



**Institute of Geophysics
Polish Academy of Sciences**

UNCERTAINTY-DRIVEN GEOPHYSICAL IMAGING IN ENVIRONMENTAL STUDIES

*A thesis submitted in fulfilment of the requirements for the degree of
Doctor of Philosophy*

Author:

Artur Marciniak

Supervisor:

Mariusz Majdański, PhD

Warsaw, September 2022

“The most beautiful experience we can have is the mysterious. It is the fundamental emotion that stands at the cradle of true art and true science.”

Albert Einstein

Contents

| | |
|--|----|
| List of Acronyms..... | 5 |
| Summary | 6 |
| Summary in English..... | 6 |
| Summary in Polish..... | 7 |
| Introduction..... | 8 |
| <i>The motivation behind the integration of geophysical techniques for environmental studies</i> | 9 |
| <i>Primary research objectives and organization of the thesis</i> | 10 |
| The scientific contribution of the presented research | 11 |
| <i>Data used in the thesis</i> | 12 |
| The problem of environmental studies in the subsurface | 14 |
| The changes in soil moisture and its properties | 14 |
| The limitations of geophysical techniques in near-surface studies | 15 |
| The seismic methods in environmental studies | 16 |
| The uncertainty of geophysical imaging..... | 17 |
| Summary of the papers..... | 19 |
| Paper I: Uncertainty based multi-step seismic analysis for near-surface imaging..... | 19 |
| Paper II: Seismic Imaging of the Mesozoic Bedrock Relief and Geological Structure under Quaternary Sediment Cover: The Bolmin Syncline (SW Holy Cross Mountains, Poland) | 20 |
| Paper III: Spatial distribution and controls of permafrost development in non-glacial Arctic catchment over the Holocene, Fuglebekken, SW Spitsbergen | 21 |
| Paper IV: Variations of permafrost under freezing and thawing conditions in the coastal catchment Fuglebekken (Hornsund, Spitsbergen, Svalbard)..... | 22 |
| Paper V: Multi-method geophysical mapping of ground properties and periglacial geomorphology in Hans Glacier forefield, SW Spitsbergen; Polish Polar Research ... | 23 |
| Paper VI: Integrated geophysical imaging of a mountain landslide – A case study | 24 |
| from the Outer Carpathians, Poland | 24 |
| Summary and conclusions | 25 |
| The problem of near-surface recognition in environmental studies | 25 |
| Integrations of multiple geophysical methods for effective near-surface imaging | 25 |
| Significance of result uncertainty estimation..... | 26 |
| Near-surface imaging in a seasonally evolving environment | 27 |
| Final remarks: general processing recommendations | 28 |
| Final remarks: future research | 29 |

| | |
|--------------------------------------|-----|
| Bibliography | 31 |
| List of the papers | 38 |
| Other contributions | 39 |
| Articles | 39 |
| Extended Abstracts | 39 |
| Scientific Projects | 40 |
| Acknowledgements | 41 |
| Reprints | 43 |
| Paper I: | 44 |
| Paper II: | 56 |
| Paper III: | 70 |
| Paper IV: | 88 |
| Paper V: | 102 |
| Paper VI: | 126 |
| Author contribution statements | 139 |

List of Acronyms

DAS - Distributed acoustic sensing

ERT- Electrical Resistivity Tomography

FWI - Full waveform inversion

GPR - Ground Penetrating Radar,

GPS - Global Positioning System

LVL – Low-Velocity Layer analysis

MASW - Multichannel Analysis of Surface Waves

RI - Reflection Imaging

RTM - Reverse Time Migration

S/N - Signal-to-noise ratio

SRT - Seismic Refraction Tomography

VP - P-wave velocity

VS - S-wave velocity

Summary

Summary in English

Main objective of the doctoral thesis: An attempt to image the subsurface in cases where it is strongly correlated with environmental factors and estimate changes due to varying climatic conditions and the current climate state.

The environmental changes observed during the 20th and 21st centuries constitute a significant challenge for modern natural and mathematical sciences (Barnett, 2009; Mieszkowska, 2021). In addition, they pose a challenge to modern geophysics, the only advanced method that allows for a precise and accurate study of spatial changes resulting from climate evolution (Bergamo et al., 2016). It is not without significance that, along with environmental changes, also geohazards, both locally and globally, are evolving (Barnett, 2009). While changes on the surface are well documented and monitored, underground imaging changes still require far-reaching further methodological research. A particular case is understanding changes and structures visible to a depth not exceeding 500 m below the ground surface where climate evolution-related changes occur. Therefore, adapting and integrating more advanced data processing and interpretation techniques are necessary to solve the mentioned challenges.

The methodology presented in this thesis integrates the classically used geophysical research methods, such as electrical resistivity tomography, ground penetrating radar imaging and refraction seismic, with more advanced and newer techniques of reflection imaging and multichannel analysis of surface waves (Marciniak et al., 2019, 2021). Furthermore, the presented approach and scheme of data processing treat the uncertainty of each method separately, not only as an interpretative parameter but as a fundamental value affecting data processing. As a result, the scientific value of the results is much greater than the sum of the individual methods used separately, and the final data are characterized by higher accuracy and lower interpretive uncertainty.

Among the applications of the methodology for the classical recognition of geological formations, exceptional cases are solutions to environmental problems representing the local scale, such as landslides, and global issues, which include the increase in the thickness of the active layer in polar regions. In both cases, a particular problem is the challenging data acquisition and the complex geological structure of the study area. The solution to this problem can only be provided by a comprehensive geophysical approach using several techniques that allow an unambiguous and high-resolution separation of environmental variables from the geological structure. An important parameter is the water content spatial and temporal variability in both the landslide and the thickness of the active layer problem. This parameter is directly (polar studies) or indirectly (landslide studies) induced by climate change.

Summary in Polish

Główny cel pracy: Próba zobrazowania podłoża w przypadkach, gdy jest ono silnie skorelowane z czynnikami środowiskowymi, oraz oszacowania zmian spowodowanych zmiennymi warunkami klimatycznymi i aktualnym stanem klimatycznym.

Obserwowane w ciągu XX i XXI wieku zmiany środowiskowe stanowią istotne wyzwanie dla współczesnych nauk przyrodniczych i matematycznych (Barnett, 2009; Mieszkowska, 2021). Stawiają one szczególne wyzwanie współczesnej geofizyce, której zaawansowane metody jako jedyne pozwalają w sposób precyzyjny i dokładny badać przestrzenne zmiany wynikające z ewolucji klimatu (Bergamo et al., 2016). Nie bez znaczenia pozostaje fakt, iż wraz ze zmianami środowiskowymi, ewoluują także geozagrożenia zarówno w ujęciu lokalnym jak i globalnym (Barnett, 2009). O ile zmiany zachodzące na powierzchni są dobrze udokumentowane i monitorowane, o tyle obrazowanie zmian zachodzących pod powierzchnią ziemi wciąż wymaga dalszych badań metodologicznych. Szczególnym przypadkiem jest zrozumienie zmian i struktur widocznych do głębokości nieprzekraczających 500 m pod powierzchnią terenu, gdzie widoczne są efekty związane z ewolucją klimatu. W celu rozwiązania wyżej wymienionych wyzwań, konieczne jest zaadoptowanie oraz zintegrowanie coraz bardziej zaawansowanych technik przetwarzania danych i ich interpretacji.

Przytoczona w pracy metodyka w sposób prosty i przejrzysty integruje klasycznie wykorzystywane metody badań geofizycznych takie jak tomografia elektrooporowa, obrazowanie georadarowe i sejsmika refrakcyjna, z bardziej zaawansowanymi i nowszymi technikami obrazowania refleksyjnego i analizy fal powierzchniowych (Marciniak et al., 2019, 2021). Przedstawione podejście i schemat przetwarzania danych traktuje niepewność każdej metody z osobna nie tylko jako parametr interpretacyjny, lecz jako realną wartość mającą wpływ na przetwarzanie danych. W rezultacie wartość naukowa wyników jest znacznie większa niż suma poszczególnych użytych metod osobno, a same finalne wyniki cechują się większą dokładnością i mniejszą niepewnością interpretacyjną.

Pośród zastosowań metodyki dla klasycznego rozpoznania utworów geologicznych, specyficznymi przypadkami są rozwiązania problemów środowiskowych reprezentujących skalę lokalną, takich jak osuwiska, oraz zagadnienia globalne, do których należy zaliczyć wzrost miąższości warstwy czynnej w rejonach polarnych. W obu wymienionych przypadkach problemem jest zarówno trudna akwizycja danych, jak i skomplikowana budowa geologiczna badanego obszaru. Szczególnym problemem, możliwym do rozwiązania tylko poprzez kompleksowe podejście geofizyczne wykorzystujące kilka technik, jest fakt rozdzielenia zmiennych środowiskowych od budowy geologicznej w sposób jednoznaczny i wysokorozdzielczy. Zarówno w zagadnieniu osuwiskowym jak i zmienności miąższości warstwy czynnej istotnym parametrem jest zmienność zawodnienia gruntu. Zmienność tego parametru zarówno w czasie jak i przestrzeni jest w sposób bezpośredni (badania polarne) lub pośredni (badania osuwiskowe) powiązana ze zmianami klimatycznymi.

Introduction

In recent years, environmental and geophysical studies have been gaining importance and popularity. One of the main reasons is accelerated climate change, which requires monitoring and predicting variations at and below the earth's surface (Kaushik et al., 2021; Reygondeau, 2019). Currently, only the geophysical techniques are sufficient for imaging the fast-developing changes beneath the surface in a spatial and non-destructive way. Of the many potential scientific targets related to the described topic, two are especially suitable to be studied by using modern geophysical imaging. One of them, representing the global scale of changes is the permafrost degradation in the polar regions (Christiansen et al., 2016; Majdański et al., 2022). The other local problem is related to the anthropogenic triggering of landslides in high mountain regions (Marciniak et al., 2021). Since the described scientific targets mainly occur in terrain with complex geological conditions, a single geophysical method is not sufficient for the precise imaging of related problems (Cardarelli et al., 2010; Hammock et al., 2022; Marciniak et al., 2019; Owoc et al., 2019).

The classical approach for near-surface studies uses ERT, GPR, and SRT techniques as standalone interpreted methods (Draebing, 2016; Feroci et al., 2000; Rossi et al., 2018; Samouëlian et al., 2005; Zhao et al., 2016). Recently, the MASW technique (Park et al., 1999; Park & Miller, 2008; Xia et al., 1999) seems very popular across environmental studies as a solution for estimating rock mechanical parameters (Hilbich, 2010; Ullemeyer et al., 2006). In addition, recent developments in computational powers allow for the use of more advanced techniques. The leading example is RI, which provides a more detailed image of the subsurface (Hobro et al., 2003). However, each of the methods mentioned has its limitations. Therefore, more integrated studies in data processing and interpretation are required to extract the maximum geological information from the datasets. It is crucial when information from boreholes is not available or sufficient, which is typical in near-surface experiments.

For studying environmental processes, where changes can be at the limit of methods resolution, an important aspect of uncertainty estimation has to be stated and concerned (Fernández-Martínez et al., 2017; Marciniak et al., 2019; Tompkins et al., 2011). In many geophysical studies, the critical aspect of results reliability is omitted. However, in studies where multiple methods are used on the same dataset or performed at the exact location, the problem of data correlation arises when comparing results from each interpretation technique. As a solution, the uncertainty information from each method should be treated as a processing parameter and used during data processing and interpretation.

There is an increasing number of studies related to problems described in previous paragraphs, treating them standalone (Kasprzak, 2015; Lindner et al., 1992; Maurer & Hauck, 2007; Wawrzyniak et al., 2016; Zhao et al., 2016). However, precise recognition of the subsurface where environmental changes occur particularly rapidly requires an approach to solving problems of method integration and result uncertainty. This thesis describes an approach to solving these problems by investigating the permafrost thawing-freezing effect and landslide triggering related to the current climate state.

The motivation behind the integration of geophysical techniques for environmental studies

The motivation behind studies discussed in the thesis can be split into methodological development of imaging techniques and the studying subsurface effects of climate evolution. When computational power allows more advanced methods to be applied to near-surface experiments, there is necessary to apply these methods to study environmental problems, mainly geohazards. The issues that have to be addressed and solved for the application of those methods are the methodological motivation of the dissertation. On the other hand, understanding how climate evolution affects geohazards is the scientific motivation behind the thesis. As such studies are long-term due to the characteristics of the problem, it is essential to gather information about the current state of the environment and observe fast-developing changes beneath the surface. The additional aspect behind the presented case studies is the importance of the topic to Poland, especially the discussion of the problem of subsurface evolution in the context of current climate dynamics.

The near-surface experiments, industrial prospecting and deep seismic soundings form the three groups that subsurface methods can be divided according to the depth of the target. Although similar and using almost the same processing and interpretation algorithms, all three groups are characterized by unique scientific problems according to the physical limitations of imaging techniques and the size of subsurface structures that must be recognized. Confusingly, near-surface studies have many similarities with crustal-scale experiments. The justification for this is the lack of borehole geophysical information in most cases, the complicated wavefields in which both refractions and reflections are mixed, and often poor S/N ratio. Nevertheless, a multi-method approach can be used to address these issues.

The problem of climate change is widely discussed and can be defined as a leading scientific topic worldwide. However, as well defined in terms of temperature increase, the changes under the surface are rarely studied and described. As climate changes induce global and local consequences both rapidly and slowly, these variations have to be described and monitored. Moreover, as such a task requires a time-lapse approach (data is gathered a few times in an assumed and often long period), it is necessary to gather information about the current state of subsurface structures. It is also essential to predict future changes, which is possible based on already estimated changes observed during previous monitoring. The articles forming the dissertation indicate only a small part of the scientific issues related to the imaging of subsurface environmental changes. However, they describe two fundamental problems that can represent the whole group. Such issues are highly sensitive to the impact of climate change, so even small disturbances can have disproportional consequences for the entire system. Especially the studies of landslides, which are triggered by natural disasters like heavy rainfalls and anthropogenic activity, significantly impact the policy toward endangered regions.

The work pointed out the importance of environmental studies and the validity of the development of geophysical techniques for studying related issues. Even though the problems addressed in the thesis represent only a small part of the broad topic of environmental studies, I believe they are of significant scientific importance. Additionally, the aspect of uncertainty analysis of the result was stated as an essential parameter that should not be omitted in geophysical research.

Primary research objectives and organization of the thesis

The main objective of the presented thesis was an attempt to image the subsurface in the near-surface area where it is strongly correlated with environmental factors and the current climate state. Thus, the key aim is to recognize the subsurface with noninvasive geophysical methods and estimate changes due to varying climatic conditions. Multiple problems have to be addressed and efficiently solved to achieve this goal:

- The gathering of the data in a challenging environment
- Integration of near-surface geophysical imaging techniques
- Reliable estimation of data uncertainty
- Development of optimal processing approach for near-surface environmental studies
- Correlation of obtained results with current climate state
- Interpretation of multiple datasets for recognition of seasonal changes in the subsurface

For that purpose, an integrated methodology for near-surface geophysical studies was developed. The approach was then applied and tested both in classical geological problems and time-lapse experiments directly covering the main problem stated in the thesis. The dissertation is constructed in the form of six articles covering the described topic:

Paper I – Uncertainty-driven seismic analysis for near-surface imaging

Paper II – Effective use of uncertainty-driven analysis in the imaging of the subsurface

Paper III – The use of ERT and MASW for initial recognition of permafrost development in S.W. Spitsbergen

Paper IV – Imaging of seasonal evolution of the permafrost in the coastal catchment in S.W. Spitsbergen

Paper V - Application of geophysical methods in recognition of ground properties and periglacial geomorphology in S.W. Spitsbergen

Paper VI - Integrated geophysical imaging of a mountain landslide in Southern Poland

The presented papers cover the problem of reliable near-surface imaging by utilizing at least two geophysical techniques. The first two articles introduce the concept of integration geophysical methods by using uncertainty as a processing and interpretation parameter. The later works present an attempt to image climate-related environmental processes using components of the developed methodology.

The thesis is divided into two main sections. The core of the work is based on the reprints of peer-reviewed published research articles forming the thesis. In the Summary of the papers section, each paper's main scientific objectives and results are briefly presented. The primary outcomes and thoughts based on findings from the publications are summarised in the second part, Summary and Conclusions. Finally, the general recommendations and future studies related to environmental near-surface studies are described and summarised in this chapter.

The scientific contribution of the presented research

The articles forming the thesis contribute to the topics of the imaging environment's current state and its changes. The most important concerns are polar and landslide studies, related to the current climate state and geohazards. The fundamental discoveries and developments are:

- Proof that thermally-related seasonal changes in Svalbard are reaching deeper into the subsurface than previously believed. It was shown that up to even 40 m under the subsurface, the indirect influence of thermal changes through water percolation could be observed. Previous knowledge states that changes do not exceed the active layer's thickness in most cases. The gathered data, with estimated uncertainty, directly show a statistically significant change in VP velocity caused by fluctuations in the water saturation of the structures. It also states that the subsurface in Arctic regions is prone to climate change more rapidly and broadly. The results significantly contribute to climate prediction models, which should be updated with findings and new data. Moreover, further studies of the phenomenon are required.
- Recognition of post-glacial and periglacial structures in the Fuglebekken catchment and Hans Glacier Forefield. In Papers III, IV and V, the first seismic and ERT experiments of such scale were conducted in a time-lapse manner. The outcomes are one of the first such insights into the geology and glaciology of the Hansbreen region.
- Precise imaging of the structure of anthropogenically triggered landslide in Beskid Żywiecki, i.e. the region strongly endangered by this type of geohazards. In Paper VI, successfully applied the methodology described in the thesis, delivering an accurate image of a potentially dangerous landslide for infrastructure. By integrating the geophysical methods, it was demonstrated that this landslide has a complex structure with multiple sliding bodies and faults. Moreover, we discovered that the rupture surface has a multi-layered form, proving that the landslide has been repeatedly activated. Deeper structures have also been identified that may indicate older landslide development, but such studies cannot be described better without further studies. Thus, they are not discussed in Paper VI. The measured physical parameters correlate with previous, less advanced studies of similar structures in the region. Therefore, conducted studies can be treated as a methodological benchmark for similar research in the region, which should be conducted more broadly due to the topic's significance.
- Geophysical imaging of Mosty region, in Holy Cross Mountains, Świętokrzyskie voivodeship, Poland. The gathered data enhanced geological knowledge about rock formations and their formation in this part of Poland. Furthermore, as the Holy Cross Mountains are interesting in terms of their complicated geological evolution, our research allowed for a better understanding of these processes, especially those related to forming the Mesozoic bedrock.

Data used in the thesis

To achieve the research objectives of the thesis, data from three research projects and four study sites were used. Data from three study sites in Poland and one in Spitsbergen were used in the order of the presented papers. These study sites significantly differ in terms of geology and thus acquisition requirements and opportunities. However, in all cases, the near-surface methodology has been used for efficient geophysical investigations. Seismic gatherings are the core methods used for studying the subsurface. Additionally, ERT and GPR methods were later integrated with cases where information from that method significantly impacts the final interpretation. This paragraph presents a brief description of datasets in the order of the article presented.

The first dataset was gathered in the Central Geophysical Observatory in Belsk (Mazowieckie voivodeship, Poland). 60 Omnirecs DATA-CUBE and 40 Reftek Texan stations with geophones having a natural frequency of 4.5Hz were used for recording. The signal excitation was carried out by an automatic PEG 40 car-mounted seismic source. A 400 m profile with 4 m geophone spacing was used for methodological tests. Due to the relatively flat elevation, the geodesy measurements were made manually using measuring tapes.

The dataset gathered in Mosty (Świętokrzyskie voivodeship, Poland) was oriented into Mesozoic bedrock relief's recognition using the previously developed methodology. The seismic line length was 840 m. Sixty standalone GPS-based DATA-CUBE recorders with 4.5 Hz geophones and a PEG 40 seismic source mounted on an in-house developed trolley were used. The receiver spacing was 5 m, and the shot spacing was 2.5 m consecutively. To cover the whole line, walk along scheme of data acquisition was used, where three smaller deployments were used to cover the whole profile. For geodetical measurements, RTK GPS was used.

The datasets presented in Papers III, IV and V were gathered during three expeditions to Svalbard (Southern Spitsbergen) in the years 2015, 2017 and 2018. The data for ERT measurements were collected during the summer of 2015, using multiple acquisition geometries on a few geophysical profiles covering the Fuglebbeken catchment and moraines of Hans Glacier. The GPR dataset was gathered in September 2018, using 30 Mhz RTA Antena from Mala, and covers seismic line HOR 22Z described in Paper V. In the seismic surveys, the same PEG 40 as a signal source with an additional 8 kg sledgehammer in places with difficult access was used. In total, four seismic lines were used with geophone spacing of 5 m in all cases and variable shooting offset (2.5 m for HOR 3 line from 2017 and 5 m for the rest of the profiles). The geodetic measurements were done by manual tape measurements and later correlated with the position obtained from GPS for each recording CUBE station.

The data for Paper VI was gathered in Cisiec (Silesian Voivodeship, Poland). Abernether and Teralog as an acquisition system were used for ERT and seismic gatherings. The data from four ERT lines of 375 m each were gathered using a gradient system. The seismic line was shorter, covering only 240 m in a place where the main landslide body was supposed to be identified. For ERT and seismic measurements, both geophone and electrode spacing was 5 m. The signal excitation for seismic studies was done manually, using an 8 kg sledgehammer. The shot spacing was 5 m, without offsets in the front and end of the line. The geodetic information was obtained by use of a GPS RTK system, as well as drone photogrammetry.

The acquisition schemes used were selected based on scientific targets and our previous experience, which can be noticed during the reviewing of the thesis articles. The author of the dissertation personally was a member or leader of all field groups, excluding the Svalbard expedition in October 2017 (I was co-organizer of the fieldwork) and 2015. The datasets used in the thesis were founded on multiple financing sources:

National Science Centre, Poland (NCN) Grants:

UMO-2012/07/B/ST10/04268, "Glacier - permafrost interaction as an environmental continuum between glacial and periglacial domain in Tarfala (Scandinavia) and Hornsund area, Spitsbergen"

UMO-2015/19/B/ST10/01833, "Three dimensional model of the lithosphere in Poland with verification of seismic parameters of the wave field"

UMO-2016/21/B/ST10/02509, "Relationship of permafrost with geomorphology, geology and cryospheric components based on geophysical research of the Hans glacier forefield and its surroundings. Hornsund, Spitsbergen"

Statutory activity No. 3841/E-41/S/2018 of the Ministry of Science and Higher Education of Poland.

The problem of environmental studies in the subsurface

One of the main difficulties in studying environmental changes in the subsurface is related to the spatial anisotropy of the studied environment (Glazer et al., 2020; Ullemeyer et al., 2006). Even in a relatively small area, the changes in the geology and rock structures can have significantly different responses to both seasonal and long-term variability.

The common in situ way of gathering rock samples from boreholes is undoubted in terms of data reliability (Lococo et al., 2021). However, raw samples from the cores, even supported with data from geological logs, are strongly limited to the local zone of radius not exceeding a few metres (Niitsuma et al., 1999). Moreover, the additional cost of even shallow drillings is also a strongly limiting factor of near-surface environmental studies and, as an invasive method, cannot be possible to use in many cases.

The ideal situation where both geological and geophysical data in terms of logs and surface gatherings are available is rare (Uhlemann et al., 2022). Moreover, in cases where a priori data are available, their quality is relatively poor. Additionally, the reliability problem arises due to a long period of observations, where data from the same study site must be collected multiple times, often in different seasons. As a solution, new approaches for similar studies have to be developed and introduced in terms of data acquisition and processing, especially in databases and the overall availability of high-quality information.

The changes in soil moisture and its properties

The environmental changes are widely observed in terms of annual temperature fluctuations (Christiansen et al., 2016; Osuch & Wawrzyniak, 2017; Wawrzyniak et al., 2016; Wawrzyniak & Osuch, 2020). Such variability strongly affects the water cycle on the surface, air, and subsurface. The way that water percolation is affected by temperature is multidirectional (Hornum et al., 2021; Matsuura et al., 2014). The effects of precipitation changes, glaciers degradation and permafrost thawing or even sea current changes can be described as direct and often global (Mieszkowska, 2021). However, indirect effects in the form of changes in water retention periods are caused by anthropogenic activities, e.g. dams and lakes built for flood prevention or artificial snowmaking, which change the local hydrogeology. Although on a micro scale, these activities can have a considerable impact on the whole regional ecosystem, especially in the mountains. Because the geophysical methods in the great majority are susceptible to water content in the media, there are ideal tools for studying environmental effects under the surface (Adepelumi et al., 2001; Boiero et al., 2010). The direct relation between water content and physical parameters like VP, VS, resistivity, and conductivity of the electrical current can be used for indirect studies of environmental evolution. Such a situation was described in Papers IV, V and VI (Marciniak et al., 2021, 2022; Majdański et al., 2022), where changes in the water saturation are the main factors for recognizing the active layer evolution and landslide structure.

Currently, one of the biggest challenges is estimating the water amount and properties of the rock structures. Because physical water parameters can vary by a high margin due to its state, salinity, temperature, and mineralization, the precise separation between water content and its parameters is challenging. One of the critical aspects is estimating water temperature, which is especially important in permafrost and hydrothermal targeted studies (Dobiński et al., 2017). Unfortunately, the temperature of the water can be

measured only directly. Because water can be in liquid form even under negative temperatures due to its salinity or pressure in rock matrices, the final result interpretation can be misleading. Therefore, the indirect effects of the water state have to be measured based on water's unique properties during its state transformations (Carcione & Seriani, 1998; Wu et al., 2017). Paper III (Glazer et al., 2020) shows that the vital aspect is separating ice and water-saturated structures in the polar experiments, which can be done using ERT and seismic techniques like MASW.

The limitations of geophysical techniques in near-surface studies

As a non-direct method of studying subsurface structures, all geophysical methods have limitations. The seismic methods are mainly limited by problems with recorded noise and challenging acquisition (Feroci et al., 2000; Marciniak et al., 2019) or the strength of the signal at the source (Atanackov & Gosar, 2013). In terms of electric methods like ERT (Revil & Glover, 1998), the limitation lies in current propagation through high resistivity media. Those can be divided into general, whose origins lie in general mathematical and statistical principles and unique ones specific to the measured physical field. The critical limitation that affects the geophysical techniques is the amount of obtained data and, thus the lack of uniqueness of the solution (Hobro et al., 2003; Owoc et al., 2019). The near-surface geophysical studies are the non-exception. However, some possibilities and drawbacks can be assigned to the relatively small scale of experiments. The critical issue, where in most cases, not a sufficient amount of data (underestimated problem), leads to the situation where not only multiple models describing earth structure can be fitted to the same dataset, but also resolution and uncertainty can vary. Although highly scarce, the opposite situation with a too high number of data (overestimated problem) leads to a significant problem. However, in this case, it can be relatively easily solved. The additional issue to be addressed is the quality of obtained data.

Opposite to the laboratory environment, where study conditions can be controlled with high accuracy, the outdoor geophysical data are gathered in a rapidly changing environment (Philips Aizebeokhai, 2010). Such a situation induces two problems that are difficult to solve. The first one is the variation of parameters of the studied structures during data collecting, and the second is changing the precision of the equipment. In both cases, the estimation of mistakes related to those changes is almost impossible in real case studies. However, the newest developments in terms of measurement devices are still far more precise than the other factors and limitations. The current state of knowledge and computational possibilities still do not allow for utilizing the datasets to their full potential. The other limitations of geophysical techniques are specific to each method uniquely. Most of those properties are the effects of physical laws and the simplifications used to describe those phenomena (Butler, 2005). Acoustic estimation of seismic wave propagation or spherical propagation of electric current in the subsurface can be a good example. The other problems are related to the measurement approach, which assumes doing experiments at the surface. Because there is no other possibility to assume the non-invasiveness of the study in most cases, the limitations in vertical recognition of the subsurface are unavoidable. This fact is related to the impact of underlying structures and layers on the deepest ones. The electric impulse in ERT or seismic wave in exploration seismology can be treated as an information carrier. Such information from deeper layers is biased by effects occurring in overlaying layers. It leads to a resolution decrease with

the depth and thus increases the uncertainty of the result. Across those effects, signal attenuation and conversions are the main difficulties that must be solved or approximated.

As previously stated, near-surface studies have some unique limitations and possibilities. One of the main is that the scientific target is complicated near-surface structures with multiple geological effects. In deeper experiments, the first meters are treated as noise, which can be easily removed from the data. In near-surface studies, complicated geological structures have to be reconstructed in geophysical models, which is difficult due to the physical limitations of each used technique. Moreover, very often, the data quality is worse in comparison to larger-scale experiments. It results from a limited number of acquisition channels and relatively weaker signal sources. Because the nearest surface substantially impacts seismic wave propagation, using a strong source is recommended, although in most cases not possible due to environmental restrictions or cost limitations. Moreover, as stated previously, the lack of geophysical information from shallow boreholes is also a limiting factor. Electrical methods like GPR and ERT, almost always exclusively used for near-surface studies, also have limitations. They resulted from the scientific target's size and balance between cost-effectiveness and recorded data quality. However limited, the near-surface studies can be relatively quickly conducted altogether in the same study site without a significant increase in the cost of the experiment. In general, the higher cost of data gathering is related to the logistics and accommodation of the field team. Because near-surface geophysical equipment is relatively portable, and data gatherings are fast due to the limited size of the study site, the multi-method approach can be introduced. This fact leads to the possibility of utilizing of multi-method approach, which is one of the critical issues of the presented thesis.

The seismic methods in environmental studies

Together with electrical methods like ERT and GPR, seismic methods like MASW and SRT are the main techniques in near-surface studies (Everett, 2013). In most cases, they are used standalone, according to the target (Draebing, 2016; Feroci et al., 2000; Hilbich, 2010; Krawczyk et al., 2012). One of the most substantial limitations of those methods is the trade-off between resolution and information about the mechanical parameters of rock structures. In the cases where the scientific target is to estimate the shape of the anomaly or localization of the boundary, electric methods are considered to be more precise. However, where geomechanical properties such as VS 30 (Allen & Wald, 2009; Ismet Kanli et al., 2006) need to be estimated, only seismic methods are applicable for solving those tasks indirectly. However, in the group of seismic methods, RI and the Full Waveform Inversion (FWI) technique can fill the gap between resolution and information about physical parameters. Those methods were not used on the near-surface due to the required processing power and/or correlation with in-situ information for detailed initial velocity field estimation. The latest development that has started to be used in environmental experiments is FWI (Adamczyk et al., 2014; Dou & Ajo-Franklin, 2014). That technique allows for obtaining much more detailed velocity estimation and increases the overall resolution of seismic methods even further (Virieux & Operto, 2009). The more mature in near-surface studies are RI techniques (Feroci et al., 2000; Krawczyk et al., 2012). In early near-surface studies, RI stacks were shown in the time domain or without horizontal stacking, as it was not possible to estimate seismic wave velocities in individual layers with sufficient precision. Another important contribution of this work is the presentation of the solution that allows the use of these techniques in environmental

studies, utilizing information from basic seismic and electric methods (Marciniak et al., 2019, 2021). It has to be stated that combining less precise methods and information about the uncertainty of the result is crucial for RI. As a result, seismic methods as a group can provide reliable information about the geomechanical properties of studied structures and deliver images with resolution exceeding previously used classical approaches, as shown in Paper VI (Marciniak et al., 2021).

Another critical point of environmental studies is the relation of water with rock structures (Boiero et al., 2010; Matsuura et al., 2014; Uhlemann et al., 2022). Showing changes in geophysical parameters and imaging structural changes in the subsurface based on those fluctuations leads to a more precise interpretation. It is essential in time-lapse measurements (Leroux and Dahlin, 2006; Bergamo et al., 2016). Those variations may be on the limit of statistical significance, and thus quantitative and qualitative estimation based on the same dataset significantly enhance the reliability of obtained information.

One of the critical aspects of using seismic methods in environmental studies is their usability and scalability in prospecting for hydrothermal and geothermal resources (Farina et al., 2019; Poletto et al., 2018). Those experiments are often on the boundary between industrial and near-surface studies. One of the key points here is that methodology previously only used in recognition of the first 50 m of the subsurface can be adopted to study subsurface up to 1000 m without using expensive vibroseis or dynamite methods for signal excitation.

The uncertainty of geophysical imaging

An additional issue related to all geophysical studies is the uncertainty of the final model (Broadhead & Ahmed, 2005; Fernández-Martínez et al., 2017; Fournier et al., 2013). The resulting uncertainty is strictly connected with the resolution of the received images. However, where much effort is put into the increasing resolution of geophysical research in general, only a few works treat about increasing their reliability (Routh, 2008). Often opposite relations of increased resolution over worse parameters of the uncertainty of the geophysical and later geological interpretation can be observed. The problem of uncertainty estimation can be described as both qualitative and quantitative and as a single value or multidimensional matrix of values (Malinverno & Briggs, 2004). The most often used uncertainty estimation is the Chi-square parameter, which is helpful in 1D modelling and can be misleading in 2D or 3D, where information about mistakes across the resulting data matrix is essential. As presented in Paper I (Marciniak et al., 2019), the two trends can be noticed in geophysical studies. The first one shows a decrease in the resolution of images with depth and an increase in result uncertainty. Secondly, higher data coverage, as presented by ray coverage images, strongly increases the reliability of the results in parts with good signal coverage.

One of the aspects discussed in Paper I (Marciniak et al., 2019) is treating uncertainty as a parameter limiting the solution space of each later method. Such an approach has two main advantages over approaches where results of experiments are used in the following methods, but without transferring uncertain information. The first one is an increase in data reliability. It results from adding "first guess" bounds derived from previous techniques to the equations during the inverse process, which limits the possible solution space significantly. According to the previously used technique, these "bounds" are based on physical parameters, and links result from the following method. Finally, despite being

based on different parameters, the last method in the processing scheme includes information from much more physical phenomena. Thus, the second added value is limited processing effort and computational cost. It is due to a significantly smaller solution area that has to be searched during the inversion process of the data for each method. Therefore, it is a significant gain in cases where big datasets gathered in a time-lapse scheme must be interpreted with the latest FWI and RTM (Baysal et al., 1983) techniques.

The problem of uncertainty analysis is significant in terms of environmental studies. As presented in Papers IV to VI (Majdański et al., 2022; Marciniak et al., 2021, 2022), geophysical techniques are not limited to recognizing geological structures but can visualize seasonal thermal and water content-related effects. Such variations can be rapid and significant in physical parameter changes like seismic velocity, as described in Papers IV and V (Majdański et al., 2022; Marciniak et al., 2022). However, those changes can be slow and on the boundary of method resolution. In such cases, uncertainty estimation is essential for stating the hypothesis about changes occurring in the studied environment.

Summary of the papers

Paper I: Uncertainty based multi-step seismic analysis for near-surface imaging

Main aim: Development of methodology for near-surface studies integrating multiple geophysical methods.

In the first article, which composes the thesis, the concept of multi-stage seismic analysis based on uncertainty was introduced for near-surface imaging. The paper shows the close integration of results from MASW, ray-based SRT and RI. The study area was the Central Geophysical Observatory in Belsk, the IG PAS test site. The proposed approach allowed the use of RI when velocity information from boreholes was not available. In addition, a concept was introduced in which the data obtained with less precise methods is used in the subsequent processing stages using more accurate techniques. Moreover, this approach simplifies data processing because the final model from the previous analysis is treated as a starting point for the next ones. One of the critical aspects of the study was the problem of uncertainty analysis of results in the near-surface methodology.

The direct use of information about the uncertainty between the methods allowed the authors to narrow down the area of possible solutions for subsequent methods. The assumption that deviations in the results obtained from the previous methods limit the possible range of solutions for more accurate subsequent methods leads to a more reliable interpretation. The case study presented by the authors shows that the propagation of information about the uncertainty of the model should be treated equally as direct outcomes in the results. Moreover, consecutive methodologies are characterized by deeper imaging potential. The findings of the work demonstrate the importance of verification of the results and thus show that the final result, which is a seismic reflection stack, may differ in the depth of the reflection horizons. In the presented study, the example of determining the velocity field for seismic imaging allowed for the retrieval of information about the reflection horizons in the data set. The work is a fundamental introduction to the methodology that has been applied and developed in various forms for the case studies presented in the following articles. A similar methodology could be applied to solve other particular geophysical problems.

Paper II: Seismic Imaging of the Mesozoic Bedrock Relief and Geological Structure under Quaternary Sediment Cover: The Bolmin Syncline (SW Holy Cross Mountains, Poland)

Main aim: Recognition of structures under quaternary sediments in localization with relatively unknown geological construction.

The methodology presented in Paper I was used to identify the Mesozoic bedrock in the Holy Cross Mountains. Geophysical methods provide the only opportunity to obtain information about subsurface structures in areas with poor geological and geophysical information, without deep boreholes and outcrops. A multi-method approach that allows the use of main recorded wave types (surface waves for MASW, wide-angle refractions for FATT, vertical reflections for seismic imaging) provided detailed, high-resolution images up to 200 m. Combined with good and dense coverage of the study area with seismic recorders and shooting points, the multi-method approach resulted in well-separated and detailed images of geological structures. The overall data obtained during processing consisted of the VS, VP and reflection image. Applying uncertainty-based processing and overall subsurface recognition down to a depth of 200 m was possible. A primary reflecting horizon at depths of 50 to 120 m was recognized as the "hard" (Mesozoic) bedrock.

There was also a depression in the horizon, corresponding to the erosion of the structure. Its shape resembles the structure of the basement syncline and erosive processes. The axis of the syncline lies at the Grzywy Korzeczkowskie foothills. The flattened shape of the bedrock in the studied part of the Holy Cross Mountains may indicate a limited erosive activity of glaciers. A narrow and deep depression was found in the Mesozoic bedrock in the northeast. This structure is probably related to the erosion of the river during one of the interglacials. Four steeply sloping branches were identified in the Mesozoic rocks, probably related to a local fault. Their configuration is related to the surface morphology. Due to the high resolution of the seismic image, numerous faults were also distinguished. Research results have increased the understanding of the geology of the Mosty region, where complex rock formations are difficult to visualize using just one method. In addition, the methodology developed appeared to be cost-effective in terms of data collection, processing, and interpretation work.

Paper III: Spatial distribution and controls of permafrost development in non-glacial Arctic catchment over the Holocene, Fuglebekken, SW Spitsbergen

Main aim: General recognition of the near-surface structures and permafrost development in the Svalbard area, SW Spitsbergen

The geophysical survey of the Fuglebekken catchment in southern Svalbard presented in Paper III integrates the MASW with the ERT methodology. In this article, the main issue was to illustrate the seasonally evolving structure of permafrost and its active layer. The application of MASW with ERT was essential for distinguishing sedimentary cover from bedrock formation and thus identification of ice-bearing permafrost. As the ERT method used as the main one in the study revealed limitations in recognition of the thermal state of the ground, an additional seismic method was necessary. The paper described the occurrence and nature of permafrost in ice-bearing and cryotic states. The Fuglebekken catchment was selected for the research as a unique site where the Holocene glacial area intersects with well-preserved sea terraces along with the river and slope sediments. The area stretches from the mountain range to the coast near the Polish Polar Station in Hornsund.

The collected data in the form of multiple ERT profiles and MASW seismic lines allowed for obtaining unique results that were the first integration of these methods to illustrate the current state of this rapidly evolving environment. After data interpretation, especially from the HOR3 line, a strong dependence on permafrost development according to environmental factors was noticed. Different permafrost structures related to Quaternary marine terraces in obtained data were noted. A nearby glacier, as well as marine transgressions, influenced those formations and their degradation. Its presence is strongly connected with surface watercourses, and their velocity flows. Moreover, a strong impact of seawater on coastal permafrost was observed. In the foothills of Fugleberget, the effect of thawing water and meteoric flows significantly increases the active layer's depth. The strong zonation of ice-bearing sediments can be observed based on recognised effects and structures, ranging from coastal to the foothill area. Due to this and the varying thickness of the active layer, it was denoted that the permafrost in the Fuglebekken catchment is sensitive to climatic effects. It is especially important in the context of climate evolution and global warming for future forecasts and their verification. Such studies pose a new challenge to modern geophysics in monitoring geological structures and thermal effects. The integration of both methods during the final interpretation allowed to solve the problem of distinguishing between geological structures, such as the boundary of the sedimentary cover-subsoil and the active layer. The work introduces a more extensive study of the Hornsund area and the Hansa Glacier moraine, wherein a modified form of a more advanced approach proposed in the previous methodology was applied.

Paper IV: Variations of permafrost under freezing and thawing conditions in the coastal catchment Fuglebekken (Hornsund, Spitsbergen, Svalbard)

Main aim: Multimethod investigation of permafrost seasonal evolution and near-surface structures in Fuglebekken catchment, with correlation to temperature from local boreholes.

Paper IV describes the variability of permafrost during the freezing and thawing processes of the Paper III test site. Due to the dominance of climate warming, the form and condition of permafrost change, which requires additional validation in the study area. Multiple seismic methods (MASW, seismic refraction and travel time tomography) and borehole data have provided new high-resolution observations and insight into the permafrost state in Fuglebekken Catchment. In the study, information from the boreholes showed the local thermal regime of the ground and high spatial conditions variability. The modified processing approach introduced in Paper I and proven in Paper II has been applied to obtain an integrated result with plausible uncertainty. Seismic surveys can also provide information about the thickness of the active layer and compare it with the distance from the shoreline, elevation, and the presence of water from the streams. Based on two experiments conducted in spring and late summer, the study estimates the minimum depth of thaw and the thickness of the active layer, the depth of the influence of surface temperature on permafrost, and the extent of permafrost in the Fuglebekken coastal catchment area. The data showed the relationship between permafrost characteristics (freezing and freezing zones) and the distance from the coast, slope and geology. Comparing the observations from the two seasons, the significant impact of seasonal changes in the active layer on seismic wave fields can be seen. The analysis of the short offsets indicates that the sediment thickness and the top of the bedrock are not changing over time. Travel time tomography detects seasonal variability in seismic velocities due to the medium's partial or complete changes in the water state. MASW cannot be used in the time-lapse mode because surface waves are only sporadically observed in the area covered by snow. In a region characterized by cryogenic permafrost, it is only possible to distinguish the active layer from permafrost by directly measuring the temperature in the ground.

However, time-lapse geophysical observations show that the characteristics of permafrost change over time. Therefore, the region can be an example of a field laboratory where permafrost degradation is evident. The interactions of water and cryotic structures have a significant impact and are expected to enhance in the future, further increasing the slope processes and causing more significant geomorphological changes. The permafrost on the Hornsund seacoast is rapidly degrading. This is induced by the accelerated increase of air temperature, the intrusion of seawater into the shore and the deep penetration of freshwater into the fractured rocks. The high spatial resolution of the velocity field imaging using the seismic method and direct monitoring of the ground temperature allows for confirming the hypothesis that there is a wide range of unfrozen ground near the coast. It is probably affected by saltwater intrusion and groundwater mineralization. Another interesting structure is the boundary between the sedimentary material and the underlying solid rock. In these two media, the velocities of seismic waves may be different, and they may change seasonally depending on the depth of ground freezing.

Paper V: Multi-method geophysical mapping of ground properties and periglacial geomorphology in Hans Glacier forefield, SW Spitsbergen; Polish Polar Research

Main aim: Multimethod investigation of ground properties and periglacial geomorphology in strongly evolving and prone to climate-related factors area of retreating Hans Glacier, SW Svalbard.

The article presents the results of geophysical surveys from which detailed images of the postglacial and periglacial terrain forms and subsurface structures were obtained. A common interpretation of three non-invasive geophysical methods, namely ERT, GPR, and time-lapse SRT, was used to receive spatial information from the complex geomorphological terrain. They were applied to identify subsurface structures in the forefield of the retreating Hans Glacier on SW Spitsbergen in Svalbard. This is the first comprehensive description of the periglacial structures in the Hans Glacier forefield, using the longest ERT profile (1500 m) in Svalbard along with deep georadar and precise seismic tomography. The data highlight the merits of combining geophysical techniques to assess permafrost characteristics, bedrock and sedimentary cover extent, identify active layer behaviour, and resolve complex geological structures. Three main zones were recognized and described, i.e. the outwash plain, terminal moraine and glacial forefield proximal to the glacier front. Each recognised zone responds differently to the freeze-thaw effect.

Based on observations from two seasons, thermal and hydrogeological influences on geophysical data can be distinguished from non-seasonal effects of sediment thickness and bedrock topography. Geophysical profiles in these zones provide information on the thickness and structure of the sediments and ice and the topography of the bedrock. It has been estimated that the boundary between the sediment-substrate layers is 5 to 20 m deep. The freeze-thawing effect of the active layer has a strong and profound influence, as evidenced by the variability of the VP in the results obtained. The observed impacts are stronger than expected from previous studies due to the indirect effect on deeper structures reaching about 40 m below the surface due to deep water penetration. This supports the hypothesis that the leading cause of deep seasonal variability is water circulation and percolation within the permafrost in the bedrock. Recently, snow cover, temperature and precipitation have changed rapidly in the Arctic, especially in Spitsbergen. As there is a clear need to identify subsurface changes due to climate warming, geoelectric, seismic, and GPR measurements should be carried out and repeated along with common profiles. Geophysical methods provide images of subsurface features related to the interplay of permafrost, water, and ice in the ground and provide an excellent basis for comparative studies.

Paper VI: Integrated geophysical imaging of a mountain landslide – A case study from the Outer Carpathians, Poland

Main aim: Investigation of the developing landslide triggered by anthropogenic actions caused by climate evolution.

In the presented case study, a multi-method approach using geophysical imaging was applied to investigate the landslide in Cisiec in southwestern Poland. The application of MASW, ERT, SRT, and RI allowed high-resolution imaging of the subsurface of the landslide in the geologically and tectonically complex environment. Drone-based digital terrain models (DTMs) supported subsurface imaging, providing a detailed view of the landslide surface. Accurate GPS-based surveying was performed during data collection to supplement information on the area's topography and the correlation of geophysical results. The connection and transfer of information between methods allow for solving the problems associated with multiple RI, especially the lack of information about the boreholes. MASW enabled the identification and distinguishing of individual layers in the sliding zone. ERT data was used to differentiate lithological structures in a case where strongly dipping layers cannot be visualized using seismic methods. The result of seismic ray-based tomography allowed for recognising velocities necessary for reflecting imaging.

The obtained velocity field is comparable with other seismic surveys of related problems in the Polish Carpathians. The model obtained by the ERT method allowed us to estimate the north-eastern direction of the slope motion. Seismic imaging enabled the identification of discontinuities inside and under the landslide body. Uncertainty analysis was necessary to directly compare the results and correct correlation of information between them. In ERT and reflection seismic method, the interpreted depth of the slip surface shows a high degree of convergence, confirming the narrow uncertainty of the obtained results. The resolution of ERT methods was estimated at 5.6 m at a depth of approx. 35 m, while the uncertainty of mapping the reflection at a depth of 30–40 m was ± 3 m. The final finding shows detailed geophysical images of a landslide with a recognized depth of the main slip surface of 16 to 36 m. As the survey site is used as a ski slope, detailed information about the landslide structure is needed to ensure the safety of the nearby structures. The methodology proposed in this article can be used in similar case studies where fast and cost-effective landslide identification is required.

Summary and conclusions

The dissertation highlights the problem of reliable environmental studies based on geophysical techniques. One of the key findings of the work is the importance of uncertainty estimation of the results and the integration of multiple techniques to obtain accurate geological interpretation. The outcomes of previously described case studies reveal that multiple scientific issues must be addressed and generally established before planning similar research. Moreover, further studies in the much broader aspect of near-surface and general geophysical methodology should be concerned with an increased number and quality of datasets from high-resolution DAS systems. With improved data reliability, the element of processing and result precision cannot be omitted. In terms of presented studies, the key four outcomes related to the environmental studies are: (i) The problem of near-surface recognition in environmental studies, (ii) Integrations of multiple geophysical methods for effective near-surface imaging, (iii) Significance of result uncertainty estimation and (iv) Near-surface imaging in a seasonally evolving environment. The following paragraphs provide conclusions based on the results of presented studies related to the topic.

The problem of near-surface recognition in environmental studies

As presented in the thesis, the methodological problem of environmental near-surface imaging lies in the complicated geology and the lack of in situ information from boreholes (Hammock et al., 2022; Rossi et al., 2018). To solve these problems and apply more precise techniques, the concept of uncertainty-driven multi-method imaging in Papers I and II (Marciniak et al., 2019; Owoc et al., 2019) was introduced. The significant outcome of this work is that the application of multiple methods as a straightforward way of obtaining more geophysical information has to be conducted in a particular order. Initially applying the shallower and less accurate, and thus requiring less input and assumptions, method of MASW and SRT, the results obtained from them can be used as initial models for more precise techniques. It is worth noticing that the proposed processing scheme is not only limited to seismic methods but can also integrate techniques like ERT, as shown in Paper VI (Marciniak et al., 2021).

Integrations of multiple geophysical methods for effective near-surface imaging

Based on gathered experience during the data preparation for publications forming the presented thesis, the cons and pros of the multi-method approach can be stated. The key outcomes from utilizing at least two geophysical methods in a strict, uncertainty-driven approach can be divided into processing and interpretation gains.

Although time-consuming and initially complex, the integration of multiple seismic methods to study the same dataset can significantly simplify data processing (Foti et al., 2003). It is especially visible in solving static corrections and velocity field estimation problems. Since, in environmental studies, changes in the subsurface can have strong contrast in physical parameters over a relatively small area, it is necessary to distinguish and estimate these effects. The key example is water-saturated zones with lower than surrounding velocities. Such structures, invisible on refraction methods, can be recognized using MASW, GPR,

or ERT techniques (Crook et al., 2008; Matsuura et al., 2014; Park et al., 2007). Another benefit of utilizing the multi-method approach is a simplified estimation of the velocity field, where the results of previously used techniques limit solution space for this task. Finally, depending on the case study, the results of other geophysical methods can be transferred to different parts of the processing step, overcoming or simplifying the problems that may significantly affect the result or exclude it from interpretation.

The interpretation gains result from the increased amount of information about the studied environment, with the possibility to correlate the outcomes from each method (Sausse et al., 2010). As each geophysical technique has unique limitations or possibilities, a good design experiment using properly chosen methods to study the target can benefit from supportive possibilities. In polar studies related to permafrost, the combination of SRT, GPR, and ERT methods can accurately estimate environmental changes. Despite the results of MASW analysis presented in Paper III and IV, application of this technique in Svalbard is problematic and not always possible due to the attenuation of surface waves by snow coverage and noticed effect of the proportional increase of the VS with decreasing frequency. As a result surface wave is not always developing. In landslide studies, the combination of MASW, SRT, and RI techniques with ERT has provided satisfactory results. In this case, the GPR technique application may be insufficient due to the limited depth of recognition due to antenna frequency.

The obtained findings from each method can be correlated both qualitatively and quantitatively. The integrated data will result in a more detailed interpretation with information about uncertainty estimation. Moreover, qualitative estimation of seasonally variable changes can be done more simply when geological horizons can be fixed as constant, and thus only changes in physical parameters can be modelled. Such an approach was presented in Paper IV (Majdański et al., 2022), where differentiation of sediment cover and the bedrock based on MASW SRT and ERT data allowed for using thicknesses as constant. It finally enabled the separation of the seasonal effects of thawing and freezing permafrost from the geological structure of the study site. As a result, the complex glacial and periglacial structures of the Fuglebbeken catchment and Hans Glacier forefield (Paper V), were recognised. Also, the images of permafrost structures proved that seasonal changes are stronger and reach deeper than previously believed. Using each method separately, such a task is not possible or at least much more complicated.

Significance of result uncertainty estimation

One of the key aspects stated in the thesis is the uncertainty estimation of each method. It is essential to use that information during the processing stage of geophysical data analysis and final geological interpretation. As presented in Papers I and II, such an approach is beneficial in enhancing data quality and reliability. One of the most favourable aspects of uncertainty analysis is shortening and thus increasing the cost-effectiveness of the whole experiment. Additionally, the influence of the human factor in the processing is limited because initial parameters have to be guessed or based on a priori information, mainly for the first technique in a workflow. Finally, during the interpretation process, information in the form of a ray-coverage mask or graphs showing the mean and best-fitted model to the data can precisely estimate the parts of images that can be certainly interpreted. With information about how accurately each horizon is estimated, a complete interpretation can be made. Furthermore, it is vital to merge information from techniques that were processed separately and joined together during result verification.

This enables the distinction between geological layers, structures, and environmental effects as presented in Papers III to VI (Glazer et al., 2020; Majdański et al., 2022; Marciniak et al., 2021). The effectiveness of the proposed approach is evident in permafrost and periglacial study. In Papers IV and V, imaging of the Fuglebekken catchment, where complicated elevated marine terraces, post-glacial sediments, and thermal effects had to be visualized and described, the information about uncertainty was essential. As a result, it was recognized that seasonal thermal effects affect deeper rock structures through changes in water percolation up to 40 m under the surface. It is also direct proof that coastal permafrost is not continuous in its form. Treating uncertainty as an additional interpretation parameter in similar cases allows for the creation of precision intervals for each method to correlate individual characteristic reapers and structures accurately.

Near-surface imaging in a seasonally evolving environment

The problem of recognizing seasonally varying effects in near-surface studies significantly increases the difficulty level of the study. In such cases, geological structures and environmental factors have to be recognized and estimated (Dou et al., 2017a; Hornum et al., 2021; Justice & Zubaj, 1986; Kneisel et al., 2008). Therefore, more geophysical information is required as the number of unknown parameters is higher. A scientific approach using multiple interpretation techniques in a time-lapse scheme should be used to investigate this issue effectively. As described in the thesis, an increased number of used techniques leads to a problem of precise result correlation and interpretation. One of the work outcomes is the importance of choosing the correct technique and its parameter for each problem (Atanackov & Gosar, 2013; Carcione et al., 2020; Carcione & Seriani, 1998). Misuse of the method can often lead to misinterpretation, even though other results indicate the correct solution. Although difficult in relatively unexplored environments such as polar regions, the solution to this problem can be straightforward in landslide studies, where some initial information can be gathered by observing outcrops and surface discontinuities. The factor that has the most significant effect on each method is water content in rock matrices, porous structures, and cracks. Because of water and its state, the usability of the ERT technique can be misleading, where dry sands at the nearest surface effectively block the current. Such an effect can be noticed on the frozen ground in polar and subpolar areas.

Similarly, the water content can attenuate surface waves in swamp areas during MASW studies reducing the penetration range or slow P-waves in tomographic results. The described situations show that gathered data must be fully understood and recognized effects and structures synthetically modelled when possible (Xiujun et al., 2005). Additional information about uncertainty increases the reliability of near-surface imaging in a harsh environment. Carefully chosen techniques, processing workflow supported with additional external data, synthetic models, and uncertainty estimations are critical for successful near-surface imaging in environmental studies.

Final remarks: general processing recommendations

General processing recommendations can be stated to conclude the efforts and outcomes gathered during the processing of six different datasets from four different localizations. As the studies were conducted in different environments, often in tough and challenging conditions, I believe our thoughts can be broadly helpful for planning similar studies. Even though every case requires an individual approach, some general recommendations can be given. However, they should not be incorporated directly as a blind processing approach. During the planning stage of each experiment, the limitations of equipment, human resources, and available interpretation tools and software have to be considered to maximize the outcome of each research.

The recommendations at the presented stage of methodology development of near-surface environmental imaging are:

- I recommend using as dense as possible data acquisition on the study site (optimally 1 m source and receiver spacing) and the strongest possible signal sources in case of seismic techniques. It significantly reduces the processing effort during signal normalization, which can be difficult in a near-surface environment where complicated attenuation processes occur.
- Geophysical imaging, mainly based on seismic methods, can provide detailed subsurface information, filling the gap between resolution and estimation of geomechanical parameters. Moreover, it can be done using a single seismic dataset, which, optimally deployed, can fulfil requirements for multiple seismic techniques like SRT, MASW, and RI.
- As presented in the Papers, the multi-method approach is reliable and significantly increases the quality and reliability of the outcomes. However, the used geophysical techniques should be applied in particular order providing information for each following used technique. As a result, the results can be revalidated and easily integrated, forming a more uniform dataset about the studied environment.
- The limitations that made methods of RI useless in near-surface studies can be omitted by using of multi-method approach. However, it has to be stated that received velocity fields for NMO and Time-to-depth migrations are assumptions and require later manual fitting and further methodology development. This is also another reason for the precise estimation of the interpretation of the result.
- The recorded datasets have to be verified with already known a priori information at the data pre-processing stage. Therefore, I recommend performing synthetic verification of the results after obtaining the first outcomes. It will allow for an understanding of the observed effects and validation of data usability in environmental studies.
- As presented in Papers IV and V, the seasonal effects increase the difficulties of interpretation. For estimation, if seasonal factors occur, the outcomes must be presented with estimated result uncertainty. This is direct proof that the presented

information is not significantly biased by processing approximations and limitations and thus provides reliable information about seasonal or rapidly developing changes in the subsurface.

- The Papers III to VI result indicates that environmental changes can significantly impact measured physical parameters. Moreover, the effect of these variations can reach deeper than previously believed. Therefore, it is necessary to clearly distinguish between the impact of temperature and water saturation changes from geological formations. It can be done with multi-method and time-lapse approaches to data gathering.

Final remarks: future research

The primary outcomes that conclude the presented thesis can be treated as key fields of future development of near-surface geophysical imaging. The dissertation introduces methodological and practical case studies with complete workflows for geophysical research of environmental changes, especially using seismic methods as core techniques. Despite being effective in terms of generated output and costs of studies, the application of imaging techniques has its limitations that have to be overcome. Moreover, the multi-method approach integrating seismic reflection techniques is still not on par in development compared to industrial-scale experiments. Nevertheless, two key study directions can be identified based on the presented studies: more precise estimation of velocities in the subsurface and integration of methods based on different physical parameters.

The key aspect of using seismic studies as a core technique for near-surface studies is that a single dataset can be used for multiple interpretation techniques, and thus, multiple geophysical and geomechanical parameters can be estimated. However, as presented in the Papers forming the thesis, reliable estimation of velocity inside the studied structure can be challenging and time-consuming. The exact solution for the velocity field has key significance for reflection-based techniques, especially RI. Without NMO velocity estimation, it is impossible to reconstruct reflecting horizons or even distinguish reflections from shallow refractions in high-velocity rock structures. As a solution, FWI techniques can be applied (O'Neill et al., 2003; Virieux and Operto, 2009; Warner et al., 2013; Dou and Ajo-Franklin, 2014). Those techniques treated as a "holy grail" of seismic methods are under strong development for industrial and purely scientific use. With the recent development in computational powers, mainly high-quality and dense seismic acquisition based on DAS systems (Dou et al., 2017b; Parker et al., 2014), inversion concerning almost all available on gathers information is possible. As a result, high-resolution velocity models can be applied to reflection-based techniques. With advanced RTM methodology (Baysal et al., 1983), this combination can provide subsurface models with resolution unseen in environmental studies, which can significantly increase understanding of climate-related and anthropogenic processes affecting the subsurface. However, there have to be noted that the FWI technique, based on multiple parameters, especially in full viscoelastic software implementations, has many parameters and, thus wide solution space that must be limited. As a solution, the approach proposed and proven in this dissertation can be treated as a priori information for this technique. It is similar to large-scale implementations, where refraction and reflection tomographic techniques are used for initial model generation. In the case of near-surface experiments, information from

surface waves, tomography or even electrical methods can be used to introduce the FWI method into environmental studies effectively.

Discussed in the previous paragraph, the problem of velocity field estimation (Amaru et al., 2017; Majdański et al., 2016; Socco et al., 2010; Xia et al., 1999) and the potential application of the FWI method can be effectively supported by integrating results from study techniques based on the electrical or magnetic properties of the rocks. This term, relatively rarely studied, starts to become interesting in the context of the latest achievements in artificial intelligence and neural networks. In most cases, results of methods based on different physical fields were shown separately or at least presented in the final interpretation images. In the presented Papers IV, V and VI, basic information about the approximated depth of the layers during processing for the structures that certainly can be distinguished and correlated was essential. In Paper VI, the information about the shape of the rupture surface during recalculations of the tomographic field into NMO velocities was used. However, the correlation of results based on different physical fields can significantly increase our understanding of the studied environment, so an enhanced integration of techniques is required. Developments in artificial intelligence, especially machine learning in both supervised and unsupervised approaches (van der Baan & Jutten, 2012; Wan et al., 2018) allows for new ways of data interpretation. Such data classification and clusterization techniques can fast and effective integrated models from seismic, magnetic or electric-based methods. In combination with accurately estimated uncertainty and a priori information about the studied environment, a complete dataset about the parameters of each structure can be obtained, even further increasing the interpretational possibilities. It is crucial in environmental studies, where differentiating dynamical changes from geology is one of the main problems of time-lapse studies. Using the machine learning approach, classifying which parts of the subsurface changed and which parameter has the most substantial impact on these processes will allow for qualitative and quantitative estimation of subsurface evolution. As a result, more precise predictive models will be created, significantly increasing our understanding of environmental processes, mainly geohazards, that impact human safety.

As presented in the thesis, geophysical imaging must be treated as a significant research tool for understanding climate evolution and related changes. Current imaging possibilities are not fully implemented in environmental studies. Despite its similarity to classical near-surface recognition studies, imaging of temperature and, thus related hydrological effects require a particular time-lapse approach and further developments in two key fields described in the dissertation.

Bibliography

- Adamczyk, A., Malinowski, M., & Malehmir, A. (2014). High-resolution near-surface velocity model building using full-waveform inversion-a case study from southwest Sweden. *Geophysical Journal International*, 197(3), 1693–1704. <https://doi.org/10.1093/GJI/GGU070>
- Adepelumi, A. A., Ako, B. D., & Ajayi, T. R. (2001). Groundwater contamination in the basement-complex area of Ile-Ife, southwestern Nigeria: A case study using the electrical-resistivity geophysical method. *Hydrogeology Journal*, 9(6), 611–622. <https://doi.org/10.1007/s10040-001-0160-x>
- Allen, T. I., & Wald, D. J. (2009). On the use of high-resolution topographic data as a proxy for seismic site conditions (Vs30). *Bulletin of the Seismological Society of America*, 99(2 A), 935–943. <https://doi.org/10.1785/0120080255>
- Amaru, M., Hoelting, C., Ivanova, N., & Osypov, K. (2017). Introduction to this special section: Velocity-model uncertainty. *Leading Edge*, 36(2), 126. <https://doi.org/10.1190/TLE36020126.1>
- Atanackov, J., & Gosar, A. (2013). Field comparison of seismic sources for high resolution shallow seismic reflection profiling on the Ljubljana Moor (central Slovenia). *Acta Geodynamica et Geomaterialia*, 10(1), 19–40. <https://doi.org/10.13168/AGG.2013.0002>
- Barnett, J. (2009). Environmental Security. *International Encyclopedia of Human Geography*, 553–557. <https://doi.org/10.1016/B978-008044910-4.00774-4>
- Baysal, E., Kosloff, D. D., & Sherwood, J. W. C. (1983). Reverse time migration. *Geophysics*, 48(11), 1514–1524. <https://doi.org/10.1190/1.1441434>
- Bergamo, P., Dashwood, B., Uhlemann, S., Swift, R., Chambers, J. E., Gunn, D. A., & Donohue, S. (2016). Time-lapse monitoring of climate effects on earthworks using surface waves. *Geophysics*, 81(2), EN1–EN15. <https://doi.org/10.1190/GEO2015-0275.1>
- Boiero, D., Godio, A., Naldi, M., & Yigit, E. (2010). Geophysical investigation of a mineral groundwater resource in Turkey. *Hydrogeology Journal*, 18(5), 1219–1233. <https://doi.org/10.1007/s10040-010-0604-2>
- Broadhead, M. K., & Ahmed, F. Y. (2005). Assessing and using seismic amplitude and acoustic impedance uncertainty in Saudi Arabia. *Leading Edge (Tulsa, OK)*, 24(8), 837–839. <https://doi.org/10.1190/1.2032260>
- Butler, D. K. (2005). Near-Surface Geophysics. *Near-Surface Geophysics*. <https://doi.org/10.1190/1.9781560801719>
- Carcione, J. M., Farina, B., Poletto, F., Qadrouh, A. N., & Cheng, W. (2020). Seismic attenuation in partially molten rocks. *Physics of the Earth and Planetary Interiors*, 309. <https://doi.org/10.1016/j.pepi.2020.106568>
- Carcione, J. M., & Seriani, G. (1998). Seismic and ultrasonic velocities in permafrost 1. *Geophysical Prospecting*, 46, 441–454.

- Cardarelli, E., Cercato, M., Cerreto, A., & di Filippo, G. (2010). Electrical resistivity and seismic refraction tomography to detect buried cavities. *Geophysical Prospecting*, 58(4), 685–695. <https://doi.org/10.1111/j.1365-2478.2009.00854.x>
- Christiansen, H. H., Gilbert, G. L., Demidov, N., Guglielmin, M., Isaksen, K., Osuch, M., & Boike, J. (2016). *Permafrost thermal snapshot and active-layer thickness in Svalbard*.
- Crook, N., Binley, A., Knight, R., Robinson, D. A., Zarnetske, J., & Haggerty, R. (2008). Electrical resistivity imaging of the architecture of substream sediments. *Water Resources Research*, 46(4). <https://doi.org/10.1029/2008WR006968>
- Dobiński, W., Grabiec, M., & Glazer, M. (2017). Cold-temperate transition surface and permafrost base (CTS-PB) as an environmental axis in glacier-permafrost relationship, based on research carried out on the Storglaciären and its forefield, northern Sweden. *Quaternary Research (United States)*, 88(3), 551–569. <https://doi.org/10.1017/qua.2017.65>
- Dou, S., & Ajo-Franklin, J. B. (2014). Full-wavefield inversion of surface waves for mapping embedded low-velocity zones in permafrost. *GEOPHYSICS*, 79(6), EN107–EN124. <https://doi.org/10.1190/geo2013-0427.1>
- Dou, S., Nakagawa, S., Dreger, D., & Ajo-Franklin, J. (2017a). An effective-medium model for P-wave velocities of saturated, unconsolidated saline permafrost. *Geophysics*, 82(3), EN33–EN50. <https://doi.org/10.1190/GEO2016-0474.1>
- Dou, S., Lindsey, N., Wagner, A. M., Daley, T. M., Freifeld, B., Robertson, M., Peterson, J., Ulrich, C., Martin, E. R., & Ajo-Franklin, J. B. (2017b). Distributed Acoustic Sensing for Seismic Monitoring of The Near Surface: A Traffic-Noise Interferometry Case Study. *Scientific Reports 2017 7:1*, 7(1), 1–12. <https://doi.org/10.1038/s41598-017-11986-4>
- Draebing, D. (2016). Application of refraction seismics in alpine permafrost studies: A review. In *Earth-Science Reviews* (Vol. 155, pp. 136–152). Elsevier B.V. <https://doi.org/10.1016/j.earscirev.2016.02.006>
- Everett, M. E. (2013). Near-Surface Applied Geophysics. *Near-Surface Applied Geophysics*, 1–399. <https://doi.org/10.1017/CBO9781139088435>
- Farina, B., Poletto, F., Mendrinós, D., Carcione, J. M., & Karytsas, C. (2019). Seismic properties in conductive and convective hot and super-hot geothermal systems. *Geothermics*, 82, 16–33. <https://doi.org/10.1016/J.GEOTHERMICS.2019.05.005>
- Fernández-Martínez, J. L., Xu, S., Sirieix, C., Fernández-Muniz, Z., & Riss, J. (2017). Uncertainty analysis and probabilistic segmentation of electrical resistivity images: the 2D inverse problem. *Geophysical Prospecting*, 65, 112–130. <https://doi.org/10.1111/1365-2478.12559>
- Feroci, M., Orlando, L., Balia, R., Bosman, C., Cardarelli, E., & Deidda, G. (2000). Some considerations on shallow seismic reflection surveys q. In *Journal of Applied Geophysics* (Vol. 45). www.elsevier.nl/locate/jappgeo
- Foti, S., Sambuelli, L., Socco, V. L., & Strobbia, C. (2003). Experiments of joint acquisition of seismic refraction and surface wave data. *Near Surface Geophysics*, 1(3), 119–129. <https://doi.org/10.3997/1873-0604.2003002>

- Fournier, A., Mosegaard, K., Omre, H., Sambridge, M., & Tenorio, L. (2013). Assessing uncertainty in geophysical problems — Introduction. *Http://Dx.Doi.Org/10.1190/Geo2013-0425-SPSEIN.1*, 78(3). <https://doi.org/10.1190/GEO2013-0425-SPSEIN.1>
- Glazer, M., Dobiński, W., Marciniak, A., Majdański, M., & Błaszczuk, M. (2020). Spatial distribution and controls of permafrost development in non-glacial Arctic catchment over the Holocene, Fuglebekken, SW Spitsbergen. *Geomorphology*, 358. <https://doi.org/10.1016/j.geomorph.2020.107128>
- Hammock, C. P., Kulesa, B., Hiemstra, J. F., Hodson, A. J., & Hubbard, A. (2022). Seismic and Electrical Geophysical Characterization of an Incipient Coastal Open-System Pingo: Lagoon Pingo, Svalbard. *Earth and Space Science*, 9(3). <https://doi.org/10.1029/2021ea002093>
- Hilbich, C. (2010). Time-lapse refraction seismic tomography for the detection of ground ice degradation. *Cryosphere*, 4(3), 243–259. <https://doi.org/10.5194/tc-4-243-2010>
- Hobro, J. W. D., Singh, S. C., & Minshull, T. A. (2003). Three-dimensional tomographic inversion of combined reflection and refraction seismic traveltimes data. In *Geophys. J. Int* (Vol. 152). <https://academic.oup.com/gji/article/152/1/79/704063>
- Hornum, M. T., Betlem, P., & Hodson, A. (2021). Groundwater Flow Through Continuous Permafrost Along Geological Boundary Revealed by Electrical Resistivity Tomography. *Geophysical Research Letters*, 48(14). <https://doi.org/10.1029/2021GL092757>
- Ismet Kanli, A., Tildy, P., Prónay, Z., Pinar, A., & Hermann, L. (2006). Vs30 mapping and soil classification for seismic site effect evaluation in Dinar region, SW Turkey. *Geophysical Journal International*, 165(1), 223–235. <https://doi.org/10.1111/J.1365-246X.2006.02882.X/3/165-1-223-FIG016.JPEG>
- Justice, J. H., & Zubaj, C. (1986). Transition zone reflections and permafrost analysis. In *GEOPHYSICS* (Vol. 51, Issue 5). <http://library.seg.org/>
- Kasprzak, M. (2015). High-resolution electrical resistivity tomography applied to patterned ground, Wedel Jarlsberg Land, south-west Spitsbergen. *Polar Research*, 34(2015). <https://doi.org/10.3402/polar.v34.25678>
- Kaushik, H., Ramanathan, A., Soheb, M., Shamurailatpam, M. S., Biswal, K., Mandal, A., & Singh, C. (2021). Climate change-induced high-altitude lake: Hydrochemistry and area changes of a moraine-dammed lake in Leh-Ladakh. *Acta Geophysica*, 69(6), 2377–2391. <https://doi.org/10.1007/s11600-021-00670-x>
- Kneisel, C., Hauck, C., Fortier, R., & Moorman, B. (2008). Advances in geophysical methods for permafrost investigations. In *Permafrost and Periglacial Processes* (Vol. 19, Issue 2, pp. 157–178). <https://doi.org/10.1002/ppp.616>
- Krawczyk, C. M., Polom, U., Trabs, S., & Dahm, T. (2012). Sinkholes in the city of Hamburg-New urban shear-wave reflection seismic system enables high-resolution imaging of subsurface structures. *Journal of Applied Geophysics*, 78, 133–143. <https://doi.org/10.1016/j.jappgeo.2011.02.003>
- Leroux, V., & Dahlin, T. (2006). Time-lapse resistivity investigations for imaging saltwater transport in glaciofluvial deposits. *Environmental Geology*, 49(3), 347–358. <https://doi.org/10.1007/s00254-005-0070-7>

- Lindner, L., Marks, L., & Szczęsny, R. (1992). Quaternary landforms, sediments and morphogenetic evolution of Hansbreen-Sofiekammen region, Wedel Jarlsberg Land, Spitsbergen. *Polish Polar Research*, 13(2), 91–101.
- Lococo, J., Co, D., Stowell, J., & Sopris, M. (2021). Evolution and application of slimhole borehole geophysical logs over the last 50 years. *Symposium on the Application of Geophysics to Engineering and Environmental Problems*, 137–139. <https://doi.org/10.4133/SAGEEP.33-071>
- Majdański, M., Trzeciak, M., Gaczyński, E., & Maksym, A. (2016). Seismic velocity estimation from post-critical wide-angle reflections in layered structures. *Studia Geophysica et Geodaetica*, 60(3), 565–582. <https://doi.org/10.1007/s11200-015-1268-0>
- Majdański, M., Dobiński, W., Marciniak, A., Owoc, B., Glazer, M., Osuch, M., & Wawrzyniak, T. (2022). Variations of permafrost under freezing and thawing conditions in the coastal catchment Fuglebekken (Hornsund, Spitsbergen, Svalbard). *Permafrost and Periglacial Processes*. <https://doi.org/10.1002/ppp.2147>
- Malinverno, A., & Briggs, V. A. (2004). Expanded uncertainty quantification in inverse problems: Hierarchical Bayes and empirical Bayes. *Geophysics*, 69(4), 1005–1016. <https://doi.org/10.1190/1.1778243>
- Marciniak, A., Stan-Kłeczek, I., Idziak, A., & Majdański, M. (2019). Uncertainty based multi-step seismic analysis for near-surface imaging. *Open Geosciences*, 11(1), 727–737. <https://doi.org/10.1515/geo-2019-0057>
- Marciniak, A., Kowalczyk, S., Gontar, T., Owoc, B., Nawrot, A., Luks, B., Cader, J., & Majdański, M. (2021). Integrated geophysical imaging of a mountain landslide – A case study from the Outer Carpathians, Poland. *Journal of Applied Geophysics*, 191. <https://doi.org/10.1016/j.jappgeo.2021.104364>
- Marciniak, A., Osuch, M., Wawrzyniak, T., Owoc, B., Dobiński, W., Glazer, M., & Majdański, M. (2022). Multi-method geophysical mapping of ground properties and periglacial geomorphology in Hans Glacier forefield, SW Spitsbergen. *Polish Polar Research*, 43(2), 101–123. <https://doi.org/10.24425/ppr.2022.140363>
- Matsuura, S., Okamoto, T., Osawa, H., Shibasaki, T., Abe, K., & Okada, Y. (2014). Fluctuations in the pore-water pressure of a reactivated landslide in a Snowy district. In *Landslide Science for a Safer Geoenvironment: Volume 3: Targeted Landslides* (pp. 499–502). Springer International Publishing. https://doi.org/10.1007/978-3-319-04996-0_76
- Maurer, H., & Hauck, C. (2007). Instruments and Methods Geophysical imaging of alpine rock glaciers. *Journal of Glaciology*, 53(180), 110–120. <http://www.abem.se/>
- Mieszkowska, N. (2021). Intertidal indicators of climate and global change. *Climate Change: Observed Impacts on Planet Earth, Third Edition*, 465–482. <https://doi.org/10.1016/B978-0-12-821575-3.00022-0>
- Niitsuma, H., Fehler, M., Jones, R., Wilson, S., Albright, J., Green, A., Baria, R., Hayashi, K., Kaieda, H., Tezuka, K., Jupe, A., Wallroth, T., Cornet, F., Asanuma, H., Moriya, H., Nagano, K., Phillips, W. S., Rutledge, J., House, L., ... Aster, R. (1999). Current status of seismic and borehole measurements for HDR/HWR development. *Geothermics*, 28(4–5), 475–490. [https://doi.org/10.1016/S0375-6505\(99\)00024-3](https://doi.org/10.1016/S0375-6505(99)00024-3)

- O'Neill, A., Dentith, M., & List, R. (2003). Full-waveform P-SV reflectivity inversion of surface waves for shallow engineering applications. In *Exploration Geophysics* (Vol. 34).
- Osuch, M., & Wawrzyniak, T. (2017). Inter- and intra-annual changes in air temperature and precipitation in western Spitsbergen. *International Journal of Climatology*, 37(7), 3082–3097. <https://doi.org/10.1002/joc.4901>
- Owoc, B., Marciniak, A., Dzierżek, J., Kowalczyk, S., & Majdański, M. (2019). Seismic imaging of the mesozoic bedrock relief and geological structure under quaternary sediment cover: The bolmin syncline (SW holy cross mountains, Poland). *Geosciences (Switzerland)*, 9(10). <https://doi.org/10.3390/geosciences9100447>
- Park, C. B., Miller, R. D., & Xia, J. (1999). Multichannel analysis of surface waves. *Geophysics*, 64(3), 800–808. <https://doi.org/10.1190/1.1444590>
- Park, C. B., & Miller, R. D. (2008). Roadside passive multichannel analysis of surface waves (MASW). *Journal of Environmental & Engineering Geophysics*, 13(1), 1–11. <https://doi.org/10.2113/jeeeg13.1.1>
- Park, Y. H., Doh, S. J., & Yun, S. T. (2007). Geoelectric resistivity sounding of riverside alluvial aquifer in an agricultural area at Buyeo, Geum River watershed, Korea: An application to groundwater contamination study. *Environmental Geology*, 53(4), 849–859. <https://doi.org/10.1007/s00254-007-0698-6>
- Parker, T., Shatalin, S., & Farhadiroushan, M. (2014). Distributed acoustic sensing – a new tool for seismic applications, Normal access. *First Break*, 32(2), 61–69. <https://doi.org/10.3997/1365-2397.2013034>
- Philips Aizebeokhai, A. (2010). 2D and 3D geoelectrical resistivity imaging: Theory and field design. *Scientific Research and Essays*, 5(23), 3592–3605. <http://www.academicjournals.org/SRE>
- Poletto, F., Farina, B., & Carcione, J. M. (2018). Sensitivity of seismic properties to temperature variations in a geothermal reservoir. *Geothermics*, 76, 149–163. <https://doi.org/10.1016/j.geothermics.2018.07.001>
- Revil, A., & Glover, P. W. J. (1998). Nature of surface electrical conductivity in natural sands, sandstones, and clays. *Geophysical Research Letters*, 25(5), 691–694. <https://doi.org/10.1029/98GL00296>
- Reygondeau, G. (2019). Current and future biogeography of exploited marine exploited groups under climate change. *Predicting Future Oceans: Sustainability of Ocean and Human Systems Amidst Global Environmental Change*, 87–101. <https://doi.org/10.1016/B978-0-12-817945-1.00009-5>
- Rossi, G., Accaino, F., Boaga, J., Petronio, L., Romeo, R., & Wheeler, W. (2018). Seismic survey on an open pingo system in Adventdalen Valley, Spitsbergen, Svalbard. In *Near Surface Geophysics* (Vol. 16, Issue 1, pp. 89–103). EAGE Publishing BV. <https://doi.org/10.3997/1873-0604.2017037>
- Routh, P. S. (2008). Resolution and uncertainty in geophysical inverse problem: A practical approach. *SEG Technical Program Expanded Abstracts*, 27(1), 3577. <https://doi.org/10.1190/1.3064070>

- Samouëlian, A., Cousin, I., Tabbagh, A., Bruand, A., & Richard, G. (2005). Electrical resistivity survey in soil science: A review. In *Soil and Tillage Research* (Vol. 83, Issue 2, pp. 173–193). <https://doi.org/10.1016/j.still.2004.10.004>
- Sausse, J., Dezayes, C., Dorbath, L., Genter, A., & Place, J. (2010). 3D model of fracture zones at Soultz-sous-Forêts based on geological data, image logs, induced microseismicity and vertical seismic profiles. *Comptes Rendus - Geoscience*, 342(7–8), 531–545. <https://doi.org/10.1016/j.crte.2010.01.011>
- Socco, L. V., Foti, S., & Boiero, D. (2010). Surface-wave analysis for building near-surface velocity models - Established approaches and new perspectives. *Geophysics*, 75(5), 75A83-75A102. <https://doi.org/10.1190/1.3479491>
- Tompkins, M. J., Fernández Martínez, J. L., Alumbaugh, D. L., & Mukerji, T. (2011). Scalable uncertainty estimation for nonlinear inverse problems using parameter reduction, constraint mapping, and geometric sampling: Marine controlled-source electromagnetic examples. *Geophysics*, 76(4). <https://doi.org/10.1190/1.3581355>
- Uhlemann, S., Dafflon, B., Wainwright, H. M., Williams, K. H., Minsley, B., Zamudio, K., Carr, B., Falco, N., Ulrich, C., & Hubbard, S. (2022). Surface parameters and bedrock properties covary across a mountainous watershed: Insights from machine learning and geophysics. *Science Advances*, 8(12). <https://doi.org/10.1126/sciadv.abj2479>
- Ullemeyer, K., Siegesmund, S., Rasolofosaon, P. N. J., & Behrmann, J. H. (2006). Experimental and texture-derived P-wave anisotropy of principal rocks from the TRANSALP traverse: An aid for the interpretation of seismic field data. *Tectonophysics*, 414(1–4), 97–116. <https://doi.org/10.1016/j.tecto.2005.10.024>
- van der Baan, M., & Jutten, C. (2012). Neural networks in geophysical applications. <https://doi.org/10.1190/1.1444797>, 65(4), 1032–1047. <https://doi.org/10.1190/1.1444797>
- Virieux, J., & Operto, S. (2009). An overview of full-waveform inversion in exploration geophysics. *Geophysics*, 74(6). <https://doi.org/10.1190/1.3238367>
- Wan, S., Chang, S. H., Chou, T. Y., & Shien, C. M. (2018). A Study of Landslide Image Classification through Data Clustering using Bacterial Foraging Optimization. *Journal of Chinese Soil and Water Conservation*, 49(3), 187–198. [https://doi.org/10.29417/JCSWC.201809_49\(3\).0006](https://doi.org/10.29417/JCSWC.201809_49(3).0006)
- Warner, M., Ratcliffe, A., Nangoo, T., Morgan, J., Umpleby, A., Shah, N., Vinje, V., Štekl, I., Guasch, L., Win, C., Conroy, G., & Bertrand, A. (2013). Anisotropic 3D full-waveform inversion. *Geophysics*, 78(2). <https://doi.org/10.1190/GEO2012-0338.1>
- Wawrzyniak, T., Osuch, M., Napiórkowski, J., & Westermann, S. (2016). Modelling of the thermal regime of permafrost during 1990-2014 in Hornsund, Svalbard. *Polish Polar Research*, 37(2), 219–242. <https://doi.org/10.1515/popore-2016-0013>
- Wawrzyniak, T., & Osuch, M. (2020). A 40-year High Arctic climatological dataset of the Polish Polar Station Hornsund (SW Spitsbergen, Svalbard). *Earth System Science Data*, 12(2), 805–815. <https://doi.org/10.5194/essd-12-805-2020>
- Wu, Y., Nakagawa, S., Kneafsey, T. J., Dafflon, B., & Hubbard, S. (2017). Electrical and seismic response of saline permafrost soil during freeze - Thaw transition. *Journal of Applied Geophysics*, 146, 16–26. <https://doi.org/10.1016/j.jappgeo.2017.08.008>

- Xia, J., Miller, R. D., & Park, C. B. (1999). Estimation of near-surface shear-wave velocity by inversion of Rayleigh waves. *Geophysics*, 64(3), 691–700. <https://doi.org/10.1190/1.1444578>
- Xiujun, G., Xiaoyu, H., & Yonggang, J. (2005). Forward Modeling of Different Types of Landslides with Multi-electrode Electric Method*. In *APPLIED GEOPHYSICS* (Vol. 2, Issue I).
- Zhao, W., Forte, E., Colucci, R. R., & Pipan, M. (2016). High-resolution glacier imaging and characterization by means of GPR attribute analysis. *Geophysical Journal International*, 206(2), 1366–1374. <https://doi.org/10.1093/gji/ggw208>

List of the papers

This thesis is based on the following papers:

- I. **Marciniak, A.**, Stan-Kłeczek, I., Idziak, A., & Majdański, M. (2019). Uncertainty based multi-step seismic analysis for near-surface imaging. *Open Geosciences*, 11(1), 727–737. <https://doi.org/10.1515/geo-2019-0057>
- II. Owoc, B., **Marciniak, A.**, Dzierżek, J., Kowalczyk, S., & Majdański, M. (2019). Seismic Imaging of the Mesozoic Bedrock Relief and Geological Structure under Quaternary Sediment Cover: The Bolmin Syncline (SW Holy Cross Mountains, Poland). *Geosciences (Switzerland)*, 9(10). <https://doi.org/10.3390/geosciences9100447>
- III. Glazer, M., Dobiński, W., **Marciniak, A.**, Majdański, M., & Błaszczuk, M. (2020). Spatial distribution and controls of permafrost development in non-glacial Arctic catchment over the Holocene, Fuglebekken, SW Spitsbergen. *Geomorphology*, 358. <https://doi.org/10.1016/j.geomorph.2020.107128>
- IV. Majdański, M., Dobiński, W., **Marciniak, A.**, Owoc, B., Glazer, M., Osuch, M., & Wawrzyniak, T. (2022). Variations of permafrost under freezing and thawing conditions in the coastal catchment Fuglebekken (Hornsund, Spitsbergen, Svalbard). *Permafrost and Periglacial Processes*. <https://doi.org/10.1002/ppp.2147>
- V. **Marciniak, A.**, Osuch, M., Wawrzyniak, T., Owoc, B., Dobiński, W., Glazer, M., & Majdański, M. (2022). Multi-method geophysical mapping of ground properties and periglacial geomorphology in Hans Glacier forefield, SW Spitsbergen. *Polish Polar Research*, 43(2), 101–123. <https://doi.org/10.24425/ppr.2022.140363>
- VI. **Marciniak, A.**, Kowalczyk, S., Gontar, T., Owoc, B., Nawrot, A., Luks, B., Cader, J., & Majdański, M. (2021). Integrated geophysical imaging of a mountain landslide – A case study from the Outer Carpathians, Poland. *Journal of Applied Geophysics*, 191. <https://doi.org/10.1016/j.jappgeo.2021.104364>

The original publisher versions of the papers are included in the Reprint chapter of the thesis.

Author contribution statements are attached at the end of the thesis.

Other contributions

During my MSc and PhD studies, I also contributed to the following extended abstracts, not included in this thesis as well as scientific projects:

Articles

- I. Stan-Kłeczek, I., & **Marciniak, A.** (2016). Zastosowanie MASW i sejsmiki refrakcyjnej do badania anizotropii prędkości w masywie skalnym. *Zeszyty Naukowe Instytutu Gospodarki Surowcami Mineralnymi i Energią PAN*, (93), 123-131.
- II. Stan-Kłeczek, I., Pierwoła, J., **Marciniak, A.**, Sutkowska, K., & Tomaszewska, R. (2022). Multimethod geophysical investigation in karst areas: case studies from Silesia, Poland. *Bulletin of Engineering Geology and the Environment*, 81(6), 1-16.

Extended Abstracts

- I. **Marciniak, A.**, Stan-Kłeczek, I., Idziak, A., & Majdański, M. (2018). Uncertainty Based Multi-Step Seismic Analysis for the Near Surface Imaging. *24th European Meeting of Environmental and Engineering Geophysics*, 2018(1), 1–5. <https://doi.org/10.3997/2214-4609.201802562>
- II. **Marciniak, A.**, Kowalczyk, S., Gontar, T., Owoc, B., & Majdański, M. (2019). Multimethod High-Resolution Geophysical Imaging of Landslides in Mountain Area-A Case Study from Cisiec, Poland. In *25th European Meeting of Environmental and Engineering Geophysics* (Vol. 2019, No. 1, pp. 1-5). European Association of Geoscientists & Engineers.
- III. **Marciniak, A.**, Owoc, B., Wawrzyniak, T., Nawrot, A., Glazer, M., Osuch, M., & Majdański, M. (2019). Near-Surface Geophysical Imaging of the Permafrost—Initial Result of Two High Arctic Expeditions to Spitsbergen. In *25th European Meeting of Environmental and Engineering Geophysics* (Vol. 2019, No. 1, pp. 1-5). European Association of Geoscientists & Engineers.
- IV. Owoc, B., **Marciniak, A.**, Kowalczyk, S., Dzierzek, J., & Majdanski, M. (2019). An Optimal Combination of Geophysical Methods to Image Geological Structures. In *25th European Meeting of Environmental and Engineering Geophysics* (Vol. 2019, No. 1, pp. 1-5). European Association of Geoscientists & Engineers.

Scientific Projects

- I. **Principal Investigator Artur Marciniak**, Supervisor prof. Mariusz Majdański - Preludium 19 from NCN No. UMO-2020/37/N/ST10/01486, "Anthropogenic triggering of landslides in the environment modified due to climate change - geophysical investigation"
- II. Principal Investigator Mariusz Majdański, **Co-investigator Artur Marciniak** - Opus from NCN No. UMO-2016/21/B/ST10/02509, "Relationship of permafrost with geomorphology, geology and cryospheric components based on geophysical research of the Hans glacier forefield and its surroundings. Hornsund, Spitsbergen"
- III. Principal Investigator Mariusz Majdański, **Co-investigator Artur Marciniak** - Opus from NCN No. 2015/19/B/ST10/01833, "Three dimensional model of the lithosphere in Poland with verification of seismic parameters of the wave field"

Acknowledgements

It can be said without any doubt that the defense of a doctoral dissertation is a symbolic and summarizing stage in the career of every scientist. It is a stage that covers not only the research period related to the creation of the dissertation itself but the entirety of the achievements and events that have led to this moment.

During my scientific career, I have encountered several people without whom it would be impossible to achieve this stage. In addition to the immediate family, they were both teachers, colleagues and friends. At this point, I would like to thank quite a large group of people, without whom the creation of this work, as well as the very achievement of the PhD studies, would not be possible.

I would like to start by thanking the two science teachers who initiated my greater involvement in Earth science. At this point, I would like to thank Antoni Motyka and Jacek Seweryn, who taught me successively in middle school and high school and encouraged me to take part in local and regional competitions. Next, I would like to thank the lecturers at the Faculty of Earth Sciences at the University of Silesia (now the Faculty of Natural Sciences) for the knowledge in the field of Geophysics, Geology and Geomorphology provided to me. In particular, I am grateful to dr hab. Iwona Stan-Kłeczek, who was the supervisor of my Bachelor's thesis and with whom I have maintained fruitful scientific cooperation so far. Also, dr Maciej Mendecki, the supervisor of the geophysicists club of the University of Silesia, PREM, as well as Professors Adam Idziak and Wacław Zuberek, had a significant impact on my further scientific career through valuable advice and suggestions, and the kindness shown at the early stage of my scientific career. I also cannot forget about dr hab. Wojciech Dobiński, whom I met for the first time as a student. Currently, I am conducting research on the evolution of permafrost in polar regions, which would be impossible without his invaluable help and valuable suggestions, for which I am grateful.

During my further scientific development at the Institute of Geophysics of the Polish Academy of Sciences, lasting since 2015, first as an apprentice, and then as a graduate student, until my current doctoral studies, I have met many supportive people. I think that every morning would be difficult without coffee with Edward Gaczyński and Monika Bociarska as regulars (but not the only ones) in morning meetings. Then I would like to thank my colleagues, both former and presently working in the Geophysical Imaging Department. They are Marta Czyż, Michał Chamarczuk, Miłosz Mężyk, Andrzej Górszczyk, Wojtek Gajek, Jacek Trojanowski, Brij Singh, Quang Nguyen, dr hab. Mariusz Białecki, and Silvan Magnia with whom I had good contact, and I could ask them for help in case of problems. I would like to express individual thanks to the head of the department, Professor Michał Malinowski, for valuable advice and suggestions, especially regarding grant and research project writing. Additionally, I would like to thank Piotr Środa and Emilia Karamuz for their help, mainly on technical and geodetic aspects during my doctorate. I cannot fail to mention Michał Glazer, Rafał Czarny, and Adam Nawrot with whom I have conducted and are currently conducting research. Then I would like to thank my friends Julia Rewers and Krzysztof Śliwiński who have shown me a lot of support in the last 2 years.

Finally, I would like to mention and thank the people who have had the most significant impact on my scientific path so far and deserve a separate distinction.

I would like to thank my parents, Lucyna and Leszek Marciniak, who encouraged me to learn from an early age and tried to provide me with the best conditions for its implementation. They both spent hundreds, if not thousands of hours from an early age helping me with my lessons or taking me to an additional English language. I am grateful to them for this, especially knowing that I was not always a patient student. I love you very much and I am grateful for your understanding, love and patience.

Then I would like to thank my beloved, more beautiful half, Justyna Cader, who, as a scientist, supports me in my work and has shown a lot of persistence since 2015, which is, after all, not an easy task. Without her, my life would not be as happy as it is today.

I would also like to thank the scientific duo, Marzena Osuch and Tomasz Wawrzyniak, from whom I have learned a lot in the field of effective research paper writing, scientific integrity and diligence. I cannot ignore my colleague from the department with whom I shared my room at the Institute and worked on research projects, namely Bartosz Owoc. Without his advice, work and suggestions, the implementation of grants and projects on which we worked together would not be possible. I am especially grateful for the support that has been shown to me so far, mainly from 2020.

Finally, it is important to mention the person who has had the greatest and most direct impact on the last 7 years of my scientific output and who supervised my Master's thesis and PhD dissertation presented here, dr hab. Mariusz Majdański. I am especially grateful to him for his very fruitful cooperation, valuable advice on my research career, and also for his understanding and patience. I think that an interesting coincidence ultimately contributed to the implementation of my doctoral dissertation. My scientific career in the full sense began with an interview in 2014 when as a student, I visited the IGF PAS. I had an almost 2-hour conversation with a young habilitated doctor who encouraged me to start an internship at Institute.

Finally, I cannot refer to the event at the beginning of 2020 that had a significant impact on my life, namely an unfortunate accident during a ski competition. Many employees of the Institute supported me and still support my further recovery. Since I have never had the opportunity to personally thank them for their support, I will do so by dedicating this doctoral dissertation to the employees and doctoral students of the Institute of Geophysics of the Polish Academy of Sciences.

Once again, I would like to thank you for the support you have shown me, for which I thank you with all my heart.

Reprints

Paper I:

Marciniak, A., Stan-Kłeczek, I., Idziak, A., & Majdański, M. (2019). Uncertainty based multi-step seismic analysis for near-surface imaging. *Open Geosciences*, 11(1), 727–737. <https://doi.org/10.1515/geo-2019-0057>



Research Article

Artur Marciniak*, Iwona Stan-Kłeczek, Adam Idziak, and Mariusz Majdański

Uncertainty based multi-step seismic analysis for near-surface imaging

<https://doi.org/10.1515/geo-2019-0057>

Received Oct 17, 2018; accepted Mar 27, 2019

Abstract: Near-surface seismic surveys are often designed for surface wave and seismic tomographic analysis. In recent years, seismic imaging methods have been more frequently used at this scale. Recognition of near-surface structures using a single method is insufficient because of the ambiguity of the inversion problem. As a solution, the authors propose a multi-step approach, where several different seismic methods are used in a particular order, to achieve an optimal model. A multi-method approach allows utilisation of a whole spectrum of recorded data, even the elements that are treated as background noise in other techniques. In classical processing approach, information about data uncertainty is often omitted or used in the simplest way for the single method only. This work presents an updated approach to uncertainty analysis by transferring estimated uncertainty between processing steps. By assuming that every consecutively applied method is more certain, the authors were able to obtain accurate velocity fields for seismic imaging, as the main information received from the previous steps. Based on information from multiple methods, a seismic stack in the depth domain was created as a final result, with an estimate of uncertainty.

Keywords: MASW, Seismic Imaging, Seismic Tomography, Uncertainty

1 Introduction

Imaging of near-surface structures is often performed rapidly using a single method. In most commercial applications, this comprises the analysis of surface wave dispersion curves (MASW) [1], or first breaks travel time tomography alone. The inversion of seismic data in the near-surface is a problem and is a non-unique procedure, without other geophysical measurements [2–9]. To limit this shortcoming, it is possible to use more data or to use interpretation techniques that utilise the whole of the recorded data [10–19]. These techniques have different resolution capabilities. One interpretation method is to focus on the most precise technique for a given problem. We are convinced that a combination of several techniques will result in better recovery of data for a studied structure, but it is necessary to understand the limitations of the techniques used, especially its uncertainty [20, 21]. Here, using simple field data, we present a complex approach to combine three seismic methods in a strict uncertainty guided procedure, in order to interpret near-surface structure. The results obtained are optimally fitted to the given data and are presented with the uncertainty analysis at each processing step.

2 Motivation

Near-surface geophysical studies have to be simple and cost-effective. In most cases, studied geological structures are rather simple. Our motivation for this work is to develop a simple but effective method that will use shallow seismic data more completely (Figure 1). The application of similar procedures to those used for deep experiments [22, 23] but in a simplified form, would allow us to overcome multiple processing problems and obtain a final result with an estimated uncertainty. The use of additional analyses which are effective in near-surface studies (e.g. MASW), will provide additional information for the correct interpretation of the subsurface.

*Corresponding Author: Artur Marciniak: Institute of Geophysics, Polish Academy of Sciences, Poland; Email: amarciniak@igf.edu.pl; Tel.: +22-6915-905; ORCID ID: 0000-0003-1715-0956

Iwona Stan-Kłeczek, Adam Idziak: University of Silesia in Katowice, Faculty of Natural Sciences, Institute of Earth Sciences, Sosnowiec

Mariusz Majdański: Institute of Geophysics, Polish Academy of Sciences, Poland

Open Access. © 2019 A. Marciniak et al., published by De Gruyter.



This work is licensed under the Creative Commons Attribution

4.0 License

Unauthenticated
Download Date | 12/13/19 11:49 AM

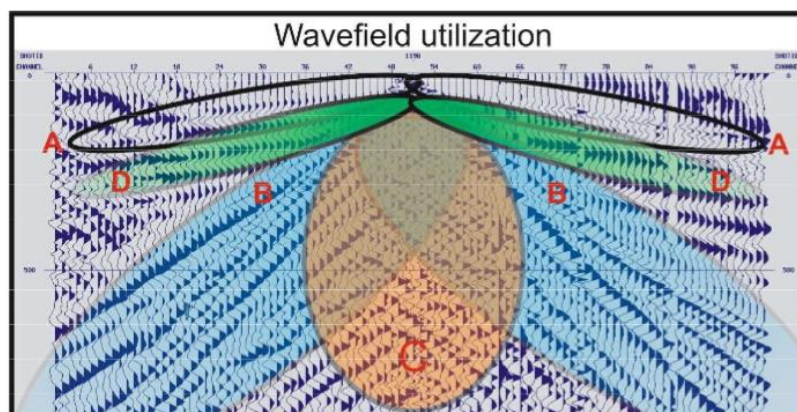


Figure 1: Example of real data with specified different types of seismic waves. The utilisation of Refracted Waves (A), Surface Waves (B), Reflected Waves (C) and wide-angle Reflected Waves (D) increases the certainty of the final result.

3 Geology

Data acquisition in this case study was conducted at the test site of the Central Geophysical Observatory in Poland. The geology of the region consists of thick Quaternary sediments (definitely thicker than 100 m), which are post-glacial and were created in the Pleistocene. According to the Central Geological Database (<http://bazagis.pgi.gov.pl>), in the vicinity of the test site, three shallow boreholes were drilled. All of them show quaternary deposits (Mała Wieś borehole 97.8m depth, Belsk 1/6 borehole 15m depth, Pgr Stara Wieś borehole 53m depth). Under the Cainozoic deposits, the Maastrichtian deposits are present [24]. However simple, the geology of the research area is difficult for the near-surface seismic methods because of the high wave attenuation. The well-mixed post-glacial sediments, with small velocity differences, are characterised by the small reflection coefficient differences between the layers. For that reason, the proposed research area is well suited as a test site for the proposed approach to data processing, that will be mainly applied in similar geological conditions. The most interesting geological boundary between Cainozoic and Mesozoic is lying on the depth that exceeds the penetration range of the author's seismic equipment.

4 Fieldwork

During fieldwork, a 400 m seismic line (Figure 2) covered by 100 stations (60 Data-Cube type (light-blue pointer) and 40 Reftek 130 (orange pointer) 4.5 Hz type receivers (Table 1) was set. The spacing between geophones was 4 m (Figure 2). As a seismic source, the authors used a car-mounted PEG 40 accelerated weight drop in the shooting scheme, assuming signal excitation between geophones (Figure 2 blue stars). Terrain coverage in the fieldwork area changed with distance from the east side of the profile to the forest zone in the west. Because of this, the application of a car-mounted PEG 40 accelerated hammer provided the best possible signal to noise (S/N) ratio for the first 332 m of the profile, while the rest of the shots were executed with a sledgehammer (Figure 2 white stars). At every shot point, a total of six signal excitations was conducted for further vertical stacking. This was an unconventional data acquisition system for a geoenvironmental purpose (with a single channel, stand-alone stations) and required very careful time measurement for the duration of the experiment. The timing device used was based on a GPS and allowed us to measure each source with a precision better than 2 ms. Because of negligible elevation changes of less than 1m, geodesy measurements were not needed.

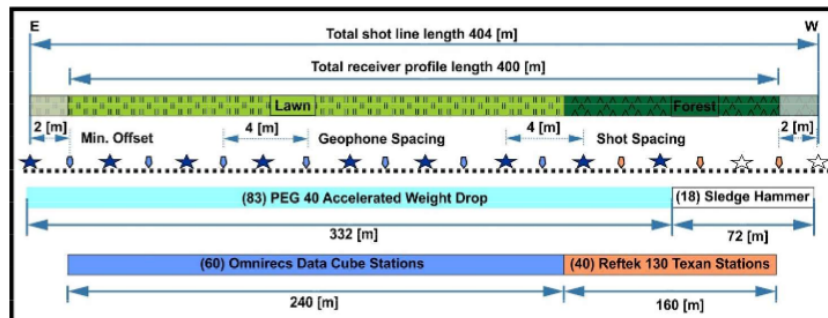


Figure 2: The geometry of acquisition profile from project GPB Belsk. The total range of 400 m long line was regularly covered with 100 seismic stations. Sources were regularly spaced at 4 m intervals. After 300 m along the profile, the application of a car-mounted, accelerated weight drop was impossible due to rough terrain. The last 72 m of the acquisition line was shot by sledgehammer.

Table 1: Acquisition parameters for the GPB seismic line.

| Parameter | Value |
|-------------------|---------|
| Vertical Stack | 6 |
| Sampling interval | 2.5 ms |
| Record length | 2 s |
| Receivers | 4.5 Hz |
| Station interval | 4 m |
| Shot interval | 4 m |
| Active channels | 100 |
| Fold | 100 |
| Offset | 0-398 m |

5 MASW data analysis

The application of multi-method, seismic data analysis requires a careful approach to the data quality and an estimation of the uncertainty of the results. Careful quality control was conducted to eliminate errors in the data due to possible timing problems. During that process, some outlier records with time deviations greater than 2 ms, were deleted. The verified data was vertically stacked, with the application of the seismic line geometry. To recover information about the layers nearest to the ground surface, classical MASW analysis was conducted [1, 25–28]. Dispersion curves for 100 regularly spaced shots were obtained and inverted by applying the genetic algorithm [29] (Eiben *et al.* 1994). During the MASW processing procedure, the raw data was filtered using the band-pass filter in the range 3 to 60 Hz. Moreover, automated gain control correction and the manual muting of refraction was applied to im-

prove the S/N ratio. For correct tracing of surface waves, 50 channels for every shot point were selected, as an optimal range where energy was visible. 1D V_s models were merged by kriging interpolation and with the assumption that each location in the 2D profile is determined to be in the centre of the spread of the single shot modelling (Figure 3A). Uncertainty estimation (Figure 3B) for the results obtained was based on a statistical comparison between inversion results. However 1D and 2D uncertainties are not the same [30, 31]. In simple cases, a proposed approximation is sufficient. To achieve 2D V_s uncertainty decay in the subsurface model, a similar kriging interpolation method was applied to the results. In the final model (Figure 3A), the authors were able to recognise a dipping layer, with a high V_s velocity contrast. The results obtained by the MASW method were recalculated to V_p by the genetic algorithm (with corresponding uncertainty information) and used in the seismic tomography stage of processing for further analysis [32]. The MASW modelling results provide useful information about low-velocity zones despite their significant uncertainty. Because classical First Arrival Seismic Tomography is blind to the presence of such structures [33], solving the methodological problem is essential to near-surface research. Moreover, the best possible recognition of the shallowest layers is essential for proper static and residual corrections in seismic reflection imaging. In the presented case study, however, MASW analysis proved that there was no low-velocity zone in the research area.

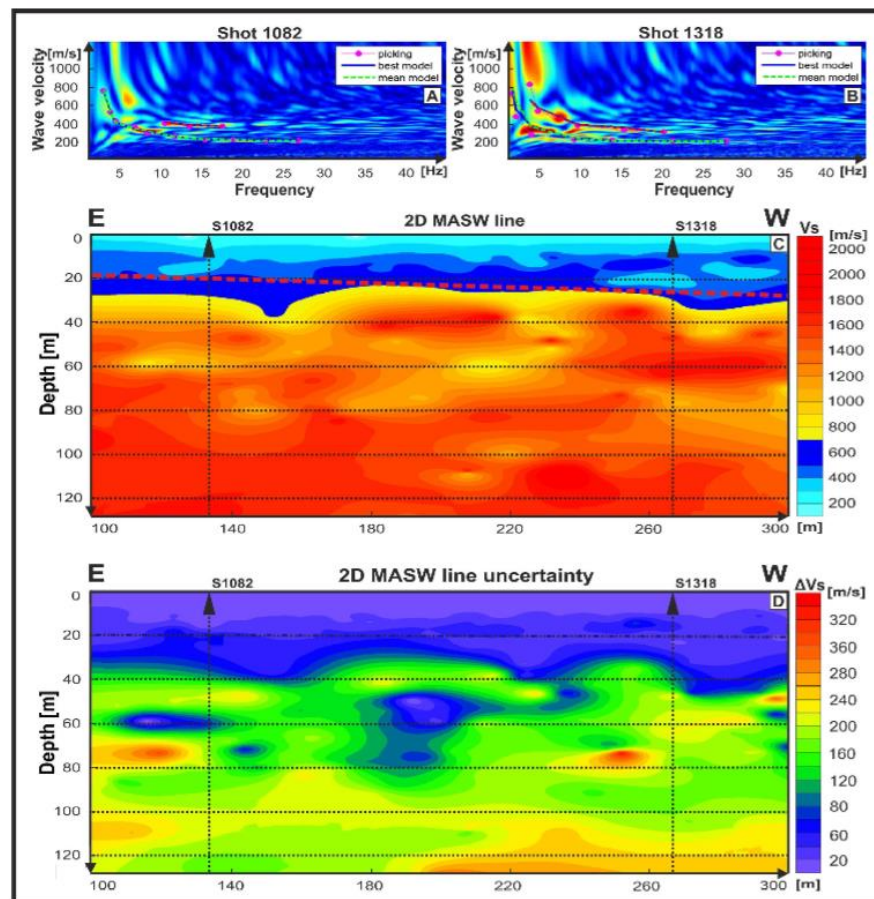


Figure 3: Results of the multichannel analysis of surface waves. To achieve the best possible data utilisation, 101 1D models were created and then interpolated to produce a 2D model (C). For the dataset under consideration: at each shot point, the fundamental and first higher-mode of Rayleigh wave dispersion was visible (A, B). To obtain a 2D model, single 1D models were interpolated. The final 2D model (C) revealed a high-velocity change, visible with a slight dip at 30 m under the surface. Panel (D) presents uncertainty analysis based on the misfit of curves during the inversion process, which revealed a fast degradation of the model precision with depth.

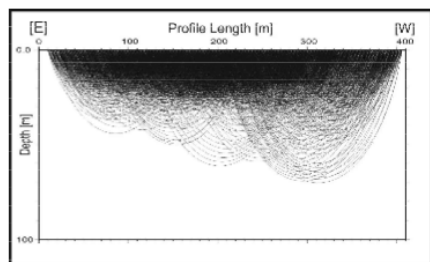


Figure 4: Ray coverage for the last iteration of tomographic inversion. Model is well resolved down to 30 m, and the maximum penetration depth is about 70 m.

6 Seismic travel-time tomography analysis

Application of the MASW method as the first processing procedure, allowed the authors to receive information about the nearest subsurface. However, because of the high levels of uncertainty in the method, particularly the fast degradation of results with depth, the modelling of layers deeper than 20 to 30 m is ineffective in the presented case. Information about uncertainty in the deeper parts of the subsurface can be treated as boundary conditions in a more accurate method. Such approximations are very useful as a priori information to seismic travel time tomography. The results obtained by this method strongly depend on the starting model. This study presents a novel approach to utilising this information. By assuming that deviations in the results received from MASW limit the intervals of possible velocities, the authors created multiple (40 in total) starting models restricted by the results of the surface analysis method. For seismic tomography modelling, the authors used JIVE3D code [34], based on ray approximation. The starting model, based on MASW results, was further smoothed by including additional information about near-surface velocities from shallow refractions. As a result of seismic tomography modelling, the authors received a smooth velocity image, with the ray coverage shown in Figure 4, and statistically estimated the uncertainty (Figure 5) of the results to be similar to the method used by [35] Melendez *et al.* in Tomo3D code.

In the method proposed by [35] Melendez *et al.*, multiple initial models are created and analysed using basic statistics. In this study, the best initial tomography model (obtained from inversion) was randomly modified in the range of uncertainty from previous MASW analysis. As

mentioned above, 40 models were created with different velocities and gradients. For every obtained model, the same inversion path was applied. For all of the results obtained, a mean value (Figure 5A) and standard deviation (Figure 5B) was calculated. The travel-time tomography results obtained show higher accuracy down to a depth of 40 m (Figure 5B) when compared to the MASW method (Figure 3D). Moreover, possible dipping of the layers is also visible in the image (Figure 5A). Information received about horizontal velocities, and the uncertainty of the results was used in the velocity analysis of the seismic imaging, which is the final step of the multi-step seismic analysis. Even though only 70 m of the model were covered by the rays (Figure 4), the deeper velocities were obtained by extrapolation of the velocity field. When compared to seismic tomography, MASW results are more certain between a depth range of 20 to 50 m, with an average difference of 120 m/s. This almost corresponds to a 50% increase in model accuracy for that depth range, assuming that the V_p to V_s ratio is a factor of 1.7. However large this may appear to be, such an approximation for near surface data is effective. Moreover, the combination of results obtained from two different, but connected, physical phenomena increases the reliability of the velocity model. The results obtained from surface wave modelling are more certain in the utmost 10 m, with an estimated uncertainty of 20 m/s of V_s , which is about 35 m/s of V_p assuming the V_p/V_s factor of 1.7.

In comparison, the uncertainty of seismic V_p tomography is much larger (150 m/s) for that part of the model. However, when the results are compared directly, the average V_p velocity recalculated from V_s for the first 10m of the model (with a ratio factor of 1.7) was 680 m/s, where the tomographic velocity average from the first breaks for that area was 750 m/s. If we assume an extreme value of V_p/V_s ratio (of, say, 2.0), with an uncertainty of 35 m/s of V_s , then the results are comparable. For that reason, the authors decided to apply tomographic velocity to the reflection imaging.

7 Seismic imaging

There is a difficulty in applying seismic imaging to shallow results obtained from velocity analysis as in many cases no external data is available and so gathering any information about vertical velocities is problematic. The problem results from the presence of strong surface waves and refractions mixing with observed reflections and, as a result, the S/N ratio is low enough to disturb classical, semblance-

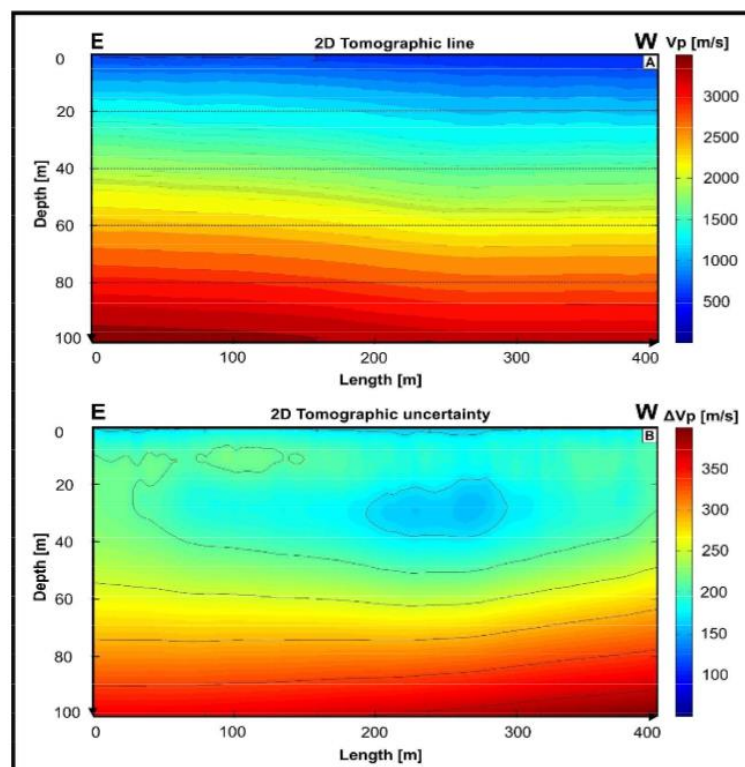


Figure 5: (A), Travel time tomography result, obtained with JIVE3D code, with uncertainty analysis (B) based on a modification of initial model introduced in Tomo3D [35]. Obtained results reveal a smooth gradient of velocity with depth and decrease of velocity towards the west. Uncertainty analysis displays high reliability of received model down to 50 m.

based velocity analysis. In the presented work, the authors used a classical image processing scheme [36] (Table 2).

At every step of the processing, multiple parameter settings were tested. During the data quality control step, multiple “death” traces were removed, and the corrected polarity of the traces was recorded by the Reftek 130 Texan stations. Moreover, panel comparison of vertical stacking algorithms was conducted in order to receive the best possible signal correlation. Because there were two types of receiver station, a geometry database was created manually, to obtain residual and static corrections. To improve the S/N ratio, simple noise suppression based on 1D and 2D F-K filters was conducted, with later deconvolution. In-

stead of applying stand-alone semblance velocity analysis, a smooth tomographic velocity model with estimated uncertainties was used. It is worth noting that the semblance-based analysis applied to the GPB Belsk data-set before adding the information from external methods, was not working properly. In the case of difficult data (e.g. where it was difficult to distinguish between noise and possible reflections), the application of an external velocity field was the only solution in order to obtain useful results. Due to anisotropy, refraction velocities are much faster than stacking ones. In order to fit refraction velocities to the reflection seismic, Dix’ equation [37], and semblance analysis was used for correcting the data fit. As a quality factor of the

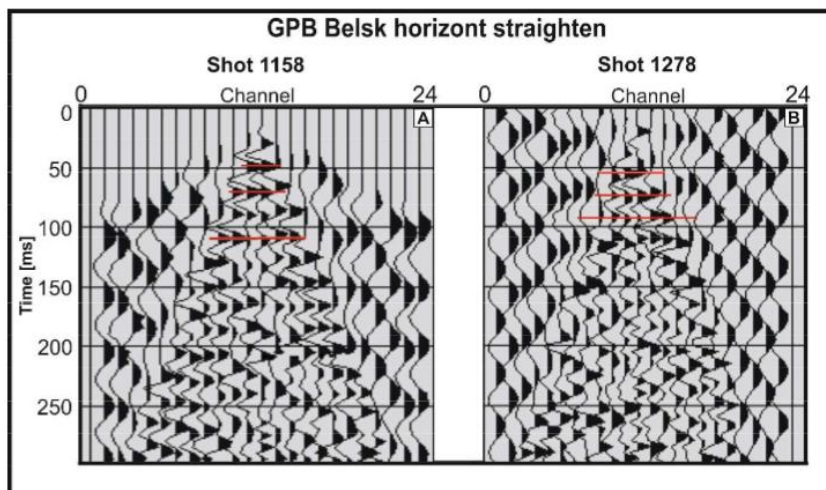


Figure 6: Application of the velocity model received from tomographic modelling to the reflection seismic analysis (NMO), allowing recognition of possible reflectors. Shot gathers in front of the profile (A), and the rear (B) reveal a straightening effect after application of the velocity model, which was impossible to obtain by the classic semblance analysis method.

Table 2: Steps of data imaging.

| Nr. | Processing Step |
|-----|---------------------------------|
| 1 | Data quality control |
| 2 | Vertical Stacking |
| 3 | Geometry building |
| 4 | Static corrections |
| 5 | Data filtering and gain control |
| 6 | Deconvolution |
| 7 | NMO with tomographic velocity |
| 8 | Horizontal stacking |
| 9 | Depth conversion |

velocity field, horizontal straightening was observed and analysed. The best results received from the depth-based, estimated velocity field (Table 3) presented a visible NMO correction (Figure 6).

Next, to the main velocity model, two disturbed velocity fields (faster and slower) were calculated, based on tomographic uncertainty. After applying an identical fitting procedure for all velocity fields, horizontal stacking, post-stack F-K filtering, deconvolution and time to depth conversion were carried out. As a result, the authors received the main seismic stack (Figure 5A) with two other deviation-

based results. Comparison between images and manual picking of selected reflecting horizons, allowed us to estimate the difference in depth of the given reflections (Figure 7B). The authors were able to distinguish the main reflectors in the structure and estimate the uncertainty of those horizons in the depth domain (Figure 7A). Application of the tomographic velocity field, not only allowed the authors to solve the problem of correct velocity field estimation, but also resulted in additional information about results uncertainty in the depth domain that could easily be related to the real rock structures. In comparison with the classical approach to velocity analysis for NMO and TTD migration, the approach presented here allowed for fast recognition of the velocity field. However, only extrapolated values from the tomographic field were used for imaging depths greater than 50 m because it was properly recognised that the shallow subsurface allowed for correct correlations of the velocity field with possible reflectors at greater depths.

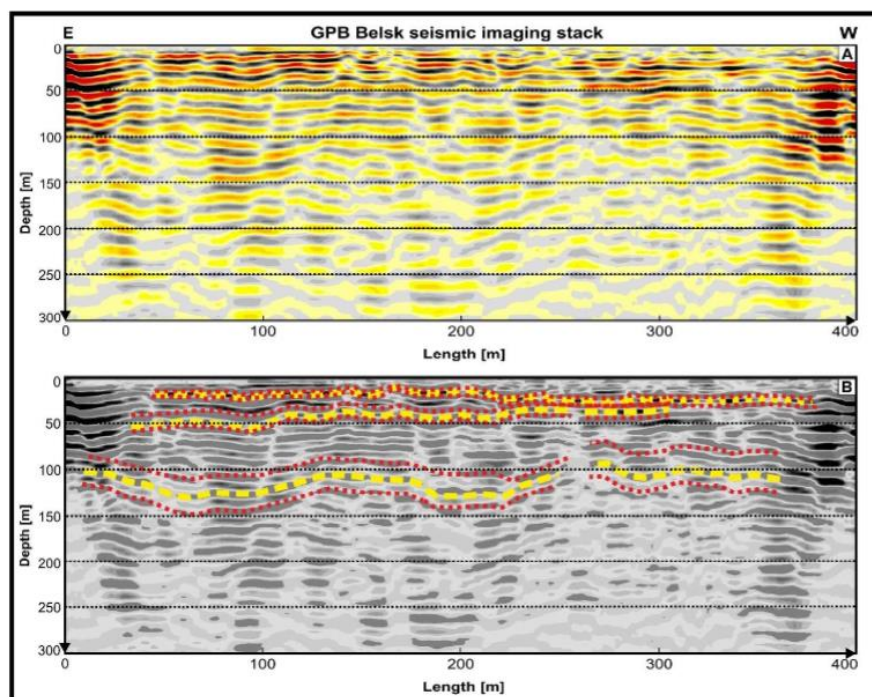


Figure 7: (A) Seismic stack obtained after data imaging of the GPB Belsk profile. Application of the velocity model received from external methods allowed correct stacking of the data, which is visible for the shallow structures, down to 50 m depth. Since tomographic methods allow for uncertainty estimation, stacks with extreme models allowed us to estimate the uncertainty of recognised reflectors (B).

8 Discussion of the results

In comparison to the standard processing flow that uses only a single data type, the methodology presented in this paper provides a better and more complete result. The main idea of every data assimilation procedure is to utilise every bit of additional information. This in all cases will lead to increases in the final result quality. As proved in the article [22], propagation of uncertainty between methods allows obtaining detailed information about the in-depth structures, even for difficult sub-salt structures. Even in the industrial seismic profiling, where both high-resolution data, and geophysical information from borehole soundings are available, estimation of the results uncertainty is extremely useful for a correct correlation of the geophysical and geological information. The migration of

the information between methods allows tightening the possible space of solutions and limits the interpretation errors. However, in the near-surface experiments, obtaining a certain geological model of the subsurface is more complicated.

In most cases, shallow experiments are conducted in places where no geophysical (e.g. VSP profiling) or geological information from boreholes is available. Even if they exist, in most cases usability of such data is limited to the final geological interpretation of the upper-most part of the seismic image. Moreover, the biggest problem with the estimation of the velocity field for seismic migration is unresolved. Adding the fact, that due to the scale of survey targets, all topographic and residual shifts have a much higher impact on the final result, the situation seems to be unresolvable. The methodology presented in work is

Table 3: Example of stacking velocities from the centre of the profile.

| Time [s] | Tomographic velocity [km/s] | Reflection velocity [km/s] | % of velocity |
|----------|-----------------------------|----------------------------|---------------|
| 0,00 | 0.75 | 0.75 | 100.00 |
| 25,00 | 0.95 | 0.95 | 100.00 |
| 50,00 | 1.14 | 1.14 | 100.00 |
| 75,00 | 1.32 | 1.32 | 100.00 |
| 100,00 | 1.49 | 1.34 | 90.00 |
| 125,00 | 1.66 | 1.49 | 90.00 |
| 150,00 | 1.82 | 1.55 | 85.00 |
| 175,00 | 1.98 | 1.58 | 80.00 |
| 200,00 | 2.15 | 1.72 | 80.00 |
| 225,00 | 2.32 | 1.74 | 75.00 |
| 250,00 | 2.49 | 1.74 | 70.00 |
| 275,00 | 2.66 | 1.86 | 70.00 |
| 300,00 | 2.83 | 1.84 | 65.00 |
| 325,00 | 3.00 | 1.80 | 60.00 |
| 350,00 | 3.16 | 1.90 | 60.00 |
| 375,00 | 3.33 | 2.00 | 60.00 |
| 400,00 | 3.50 | 2.10 | 60.00 |
| 425,00 | 3.67 | 2.20 | 60.00 |
| 450,00 | 3.84 | 2.30 | 60.00 |
| 475,00 | 4.01 | 2.40 | 60.00 |

a solution to those problems. Because of relatively shallow geological structures, estimation of migration velocity by the refraction methods is effective. To overcome the strong dependence of the final result on the initial model, the MASW and LVL based model was used. In addition to limiting the space of solution, such approach considers nearest surface effects, that are beyond the resolution of travel time tomography. In this paper, the results obtained by the MASW method correlate well with the tomographic solution. As presented, the application of such methodology requires information about result uncertainty, on each step of the processing. That information, not only improve the overall result's quality but also allow for correct migration of the data between the methods. The seismic stack (Figure 7), where the increase of the horizon uncertainty with depth is visible, explicitly presents the need for such estimations. In the presented case study, the Quaternary post-glacial Pleistocene sediments were the main imaging target. All possible reflections are connected with structures formed during that period. The correlation of our results, with the data from shallow boreholes, especially the deepest ones in "Mała Wieś" and "Stara Wieś" validated, that the thickness of Quaternary sediments is much higher

than 100 meters because there are no strong reflections from larger depths on the seismic stack. Any deeper investigation requires more powerful seismic source and additional acquisition channels for better recording of the post-critical reflections. In the presented methodology, many assumptions which cannot be used for more complex geology was applied. In cases of rough geology, the joint 2D inversion of MASW results should be applied, instead of the interpolation of single 1D models.

Presented case study proves that the applied methodology was effective, as should be easily applied in similar near-surface studies. As a cost and time effective method, presented procedure greatly simplifies and improves the results of near-surface surveys without the need for additional data. In addition to modern high-resolution seismic surveys [39, 40], presented methodology increases the overall quality of the final result. Additionally, the presented methodology can be used in other scales, where layer stripping approach is used, for example in industrial scale [41], or even lithospheric research [42]. For further improvement of the results of the presented methodology, the information from additional geophysical methods, based on the different physical parameter (e.g. ERT, GPR) can be used [43]. The scalability of the technique, to other scales, makes it cost and time efficient, and allows to solve multiple processing problems. Additional uncertainty parameter of the final seismic image will greatly simplify the interpretation, which is extremely useful not only in small scale experiments but also industrial-scale projects.

9 Conclusions

This work presents an uncertainty-based, multi-step seismic analysis that allows us to obtain final results with estimated reliability. Direct use of the uncertainty information between the methods allowed the authors to restrict the area of possible solutions for the consecutive methods. That approach leads to final results which showed detailed information about the subsurface through seismic imaging. Moreover, the application of external methods to the reflection seismic, allowed us to find solutions where the classical approach to velocity analysis was ineffective. The case study presented by the authors reveals that propagation of the information about model uncertainty should be treated equally in the results. The assumption that deviations in the results received from previous methods limit the possible solution range of more accurate consecutive ones leads to more certain results. Moreover, that approach allowed simplified processing of the

data because the final model from the previous analysis is treated as a starting point for subsequent ones. The presented methodology allows us to overcome the problems that arise in near-surface surveys that are unsolvable using classical processing tools. In the presented study, an example of finding the velocity field for seismic imaging allowed for recovery information about reflection horizons in the dataset. The methodology presented by the authors is correct only if information about uncertainty is estimated and treated with caution. This approach allows correct, partial results transfer between methods, which results in less processing mistakes and a correct final solution. A similar methodology could be used for solving other special geophysical problems.

Acknowledgement: This research was funded by the National Science Centre, Poland (NCN) Grant UMO-2015/19/B/ST10/01833 and part of the work was supported within statutory activity No. 3841/E-41/S/2018 of the Ministry of Science and Higher Education of Poland.

References

- [1] Park, C. B., Miller, R. D., Xia, J., (1999). Multichannel analysis of surface waves: *Geophysics*, 64(3), 800–808. Report 2005-22.
- [2] Miller, R. D., Xia, J., Park, C. B., Ivanov, J., (1999). Using MASW to map bedrock in Olathe, Kansas [Exp. Abs.]: *Soc. Explor. Geophys.* 433–436.
- [3] Stokoe, K. H. II, Wright, S. G., Bay, J. A., Roesset, J. M., (1994). Characterization of geotechnical sites by SASW method, *Geophysical Characterization of Sites*, Oxford & IBH Publishing, New Delhi, India, pp. 15–25.
- [4] Ezersky, M., Legchenko, A., (2015). Mapping of Salt Consolidation and Permeability Using MASW Method in the Dead Sea Sink-hole Problem., *Engineering Geology for Society and Territory - Volume 5*. Springer.
- [5] Fokin, I.V., Basakina, I.M., Kapustyan, N.K., Tikhotskii, S. A., Schur, D. Yu., (2012). Application of travel-time seismic tomography for archaeological studies of building foundations and basements, *Seismic Instruments* (2012) 48: 185. <https://doi.org/10.3103/S074792391202003X>.
- [6] Bruno, P. P., Improta L., Castiello A., Villan F., Montone P., (2010). The Vallo di Diano Fault System: New evidence for an active range-bounding fault in southern Italy using shallow, high-resolution seismic profiling, *Bull. Seismol. Soc. Am.* 100, no. 2, doi: 10.1785/0120090210.
- [7] Dolan, J. F., Pratt, T. L., (1997). High-resolution seismic reflection profiling of the Santa Monica fault zone, West Los Angeles, California, *Geophys. Res. Lett.* 24 (16), 2051–2054.
- [8] Uhlemann, S., Hagedorn, S., Dashwood, B., Maurer, H., Gunn, D., Dijkstra, T., Chambers, J., (2016). Landslide characterization using P- and S-wave seismic refraction tomography — the importance of elastic moduli, *Journal of Applied Geophysics.*, 134, 64–76.
- [9] Adelinet, M., Domínguez, C., Fortin, J., Violette, S., (2018). Seismic-refraction field experiments on Galapagos Islands: A quantitative tool for hydrogeology, *Journal of Applied Geophysics*, 148, 139–151.
- [10] Gallardo, L. A., Max, A., Meju, M. A., (2003). Characterization of heterogeneous near-surface materials by joint 2D inversion of dc resistivity and seismic data, *Geophys. Res. Lett.*, 30(13), 1658, doi:10.1029/2003 GL017370, 2003.
- [11] Gallardo, L. A., Fontes, S. L., Meju, M. A., Buonora, M. P., de Lugao, P. P., (2012). Robust geophysical integration through structure-coupled joint inversion and multispectral fusion of seismic reflection, magnetotelluric, magnetic, and gravity images: Example from Santos Basin, offshore Brasil: *Geophysics*, 77(5), 237–251, doi: <https://doi.org/10.1190/GEO2011-0394.1>.
- [12] Colombo, D., de Stefano, M., (2007). Geophysical modelling via simultaneous joint inversion of seismic, gravity and electromagnetic data: Application to pre-stack depth imaging: *The Leading Edge*, 26, 326–331, doi: <https://doi.org/10.1190/1.2715057>.
- [13] de Stefano M., Andreasi, F. G., Re, S., Virgilio, M., Snyder, S. F., (2011). Multiple-domain, simultaneous joint inversion of geophysical data with application to subsalt imaging, *Geophysics*, 76(3), R69–R80, doi: <https://doi.org/10.1190/1.3554652>.
- [14] Doetsch, J., Linde, N., Coscia, I., Greenhalgh, S. A., Green, A. G., (2010). Zonation for 3D aquifer characterization based on joint inversions of multimethod cross-hole geophysical data, *Geophysics*, 75(6), G53–G64, doi: <https://doi.org/10.1190/1.3496476>.
- [15] Gao, G., Abubakar, A., Habashy, T. M., Pan, G., (2012). Joint petrophysical inversion of electromagnetic and full-waveform seismic data: *Geophysics*, 77(3), 3–18, doi: <https://doi.org/10.1190/GEO2011-0157.1>.
- [16] Vozoff, K., Jupp, D. L. B., (1975). Joint inversion of geophysical data: *Geophysical Journal of the Royal Astronomical Society*, 42, 977–991.
- [17] Marciniak, A., (2017). Seismic tomography and MASW as a tool improving Imaging, MSc Thesis, Department of Earth Sciences, University of Silesia.
- [18] Giustiniani, M., Tinivella, U., Accaino, F., (2010). P and S reflection and P refraction: An integration for characterising shallow subsurface, *Journal of Applied Geophysics*, 71(4), 149–156.
- [19] Wu, Y., Nakagawa, S., Kneafsey, T. J., Dafflon, B., Hubbard, S., (2017). Electrical and seismic response of saline permafrost soil during freeze-thaw transition, *Journal of Applied Geophysics*, 146, 16–26.
- [20] Wellmann, J. F., Regenauer-Lieb, K., (2012). Uncertainties have a meaning: Information entropy as a quality measure for 3-D geological models: *Tectonophysics*, 526, 207–216.
- [21] Caers, J., (2011). Modelling Uncertainty in the Earth Sciences, John Wiley & Sons Ltd, Chichester, UK (June 2011).
- [22] Majdański, M., Trzeciak, M., Gaczyński, E., et al. (2016). Seismic velocity estimation from post-critical wide-angle reflections in layered structures, *Stud. Geophys. Geod.* 60: 565. <https://doi.org/10.1007/s11200-015-1268-0>.
- [23] Hayward, N., Andrew, J. S., Calvert, A. J., (2007). Seismic reflection and tomographic velocity model constraints on the evolution of the Tofino forearc basin, British Columbia, *Geophysical Journal International*, 168(2), 1 February, 634–646. <https://doi.org/10.1111/j.1365-246X.2006.03209.x>
- [24] Stupnicka, E., (2007), *Geologia regionalna Polski*. Wydawnictwa Geologiczne, Warszawa, ISBN 978-83-235-1787-0

- [25] Rix, G. J., Leipski, E. A., (1991). Accuracy and resolution of surface wave inversion. In: Bhatia, S. K., and Blaney, G. W., Eds. Recent advances in instrumentation, data acquisition and testing in soil dynamics: *Am. Soc. Civil Eng.*, 17–32.
- [26] McMechan, G. A., Yedlin, M. J., (1981). Analysis of dispersive waves by wave field transformation: *Geophysics*, 46, 869–874.
- [27] Park, C. B., Miller, R. D., (2005). Seismic characterization of wind turbine sites near Lawton, Oklahoma, by the MASW method: Kansas Geological Survey Open-file.
- [28] Islam, T., Chik, Z., Mustafa, M. M., Sanusi, H., (2013). Faster 2-D representation of geotechnical characteristics using MASW method: Faster tomography in MASW. *Environmental Earth Sciences*, 70(1), 329–335. DOI: 10.1007/s12665-012-2130-0.
- [29] Eiben, A. E., Raue, P. E., Ruttikay, Z., (1994). Genetic algorithms with multi-parent recombination. *Proceedings of the third international conference on parallel problem solving from nature (PPSN)*, Springer.
- [30] Fernández-Martínez, J. L., Xu, S., Sirieix, C., Fernández-Muniz, Z., Riss, J., (2017). Uncertainty analysis and probabilistic segmentation of electrical resistivity images: the 2D inverse problem. *Geophysical Prospecting*, 65, 112–130. doi: 10.1111/1365-2478.12559.
- [31] Tompkins, M. J., Fernández-Martínez, J. L., Alumbaugh, D. L., Mukerji, T., (2011). Scalable uncertainty estimation for nonlinear inverse problems using parameter reduction, constraint mapping, and geometric sampling: Marine controlled-source electromagnetic examples *Geophysics*, 76(4),
- [32] Lee, M. W., (2003). Velocity Ratio and its Application to Predicting Velocities, *U.S. Geological Survey Bulletin* 2197.
- [33] Nole, G., (2008). *A Breviary of Seismic Tomography: Imaging the Interior of the Earth and Sun*. Cambridge: Cambridge University Press. doi: 10.1017/CBO9780511984709.
- [34] Hobro, J. W. D., Singh, S., (1999). Joint interface and velocity estimation in three dimensions (JIVE3D), *LITHOS science report*, Department of Earth Sciences, University of Cambridge.
- [35] Meléndez, A., Korenaga, J., Sallares, V., Miniussi, A., Ranero, C., (2015). TOMO3D: 3-D joint refraction and reflection travel-time tomography parallel code for active-source seismic data-synthetic test. *Geophysical Journal International*, 203, 158–174. 10.1093/gji/ggv292.
- [36] Yilmaz, Ö., (2001) *Seismic Data Analysis: Processing, Inversion, and Interpretation of Seismic Data*, Society of Exploration Geophysicists, ISBN: 978-1-56080-158-0
- [37] Dix, C. H., (1955). Seismic velocities from surface measurements, *Geophysics*, 20, 68–86.
- [38] Lingli, H., Jianhang, Z., (2011). Velocity update using high-resolution tomography in Santos Basin, Brazil, *SEG Technical Program Expanded Abstracts 2011*. January 2011, 3974–3978.
- [39] Bruno, P., (2015). High-resolution seismic imaging in complex environments: a comparison among Common Reflection Surface stack; Common Midpoint stack; and pre-stack depth migration at the Ilva - Bagnoli brownfield site, Campi Flegrei, Italy. *Geophysics*. 80. 10.1190/GE02014-0488.1.
- [40] Bruno, P., Castiello, A., (2009). High-resolution onshore seismic imaging of complex volcanic structures: An example from Vulcano Island, Italy. *Journal of Geophysical Research*. 114. 10.1029/2008JB005998.
- [41] Malinowski, M., Guterch, A., Narkiewicz, M., Petecki, Z., Janik, T., Środa, P., Maksym, A., Probalski, J., Grad, M., Czuba, W., Gaczyński, E., Majdański, M., Jankowski, L., (2015). Geophysical constraints on the crustal structure of the East European Platform margin and its foreland based on the POLCRUST-01 deep reflection seismic profile. *Tectonophysics*, 653, 109–126, doi: 10.1016/j.tecto.2015.03.029.
- [42] Majdański, M., Kozlovskaya, E., Świeczak, M., Grad, M., (2009). Interpretation of geoid anomalies in the contact zone between the East European Craton and the Palaeozoic Platform - I. Estimation of effects of density inhomogeneities in the crust on geoid undulations. *Geophysical Journal International*, 177, 321–333
- [43] Marciniak A., Owoc B., Wawrzyniak T., Nawrot A., Glazer M., Osuch M., Dobiński W., Majdański M., (2019). Recognition of the varying permafrost conditions in the SW Svalbard by multiple geophysical methods, EGU2019-377 | CR4.1/GM9.6, Conference Abstract

Paper II:

Owoc, B., **Marciniak, A.**, Dzierżek, J., Kowalczyk, S., & Majdański, M. (2019). Seismic Imaging of the Mesozoic Bedrock Relief and Geological Structure under Quaternary Sediment Cover: The Bolmin Syncline (SW Holy Cross Mountains, Poland). *Geosciences (Switzerland)*, 9(10). <https://doi.org/10.3390/geosciences9100447>



Article

Seismic Imaging of the Mesozoic Bedrock Relief and Geological Structure under Quaternary Sediment Cover: The Bolmin Syncline (SW Holy Cross Mountains, Poland)

Bartosz Owoc ^{1,*}, Artur Marciniak ¹, Jan Dzierżek ², Sebastian Kowalczyk ² and Mariusz Majdański ¹

¹ Institute of Geophysics, Polish Academy of Sciences, 01-452 Warsaw, Poland; amarciniak@igf.edu.pl (A.M.); mmajd@igf.edu.pl (M.M.)

² Faculty of Geology, University of Warsaw, 02-089 Warsaw, Poland; j.dzierzek@uw.edu.pl (J.D.); s.kowalczyk@uw.edu.pl (S.K.)

* Correspondence: bowoc@igf.edu.pl

Received: 24 September 2019; Accepted: 17 October 2019; Published: 18 October 2019



Abstract: The clear and detailed images of geological structures that can be obtained by seismic methods are one of the main drivers of their popularity in geological research. The quality of final geophysical images and models relies strongly on the amount of data that goes into them. Analysing several complementary seismic datasets allow an improved interpretation. Responding to this challenge, this article proposed an optimal combination of geophysical methods for near-surface applications. Multi-channel analysis of surface waves, first-arrival travel-time tomography, and ground-penetrating radar were the key supports for standard reflection seismic imaging. Ease of use and fast and cheap acquisition are some of the advantages of the mentioned methods. Considering that all recorded wave fields required minimal additional processing while offering a significant improvement in the final stack, it was worth the extra effort. Thanks to that, the better-estimated velocity field allowed high quality images to be obtained up to 200 m. The Mesozoic bedrock was a distinct and very strong reflector in the resulting reflection seismic imaging. There was also a clearly visible depression of the horizon corresponding to erosion or a structure (syncline). Deeper, it was possible to track two or even four detachments of faulting origin.

Keywords: reflection seismic imaging; multi-channel analysis of surface waves; first-arrival travel-time tomography; Mesozoic bedrock; multi-method analysis

1. Introduction

Recognition of the Mesozoic basement in the Holy Cross Mountains and the tectonic structure lying below was the main aim of this paper. During geological research, the use of geophysical methods is invaluable, especially the use of high-resolution seismic methods [1–6]. These methods image geological structures at different depths with different degrees of precision [7,8]. Seismic methods have been successfully applied in the exploration and exploitation of hydrocarbon deposits and actually in many other fields of science, for example, archaeology, construction, environmental protection, tectonics, and geomorphology [9–16]. Another application worth mentioning is sediment basin analysis [17–23].

Geophysical methods provide the only opportunity to obtain information about subsurface structures in areas with poor geological knowledge, without deep boreholes and outcrops, in both 2D or 3D. The technical solutions (e.g., source type) used during fieldwork and acquisition geometry determine

the quality of the seismic data and the depth of investigation [24]. Therefore, the combination of different complementary seismic methods may result in more consistent, accurate, and detailed interpretations.

To fulfil such a demand, multi-channel analysis of surface waves [24,25] and first-arrival travel-time tomography [26] were used along with seismic imaging. This research used the uncertainty-driven approach proposed by Marciniak et al. [27], which utilizes all possible data from various geophysical methods to accomplish a more precise and clearer result. This kind of approach requires estimation of uncertainty at each step of processing to obtain a reliable interpretation of the geophysical image as the geological result. By applying geophysical methods in sequence, where less certain methods are used at the beginning and the most precise are used at the end, and transferring information between methods, the authors were able to increase the quality of the seismic stack. Considering a few geophysical methods by using the multi-method approach gave a more detailed and accurate image of the basin.

2. Geological Setting

The research area is located approximately 5 km from the village of Chęciny in the Holy Cross Mountains, between Grzywy Korzeczkowskie and the rivers Hutka, Biała Nida, and Czarna Nida (Figure 1). The Mesozoic bedrock contains Upper Jurassic deposits, mainly Kimmeridgian [28–30]. The Upper Kimmeridgian deposits include shell limestone, oolitic limestone, marlstone limestone, and marl, as well as marly clays. The Lower Kimmeridgian deposits consist of oolitic limestones, chalky limestones, pelite, and striped limestone with flints [30]. The nearby hills are made of rocks belonging to the Lower Kimmeridgian, namely Grzywy Korzeczkowskie (over 330 m a.s.l.) and Bzowica Mountain (240 m a.s.l.) on the other side of the village of Mosty. In the vicinity of the studied area, there are also Oxfordian rocks. They include speckled limestones, chalky and marginal limestones, and limestone with flints. In some places they reach the surface, where they form the northern and eastern parts of Grzywy Korzeczkowskie [30]. The faulted and folded rocks described are a direct bedrock for Quaternary sediments.

The axial part of the Bolmin syncline is located in the Mosty region [28,29]. Its axis has a WNW direction in this area. In the SW area of the Holy Cross Mountains Margin, a number of fault zones have been found, which are partially visible in the relief of this terrain (Figure 1). Most river valleys, including Hutka, Biała Nida, and Czarna Nida, are characterized by developed fault lines [28,30,31]. The largest fault zone stretches along a length of 15 km to the NW through the Mosty region to Czarna Nida to the south of Chęciny. It cuts the rocks of the Bolmin syncline and has the character of a dextral strike-slip fault [32,33]. The existence of smaller faults can be suspected on the basis of interpretation of the relief of Grzywy Korzeczkowskie (Figure 1). Gorges that cut the hill have been formed as a result of the tectonic activity. In this part of the Holy Cross Mountains, the relation of the relief with the tectonics and lithology of Quaternary bedrock is exceptionally readable [32].

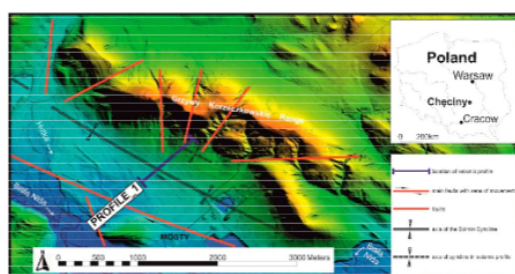


Figure 1. The studied area, Chęciny in the Holy Cross Mountains. A fluvial area (with the sand mine) is located between culminations of Mesozoic rocks (Lindner et al., 2001; Cabalski et al., 2018).

In the Mosty region, the flat surface to the SW of Grzywy Korzeczkowskie is built of Quaternary sediments. The thickness of the Quaternary overburden is estimated to be up to 90 m in this area, but is usually at the level of 30–60 m. The profile of the Quaternary sediments begins with a layer of debris and residual clays classified as the South Polish Complex [32,34]. Sand and gravel sediments of the Middle Polish Complex fill the fossil valley [35], the bottom of which was recognized in boreholes at a depth of at least 140 m a.s.l. to the east of the village of Mosty [32]. Above it, silts with an admixture of sands appear. Their genesis is associated with obstruction of the surface runoff by the forehead of the Odranian-age glacier, which is located approximately 15 km to the SW, near Małogoszcz and Łopuszna [33,35]. In the immediate vicinity of the seismic profile, these sediments occur at depths of about 30 m [36,37]. The thickness of the series can reach several metres [32]; however, it is usually smaller as a result of subsequent erosion of proglacial and extra-glacial waters. The accumulation of sand–gravel material with a thickness of 10–25 m is also related to the activities of these waters [36,37]. These sediments, which directly form a large area between the foothills of Grzywy Korzeczkowskie and the village of Mosty, represent a higher level (V) of the Biała Nida valley [38].

The lithology and texture of subsurface sediments can be traced in the walls of the nearby sandstone in Mosty. Within this layer, there are packages and interbedding of fine debris of diluvium origin on several levels. These paleoflow sediments from the slopes of Grzywy Korzeczkowskie were accompanied by the accumulation of extra-glacial rivers in periglacial conditions. The debris layers can be several metres thick, and their occurrence is irregular both in the profile of sediments and on the surface [37]. In the SW direction, the surface is made of the sands and gravels of the Biała Nida River terrace, created during the main Vistulian glaciation (Lindner et al., unpublished data). Despite being a continuous object of geological interest, the general knowledge about the Holy Cross Mountain is still incomplete. Many geological hypotheses still need to be verified, especially using seismic methods.

3. Fieldwork

Two seismic profiles were obtained during the survey. The analyzed one (Profile_1, Figure 1) was 840 m long with a receiver spacing of 5 m and a shot spacing of 2.5 m. Sixty standalone GPS-based DATA-CUBE recorders with 4.5 Hz geophones were used as seismic receivers. The source, an in-house modified weight drop (PEG-40), produced enough seismic energy to image the studied structure. Offset shooting with 10 shot points on each side was carried out along five deployments of Profile_1. This gave a good, stable seismic fold of 90 on average, without significant oscillation. To meet the need for precise topography for all methods, geodetic measurements were conducted using an GPS RTK LEICA device. Accurate shot timing was ensured using GPS-based devices, which were specially constructed and had been previously tested for geoenvironmental problems [8]. The gathered data (Figure 2), stacked using a diversity stack, were used for a few seismic methods: first-arrival travel-time tomography (FATT), multi-channel analysis of surface waves (MASW), and reflection seismic imaging. The presented data gathering scheme allowed for fast and cost-efficient acquisition.

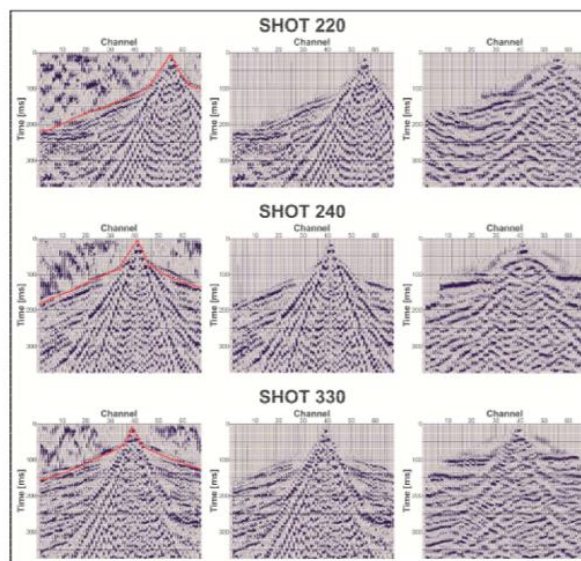


Figure 2. Shot gathers for shots 220, 240, and 330 with applied automated gain control (AGC) (100 ms). Left panels: shot gathers after diversity stacking. A carefully designated front mute (red line in left panels) removing linear refraction arrivals is presented in the middle panels. Right panels show the effect of applying normal move-out (NMO). Clear shallow reflections were visible at approximately 120 ms for shot 220, 110 and 140 ms for shot 240, and 100 and 150 ms for shot 330.

4. Methods and Data Processing

In the multi-method analysis, the order in which methods were used was not accidental, but dependent on their uncertainty and depth of investigation [27]. In the first step, the shallowest and most uncertain by resolution method, MASW, was used to identify the shallowest structures. The obtained results were used to create a preliminary model of the velocity field for FATT and for static correction. FATT was then applied to estimate the velocity field for refracted waves. In the last step of the multi-method approach, the most precise and demanding method was used: reflection seismic imaging, which utilized all of the information from MASW and FATT to give better constraints and more robust results.

Each seismic method demands a different processing scheme. However, the methods have a few common steps at the beginning. Geometry was set up and quality control was performed. These processes take a long time but are crucial to obtaining a high-quality result in all methods, especially due to the use of standalone stations and possible acquisition errors. To remove noisy channels, manual trace editing was carried out. A vertical stack of four repeated shots was performed to improve the signal-to-noise ratio.

4.1. Multi-Channel Analysis of Surface Waves

Both tomographic and reflection methods are poorly sensitive to potential low velocity zones, and also cannot image upper 10 m of the shallowest subsurface; therefore, the MASW method was applied. This analysis, widely used in geoenvironmental projects, can provide information about the

shear velocity (V_s) field [24]. Furthermore, it can be used to estimate the geotechnical parameters of the soil.

In the presented study case, a scheme where multiple single 1D profiles were interpolated to obtain a pseudo-2D model was used. The preprocessing of the data, performed using Globe Claritas software, aimed to enhance the surface waves and suppress the noise. Particular attention was paid to the removal of refraction and reflection waves from the records; these can potentially strongly affect the result. That goal was achieved by applying a combination of a 1D band pass with characteristics of 2–3–60–70 Hz and 2D FK filtration, followed by 500 ms automated gain control (AGC). The later steps of processing were standard for the classical MASW scheme [39]. The dispersion curves were picked manually and properly prepared for the inversion procedure. To obtain the best possible input data for inversion, every dispersion curve was picked 10 times, and average of them with the estimated misfit as standard deviation was used in the modeling (Figure 3). Moreover, in some noisy single shot records, the picked curve was smoothed to eliminate the impact of hand precision as much as possible. To obtain the 2D model of V_s , nine single 1D dispersion curves at points spaced at regular intervals along the seismic line were analyzed. The inversion procedure was based on the Monte Carlo and the Nearest Neighbourhood algorithms adapted to the Dinver mode of the Geopsy program [40]. The starting model created took into account information from LVL (low velocity layer) analysis and local geology. During the inversion, 50 Monte Carlo models and an additional 2500 models from the Nearest Neighbourhood algorithm were used to find the one with the best fit to the data.

As an overall uncertainty criterion, the chi-squared parameter was used. Results below 1.3 were rejected. Additionally, the theoretical dispersion curve was compared manually with the original one for each of the nine locations as a final verification. Interpolation between profiles was achieved by the kriging method in the Surfer program. Finally, a smooth 2D model showing the general trend of changes in lithology for the first 50 m was obtained (Figure 4).

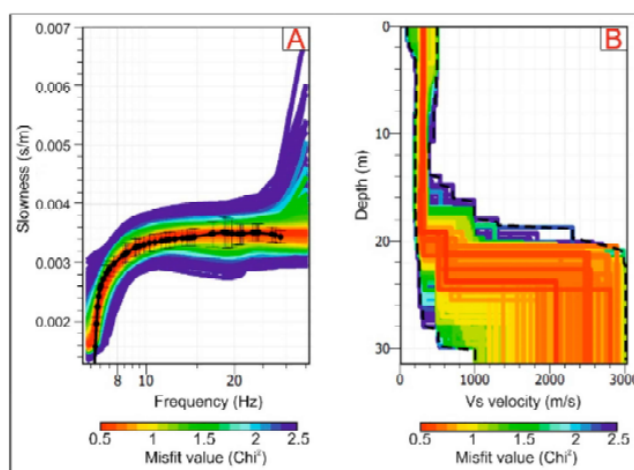


Figure 3. (A) The uncertainty of the dispersion curve modeling. The picked dispersion curve (black line) with the uncertainty of picking was well fitted to the synthetic models (colored areas). The chi-squared parameter for the best theoretical curves was less than one; (B) 1D result of the multi-channel analysis of surface waves (MASW) analysis for shot 164. The 1D velocity model presented a uniform structure up to 18 metres. Below that depth, an increase of shear velocity (V_s) was visible. Interpretation of the deeper parts was impossible, due to the penetration range of the method.

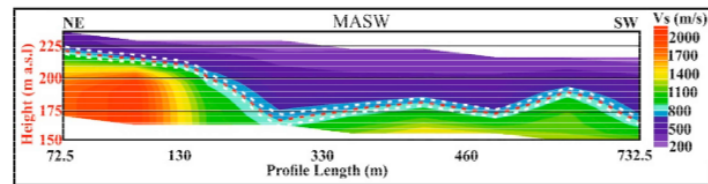


Figure 4. The result of the multi-channel analysis of surface waves (MASW). The red dashed line presents the geophysical boundary. The white dotted lines show the uncertainty of the result. The overall shape of the structure is similar to the result obtained in reflection imaging.

4.2. First-Arrival Travel-Time Tomography and Uncertainty Analysis

The velocity model spanned a rectangular grid with 85×31 cells and dimensions of 10×5 m. An inversion scheme consisting of 10 steps with six iterations per step was applied using JIVE3D software [41]. JIVE3D uses the shooting method [42] to trace ray paths through a modeled velocity field. The linearization of the relationship between travel-times and model parameters was carried out using ray perturbation theory. The inversion method was based on a set of linearized refinements to the initial velocity field to achieve a better match between the starting model and the raw data.

Clearly visible at all offsets, P-wave first-arrival travel-times were picked manually along the profile. Similarly to Korenaga et al. [43], a large number of starting models were tested to find the optimal one—that is, the one which gave the best fit to the travel time at a given parameterization. Instead of Monte Carlo sampling, a simple grid search approach was adopted. Our starting models were generated by a set of 1D linear vertical velocity gradients with defined topography. Each gradient was parameterized with two values: the velocity at the surface ($V1$, above topography) and the velocity at the bottom of the model ($V2$). Interpolation of the velocity value for each model's cell was performed using standard b-spline methods. Table 1 summarizes the gradient parameters with the corresponding steps that were tested.

Table 1. Range of values of the upper ($V1$) and lower ($V2$) velocities in the experimental setting.

| Velocity | Elevation (m) | Minimum (m/s) | Maximum (m/s) | Step (m/s) | Final Model (m/s) |
|----------|---------------|---------------|---------------|------------|-------------------|
| $V1$ | 300 | 200 | 300 | 10 | 260 |
| $V2$ | 150 | 1200 | 1800 | 60 | 1500 |

In total, 121 starting models were found to have adequate statistics for evaluating the uncertainty using hit-count normalization [44]. In this approach, the standard deviation normalized by the sum of rays in each cell was treated as the uncertainty estimator, called a weighted error (WE). Inversion was carried out for all 121 starting models of the velocity field. To find the optimal velocity field, the travel-time fitting was estimated as a ratio of chi-squared to the hit-rate—that is, the percentage of the picked travel-times for which synthetics were successfully obtained during two-point ray-tracing. The best travel-time fit was obtained for the model where $V1 = 260$ m/s and $V2 = 1500$ m/s. The inversion of this model was considered to be the final result of tomography. In the next step of the multi-method analysis, it was used as the subsurface velocity field and for correct front mute in reflection seismic imaging. Figure 5A presents the velocity distribution from inversion using JIVE3D code with the mask. The velocity field was rather smooth. The unconfirmed area (without sufficient ray coverage) has been greyed out.

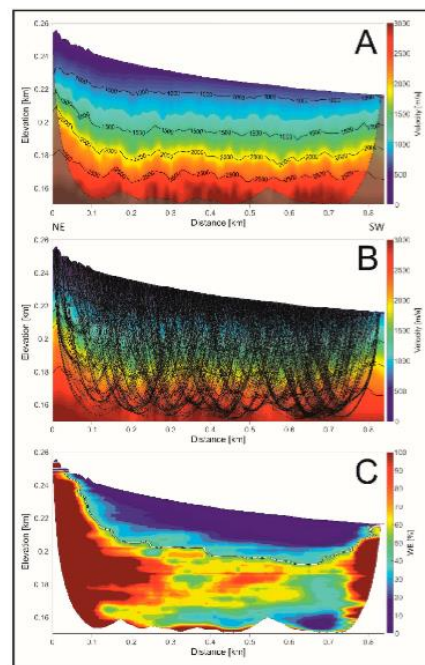


Figure 5. The best result of the first-arrival travel-time tomography (FATT): (A) The velocity field. The unconfirmed area without ray coverage was greyed out. The color contour corresponds to the resolved part of the result with high-density ray coverage; (B) ray paths; (C) the map of uncertainty normalized by the ray coverage – WE (weighted error). The black and white line corresponds to the edge of the area well-resolved by rays (in this particular case, a value of 50%).

The estimated uncertainty is presented in the form of uncertainty maps (Figure 5C). Each cell of these maps was calculated separately as the standard deviation of the velocity from the respective cells, extracted from the models. Masks in Figure 5A were created considering only those parts of the given panels covered by rays (Figure 5B). Hit-count normalization in Figure 5C did not require masks because it occurred automatically, due to the nature of this procedure.

The FATT result showed an almost-flat smooth structure slightly inclining to the SW. There were also visible small-scale undulations in the shallow part of the section.

4.3. Reflection Seismic Imaging

With a limited offset of 100 m, refraction statics were estimated by applying standard techniques from Globe Claritas. The seismic imaging processing also included a carefully designated front mute (red line) to extract linear refraction arrivals without distorting wide-angle shallow reflections (Figure 2, middle panels). Its meaning has been demonstrated in many articles [45,46]. The outcome of the NMO (normal move-out) correction is shown in Figure 2 (right panels) as flattened shallow reflections. Straightening of reflections confirmed the correctness of the velocity field used. The appearance of strong surface waves is problematic for seismic imaging. They interfere with wide-angle reflections, which are treated as a useful signal. A simple high-pass filter with frequencies of >30 Hz proved to

be sufficient to suppress almost all surface wave amplitudes. In the next step, a surface-consistent deconvolution was performed in order to improve the resolution of the seismic image by amplifying high frequencies. The data were filtered in the FK domain using a band pass filter with characteristics of 2–3–100–120 Hz before stacking the shot gathers in the seismic section to cut frequencies above 100 Hz. Final time to depth conversion was performed using the velocity model from the previous FATT and further extrapolated downward with the standard common velocity stack (CVS) method. The final result in the depth domain is shown in Figure 6B.

Due to the lack of boreholes, verification of the interpreted structures was impossible. To evaluate the uncertainty of the main reflector determination, the velocity field used for the time to depth migration was changed by applying extreme values of velocity. These velocities were estimated for $\pm 30\%$ of the optimal one according to knowledge from MASW, FATT results, and previous works [7]. Figure 6C shows the estimated uncertainty in the form of white bars with the geological interpretation.

The reflection imaging provided the possibility of recognition of the Mesozoic basement visible as a strong reflector. Application of the proposed approach gives information about the uncertainty of the result.

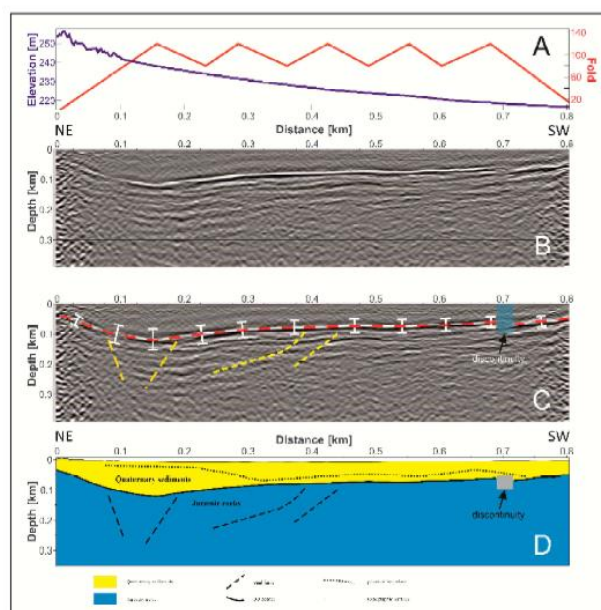


Figure 6. The result of the reflection seismic imaging: (A) Elevation and fold. Thanks to acquisition geometry in the form of six deployments, a good seismic fold along the whole profile was achieved; (B) seismic stack in the depth domain; (C) interpretation of the seismic image. Considered as the Mesozoic bedrock, the main reflecting horizon (red dashed line) is clearly visible in the seismic section. Its depression in the NE is probably related to the syncline structure and/or erosion. In the middle of the seismic stack (yellow dashed line), there are four detachments, probably connected to a local fault. White bars show the estimated uncertainty of determination of the interpreted horizon. The blue area corresponds to the discontinuity of the Mesozoic bedrock; (D) geological interpretation of all results.

5. Discussion

The presented model of Quaternary sediments indicates that regardless of origin and age, their lithological variation is small, with the exception of the thick packages of limestone debris. This issue certainly hinders their spatial recognition and interpretation in seismic results [36,37]. The pronounced contrast between the physical properties of Quaternary sediments and those of the Jurassic rocks was the main basis for undertaking the research.

The result from MASW showed simple flat-lying structures according to shear velocity to a depth of approximately 40 m, but smoothly inclining to the SW (Figure 3). Therefore, static correction was not required for this dataset. The FATT result showed an almost-flat smooth structure with small-scale undulations slightly inclining to the SW. The places where velocity decreased are related to thicker deposits of loose material (Figure 5A, at approximately 120 m). The uncertainty map presented in Figure 5C was computed as shown in Owoc et al. [44]. The well-resolved part of the velocity field, which is crucial for the most critical processing step in the seismic imaging, the manual front mute, is visible as the upper bluish zone with the lowest values of WE. During stacking of the seismic data and time to depth conversion of the final stack, this part of the velocity field was also used.

As shown in Figure 6B, the obtained image was not distorted by any amplitude variation and was therefore easy to interpret (Figure 6C,D). This feature was due to an almost uniform seismic fold (Figure 6A). At a depth of approximately 50 to 120 m, the main reflecting horizon was clearly visible due to the high contrast of impedance between the soft Quaternary sediments and the hard Jurassic rocks (Figure 6B–D). This reflector was interpreted as the Mesozoic bedrock. It definitely inclined to the NE direction, where there was an important feature: a depression at approximately 120 m of the profile with its bottom around 120 m below the subsurface. From this location on the profile in both directions, this horizon rises to 40–50 m depth. In the SW part of the seismic result, the Mesozoic bedrock became almost flat. In the vicinity of 700 m of the profile, the signal suddenly weakened, which was visible as a rapid discontinuity of the reflector in the result of the reflection seismic imaging. In general, the shape of this line referred to the gently curved syncline with the axis in the northern part of the presented seismic profile (Figure 6B,C,D). This would mean that the axis of syncline should be moved several hundred metres to the north compared to the previously developed interpretation [32]. However, the gentle nature of the Quaternary basement line suggests a glacial erosion. The glacier adapted to the existing shape of the syncline bedrock, deepening the axis zone and leveling the adjacent areas. The first glacier in this area during the Sanian 1 (MIS 16) glaciation [28,41] entered with a lobe from the SE. A slight residue of glacial tills proved the small thickness of ice in this region [28]. Therefore the results of the glacial erosion may not be significant. The river erosive genesis seems to have had a narrow and deep refraction of the basement line in the southern part of the seismic image. The existence of fossil river valleys from the Mazovian interglacial was documented by Lindner et al. [32] in the SE region of Mosty. Perhaps it is a continuation of this valley form, although the bottom of visible discontinuity (valley) on the discussed profile reaches about 100 m from the surface.

The seismic signal below the line interpreted as the Mesozoic bedrock allowed two types of reflections to be recognized. The first ones were gentle lines or sets of lines approximately parallel to each other and with the same shape as the basement. The second type consisted of steep lines or interruption zones of the seismic signal (Figure 6B). It is very likely that the bending of the lines reflected the variation of sediment layers within the axial part of the Bolmin syncline. Its inflection point corresponded to the intersection of the cross-section with its axis. The syncline axis was located near the foothills of the Grzywy Korzeczkowskie within marly Kimmeridgian limestones [30]. The visibility of the syncline layering disappeared below the depth of 350 m. This was probably related to the occurrence of signal-suppressing rocks: clays, claystone, siltstones, and the Lower Jurassic and Upper Triassic marly limestones. The steep lines in the seismic image were identified as discontinuities of rock layers, locally with vertical displacements—faults. Four detachments were found under the main horizon in the middle of the seismic image: two in the middle part of the profile and the other two in its northern end, accompanying the inflection zone of the syncline. They correlated well with the

faults that cut through the Grzywy Korzeczkowskie Range (Figure 1). The extensions of the fault lines coincided with the seismic record discontinuities. The inclination angles of the upper sections on the discontinuity line (apparent dip) were from approximately 40° to 55° . Considering the intersection angle of the fault line on the plan with the section line gave the approximate value of the fault slope in the range from 51° to 65° .

The diversification of the Quaternary sediments in the seismic image was definitely less spectacular. Signal gain zone, parallel to the surface, was recognized at a depth of 5 to 20 m, especially in the NW part of the profile. The second lay at a depth of 30–90 m; however, it sometimes disappeared. These signal amplifications could have been the result of reflection from layers with a large admixture of limestone debris or increased content of gravel. Zones without clear reflections can be interpreted as attenuation of the seismic energy by silty and fine-grained layers.

The obtained seismic image generally confirmed the current interpretation of the geological structure of the studied area, but structures are at different locations (Figure 6B–D). However, it provides new details in several places. The synclinal arrangement of the layers was confirmed; however, the axis of the syncline should be located in the area of the southern foothills of the Grzywy Korzeczkowskie. In the case of strongly faulted terrain, local changes in the course of the syncline axis do not arouse controversy even in short sections. The shape of the sub-Quaternary bedrock was in line with the geological structure of Mesozoic rocks. Namely, the lowest surface is located on the axial part of the syncline. Strong tectonic involvement of this area, visible in the morphostructural analysis, has also been confirmed. The faults reach the ceiling surface of the Mesozoic rocks and are not visible in the quaternary overburden. However, their relationship with a deep and narrow erosion form in the Mesozoic ceiling surface at the southern end of the cross-section can be found indirectly. The Quaternary bedrock, in addition to the exception described above, was imaged on the seismic profile by a strong but gentle line. This is the result of not very intense glacial erosion rather than time-differentiated river erosion. Only the discontinuity zone in the SE part of the profile may have been associated with deep river erosion, as previously suggested by Lindner et al. [32] and Lindner and Mastella [33]. The thickness of the loose rock cover reaching a maximum of 120 m was confirmed.

The usefulness of shallow high-resolution seismic profiling in geological studies can be considered significant. However, separation of Quaternary deposits was impossible. This can be explained by the relatively weak lithological variation within the sedimentary cover and the small thickness and irregularity of the occurrence of rubble packages, giving a stronger seismic signal.

6. Conclusions

Relatively high-quality images of the subsurface with low cost of acquisition make seismic methods cost-efficient and desirable to researchers. The multi-method approach, which allows the utilization of all recorded wave fields (surfaces waves for MASW, wide-angle refractions for FATT, vertical reflections for seismic imaging), provided detailed images with high resolution down to 200 m. During acquisition, the timing device and the in-house modification of the seismic source were working properly. Combined with good and dense coverage of the studied area by seismic shot and receiver points, the multi-method approach gave well-resolved and detailed images of geological structures. The seismic energy obtained from the in-house modified weight drop during acquisition was strong enough to image the structure down to 200 m. The extra time spent on MASW processing and seismic tomography in comparison to a standard approach using only the single method of seismic imaging was worth the effort.

The strong main reflector at depths from approximately 50 to 120 m was connected with “hard” (Mesozoic) bedrock. Its shape refers to the syncline structure of the basement and erosional processes. The axis of the syncline is located near the foothills of the Grzywy Korzeczkowskie. The flattened shape of the bedrock in the studied part of the Holy Cross Mountains may be indicative of the limited erosional activity of the glaciers. In the NE, a narrow and deep depression form was found in the Mesozoic bedrock. This structure is probably related to river erosion during one of the

interglacials. In the Mesozoic rocks, four detachments with a steep inclination, probably related to local faulting, were identified. Their configuration is associated with the main surface morpholineaments. The physical limitations of reflection seismic imaging did not allow the precise imaging of the first thirty metres.

Author Contributions: Conceptualization, all authors; methodology, B.O., A.M. and M.M.; validation, all authors; formal analysis, B.O., A.M. and M.M.; writing—original draft preparation, B.O., A.M., and J.D.; writing—review and editing, all authors; visualization, all authors.

Funding: This research was funded by NCN Grant UMO-2015/19/B/ST10/01833, entitled ‘Three dimensional model of the lithosphere in Poland with verification of seismic parameters of the wave field’. Part of this work was supported within statutory activities No. 3841/E-41/S/2018 of the Ministry of Science and Higher Education of Poland.

Acknowledgments: We are grateful to M. Ludwiniak, for a fruitful discussion on the tectonics of the study region.

Conflicts of Interest: The authors declare no conflict of interest

References

1. Steeples, D.W.; Miller, R.D. Avoiding pitfalls in shallow seismic reflection surveys. *Geophysics* **1998**, *63*, 1213–1224. [\[CrossRef\]](#)
2. Steeples, D.W. A review of shallow seismic methods. *Ann. Geofis.* **2000**, *43*, 1021–1044.
3. Bruno, P.P.; Improta, L.; Castiello, A.; Villani, F.; Montone, P. The Vallo di Diano Fault System: New Evidence for an Active Range-Bounding Fault in Southern Italy Using Shallow, High-Resolution Seismic Profiling. *Bull. Seism. Soc. Am.* **2010**, *100*, 882–890. [\[CrossRef\]](#)
4. Tsuji, T.; Johansen, T.A.; Ruud, B.O.; Ikeda, T.; Matsuoka, T. Surface-wave analysis for identifying unfrozen zones in subglacial sediments. *Geophysics* **2012**, *77*, EN17–EN27. [\[CrossRef\]](#)
5. Bruno, P.P.; Castiello, A.; Villani, F.; Improta, L. High-Resolution Densely Spaced Wide-Aperture Seismic Profiling as a Tool to Aid Seismic Hazard Assessment of Fault-Bounded Intramontane Basins: Application to Vallo di Diano, Southern Italy. *Bull. Seism. Soc. Am.* **2013**, *103*, 1969–1980. [\[CrossRef\]](#)
6. Malehmir, A.; Bastani, M.; Krawczyk, C.M.; Gurk, M.; Ismail, N.; Polom, U.; Perss, L.; Persson, L. Geophysical assessment and geotechnical investigation of quick-clay landslides – A Swedish case study. *Near Surf. Geophys.* **2013**, *11*, 341–352. [\[CrossRef\]](#)
7. Majdański, M.; Trzeciak, M.; Gaczyński, E.; Maksym, A. Seismic velocity estimation from post-critical wide-angle reflections in layered structures. *Stud. Geophys. Geod.* **2016**, *60*, 565–582. [\[CrossRef\]](#)
8. Majdański, M.; Grzyb, J.; Owoc, B.; Krogulec, T.; Wysocka, A. Near-surface structure of the Carpathian Foredeep marginal zone in the Roztocze Hills area. *Acta Geophys.* **2018**, *66*, 179–189. [\[CrossRef\]](#)
9. Stewart, M.A.; Lonergan, L.; Hampson, G. 3D seismic analysis of buried tunnel valleys in the central North Sea: morphology, cross-cutting generations and glacial history. *Quat. Sci. Rev.* **2013**, *72*, 1–17. [\[CrossRef\]](#)
10. Brooks, G.R. Evidence of late glacial paleoseismicity from submarine landslide deposits within Lac Dasserat, northwestern Quebec, Canada. *Quat. Res.* **2016**, *86*, 184–199. [\[CrossRef\]](#)
11. Cheng, Y.; Wu, Z.; Yu, L.; Wang, Z.; Jia, H.; Su, W. Seismic-Reflection Imaging of a Pull-Apart Sag within Tan-Lu Strike-Slip Fault Zone: Cenozoic Structure and Evolution of the Weibei Sag, Southeastern Bohai Bay Basin, China. *J. Geol.* **2016**, *124*, 377–393. [\[CrossRef\]](#)
12. Batchelor, C.L.; Ottesen, D.; Dowdeswell, J.A. Quaternary evolution of the northern North Sea margin through glaciogenic debris-flow and contourite deposition. *J. Quat. Sci.* **2017**, *32*, 416–426. [\[CrossRef\]](#)
13. Klotzko, S.; Driscoll, N. Geomorphological and stratigraphic evidence along the northeastern U.S. margin for Laurentide glacial lake outburst floods during the MIS 2 deglaciation. *Quat. Res.* **2018**, *90*, 139–152. [\[CrossRef\]](#)
14. Montelli, A.; Dowdeswell, J.; Ottesen, D.; Johansen, S. Architecture and sedimentary processes on the mid-Norwegian continental slope: A 2.7 Myr record from extensive seismic evidence. *Quat. Sci. Rev.* **2018**, *192*, 185–207. [\[CrossRef\]](#)
15. Lenz, B.L.; Sawyer, D.E.; Phrampus, B.; Davenport, K.; Long, A. Seismic Imaging of Seafloor Deformation Induced by Impact from Large Submarine Landslide Blocks, Offshore Oregon. *Geosciences* **2019**, *9*, 10. [\[CrossRef\]](#)

16. Lebedev, M.; Dorokhin, K. Application of Cross-Hole Tomography for Assessment of Soil Stabilization by Grout Injection. *Geosciences* **2019**, *9*, 399. [\[CrossRef\]](#)
17. Hougardy, D.D.; Colman, S.M. Sedimentary architecture of the southern basin of Lake of the Woods, Minnesota and its relation to Lake Agassiz history and Holocene environmental change. *Quat. Res.* **2018**, *90*, 96–109. [\[CrossRef\]](#)
18. Rabbel, O.; Galland, O.; Mair, K.; LeComte, I.; Senger, K.; Spacapan, J.B.; Manceda, R. From field analogues to realistic seismic modelling: a case study of an oil-producing andesitic sill complex in the Neuquén Basin, Argentina. *J. Geol. Soc.* **2018**, *175*, 580–593. [\[CrossRef\]](#)
19. Archer, C.; Noble, P.; Rosen, M.R.; Sagnotti, L.; Florindo, F.; Mensing, S.; Piovesan, G.; Michetti, A.M. Lakes as paleoseismic records in a seismically-active, low-relief area (Rieti Basin, central Italy). *Quat. Sci. Rev.* **2019**, *211*, 186–207. [\[CrossRef\]](#)
20. Plets, R.M.K.; Callard, S.L.; Cooper, J.A.G.; Kelley, J.T.; Belknap, D.F.; Edwards, R.J.; Long, A.J.; Quinn, R.J.; Jackson, D.W.T. Late Quaternary sea-level change and evolution of Belfast Lough, Northern Ireland: new offshore evidence and implications for sea-level reconstruction. *J. Quat. Sci.* **2019**, *34*, 285–298. [\[CrossRef\]](#)
21. Savastano, L.; Agostinetti, N.P. Deep structure of the Southern Apennines as imaged by active and passive seismic data along the CROP-04 (crustal) reflection seismic profile. *J. Geol. Soc.* **2019**. [\[CrossRef\]](#)
22. Wiberg-Larsen, P.; Bennike, O.; Jensen, J.B. Submarine Lateglacial lake deposits from the Kattegat, southern Scandinavia. *J. Quat. Sci.* **2019**, *34*, 165–171. [\[CrossRef\]](#)
23. Yilmaz, Ö. *Seismic Data Analysis: Processing, Inversion, and Interpretation of Seismic Data*; Society of Exploration Geophysicists: Tulsa, OK, USA, 2001; ISBN 978-1-56080-098-9.
24. Park, C.B.; Miller, R.D.; Xia, J. Multichannel analysis of surface waves. *Geophysics* **1999**, *64*, 800–808. [\[CrossRef\]](#)
25. Bichler, A.; Bobrowsky, P.; Best, M.; Douma, M.; Hunter, J.; Calvert, T.; Burns, R. Three-dimensional mapping of a landslide using a multi-geophysical approach: the Quesnel Forks landslide. *Landslides* **2004**, *1*, 29–40. [\[CrossRef\]](#)
26. Nolet, G. *A Breviary of Seismic Tomography: Imaging the Interior of the Earth and Sun*; Cambridge University Press: Cambridge, UK, 2008; ISBN 978-0521882446.
27. Marciniak, A.; Stan-Kłeczek, I.; Idziak, A.; Majdański, M. Uncertainty based multi-step seismic analysis for the near surface imaging. *Open Geosci.* **2019**. (under review).
28. Czarnocki, J. *Ogólna Mapa Geologiczna Polski—Arkusz 4—Kielce (Carte Géologique Générale de la Pologne. Feuille 4: Kielce)*; Wojskowy Instytut Geograficzny: Warszawa, Poland, 1938.
29. Kutek, J. The Kimmeridgian and uppermost Oxfordian in the SW margins of the Holy Cross Mts (Central Poland). Part 1. Stratigraphy. *Acta Geol. Pol.* **1968**, *18*, 493–586.
30. Hakenberg, M. *Detailed Geological Map of Poland, Sheet Chęciny (Szczegółowa Mapa Geologiczna Polski, Arkusz Chęciny)*; Państwowy Instytut Geologiczny: Kielce, Poland, 1973. (in Polish)
31. Hakenberg, M.; Lindner, L. Quaternary deposits of the Middle Nida Valley. *Acta Geol. Pol.* **1971**, *21*, 241–264, (in Polish with English summary).
32. Lindner, L.; Mastella, L.; Semil, J. Evolution of the Mid- to Late Pleistocene river network in the southeastern part of the Holy Cross Mountains. *Geol. Q.* **2001**, *45*, 387–395.
33. Lindner, L.; Mastella, L. Origin and age of the Wierna Rzeka (Łososina) gorge in the vicinity of Bocheniec (SW Mesozoic margin of the Holy Cross Mts.). *Prace Inst. Geogr. Akad. Świętokrzyskiej Kielc.* **2002**, *6*, 21–46. (in Polish with English summary)
34. Lindner, L.; Dzierżek, J. Pleistocene deposits in the western part of the Holy Cross Mountains. *Stud. Quat.* **2019**, *36*, 75–85. [\[CrossRef\]](#)
35. Lindner, L. Pleistocene glaciations in the western part of the Holy Cross Mountains (central Poland). *Stud. Geol. Pol.* **1977**, *53*, 1–143, (in Polish with English summary).
36. Cabalski, K.; Dzierżek, J.; Kowalczyk, S. Osady Przypowierzchniowe u Podnóży Grzyw Korzeczkowskich w Mostach (Góry Świętokrzyskie) w Obrazie GPR. In Proceedings of the III Ogólnopolskie Sympozjum Geointerdyscyplinarnych Metod Badawczych – GeoSym, Chęciny, Poland, 11–13 April 2018.
37. Dzierżek, J.; Cabalski, K.; Kowalczyk, S. Relic debris flows at low altitudes in the geological and geophysical investigation: Case study of Mosty site (the Holy Cross Mountains, Poland). *Stud. Quat.* **2019**. (under review)
38. Lindner, L.; Dzierżek, J.; Cabalski, K. Quaternary valley levels and river terraces in the western part of the Holy Cross Mountains. *Stud. Quat.* **2019**, *36*, 109–118. [\[CrossRef\]](#)

39. Foti, S.; Hollender, F.; Garofalo, F.; Alberello, D.; Asten, M.; Bard, P.Y.; Comina, C.; Cornou, C.; Cox, B.; Giulio, G.D.; et al. Guidelines for the good practice of surface wave analysis: A product of the InterPACIFIC project. *Bull. Earthq. Eng.* **2018**, *16*, 2367–2420. [CrossRef]
40. Jongmans, W.M.D.; Ohrnberger, M. Surface wave inversion using a direct search algorithm and its application to ambient vibration measurements. *Near Surf. Geophys.* **2004**, *2*, 211–221.
41. Hobro, J.W.D.; Singh, S. Joint Interface And Velocity Estimation in Three Dimensions (JIVE3D). *LITHOS science report*. 1999. Available online: <https://www.yumpu.com/en/document/read/18196208/joint-interface-and-velocity-estimation-in-three-dimensions-bullard-> (accessed on 18 October 2019).
42. Červeny, V.; Klimeš, L.; Pšenčík, I. Complete Seismic Ray Tracing in Three Timensional Structures. In *Seismological Algorithms*; Doornbos, D.J., Ed.; Academic Press: Cambridge, MA, USA, 1988.
43. Korenaga, J.; Holbrook, W.S.; Kent, G.M.; Kelemen, P.B.; Detrick, R.S.; Larsen, H.C.; Hopper, J.R.; Dahl-Jensen, T. Crustal structure of the southeast Greenland margin from joint refraction and reflection seismic tomography. *J. Geophys. Res.* **2000**, *105*, 21591–21614. [CrossRef]
44. Owoc, B.; Górszczyk, A.; Majdański, M. The Discussion Of The Uncertainty In The Traveltime Seismic Tomography. In Proceedings of the 24th European Meeting of Environmental and Engineering Geophysics, Porto, Portugal, 9–13 September 2018. [CrossRef]
45. Robertsson, J.O.A.; Holliger, K.; Green, A.G.; Pugin, A.; De Iaco, R. Effects of near-surface waveguides on shallow high resolution seismic refraction and reflection data. *Geophys. Res. Lett.* **1996**, *23*, 495–498. [CrossRef]
46. Buker, F.; Green, A.G.; Horstmeyer, H. Shallow seismic reflection study of a glaciated valley. *Geophysics* **1998**, *63*, 1395–1407. [CrossRef]



© 2019 by the authors. Licensee MDPI, Basel, Switzerland. This article is an open access article distributed under the terms and conditions of the Creative Commons Attribution (CC BY) license (<http://creativecommons.org/licenses/by/4.0/>).

Paper III:

Glazer, M., Dobiński, W., **Marciniak, A.**, Majdański, M., & Błaszczuk, M. (2020). Spatial distribution and controls of permafrost development in non-glacial Arctic catchment over the Holocene, Fuglebekken, SW Spitsbergen. *Geomorphology*, 358.
<https://doi.org/10.1016/j.geomorph.2020.107128>

Geomorphology 358 (2020) 107128



Contents lists available at ScienceDirect

Geomorphology

journal homepage: www.elsevier.com/locate/geomorph

Spatial distribution and controls of permafrost development in non-glacial Arctic catchment over the Holocene, Fuglebekken, SW Spitsbergen

Michał Glazer^{a,*}, Wojciech Dobiński^a, Artur Marciniak^b, Mariusz Majdański^b, Małgorzata Błaszczuk^a

^a University of Silesia, Faculty of Natural Sciences, Bedzińska St. 60, 42-700 Sosnowiec, Poland

^b Institute of Geophysics, Polish Academy of Sciences, Księcia Janusza St. 64, 01-452 Warsaw, Poland

ARTICLE INFO

Article history:

Received 16 October 2019

Received in revised form 26 February 2020

Accepted 26 February 2020

Available online 29 February 2020

Keywords:

Coastal permafrost

Electrical resistivity tomography (ERT)

Spitsbergen

Arctic

ABSTRACT

This article presents the distribution and properties of the permafrost based on electrical resistivity tomography (ERT) and multichannel analysis of surface waves (MASW) data collected at the Fuglebekken coastal catchment area in SW Spitsbergen. This work summarizes the development of permafrost in this area during the Holocene, from the mountain environment through to the system of elevated marine terraces found around the coast. The ERT models were analysed taking into consideration the non-unique nature of the data inversion process and the physical limitations of this method. Comparing the ERT and the MASW results allows a zonal characterization of the occurring ice-bearing permafrost and its correlation with the evolution history of the catchment area. Maritime transgression as well as intensive watercourses during past degradation episodes have altered the permafrost presence and ice-accumulating abilities of different sediment zones. Permafrost development depends greatly on the presence of surface watercourses in talus slopes. The youngest elevated uplifted marine terrace did not develop an ice-rich permafrost, but the presence of permafrost in a cryotic form is possible. The significant range of the fjord water infiltration found within the sedimentary cover have influenced the development of the coastal permafrost. The current structure of ice-bearing permafrost found in the research area seems to be very sensitive to the climatic changes. Based on these results, we propose a model for the formation of the current permafrost in the studied area.

© 2020 Published by Elsevier B.V.

1. Introduction

Permafrost is a geological phenomenon caused by climate. By definition, it requires ground temperatures not to exceed 0 °C over two consecutive years; therefore, it is best described based on its thermophysical properties (Everdingen, 1998; Dobiński, 2011a). Spatial and thermal variations in permafrost are a direct consequence of climatic variations above ground. For this reason, the Global Terrestrial Observing System identifies permafrost as one of the six cryospheric indicators of global climate change (Burgess et al., 2000). On Svalbard, permafrost is generally considered continuous in non-glaciated areas (Liestøl, 1976; Christiansen et al., 2010), covering ca. 43% of the terrain (Nuth et al., 2013). It has a thickness of approximately 400–500 m in mountains rising above 500 m a.s.l., 100–200 m in the bottom of major valleys below an altitude of 90 m a.s.l., and 80–100 m near the coast (Humlum, 2005). These assumptions are confirmed by data from a limited number of boreholes up to 100 m deep (Gregersen and Eidsmoen, 1988; Isaksen et al., 2000), data from the Gruve 7 coal mine (Christiansen et al., 2005), and deep boreholes performed to search

for suitable geological conditions for CO₂ sequestration (Elvebak, 2008; Braathen et al., 2012). According to Humlum et al. (2003), the age of the permafrost could reach up to 700 ka BP in unglaciated mountains areas. On the other hand in main trunk valleys where basal sliding friction plays a significant role, the permafrost could have experienced significant degradation, possibly down to its depletion, during repeated Weichselian glaciations. In valleys and near sea level, the late Holocene age of permafrost is pointed out by pingos and ice wedge initiation (Svensson, 1971; Oliva et al., 2014).

The development of coastal permafrost and its interaction with sea-water is important to understand (Kasprzak et al., 2017), particularly in the context of response to climate change (Isaksen et al., 2007; Etzelmüller et al., 2011; Isaksen et al., 2018). Permafrost degradation due to global warming is increasingly obvious in Spitsbergen, and these changes are expected to occur considerably faster around the land-to-sea transition zone (Isaksen et al., 2007); however, the conditions of the permafrost in this zone remain unclear. In this regard, Gregersen and Eidsmoen (1988) estimated the depth of the permafrost to be approximately 100 m near the shore both at Longyearbyen and Svea, based on temperature profiles from boreholes. The depth of the permafrost at their reference sites was 190 m in Longyearbyen and 125 m in Svea, from boreholes 500 m and 200 m inland, respectively.

* Corresponding author.
E-mail address: mglazer@us.edu.pl (M. Glazer).

These data confirmed the presence of relatively “warmer” permafrost along the coast, with an average temperature of only $-1\text{ }^{\circ}\text{C}/-2\text{ }^{\circ}\text{C}$. In the study by Gregersen and Eidsmoen (1988), it was calculated that the permafrost extends 40–50 m offshore. Furthermore, they also found that on the lowland in Svea, which emerged only 0.7 ka BP, the temperature profiles are markedly warmer than those in Longyearbyen, and they have not yet reached a stable thermal condition for depths below 20 m.

The aim of this article is to identify and determine the spatial distribution, characteristics and evolution of permafrost along a transitional transect (approx. 1.1 km line) from a mountain area to the seashore near the Polish Polar Station (PPS) in Hornsund. Located in the southernmost part of Spitsbergen, the area's basic climatic parameters and the depth of the active layer have been continuously monitored for decades. Periglacial studies have been conducted here since the 1950s (Jahn, 1959a, 1959b). Yet studies from this area addressing the state of permafrost are limited due to the high cost of drilling and associated logistical difficulties in this environment (Jahn, 1982; Chmal et al., 1988). Some of the studies on permafrost near the Hornsund PPS describe it on coastal terraces in relation to fjord and scree cones at Fugleberget (Dobiński and Leszkiewicz, 2010; Dobiński, 2011b). These early studies also discuss the possibility of permafrost aggradation in newly exposed glacier forefields and the relation between glaciers and permafrost. The interaction between permafrost and seawater has also been described from the Hornsund area (Baranowski, 1968; Kasprzak et al., 2017), suggesting that seawater infiltrates under the permafrost layer. This controls the duration and effectiveness of cryo-conditioning of the evolution of rocky coastal systems (Strzelecki et al., 2017; Lim et al., 2020). The first attempt to model the permafrost distribution in the Hornsund region, carried out by Wawrzyniak et al. (2016), suggested that it could reach depths over 100 m near the PPS.

For our study the Fuglebekken catchment (Fig. 1c) has been chosen as the unique catchment crossing terrain deglaciated during the Holocene with well-preserved marine terraces alongside fluvial and slope deposits. We focus on an area with a thick layer of sediments (Baranowski, 1968) suitable for application of near-surface geophysical techniques. This facilitates the interpretation of the resistivity profiles, as in this region is still not possible to associate specific results with precise lithology based on boreholes or deep temperature measurements. Unconsolidated sedimentary rocks present a high proportion of pore spaces when compared to fissured solid rocks; consequently, they can accumulate large volumes of water/ice. This characteristic allows easy distinction between physical states based on resistivity imaging. Here we analyse electrical resistivity tomography (ERT) profiles along a longitudinal transect following the Arieskaret–Isbjørnhamna line, in Hornsund fjord, Svalbard (Fig. 1c, Profiles Hor 7 and 6). These measurements allowed us to understand the structure of the permafrost formation over an approximately 1 km transect from a scree cone site at an altitude of approx. 100 m a.s.l., to an erosional cut within the youngest marine terrace at 1.5 m a.s.l. Seismic surveys as a complementary study (Kneisel and Hauck, 2008) were also conducted in the same area.

2. Regional setting

The mean annual air temperature (MAAT) at the Svalbard archipelago is negative. However, Spitsbergen experiences large variations in its temperature range. An increase from $-9\text{ }^{\circ}\text{C}$ to $-4\text{ }^{\circ}\text{C}$ was measured in the 1920s; later the temperature dropped again by $5\text{ }^{\circ}\text{C}$ and increased gradually until the end of the century (Humlum et al., 2003). For the first time since PPS meteorological records began, MAAT approached $0\text{ }^{\circ}\text{C}$ in 2016 (Łupikasza et al., 2014; Brauer et al., 2017). This warming

trend is visible in the depth of the seasonal freezing and thawing, the thickness of the active layer and the temperature of the permafrost (Isaksen et al., 2007; Isaksen et al., 2018).

The Fuglebekken catchment presents metamorphic bedrock consisting of calcite marbles, garnet-calcite-mica schists, and paragneisses from the Arikammen and Skoddefjellet formation of the Hecla Hoek succession (Birkenmajer, 1990; Czerny et al., 1993). Abrasion platforms with different-aged marine sediments have developed as a result of isostatic uplift. These elevated marine terraces have been highly transformed through nivation and erosion, and by solifluction and colluvial accumulation in the subslopes (Pekala, 1989). For this reason, the Quaternary sediment map of the western forefield of Hansbreen in Fig. 1c shows some transitional boundaries between subsequent sections. All geophysical measurements were carried out within the Arikammen formation.

The mouth of Hornsund fjord was deglaciated 17.4 ± 1.5 ka BP (Young et al., 2018), although the ice remained near the fjord mouth for several thousand years after deglaciation. This glacial episode is probably marked by the sill separating the Hornsund basin along the Wilczekodden–Höferpynten line (Kowalewski et al., 1991). A rapid, complete deglaciation approximately 13 ka BP left the inner Hornsund fjord open (Young et al., 2018; Birkenmajer and Olsson, 1997). Considering the closest glacier, Hansbreen the maximum range in the Holocene is defined by its Little Ice Age (LIA) ice-cored moraine with an age of ca. 10 ka BP for tills from the southern part of Hansbreen ice-cored moraine (Pekala, 1989). The LIA was the coldest period during the Holocene, when most of the glaciers reached their largest extent since the end of the Pleistocene (Svendsen and Mangerud, 1992; Mangerud and Landvik, 2007; Miller et al., 2010). A similar scenario was described for other sites, e.g. south Hornsund (Wójcik and Złajka, 1993). Treskelen (Birkenmajer and Olsson, 1997; Philipps et al., 2017), and Scottbreen (Mangerud and Landvik, 2007). The dating of the shells, found in marginal moraine, eskers, and the dirt cones at Werenskiöldbreen, indicates that the ice reached lesser extents before 12.1 cal ka BP than today (Birkenmajer and Olsson, 1998; Hormes et al., 2013). Consequently, Hansbreen did not influence the development of permafrost around Fuglebekken throughout the Holocene, but beginning from the deglaciation of Hornsund 13 ka BP (Young et al., 2018). Thus, during the time frame considered here, the main non-directly climatic development stimulus was based on coastline changes driven by isostatic movements and periglacial processes on the forefield of Hansbreen.

The isostatic uplift of Spitsbergen was irregular, both spatially and in its dynamics. It depended on the distribution of past ice-sheet loads and its deglaciation history (Landvik et al., 1998). It was also altered by local tectonic activity (Lindner et al., 1986). Consequently, independent marine terrace systems have developed in different areas across Svalbard. The review of Forman et al. (2004) on postglacial rebound suggests that the difference between the location of the coastline during the Late Weichselian and that of the Holocene can be used to estimate the initial ice-sheet load in the different regions. For North Hornsund, the Late Weichselian coastline sits at approximately 25 m a.s.l. (Birkenmajer and Olsson, 1970; Chmal, 1987); in North West Søkkapp Land it reaches 42 m a.s.l. (Salvigsen and Elgersma, 1993; Salvigsen, 2005); in Ytterdalen (Belsund) it is 64 m a.s.l. (Landvik et al., 1987); and in North West Wedel Jarsberg Land it is 55–60 m a.s.l. (Salvigsen et al., 1991). These data suggest that the ice load at the Last Glacial Maximum (18 ka BP) in North Hornsund was the lowest compared to surrounding areas (Chmal, 1987). In contrast, driftwood dated to almost 10 ka BP was found at 100 m elevation on Kongsøya (Salvigsen, 1981). Pekala's (1989) classification of marine terraces is used in this paper. This classification is based on findings published by Karczewski

Fig. 1. Study area: a) Svalbard archipelago; b) Southern part of Wedel-Jarsberg Land. DEM image based on data from the Norwegian Polar Institute (S0 Terrenmodell, Creative Commons); c) Map of the Quaternary deposits in the Hansbreen glacier western forefield, modified from Pekala (1989) including the ERT and MASW profile lines.

M. Glazer et al. / Geomorphology 358 (2020) 107128

3

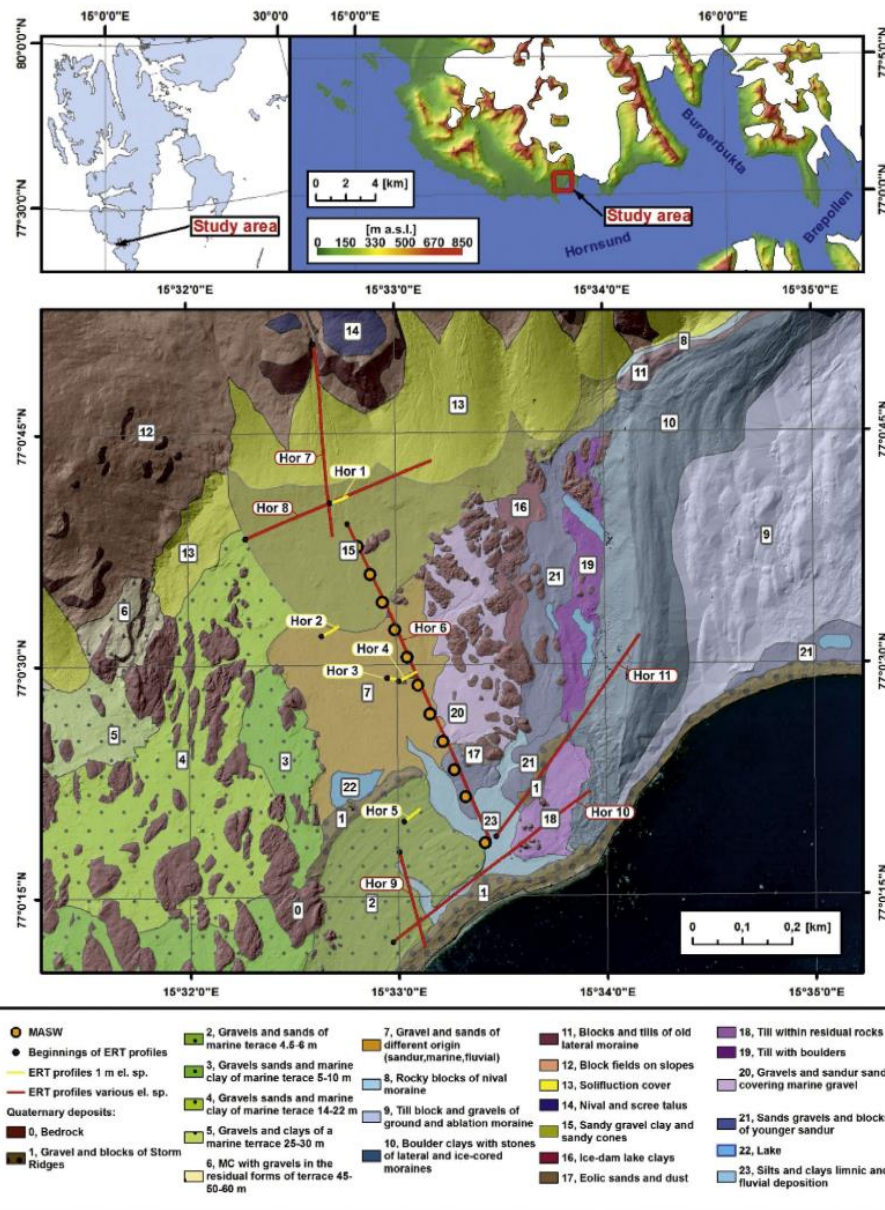


Table 1
The processing scheme applied for the data from Hor 6 profile.

| Number of Step | Processing steps |
|----------------|--|
| 1 | QC of the data set |
| 2 | Geometry building |
| 3 | Band pass filtering 2–50 Hz |
| 4 | F-K filtering |
| 5 | Dispersion curve modeling and picking |
| 6 | Manual picking uncertainty estimation |
| 7 | Smoothing of the dispersion curve |
| 9 | Inversion of the data using 100 Monte Carlo and 5000 Nearest neighborhood iterations |
| 10 | Evaluation of the results, and eventually initial model upgrade |
| 11 | Interpolation of the data to obtain 2D model |

et al. (1981), but with the generalization for local groups of marine terraces resulting from the high heterogeneity of sediments found in clusters of residual rocks (paleo-skerries) and erosional cuts (Fig. 1c). This creates a starting point for estimation of lateral sediment differentiation over pre-fluvial surface changes of Fuglebekken and provides a time frame for interpretation of the youngest Holocene marine terraces.

The relatively long gap (about 8 ka years) between the formation of the Holocene terraces between 8 and 12 m and 4.5–6 m a.s.l. may be explained by a submerged south Spitsbergen coast during that period (Birkenmajer and Olsson, 1970). The work of Chmiał published in 1987 provided four different ^{14}C dates for the 7–9 m a.s.l. terrace, suggesting a marine transgression lasting from 7.2 ka to at least 5 ka B.P., not surpassing the 9 m level. Similar transgressions have been identified in Ytterdalen (Belsund) (Landvik et al., 1987), North West Wedel Jarlsberg Land (Salvigsen et al., 1991) and North West Sørkapp Land (Salvigsen and Elgersma, 1993). On the other hand, a transgressive-regressive cycle was described for Bohemanflya and Erdmannflya with a different time frame, taking place between 8 and 7 ka BP (Salvigsen et al., 1990). The cause of this transgression and the different timings might be linked to a collapsing forebulge and the back migration of displaced mantle material (Fjeldskaar, 1994; Forman et al., 2004). These influences have been taken into consideration when preparing the expected Quaternary formations and marine limits maps of Fuglebekken used to analyse the ERT results.

3. Material and methods

3.1. DEM analysis

A digital elevation model (DEM) was constructed based on laser scanning data obtained in August 2015 using a Riegl VZ-6000 scanner. The scans were combined with an accuracy of 2 cm and spatially referenced using a UTM 33 N projected coordinate system on a EGM96 geoid with an accuracy of 30 cm. The point cloud was then converted into a TIN file. The average heights obtained using the algorithm to convert the data to TIN were used to estimate the missing values. The final product was converted to a raster with 0.5 m resolution. The obtained DEM was used to refine the Quaternary sediment map of Hansbreen's western foreground (Peckala, 1989), which was subsequently used to correlate the resistivity profiles and seismic survey and for data interpretation (Fig. 1c). Additional maps were constructed from the original to highlight the characteristics of the landform: slope inclination, slope aspect, hillshade, elevation and watershed delineation. An orthophotomap, generated from an infrared aerial photograph taken by the Norwegian Polar Institute in 1990, and subsequently colour altered to show the vegetation, was also used for the analysis (Jania et al., 2002). All the cartographic work was conducted in ArcGIS v. 10.4 software.

3.2. Electrical resistivity tomography

ERT is a method to determine the distribution of resistivity throughout a geological medium based on resistivity measurements taken at the surface. The method is well documented elsewhere (Dahlin, 2001; Schrott and Sass, 2008; Reynolds, 2011; Loke, 2018). It is a broadly applicable non-invasive ground investigation method, commonly used in permafrost research (Isaksen et al., 2002; Hauck et al., 2004; Kneisel et al., 2008; Hilbich et al., 2009; You et al., 2013; Kasprzak, 2015; Dobiński et al., 2017). This method does not provide direct information on the thermal state of the studied medium. Electrical conductivity in geological settings occurs primarily through ionic conductivity. Thus, groundwater content, mineralization and flow capacity are dominant factors influencing the resistivity of geological media. Consequently, the presence of ice significantly increases the resistivity of the medium. This is relatively easy to detect using ERT, and it could be used as an indicator of a phase transition between water and ice, implicitly at a temperature of around 0 °C. Thus, it is possible to determine indirectly the occurrence of sediments connected with the ice-bearing permafrost (i.e., ice-cemented, segregational, or dead ice blocks, as described by Everdingen, 1998, definition 269). Depending on the volume of the ice matrix, the rock type, pore system, and water saturation within the pores, permafrost resistivity can vary from few kΩm to MΩm (Telford et al., 1990; Marescot et al., 2003; Kneisel and Hauck, 2008). However, lack of the water's phase transition is not a definite indicator of the absence of permafrost. It cannot be detected in cryotic soils without ice, solely based on the resistivity criterion.

During the summer of 2015, 31 resistivity profiles were made in the area between PPS and the forefield of the Hansbreen using different lengths, distances between electrodes and orientation. Here we present the results from 11 of those, which are the most representative for the area and are at least partially located on the sedimentary cover of the Fuglebekken catchment (Fig. 1c). Their total length is 2180 m. For the ERT profile data, several electrode spacings were used: 0.5, 1.0, 2.0, and 5.0 m. Their distribution was aimed to ensure linkage between profiles with low-resolution covering large areas and high-resolution ones covering the study area only locally. Data were collected from all the profiles using two different measuring arrays, the Schlumberger and the dipole-dipole, differing in sensitivity for vertical and horizontal structures and in the strength of the signal (Loke, 2018). An ABEM Terrameter LS system was used for data acquisition. Most of the profiles were performed in an area characterized by good electrode-ground contact. Only in the higher parts of the alluvial cone and in areas directly on the shore was it necessary to remove thicker material at the surface and to place the electrodes in finer deposits.

Res2dinv v. 4.06.18 was used to invert the measurement data. For the topographic correction, the DEM model was utilized. More than 50 inversion procedures with their respective predetermined parameters were applied to test the behaviour of the resistivity models and to ensure a systematic approach. From this set, the models with the most accurate geological structure consistent with a priori knowledge were chosen for further interpretation. The type of inversion used, values of damping, and cut-off factors are specified for each model. Whenever the parameters applied were the default software values, this is indicated as "standard" alongside the inversion type. The constraints imposed by the inversion have an impact on the shape of the final models and the resistivity values of the structures surveyed, and therefore a common plane was required for comparisons (Table 2). To this end, the most stable and realistic inversion methods for the overall process, based on the geological structure assessed, were the robust data constraint (L1 norm) and the smooth model constraint (L2 norm) of the standard version. In an attempt to better understand the structure of the resistivity models, additional analysis of the Depth of investigation (DOI) index was made (Oldenburg and Li, 1999; Glazer et al., 2014; Loke, 2018). In addition, the effects observed in the models were reproduced using Res2Dmod and Res3Dmod software, to check

6

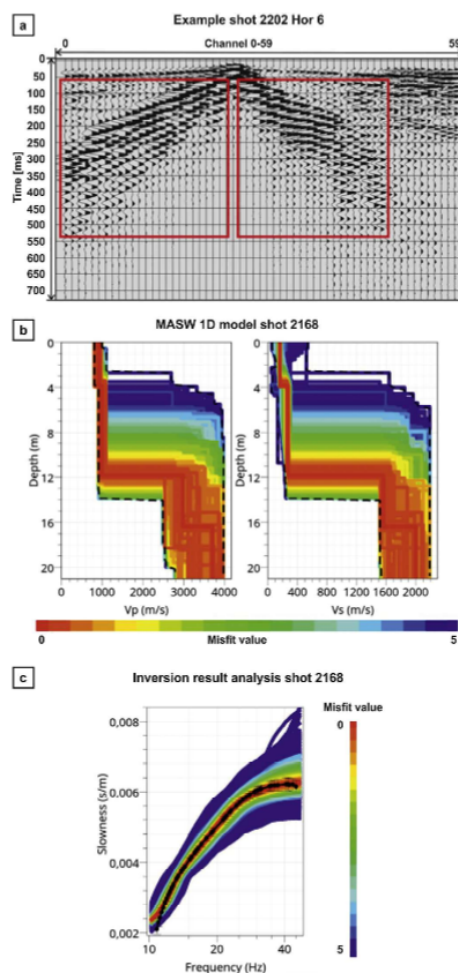
M. Glazer et al. / *Geomorphology* 358 (2020) 107128

Fig. 2. a) Example of a wave field recorded on profile Hor 6. The Rayleigh surface (red windows); b) Example of the single 1D model. Both VP and VS models were linked using a velocity scalar. The modelled max depth range was locked to 20 m, below that depth the model was unreliable; c) Results of the inversion process. The combination of a Monte Carlo approach with a more precise fitting using the nearest neighborhood method allowed obtaining a good correlation between the real and theoretical dispersion curves. (For interpretation of the references to colour in this figure legend, the reader is referred to the web version of this article.)

4.1. Short high-resolution profiles

4.1.1. Hor 1 (40 m) – distal part of a cone

The model consists of three horizontal layers (Fig. 4a). Two from the surface reach resistivity values in the range of 1–2.2 and 0.4–0.8 kΩm,

respectively. At the bottom is a sharp boarder with high-resistivity body over 4 kΩm. Its depth is considerably greater than the active layer thickness described in the interpretation key at the beginning of this section. This lower body still can be explained by the ice-bearing permafrost as the southern slope exposition and thermo-erosion caused by the presence of running watercourses observed near this site. It is expected to increase the depth of the permafrost table. The upper two resistivity layers are consistently loose sediments within an active layer distinguished by the water saturation within it.

4.1.2. Hor 2 (40 m) and 3 (20 m) – floodplain

Profile Hor 2 (Fig. 4b) (see also Kula et al., 2018) possesses two distinct horizons. The first one is characterized by very low resistivity values in the range 0.15–0.4 kΩm. At a the depth of 1.5 m the high-resistivity body appears, with values varying between 6 and 40 kΩm. This follows the initial assumptions about ice-bearing structure in loose sediments; therefore the lower body is identified as permafrost. It should be noted that it is not homogeneous, thus providing information that ice content may vary drastically over small distances.

In the case of 0.5 m electrode spacing used on Hor 3 (Fig. 4c), it was possible to greatly increase the resolution of the resistivity model. Up to 1.5 m depth, low-resistivity complex is observed. It consists of three parts, of which the two outer ones range from 0.1 to 0.5 kΩm. Between them there are lenses that reach up to 1.5 kΩm arranged in a single horizon. Below that a complex high-resistivity body up to 15 kΩm emerges. Up to 1.5 m depth, this model can be identified as a succession of depositional sequences of sediments within the active layer and the permafrost table beneath it.

4.1.3. Hor 4 (40 m) – outcrop

This profile (Fig. 4d) partially crossed outcrops of residual rocks (Fig. 3f). The obtained alternate lenticular structure cannot be marked as ice-bearing permafrost as was the case of the nearby Hor 3 profile (Fig. 4c), ending approximately 8 m away from Hor 4. In this case, a synthetic model was built to investigate the origin of the observed results. The theoretical response of a profile over a paleo-skerry flanked by a thick sedimentary cover is presented in Fig. 5. This proves that the structure observed on Hor 4 can be obtained as a result of limited current penetration into the high-resistivity medium and its increased flow along the surrounding low-resistivity zone, in a function of the size and sensitivity of the measurement array and used. Therefore, a double sequence of high- and low-resistivity bodies appears at the profile transition directly in front of the outcrop, between 14 m and 16 m of the profile length. The anomaly found in the eastern part, reaching 30 kΩm, is similar to this case. Observed effects are related only to the local presence of bedrock.

4.1.4. Hor 5 (40 m) – marine terrace 4.5–6 m

This profile (Fig. 4e) was located on the youngest elevated marine terrace built of sands and gravels, covered with ice-rafter debris (Fig. 3a).

Up to 5 m from the surface there is a relatively high-resistivity complex that possesses distinguishable horizons which can be grouped in two ranges: 2.5–7 and 0.5–1 kΩm. The uppermost layer shows signs of significant gradation from the start to the end of this profile. Beneath 5 m depth this complex rapidly ends and is replaced by a low-resistivity horizon below 0.1 kΩm. In this model there is no structure that can be identified as ice-bearing permafrost. A high-resistivity sequence is affiliated with dry marine sediments. The underlying extremely low-resistivity structure is an effect of seawater infiltration.

4.2. Hor 6 (700 m) – main profile through Fuglebekken

Resistivity models based on Schlumberger and the dipole-dipole arrays (Fig. 6a and b) show a significant inconsistency at a distance of

M. Glazer et al. / *Geomorphology* 358 (2020) 107128

7

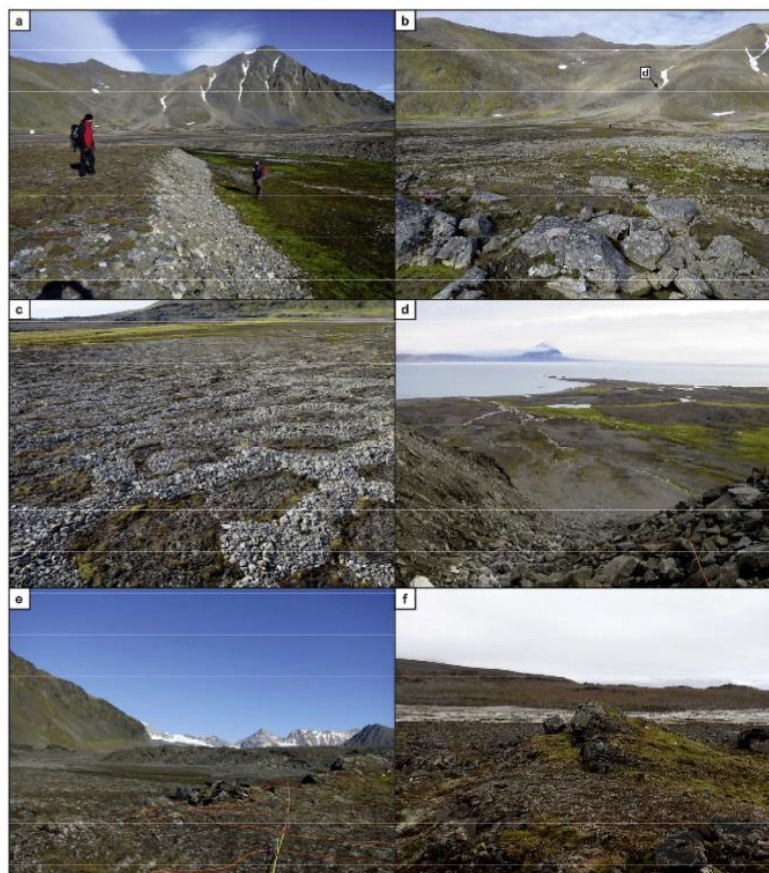


Fig. 3. a) Surface drainage erosional cut into the marine terrace found 4.5–6 m a.s.l. Location of the profile Hor 1; b) Weathered outcrop along with the profile Hor 6 including the location where photograph “d” was taken from; c) Patterned ground near the profile Hor 3; d) View of the Fuglebekken catchment from the beginning of the profile Hor7, right under a snow patch; e) Profile Hor 4 over an outcrop with a sedimentary cover and f) Different view on the same outcrop, as seen in photo “e”.

140–340 m (zone marked on Fig. 6a). In this area, a reduction of the sedimentary cover is clear and its thickness relates to the local occurrence of a bedrock outcrop (Fig. 1c; Fig. 3b and f). The mentioned effect results from the electrode array’s different sensitivities to horizontal and vertical changes of the structure and their signal strength (Loke, 2018). As the dipole–dipole array possesses higher horizontal resolution, in Fig. 6b resistivity structures that can be associated with the top of the bedrock are marked. This boundary is poorly constrained in terms of real depth due to the electrode spacing used (5 m), a high-resistivity contrast near the surface, and most probably varied bedrock topography. To assess areas where the inversion parameters strongly influence the resulting models, i.e., those not well constrained by the data, the DOI index was used (Fig. 6c). A coefficient value above 0.2 is assumed to determine inversion artefacts (Oldenburg and Li, 1999). On this basis, reliability

of the model is assumed to be down to ~40 m a.s.l. in the central and southern parts of the profile and ~20 m a.s.l. in the northern part.

A 2D synthetic modeling methodology was developed to differentiate between ice-bearing permafrost in non-lithified sediments and the solid bedrock. Fig. 7a shows a simulated geological medium with an undulated 1.5 m thick highly conductive active layer. The results can be found in Fig. 7b. For simplicity, ice-bearing permafrost sediments and bedrock are shown together, due to the relatively small differences in conductivity between them compared to the wet active layer. The sedimentary structure and the bedrock are not clearly distinguished in Hor 6, and the reliable depth range of resistivity models is significantly reduced. Therefore, to qualitatively analyse the resistivity values obtained from those layers identified as ice-bearing permafrost, areas with a thin sedimentary cover must be excluded. This prevents the

8

M. Glazer et al. / Geomorphology 358 (2020) 107128

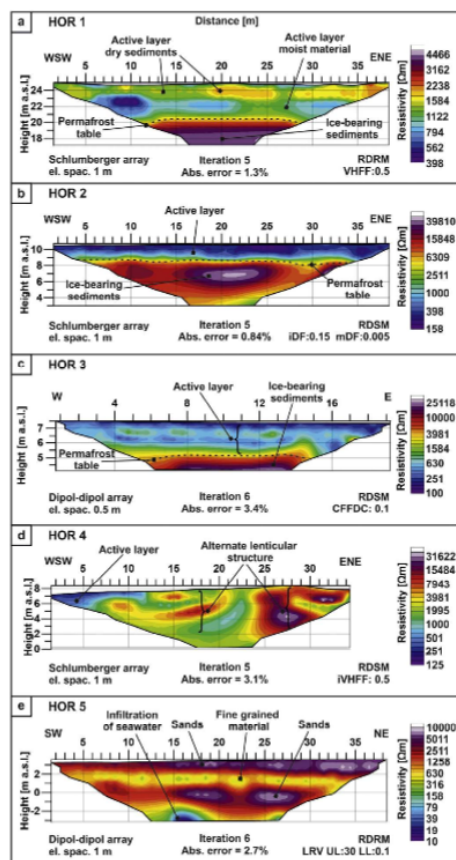


Fig. 4. High resolution ERT profiles presented in order from North to South. LRV: Limit Resistivity Values; UL: upper limit; LL: lower limit; VHFF: Vertical to horizontal flares filter ratio; CFFDC: cutoff factor for data constrain; IDFF: initial damping factor and mDF: minimum damping factor.

wrong correlation of sediments with high ice content in cases when high resistivity values are affected mainly by bedrock. The S-wave velocity model from MASW (Fig. 8) allows tracing the general bedrock top trend. This is a bimodal model, and the depth where the change occurs varies depending on the length of the profile, ranging from 3 m to 15 m below the surface. Velocities within the 100–500 m/s range are identified as non-lithified sedimentary rocks. The interval 1300–2100 m/s indicates the propagation of the S wave through the bedrock. The thickest sedimentary cover appears near the fjord. Discrepancies in resistivity models are found in those areas where the depth of velocity change becomes clearly shallower.

In Fig. 6 d resistivity model originating from the near-surface data set is presented. It includes a superimposed line of rapid velocity change obtained using MASW. A correlation between the type of structure and the bedrock depth allows us to qualitatively analyse

only areas with a thick sedimentary cover. Thus we exclude from an attempt to analyse ice-bearing permafrost content the region between 175 m and 300 m in the Hor 6 profile in which bedrock is significantly shallower. It is possible to distinguish the permafrost table on this profile from its beginning up to 520 m with the exclusion of the previously mentioned area.

4.3. Other long profiles

4.3.1. Hor 7 (400 m) – axis of a cone

The resistivity model (Fig. 9a) chosen for this profile was the one providing the most reliable representation of the general geological structure. However, this was at the cost of a significant structure unification within its two distinct parts. The first one, with relatively low values in the range of 3 to 12 kΩm, is present near the surface. Based on the presented model, it possesses from 2.5 to 15 m thickness and covers a massive high-resistivity structure that varies from 15 to 50 kΩm. This distribution of electrical properties is related to sedimentary cover of the cone and underlying bedrock. Around 150 m along the profile, a lens presenting a resistivity of up to 12 kΩm is visible within the slope sediments. It suggests the presence of buried snowpack or standard ice-bearing permafrost. Regardless of the hypothesis adopted, its occurrence can be associated with an increased thickness of the cone and a potentially deeper intra-permafrost flow of water. The high-resistivity lens further down the slope, between 240 and 290 m of the profile, is an anomaly identified by synthetic modeling as resurfacing bedrock covered by only a thin layer of sediments. Indications of this bedrock morphology, however, are not found at the slope surface. Beginning from 300 m, the lower part of this profile changes in nature. High-resistivity complex identified as bedrock is now covered by ice-bearing sediments, as was shown on Hor 1. This prevents the determination of bedrock depth. On this model, that change is connected only to a slight drop in resistivity and a significant reduction of the upper layer thickness.

4.3.2. Hor 8 (400 m) – distal part of a cone and floodplain

This model poses a lenticular structure in which its highest resistivity values are reached. They range from 10 to 40 kΩm. Up to 250 m of the profile, lenses are separated by narrow low-resistivity 0.05–0.5 kΩm anomalies. Beyond that area, the lenticular structure transforms to a continuous form. The created gaps are correlated with the presence of water streams along the slope. Connection to Hor 1 allows identification of ice-bearing formations. A general decrease in resistivity towards the floodplain in the west/south-west suggests a significant increase in the thickness of the active layer of the permafrost in this area, combined with an increase in water retention in sediments. Consequently, the high-resistivity medium disappears below 12 m depth on the ERT models in the West/South West direction. Furthermore, a decrease in the number of water streams and the level of water retention of active layer following the east/north-east direction leads to an increased continuity and thickness in the ice-bearing permafrost. This, in turn, results in ERT profiles with the characteristic underlying structures predicted by the synthetic models. As the high resistivity values peak around 40 kΩm, it is very likely that sediment cover over bedrock in these places is significantly reduced. The Hor 1 profile confirms a local lowering of the bottom of the active layer. It should be noted, however, that the high-resolution profile does not directly overlap with the resistivity reduction region of Hor 8, suggesting that the active layer might be much thicker locally as a result of the water course impact.

4.3.3. Hor 9 (200 m) – marine terrace 4.5–6 m

Fig. 9c displays an uppermost layer ranging between 1 and 7 kΩm. Beneath it is massive low-resistivity structure that does not exceed 0.1 kΩm. Within it, locally at 12–25 m depth, a structure that rises up to 0.4 kΩm appears. In accordance with the high-resolution profile of

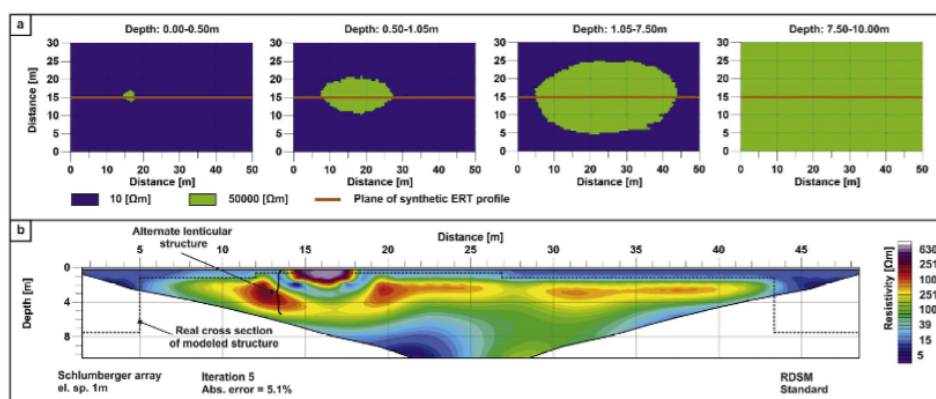


Fig. 5. 3D synthetic resistivity model of the paleo-skerry surrounded by high conductivity sediments. a) Depth profiles; b) 2D resistivity model created from data gathered from the marked plane.

Hor 5 (Fig. 4e), the near-surface high-resistivity structure is a sequence of sands and gravels without ice-bearing permafrost, but due to the low resolution of this profile it is not possible to distinguish them. A low-resistivity body in the lower part of model correlates with the presence of seawater in the sediments. A 0.4 kΩm structure within it might be connected with rising bedrock.

4.3.4. Hor 10 (500 m) and 211 (500 m) — marine terrace 4.5–6 m and ice-cored moraine

The area 300–500 m along Hor 10 and 80–260 m along Hor 11 follows a platform of residual rocks with a thin overlying layer of till. The Hansbreen moraine, reaching this place at the beginning of the 20th century, had been larger than today. Since that time it was considerably degraded and eroded in this part due to marine influence, leaving tills between residual rocks (Fig. 1c, designations 18 and 19). On both profiles passing through this area the alternating lenticular structure is observed. As a whole it is considered to be connected to solid rock formations (marked on Fig. 9d and e). Beside that area, constituting a large part of both profiles, is a massive low-resistivity body. Its values do not exceed 0.05 kΩm, which is related to the presence of seawater. Within it, on Hor 10, local anomalies that rise up to 0.5 kΩm have been marked as the possible rise of bedrock. The whole model below 30 m depth does not provide any useful information in this regard. Over the entire Hor 10 profile (Fig. 9d) no structures suggesting the presence of ice-bearing permafrost can be found. On the other hand between 300 m and 500 m of Hor 11 (Fig. 9e), on the ice-cored moraine it is confirmed how in conditions of low-resolution models the active layer for ice-rich permafrost should appear on ERT. Lenticular effects known from synthetic modeling have not been found here as the resistivity contrasts are higher and the structure itself is massive and uniform in the upper parts.

4.4. Qualitative analysis of the ERT results

In the initial assumptions, the high-resolution resistivity profiles were aimed to classify the occurrence of ice-bearing permafrost in the Fuglebekken catchment based on objective resistivity data. However, the data revealed a higher than expected variation of local conditions. For example, the active layer visible on Hor 1 (Fig. 4a) reaches far deeper than that in other places due to an

intense water flow within the cone, clearly reducing the level of resistivity in the lower layer. The Hor 3 profile (Fig. 4c) is subjected to different minimal electrode spacing, while Hor 4 passes directly over an outcrop (Fig. 3e). These profiles have contributed greatly to the understanding of other resistivity model structures, but had to be excluded from the general categorization due to a large variability in their characteristics.

The longest profiles were used to qualitatively analyse the relative occurrence of ice-bearing permafrost in the study area. To this end, it was assumed that we could make overall generalizations regarding the geological medium, allowing the identification of large areas with similar features and resistivity values. The assessment of the relative ice content in the near-surface permafrost refers only to the sedimentary cover. The resistivity models used for the correlations were obtained by application of the RDSM standard inversion on the Schlumberger array datasets. Profiles are categorized separately depending on ice-bearing permafrost structural presence or absence. In the case of confirmed permafrost, distinctive resistivity zones have been classified as characterized by very high (VH), high (H), medium (M), and low (L) values. The following ranges have been implemented: $VH > 30 \text{ k}\Omega\text{m} > H > 10 \text{ k}\Omega\text{m} > M > 2.5 \text{ k}\Omega\text{m} > L$. They are based on values obtained from distinctive surface areas on Hor 6. In the case of an absent or doubtful ice-bearing sedimentary cover, the focus was set on the distinction only between high and low resistivity values. In that case, the boundary between them was set at 3 kΩm.

The full classification of the resistivity models for the ice-bearing permafrost in the sedimentary cover (Table 2) is presented on a map together with the variability of marine limits within Fuglebekken and late Holocene Hansbreen sediments and its direct influence on this area (Fig. 10). Due to the composition of the Pleistocene terraces, these ranges should be considered as the minimum sea level based on dated sediments (Birkenmajer, 1960; Chmäl, 1987; Pekala, 1989; Lindner et al., 1991). The resistivity values clearly decrease in subsequent zones following a regular pattern, from Fugleberget to the youngest marine terrace. An area in the VH range is located above the oldest Holocene marine terrace. Below it, there are two successive H and M boundaries up to a storm ridge terrace, 4.5–6 m a.s.l. Within that 4.5–6 m a.s.l. area, ice-bearing permafrost is not found based on resistivity data.

10

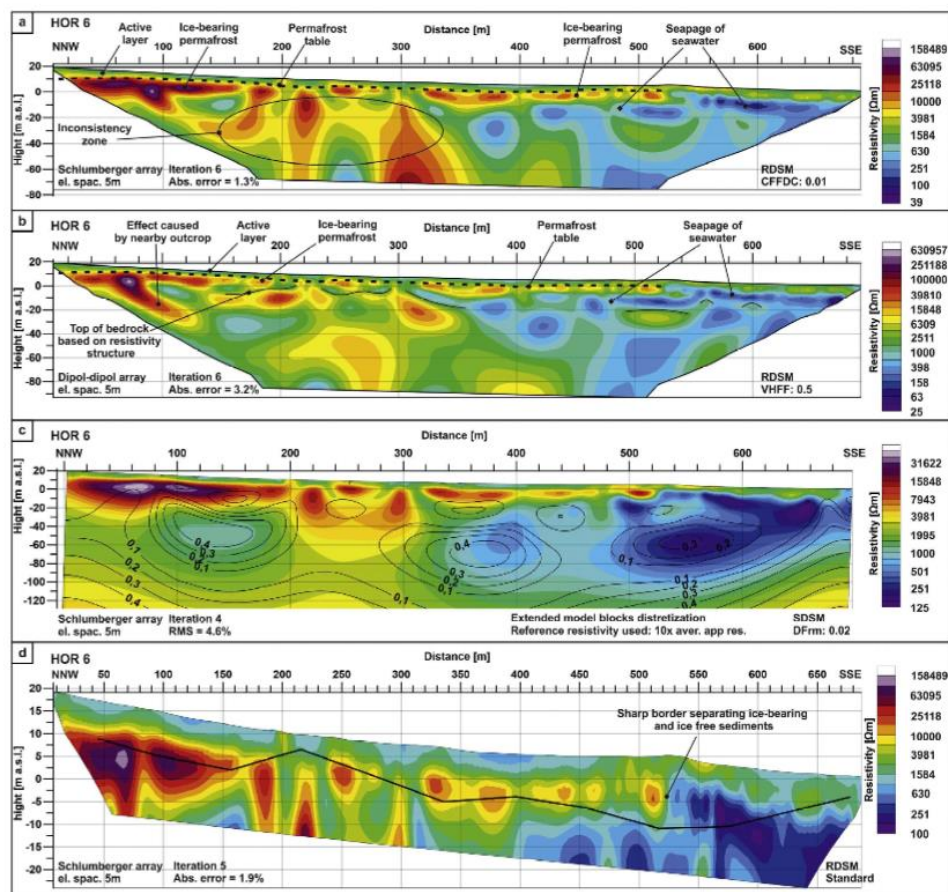
M. Glazer et al. / *Geomorphology* 358 (2020) 107128

Fig. 6. Hor6 ERT profile analysed using: a) Schlumberger array; b) Dipol-dipol array; c) DOI map overlap with the resistivity model used for its creation; d) Schlumberger array data without deeper levels of data points overlapping with the MASW bedrock surface (black line). RDSM: robust data smooth model; SDSM: smooth data smooth model; VHF: Vertical to horizontal flattening filter ratio; CFFDC: cutoff factor for data constrain and DFM: damping factor for the reference model.

5. Discussion

This chapter presents the range and variability of permafrost and the active layer in the profile from the mountain environment to the sea shore. It is associated with forms such as talus and proluvial cone, then the Late Quaternary marine terraces with ice-bearing permafrost, and marine terrace 4.5–6 m a.s.l. without ice-bearing permafrost. Sea-water infiltration is also considered. The chapter ends with a description of limitations and accuracy of the applied ERT method.

5.1. Talus and proluvial cone

Within the cone, almost throughout the entire profile, Hor 7 maintains the VH category (Fig. 10), due to solid bedrock (Fig. 9a). The high

resistivity values most probably relate to the presence of permafrost, where the ice is preventing the effective infiltration of water into bedrock cracks. Within the sedimentary cover itself, the relatively low resistivity values suggest a high content of fine material and a significant level of water retention. This is confirmed by observations of water streams not far from this profile. Some of them would disappear in the proximity of Hor 7 only to appear again further downstream, over 50 m away. The presence of high-resistivity lens (Fig. 9a) suggest that intra-permafrost water flow, and potentially the presence of buried snow that would mean periods of rapid material accumulation (Humlum, 2005), play a significant role in shaping the structure of the permafrost within the cone. This concept is shown in Fig. 11a. As near-sea-level permafrost is commonly considered to be from the late Holocene, which is evidenced by the data from ice wedges and pingos,

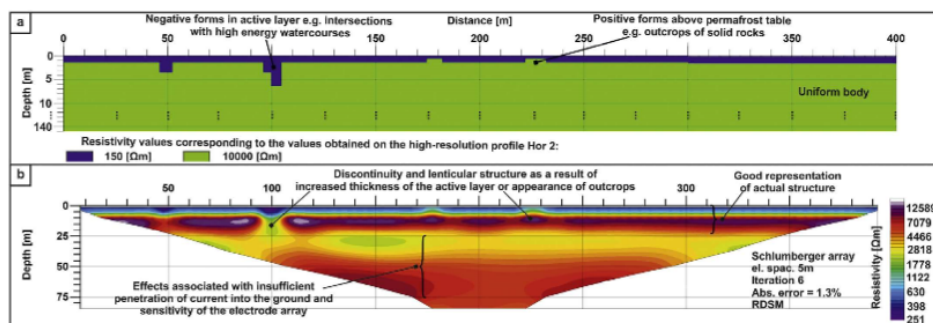


Fig. 7. 2D synthetic model to test the influence of a shallow high conductive layer on the deeper homogeneous high resistive structure. a) Simulated medium; b) Resistivity model based on data from the forward modeling.

whose origins are dated at ca. 3 ka BP (Svensson, 1971; Oliva et al., 2014), it is still an open question whether the older permafrost formulated before the Holocene Climatic Optimum could have locally survived under developing sedimentary cover of the cone. At the foot of the slope, the VH resistivity zone includes a cover of strictly ice-bearing deposits. In addition, Hor 8 shows different resistivity values for permafrost than those obtained from the lower parts of the perpendicular Hor 7 transect (Fig. 10). This is mainly the consequence of a large number of water streams running along the western section of Hor 8 and, the presence of a thicker active layer with increased water retention. Furthermore, resistivity values can differ depending on the orientation of profile lines intersecting the same non-symmetric 3D geological structure. As an extreme example of such influence, an ERT study on ice-core moraine of Theodul glacier (Switzerland) can be used (Hauck and Mühl, 2003).

5.2. Late Quaternary marine terraces with ice-bearing permafrost

There is a clear correlation between the zonation of the early Holocene marine range and the boundary separating the VH from the H resistivity zone (Fig. 10). Taking into consideration the thickness of the sediments over Fuglebekken from MASW, we can suspect that these values represent the nature of the sedimentary cover, which largely is not altered by the presence of solid bedrock. In this location, only a transitional gradient between the colluvial and alluvial deposits is observed on the cone surface (Fig. 1c). A similar situation appears between the H and M resistivity ranges. Relatively sharp boundaries between resistivity zones can be explained by environmental factors such as the presence of water streams, type of terrain, snow cover thickness, and geological history of the area. Fig. 10 shows two factors spatially correlating with the resistivity complexes and explaining the

sharp transitions between them. These factors are a sea transgression occurring at 7–5 ka BP and water drainage from Hansbreen.

Fjord waters could still influence the terrain beyond the marked 7–5 ka BP transgression line, potentially explaining the transition between the VH and the H zones. In addition, two distinct episodes can be identified in the outflow of waters from Hansbreen, represented by the oldest and the youngest parts of the sandur. These two episodes are also associated with the presence of ice-dam lake clays. At one point, the outflow was intense enough to break the storm ridge of the marine terrace found at 4.5–6 m a.s.l. On the other hand, the flow of glacial waters through the 14–25 m marine terrace system in the central part of Fuglebergsletta is still unclear (Karczewski et al., 1981; Pękala, 1989).

In the cases of both the marine transgression and outflow from the Hansbreen hypothesis, there was a high-energy water flow linked to a fast energy exchange, removing the silty and clayey sediment cover. The cover was subsequently replaced with thicker fractions, potentially increasing the infiltration of water from streams or snowmelt, concomitantly intensifying the degradation of the ice content of the sediments in the long term. The smallest fractions within the sedimentary cover can also play a significant role in increasing surface drainage (Sobota et al., 2016). This also explains the differences between the H and the M zones (Fig. 10). While the H zone is characterized by extensive outflow from a large area and the deposition of silt, the M zone is located in a dry slight elevation dominated by sands with a theoretically greater ice accumulation potential. The fractional differentiation of the sediments directly over its surface was described by Szymański et al. (2013, 2016), which also shows a clear increase in the content of the smaller fractions in the direction of the cone slope. Thus, the differences in resistivity might be related to both factors: the potential of the sediment complexes to preserve ice-bearing permafrost, and the cycle of degradation–restoration of the finer fraction cover from high to low energy fluvial activity.

5.3. Marine terrace 4.5–6 m a.s.l.

The youngest elevated marine terrace, 4.5–6 m a.s.l., is substantially free of structures indicating ice-bearing permafrost (Fig. 10). However, in the eastern part (part of Hor 10 and 11), where solid bedrock is considered under a thin till layer among paleoskeries, permafrost certainly occurs there, which argues for the influence of modern climate (Brauer et al., 2017), since the time of release from the Hansbreen moraine and because of the lack of watercourses. However, this permafrost is unlikely to be identifiable using geophysical methods which are only able to identify the phase transformation of water. Only temperature measurements can confirm its presence.

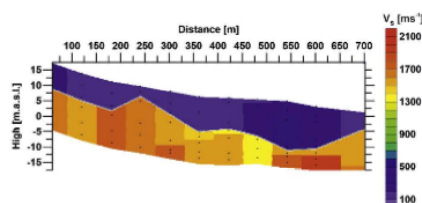


Fig. 8. 2D MASW shear wave velocity profile over the Hor 3 horizontal distances according to the ERT profile.

12

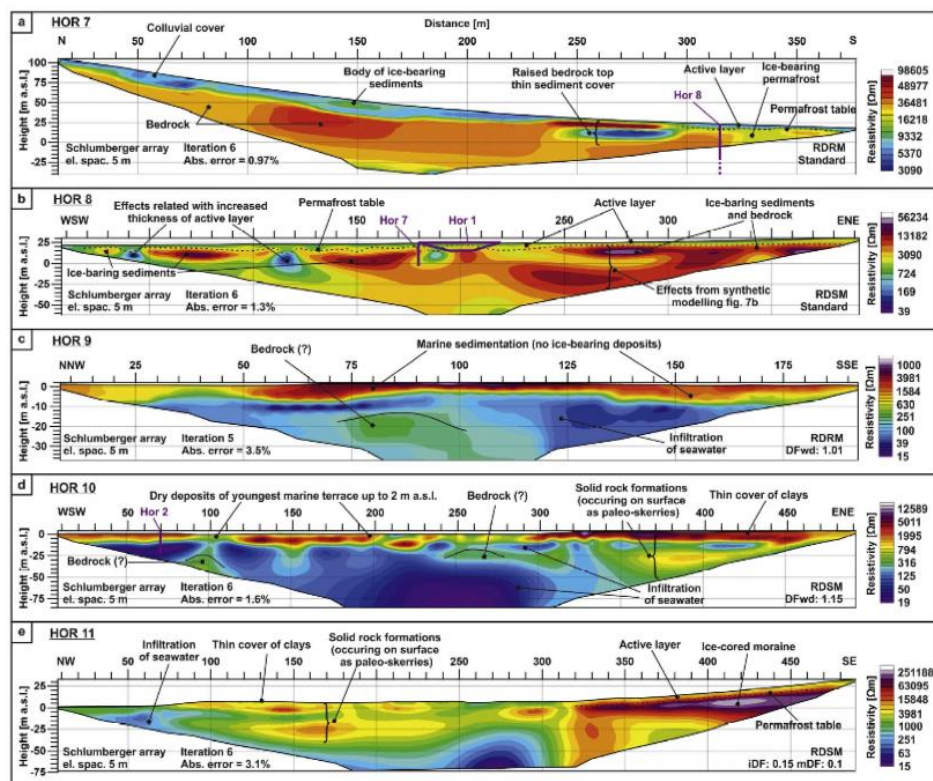
M. Glazer et al. / *Geomorphology* 358 (2020) 107128

Fig. 9. ERT profiles taken using different electrode spacing, presented in order from North to South. RDSM: Robust data smooth model; RDRM: Robust data robust model; VHHF: Vertical to horizontal flatness filter ratio; CFFDC: cutoff factor for data constrain; IDf: initial damping factor; mDF: minimum damping factor and DFwd: damping factor.

In the case of profiles found on the thicker marine deposits reaching up to 15 m below ground level, the alternating high resistivity layers on Hor 3 are associated with marine deposits, with its sequence representing the evolution of the area, taking into account a sea transgression occurring 7–5 ka BP (Karczewski et al., 1981; Chmal, 1987; Lindner et al., 1991). The underlying low resistivity layer, is a result of inland infiltration of seawater (Baranowski, 1968). In this case, the existence of a very thin layer of ice-bearing permafrost is very unlikely. A seismic refraction survey conducted near this measuring site and the lack of velocity change that could indicate increased ice content have been confirmed (Dobiński and Leszkiewicz, 2010).

This terrain was under water until ca. 1.0–0.7 ka BP. A similar exposition time on climate influence has been observed near Svea, where the surge of Paulabreen compressed the seabed sediments and lifted them above the sea level. Borehole temperature measurements indicate that the permafrost there was “warm”, with a temperature above -2.5°C below 20 m deep. These thermal conditions in the ground are not stable compared to the inland conditions (Gregersen and Eidsmoen, 1988).

Similar thermal settings are most likely to occur near the PPS (Wawrzyniak et al., 2016). Indeed, “warm permafrost” might form there as highly mineralized seawater infiltrates within the accumulated deposits while halting the development of an ice matrix. This would also explain why high-resistivity anomalies are not found near the seawater infiltration level. The marine terrace at 4.5–6 m a.s.l. (Fig. 6d) does not present an ice-bearing permafrost layer even in sediments above sea level. This could be explained by the absence of silt and clay fractions in the near-surface layer, due to a relatively recent sea regression and the absence of low-velocity watercourse sedimentation above the terrace, as nearby streams use existing cuts. This, in turn, strengthens the infiltration of rainwater and snowmelt throughout the coarse sea sediments, which results in the systematic melting and dissolving of the developing ice matrix. In addition, fast infiltration to the groundwater level, including marine intrusions, further prevents the retention of sufficiently high freshwater content within the sediments to create an ice-bearing layer. However, even if the resistivity models do not predict the presence of ice-bearing permafrost here either, the presence of a cryotic-state permafrost layer above the groundwater table cannot be

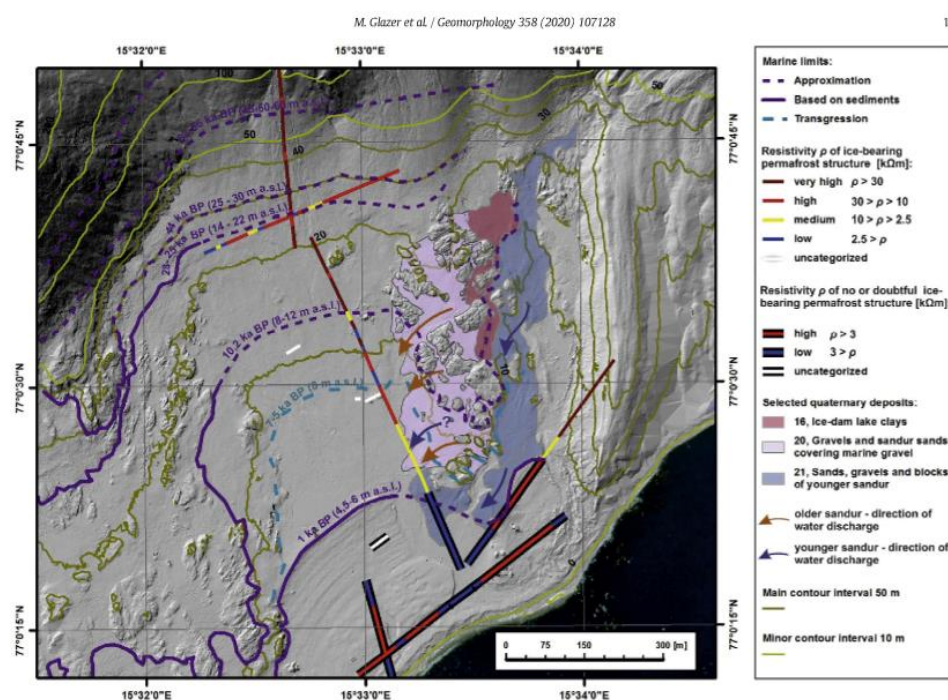


Fig. 10. Map presenting a section of the ERT models overlapping the expected Quaternary marine limits and the late Holocene fluvio-glacial/glaciolacustrine sediments from Hansbreen. The comparison has been made over the first high resistivity layer on top of the base models (Table 1).

excluded. Actually, there are no borehole temperature data from areas of preservation and interaction of permafrost within sediments with inland infiltration of fjord waters; therefore, the cryotic permafrost base is marked only as two purely hypothetical variants (Fig. 11b).

5.4. Seawater infiltration

Seawater infiltration is most likely the predominant factor altering the structure of the permafrost in the shore of the studied area, preventing the possibility of clear determination of its spatial occurrence (Baranowski, 1968; Kasprzak et al., 2017). The extent of seawater infiltration is assessed here by using the Hor 6 resistivity model, which suggests that it could reach up to 450 m inland. It should be emphasized that the study area was configured as a bay in a geologically recent past, still showing a considerably thick marine sediment cover. Fjord-water intrusions would lower the freezing point of the aquifer, potentially influencing the temperature of the layer where it is found, especially during the summer when the temperature of the bottom water in Isbjørnhamna can be as high as 3–4 °C (Wiśniewska-Wojtasik, 2005; Promińska et al., 2017). Several studies on the thermal characteristics of the active layer and the uppermost permafrost layer near the PPS show a series of temperature increase episodes, demonstrating the presence of a basal heat supply in shallow boreholes performed during winter (Baranowski, 1968; Jahn, 1982; Chmal et al., 1988). Consequently, the work by Kasprzak et al. (2017) postulated the existence of a bottom active layer, based on ERT measurements taken at two-year intervals, and defined as “the low layer of ground under the

permafrost in coastal zone, that thaws each summer and refreezes each fall in accordance with impact of seawater and permafrost body conditions”. This leads to the fair assumption that in the Fuglebekken region, a coastal “warm permafrost” (as defined by Gregersen and Eidsmoen, 1988) is thermally active (active permafrost) in the transition zone between land and sea, due to a significant infiltration of seawater inland (Harris, 2001; Dobiński, 2011b).

The rate of water exchange must also be considered when discussing the potential impact of seawater intrusion into land. In an extreme case, assuming a hypothetical factor forcing a constant flow inland and the high filtration coefficient characteristic of gravel sediments, overcoming a distance of approximately 500 m would take almost 3.8 days. The presence of seawater within the sedimentary cover of marine terraces 4.5–6 m a.s.l. is undeniable; however, which factors would have forced this inland seawater flow and the duration is perhaps less obvious. Some factors, for example, are storm surges, tidal surges or local wind-dependent currents. During a particularly heavy storm in 2011, ice growlers were thrown towards the PPS area reaching up to 40 m inland (Bania and Wawrzyniak, 2011). This indirectly shows the potential for water exchange on land. The duration of such events and the necessity of a partial replacement of water in the sediment cover must have significantly limited its range. However, this water exchange still has the potential of influencing the temperature over a larger area. The salt-water ingress into coastal “warm” permafrost might alter its state into a purely cryotic one, depriving it of the presence of ice. Furthermore, the time and the intensity of the infiltration can also alter the base of the permafrost. Considering the changes the coastline had

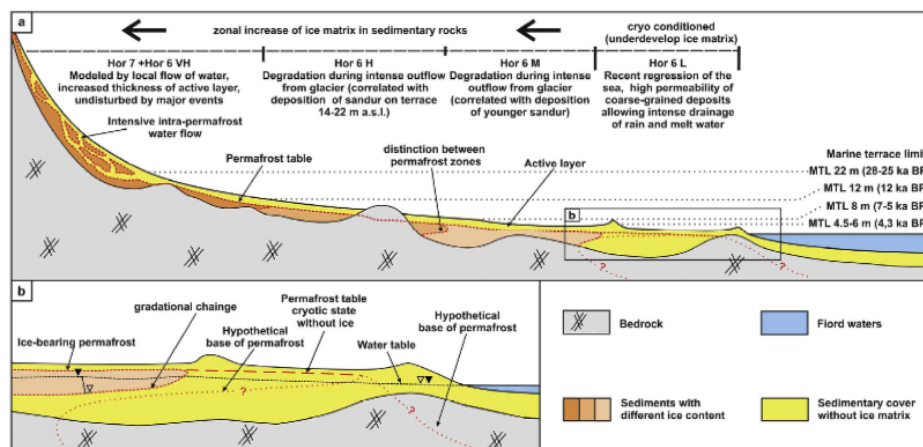


Fig. 11. Simplified model of the permafrost distribution across the Fuglebekken catchment based on ERT studies.

experienced throughout the Holocene, and the start time of the neoglaciation period, it is possible that the Fuglebekken sediment cover never fully exchanged its seawater for freshwater within the aquifer. Indeed, the development of an ice-bearing permafrost layer at the ground surface following a sea level decrease approximately 5 ka BP would have significantly obstructed this process.

5.5. Limitations of the ERT method in periglacial studies

In relation to the thermal state of the ground, by using ERT methods it is possible to identify unfrozen from frozen ground and the resistivity values which differ by 2 to 5 orders of magnitude, reaching several hundred of $\text{K}\Omega\text{m}$ at its peak. Furthermore, even frozen sediments show a wide range of resistivity values (MacKay, 1969; Larin et al., 1978; Telford et al., 1990; Kneisel and Hauck, 2008; You et al., 2013). It is also worth noting that the phase transition of water does not always happen at 0°C , and significant mineralization can lower the freezing temperature. For seawater, for example, it is ca. -1.8°C . For water present in fine-grained sediments, capillarity and adsorption effects can reduce the freezing point even further (Williams and Smith, 1989; Overduin et al., 2012). Gregersen et al. (1983) reported on laboratory studies on saline clay from Svea where over 40% of the water content remained unfrozen at -6°C . This means that ERT enables the assessment of the thermal conditions of soil only in the presence of ice-bearing permafrost and larger ice bodies. The cryotic state is a synonym for permafrost but is also a broader term; therefore, soil in the cryotic state with no ice will not show distinctive high resistivity values. In addition, during interpretation it is necessary to take into consideration effects related with the three-dimensional geological structure and its complexity, the decrease in ERT resolution with depth, possible current penetration issues, and the non-uniqueness of the generated models (Oldenburg and Li, 1999; Mościcki, 2010; Loke, 2018).

Profiles 2, 7, 8, and partially 6, 10, and 11 show a decrease in resistivity underneath a high-resistivity shallow subsurface; however, these high-resistivity structures do not necessarily represent actual geological structures. This rather shows an increased lateral propagation of the current flow and response of electrode array sensitivity to this effect, as shown by the synthetic models (Figs. 5 and 7). The identification of these anomalies may be a useful indicator of the variability of the

surface conditions, as seen in the Hor 8 profile (Fig. 9b) and parts of Hor 11 on the maximum range limit of the Hansbreen LIA moraine (Fig. 9e). Thus, we are convinced that this effect is correctly diagnosed by implementing synthetic models created in accordance with resistivity structure from high-resolution profiles. In Svalbard, where permafrost conditions prevail and its estimated thickness is known in general (Humlum et al., 2003), this effect explains the decrease in resistivity within the bedrock underneath the ice-bearing Fuglebekken sedimentary cover, rather than the thickness or form of permafrost itself. In this context, it is worth evaluating other works using geoelectrical methods for periglacial zone studies. For example, the results by Harada and Yoshikawa (1998) from electrical resistivity soundings lead to an estimation of the permafrost thickness in Moskuslagoon of 22 m. This is in contrast to other estimations from the north side of Adventfjord, opposite to Longyearbyen, where the thickness of the permafrost was estimated to be ca. 100 m at the seashore, based on temperature data from boreholes by Gregersen and Eidsmoen (1988). General geological information is essential to validate the resistivity results obtained using ERT in permafrost studies, as well as incorporating other complementary geophysical methods.

6. Conclusions

This work provides insight into the occurrence and nature of the permafrost, both ice-bearing and cryotic, in the area of Hornsund, following an altitudinal gradient from a mountain area to a system of uplifted marine terraces along the coast. Based on geophysical investigations, we draw the following conclusions:

- 1) Different ice-bearing sediment formations appear within the late Quaternary marine terraces. These formations are most likely influenced by the presence of nearby glacial ice and its degradation. Intense events in the form of glacier outflows and the creation of sand covers were also important in this case. A maritime transgression has also been suggested as a significant factor influencing the presence and nature of the permafrost in the area, potentially altering the ice-accumulating abilities of different sediment zones. This latter hypothesis would require additional studies.

- 2) Permafrost development depends significantly on the presence of surface watercourses. Higher velocity flows are associated with its degradation, while lower velocity flows lead to silt and clay deposition, which in turn may increase water outflow reducing water infiltration within the active layer, and also reducing the degradation of the permafrost. Hydrological changes associated with warming will significantly influence the nature and form of permafrost aggradations.
- 3) The youngest uplifted marine terrace, 4.5–6 m a.s.l., did not develop ice-bearing permafrost. However, the presence of permafrost in a cryotic form cannot be excluded.
- 4) The MASW is proven to be a useful method in the imaging of the sedimentary cover over the bedrock. Here, a 2D model of the subsurface allows identifying two geological layers with a strong velocity contrast between them, and helps in the identification of ice-bearing permafrost. These results suggest that the sedimentary cover of the central part of Fuglebekken can locally reach up to 15 m in thickness.
- 5) A significant range of seawater infiltration is also noticeable within the Fuglebekken sedimentary cover, confirming other studies suggesting a significant impact of seawater on coastal permafrost formation and evolution.
- 6) The zonality of ice-bearing sediments, including their small thickness within the youngest elevated marine terraces and the presence of active permafrost, makes the permafrost in the area of Fuglebekken very sensitive to the effects of climate change.
- 7) The talus and the proluvial cone present a heterogeneous structure responsible for a significant intra-permafrost flow of water. This state can potentially intensify the solifluction movements in the near future, as a response to climate warming.
- 8) Ice lenses are found in the higher parts of the cones. These potentially represent preserved buried snow, from avalanches in the stage of increased cone development.
- 9) Thawing water and meteoric water flows at the cone foothills can significantly increase the thickness of the active layer.

Declaration of competing interest

The authors declare that they have no known competing financial interests or personal relationships that could have appeared to influence the work reported in this paper.

Acknowledgements

This article is one of the results of research projects funded by the National Science Centre, Poland (NCN) DEC-2012/07/B/ST10/04268 and NCN UMO-2016/21/B/ST10/02509. Special thanks for help in acquiring ERT field data to Mr. Damian Kula. We would like to show our appreciation to two anonymous reviewers for their suggestions and comments which significantly improved the manuscript.

References

- Ajo-Franklin, J., Dou, S., Daley, T., Freifeld, B., Robertson, M., Ulrich, C., Wood, T., Eckblaw, I., Lindsey, N., Martin, E., Wagner, A., 2017. Time-lapse surface wave monitoring of permafrost thaw using distributed acoustic sensing and a permanent automated seismic source. SEG Technical Program Expanded Abstracts 2017, 5223–5227. <https://doi.org/10.1190/segam2017-17774027.1>.
- Bania, M., Wawrzyniak, T., 2011. Meteorological Bulletin Spitsbergen - Hornsund. Polish Polar Station Institute of Geophysics, Polish Academy of Sciences October 2011. <https://hornsund.igf.edu.pl> (website accessed: 2018.10.15).
- Baranowski, S., 1968. Thermic conditions of the periglacial tundra in SW Spitsbergen. Acta Universitatis Wratislaviensis 68, Studia geograficzne X (in Polish with Eng. abstract) (74 p).
- Birkenmajer, K., 1960. Raised marine features of the Hornsund area. Vestspitsbergen. – Studia Geol. Polon 5, 3–95.
- Birkenmajer, K., 1990. Geology of the Hornsund Area, Spitsbergen. Geological Map 1: 75,000. With Explanations. Polish Academy of Sciences, Committee on Polar Research, and Silesian University.
- Birkenmajer, K., Olsson, I.U., 1970. Radiocarbon Dating of Raised Marine Terraces of Hornsund, Spitsbergen and the Problem of Land Uplift. 1969. Norsk Polarinstitutt Arb., pp. 17–43.
- Birkenmajer, K., Olsson, I.U., 1997. Radiocarbon dating of marine bivalve shells from Holocene moraines at inner Hornsund, South Spitsbergen. Bulletin of the Polish Academy of Sciences Earth Sciences 451, 59–66 November.
- Birkenmajer, K., Olsson, I.U., 1998. Radiocarbon-dated late Pleistocene and Early Holocene marine shells at Werenskiöldbreen, south Spitsbergen. Bulletin of the Polish Academy of Sciences, Earth Sciences 46, 21–34.
- Braathén, A., Balum, K., Christiansen, H.H., Dahl, T., Eiken, O., Elvebakk, H., Hansen, F., Hanssen, T.H., Jochmann, M., Johansen, T.A., Johnsen, H., Larsen, L., Lie, T., Mertes, J., Mork, A., Mork, M.B., Nemec, W., Olausson, S., Oye, V., Rod, K., Titledstad, G.O., Tveranger, J., Vagle, K., 2012. The Longyearbyen CO2 Lab of Svalbard, Norway—initial assessment of the geological conditions for CO2 sequestration. Norwegian Journal of Geology 92, 353–376 (Trondheim, ISSN 029-196X).
- Brauer, H., Kucjba, S., Mandat, M., Dąbrowska, D., Wawrzyniak, T., 2017. Meteorological Bulletin Spitsbergen - Hornsund, Summary of the Year 2016, Polish Polar Station Institute of Geophysics, Polish Academy of Sciences <https://hornsund.igf.edu.pl> (website accessed: 2018.10.15).
- Burgess, M.M., Smith, S.L., Brown, J., Romanovsky, V., Hinkel, K., 2000. Global Terrestrial Network for Permafrost (GTNet-P): permafrost monitoring contributing to global climate observations. Geol. Surv. Can. Curr. Res. E14, 1–8.
- Chmal, H., 1987. Pleistocene sea level changes and glacial history of the Hornsund area, Svalbard. – Polar Res. 269–270 5 n.s.
- Chmal, H., Klementowski, J., Migala, K., 1988. Thermal currents of active layer in Hornsund area. In: Senneker, K. (Ed.), Permafrost. Fifth International Conference. August 2–5, Proceedings. Vol. 1, Tapir Pub., Trondheim, Norway, pp. 44–49.
- Christiansen, H.H., French, H.M., Humlum, O., 2005. Permafrost in the Gruve-7 mine, Adventdalen, Svalbard, Norsk Geografisk Tidsskrift - Norwegian Journal of Geography 59 (2), 109–115. <https://doi.org/10.1080/00291950510020592>.
- Christiansen, H.H., Etzelmüller, B., Isaksen, K., Juliusen, H., Farbrøt, H., Humlum, O., Johansson, M., Ingeman-Nielsen, T., Kristensen, L., Hjort, J., Holmlund, P., Sannel, A.B., Sigsgaard, C., Åkerman, H.J., Foged, N., Blikra, L.H., Pernosky, M.A., Ødegård, R.S., 2010. The thermal state of permafrost in the nordic area during the international polar year 2007–2009. Permafrost Periglacial Process. 21, 156–181. <https://doi.org/10.1002/ppp.687>.
- Czerny, J., Kieres, A., Manecki, M., Rajchel, J., 1993. Geological Map of the SW Part of Wedell Järlsberg Land Spitsbergen, 1:25 000. Institute of Geology and Mineral Deposits, Univ. of Mining and Metallurgy, Cracow.
- Dahlin, T., 2001. The development of DC resistivity imaging techniques. Comput. Geosci. 27, 1019–1029. [https://doi.org/10.1016/S0098-3004\(00\)00160-6](https://doi.org/10.1016/S0098-3004(00)00160-6).
- Dobiński, W., 2011a. Permafrost. Earth-Science Reviews. 108, 158–169. <https://doi.org/10.1016/j.earscirev.2011.06.007>.
- Dobiński, W., 2011b. Permafrost in the selected areas of Tatra Mts, the Scandinavian Mts, and Spitsbergen in the light of extensive geophysical studies and climatological analyses. Prace naukowe Uniwersytetu Śląskiego w Katowicach nr 2850. Wydawnictwo Uniwersytetu Śląskiego (in Polish).
- Dobiński, W., Leszkiewicz, J., 2010. Active layer and permafrost occurrence in the vicinity of the Polish Polar Station, Hornsund, Spitsbergen in the light of geophysical research. Problemy Klimatologii Polarnej 20, 129–142 (in Polish).
- Dobiński, W., Grabiec, M., Glazer, M., 2017. Cold-temperate transition surface and permafrost base (CTS-PB) as an environmental axis in glacier-permafrost relationship, based on research carried out on the Storglaciären and its forefield, northern Sweden. Quaternary Research 88 (3), 551–569. <https://doi.org/10.1017/qua.2017.65>.
- Dolnicki, P., Grabiec, M., Puczek, D., Gawor, I., Budzik, T., Klementowski, J., 2013. Variability of temperature and thickness of permafrost active layer at coastal sites of Svalbard. Polish Polar Res. 34 (4), 353–374. <https://doi.org/10.2478/popore-2013-0026>.
- Dou, S., Ajo-Franklin, J.B., 2014. Full-wavefield inversion of surface waves for mapping embedded low-velocity zones in permafrost. GEOPHYSICS 79 (6), EN107–EN124. <https://doi.org/10.1190/geo2013-0427.1>.
- Elvebakk, H., 2008. Results of borehole logging in CO2 wells, Dh1-CO2 - 07 and Dh2-CO2 - 07, Longyearbyen, Svalbard. NGU Report 2008.054, 25 Unis Report 2009-01. <https://www.ngu.no/publikasjon/> (date of access: 17.08.2018).
- Etzelmüller, B., Schuler, T.V., Isaksen, K., Christiansen, H.H., Farbrøt, H., Benestad, R., 2011. Modeling the temperature evolution of Svalbard permafrost during the 20th and 21st century. Cryosphere 5, 67–79. <https://doi.org/10.5194/tc-5-67-2011>.
- Everdingen, Van R.O., 1998. Multi-language Glossary of Permafrost and Related Ground-ice Terms (Definitions).
- Fjeldskaar, W., 1994. The amplitude and decay of the glacial forebulge in Fennoscandia. Nor. Geol. Tidsskr. 74, 2–8.
- Forman, S.L., Lubinski, D.J., Ingólfsson, Ö., Zeeberg, J.J., Snyder, J.A., Siegiert, M.J., Matishov, G.G., 2004. A review of postglacial emergence on Svalbard, Franz Josef Land and Novaya Zemlya, northern Eurasia. Quat. Sci. Rev. 23, 1391–1434. <https://doi.org/10.1016/j.quascirev.2003.12.007>.
- Glazer, M., Mendecki, M.J., Mycka, M., 2014. Application of DOI index to analysis of selected examples of resistivity imaging models in quaternary sediments. Studia Quaternaria 31, 109–114. <https://doi.org/10.2478/squa-2014-0011>.
- Gregersen, O., Eidsmoen, T., 1988. Permafrost conditions in the shore area at Svalbard. In: Senneker, K. (Ed.), Permafrost. Fifth International Conference. August 2–5, Proceedings. Volume 2, Tapir Pub., Trondheim, Norway, pp. 933–936.
- Gregersen, O., Phukan, A., Johansen, T., 1983. Engineering properties and foundation design alternatives in marine Svea clay, Svalbard. International Conference on Permafrost 4, Fairbanks, Alaska 1983. Proceedings. 1985. Norwegian Geotechnical Institute, Oslo, pp. 384–388 Also publ. in: Publ. No. 159.
- Harada, K., Yoshikawa, K., 1998. Permafrost thickness at Moskuslagoon, Spitsbergen. Permafrost - Seventh International Conference Proceedings, Yellowknife (Canada), Collection Nordica 55, pp. 427–431.
- Harris, S.A., 2001. Twenty years of data on climate - permafrost - active layer variations at lower limit of alpine permafrost, Marmot Basin, Jasper National Park, Canada.

- Geografiska Annaler 83 A (1–2), 1–13. <https://doi.org/10.1111/j.0435-3676.2001.00140.x>.
- Hauck, C., Mühl, D.V., 2003. Inversion and interpretation of two-dimensional geoelectrical measurements for detecting permafrost in mountainous regions. *Permafrost Periglac. Process.* 14, 305–318. <https://doi.org/10.1002/ppp.462>.
- Hauck, C., Isaksen, K., Vonder Mühll, D., Sollid, J.L., 2004. Geophysical surveys designed to delineate the altitudinal limit of mountain permafrost: an example from Jotunheimen, Norway. *Permafrost Periglac. Process.* 15, 191–205. <https://doi.org/10.1002/ppp.493>.
- Hilbich, C., Marescot, L., Hauck, C., Loke, M.H., Mausbacher, R., 2009. Applicability of electrical resistivity tomography monitoring to coarse blocky and ice-bearing permafrost landforms. *Permafrost Periglac. Process.* 20, 269–284. <https://doi.org/10.1002/ppp.652>.
- Hormes, A., Gjermundsen, E.F., Rasmussen, T.J., 2013. From mountain top to the deep sea – deglaciation in 4D of the northwestern Barents Sea ice sheet. *Quat. Sci. Rev.* 75, 78–99. <https://doi.org/10.1016/j.quascirev.2013.04.009>.
- Humlum, O., 2005. Holocene permafrost aggradation in Svalbard. *Geol. Soc. Lond., Spec. Publ.* 242, 119–129. <https://doi.org/10.1144/GSL.SP.2005.242.01.11>.
- Humlum, O., Instanes, A., Sollid, J.L., 2003. Permafrost in Svalbard: a review of research history, climatic background and engineering challenges. *Polar Res.* 22 (2), 191–215. <https://doi.org/10.3402/polar.v22i2.6455>.
- Isaksen, K., Vonder Mühll, D., Gubler, H., Kohl, T., Sollid, J.L., 2000. Ground surface-temperature reconstruction based on data from a deep borehole in permafrost at Janssonhaugen, Svalbard. *Ann. Glaciol.* 31, 287–294. <https://doi.org/10.3189/172756400781820291>.
- Isaksen, K., Hauck, C., Gudvang, E., Ødegård, R.S., Sollid, J.L., 2002. Mountain permafrost distribution in Dovrefjell and Jotunheimen, southern Norway, based on BTS and DC resistivity tomography data. *Norsk Geografisk Tidsskrift–Norwegian Journal of Geography* 56, 122–136. <https://doi.org/10.1080/002919502700056459>.
- Isaksen, K., Benestad, R.E., Harris, C., Sollid, J.L., 2007. Recent extreme near-surface permafrost temperatures on Svalbard in relation to future climate scenarios. *Geophys. Res. Lett.* 34, L17502. <https://doi.org/10.1029/2007GL031002>.
- Isaksen, K., Ertekmüller, B., Ødegård, R.S., Jansson, P., Holmlund, P., 2018. Long-term changes in permafrost temperature in Svalbard and Scandinavia. In: Deline, P., Bodin, X., Ravanel, L. (Eds.), 5th European Conference On Permafrost – Book of Abstracts. 23 June – 1 July 2018, Chamonix, France. <hal-01816115>. <https://hal.archives-ouvertes.fr/hal-01816115>.
- Jahn, A., 1959a. Postglacial development of Spitsbergen shores. —, *Czas. Geogr.* 30, 245–262.
- Jahn, A., 1959b. The raised shore lines and the beaches in Hornsund and the problem of postglacial vertical movements of Spitsbergen. *Przeg. Geogr.* 31 (Suppl.), 143–178.
- Jahn, A., 1982. Soil thawing and active layer below coastal permafrost: the impact of seawater on permafrost degradation imaged by electrical resistivity tomography (Hornsund, SW Spitsbergen). *Geomorphology* 293 (Part B), 347–359. ISSN 0169-555X. <https://doi.org/10.1016/j.geomorph.2016.06.013>.
- Kneisel, C., Hauck, C., 2008. Electrical methods. In: Hauck, C., Kneisel, C. (Eds.), *Applied Geophysics in Periglacial Environments*. Cambridge Univ. Press, pp. 3–27.
- Kneisel, C., Hauck, C., Fortier, R., Moorman, B., 2008. Advances in geophysical methods for permafrost investigations. *Permafrost Periglac. Process.* 19, 157–178. <https://doi.org/10.1002/ppp.616>.
- Kowalewski, W., Rudowski, S., Zalewski, S.M., 1991. Seismoacoustic studies in Hornsund, Spitsbergen. *Polish Polar Research* 12 (3), 353–361.
- Kula, D., Olczewska, D., Dobrzyński, W., Glazer, M., 2018. Horizontal-to-vertical spectral ratio variability in the presence of permafrost. *Geophysical Journal International* 214 (1), 219–231. <https://doi.org/10.1093/gji/ggy118> 1 July.
- Landvik, J.Y., Mangerud, J., Salvigsen, O., 1987. The Late Weichselian and Holocene shoreline displacement of the west-central coast of Svalbard. *Polar Research* 5, 29–44. <https://doi.org/10.3402/polar.v5i1.6866> n.s..
- Landvik, J.Y., Bondevik, S., Elverhøi, A., Fjeldskaar, W., Mangerud, J., Siegert, M.J., Salvigsen, O., Svendsen, J., Vorren, T.O., 1998. The Last Glacial Maximum of Svalbard and the Barents Sea area: ice sheet extent and configuration. *Quat. Sci. Rev.* 17, 43–75. [https://doi.org/10.1016/S0277-3791\(97\)00066-8](https://doi.org/10.1016/S0277-3791(97)00066-8).
- Larin, S.M., Marov, G.P., Kholmianskiy, M.A., Neizvestnov, Y.V., 1978. Certain types of geoelectric sections of the negative temperature belt in the arctic and subarctic connection with exploration for subpermafrost. In: Sanger, F.J., Hyde, P.J. (Eds.), *Permafrost Second International Conference*, 13–28 July 1973, Yakutsk U.S.S.R., USSR Contribution, National Academy of Sciences, Washington, pp. 428–430.
- Liestøl, O., 1976. Pings, springs and permafrost in Spitsbergen. *Norsk Polarinstitutt Årbok* 1975, 7–29.
- Lim, M., Strzelecki, M.C., Kasprzak, M., Swirad, Z.M., Webster, C., Woodward, J., Gjeltun, H., 2020. Arctic rock coast responses under a changing climate. *Remote Sens. Environ.* 236. <https://doi.org/10.1016/j.rse.2019.111500>.
- Lindner, L., Marks, L., Pekala, K., 1986. Outline of Quaternary chronostratigraphy of the northern Hornsund area, southern Spitsbergen. *Bull. Pol. Acad. Earth Sc.* 34, 427–436. <https://doi.org/10.3402/polar.v34i1.6866>.
- Lindner, L., Marks, L., Roszczyński, W., Semil, J., 1991. Age of raised marine beaches of northern Hornsund Region, South Spitsbergen. — *Pol. Polar Res.* 12 (2), 161–182.
- Loke, M.H., 2018. Tutorial: 2-D and 3-D electrical imaging surveys. <http://www.geoelectrical.com> (Website accessed 15.06.2018).
- Lupikasza, E., Malarzewski, L., Niedźwiedz, T., Dobrowolska, K., 2014. The trends in air temperature and number of ice and freeze-thaw days in the Atlantic and Siberian sector of arctic. *Problemy Klimatologii Polarnej* 24, 5–24 (in Polish).
- MacKay, D.K., 1969. Electrical Resistivity Measurements in Frozen Ground, Mackenzie Delta Area, Northwest Territories. Association Internationale d'Hydrologie Scientifique, Actes du Colloque de Becarest, Reprint Ser. 82, Department of Energy, Mines and Resources, Inland Waters Branch, Ceuterick, Belgium, pp. 363–375.
- Mangerud, J., Landvik, J.Y., 2007. Younger Dryas glaciers in western Spitsbergen: smaller than during the Little Ice Age. *Boreas* 36 (3), 278–285. <https://doi.org/10.1111/j.1502-3885.2007.tb01250.x>.
- Marescot, L., Loke, M.H., Chapellier, D., Delaloye, R., Lambiel, C., Reynard, E., 2003. Assessing reliability of 2D resistivity imaging in permafrost and rock glacier studies using the depth of investigation index method. *Near Surface Geophysics* 1, 57–67. <https://doi.org/10.3997/1873-0604.2002007>.
- Miller, G.H., Brigham-Grette, J., Alley, R.B., Anderson, L., Bauch, H.A., Douglas, M.S.V., Edwards, M.E., Elias, S.A., Finney, B.P., Fitzpatrick, J.J., Funder, S.V., Herbert, T.D., Hinzman, L.D., Kaufman, D.S., MacDonald, G.M., Polyak, L., Robock, A., Serreze, M.C., Smol, J.P., Spielhagen, R., White, J.W.C., Wolfe, A.P., Wolff, E.W., 2010. Temperature and precipitation history of the Arctic. *Quaternary Science Reviews* 29 (15–16), 1679–1715. ISSN 0277-3791. <https://doi.org/10.1016/j.quascirev.2010.03.001>.
- Mościcki, W.J., 2010. Remarks on application of geophysical geoelectric methods in mountain discontinuous permafrost studies, conference paper. Nauka a zarządzanie obszarem Tatry i ich otoczeniem: przyroda Tatrzańskiego Parku Narodowego a człowiek: IV konferencja: Zakopane 14–16 October 2010. Polskie Towarzystwo Przyjaciół Nauk o Ziemi. — [Kraków: PTNPoZ] (ISBN: 978-83-61788-24-9, 103 – 110 in Polish).
- Nuth, C., Kohler, J., König, M., von Deschanden, A., Hagen, J.O., Käbb, A., Moholdt, G., Pettersson, R., 2013. Decadal changes from a multi-temporal glacier inventory of Svalbard. *Cryosphere* 7, 1603–1621. <https://doi.org/10.5194/cr-7-1603-2013>.
- Oldenburg, D.W., Li, Y., 1999. Estimating depth of investigation in dc resistivity and IP surveys. *Geophysics* 64, 403–416. <https://doi.org/10.1190/1.1444545>.
- Oliva, M., Vieira, G., Pina, P., Pereira, P., Neves, M., Freitas, M.C., 2014. Sedimentological characteristics of ice-wedge polygon terrain in Adventdalen (Svalbard) – environmental and climatic implications for the late Holocene. *Solid Earth* 5, 901–914. <https://doi.org/10.5194/se-5-901-2014>.
- Overduin, P.P., Westermann, S., Yoshikawa, K., Haberlau, T., Romanovsky, V., Wetterich, S., 2012. Geoelectric observations of the degradation of nearshore submarine permafrost at Barrow (Alaskan Beaufort Sea). *J. Geophys. Res.* 117, F02004. <https://doi.org/10.1029/2011JF002088>.
- Pekala, K., 1989. Quaternary deposits of the Hans Glacier forefield (Hornsund, Spitsbergen). *Polar Session, Natural Environment Research of West Spitsbergen, Inst. Nauk o Ziemi UMCS w Lublinie*, pp. 191–204 (in Polish).
- Philipps, W., Briner, J.P., Gislefoss, L., Linde, H., Koffman, T., Fabel, D., Xu, S., Hormes, A., 2017. Late Holocene glacier activity at inner Hornsund and Scottbreen, southern Svalbard. *Quaternary Sci.* 32, 501–515. <https://doi.org/10.1002/jqs.2944>.
- Piotti, S., Yuan, A., Carcione, J.M., Horgan, H.J., Anandakrishnan, S., 2015. Anisotropy and crystalline fabric of Whillans ice Stream (West Antarctica) inferred from multicomponent seismic data. *J. Geophys. Res. Solid Earth* 120, 4237–4262. <https://doi.org/10.1002/2014JB011591>.
- Promisksa, A., Cisek, M., Walczowski, W., 2017. Kongsfjorden and Hornsund hydrography – comparative study based on a multiyear survey in fjords of west Spitsbergen. *Oceanologia* 59, 397–412. <https://doi.org/10.1016/j.oceano.2017.07.003>.
- Repelewski-Pekalowa, J., Pekala, K., 2003. Spatial and temporal variation in active layer thickness, Calypsostranda, Spitsbergen. *Proceedings of 8th International Conference on Permafrost, Zurich*, pp. 941–945.
- Reynolds, J.M., 2011. *Electrical Resistivity Methods. An Introduction to Applied and Environmental Geophysics*. Wiley, Chichester, pp. 289–372.
- Rossi, G., Accaino, F., Boaga, J., Petronio, L., Romeo, R., Wheeler, W., 2018. Seismic survey on an open pingo system in Adventdalen Valley, Spitsbergen, Svalbard. *Near Surface Geophysics* 16, 89–103. <https://doi.org/10.3997/1873-0604.2017037>.
- Salvigsen, O., 1981. Radiocarbon dated raised beaches in Kong Karls Land, Svalbard, and their consequences for the glacial history of the Barents Sea. *Geogr. Ann.* 63A, 280–291.
- Salvigsen, O., 2005. Postglacial emergence of southernmost Spitsbergen, Svalbard: supplement to article by Forman et al., 2004, QSR 23, 1391–1434. *Quaternary Science Reviews* 24 (16–17), 1961–1962.
- Salvigsen, O., Elgersma, A., 1993. Radiocarbon dating of deglaciation and raised beaches in northwestern Sørkapp Land Spitsbergen, Svalbard. *Prace Geograficzne* 94, 39–48.
- Salvigsen, O., Elgersma, A., Hjort, C., Lagerlund, E., Liestøl, O., Svensson, N.-O., 1990. Glacial history and shoreline displacement on Erdmannflya and Bohemianflya, Spitsbergen, Svalbard. *Polar Res.* 8, 261–273. <https://doi.org/10.3402/polar.v8i2.6816>.
- Salvigsen, O., Elgersma, A., Landvik, J.Y., 1991. Radiocarbon Dated Raised Beaches in Northwestern Wedel Jarlsberg Land, Spitsbergen, Svalbard. *Wyprawy Geograficzne ma Spitsbergen UMCS, Lublin*.
- Schrott, L., Sass, S., 2008. Application of field geophysics in geomorphology: advances and limitations exemplified by case studies. *Geomorphology* 93, 55–73. <https://doi.org/10.1016/j.geomorph.2006.12.024>.
- Sobota, I., Dziembowski, M., Grajewski, T., Weckwerth, P., Nowak, M., Greif, K., 2016. Short-term changes in thermal conditions and active layer thickness in the tundra of the Kaffiyra region, NW Spitsbergen. *Bulletin of Geography. Physical Geography Series* 11 (1), 43–53. <https://doi.org/10.1515/bgeo-2016-0014>.
- Strzelecki, M., Kasprzak, M., Lim, M., Swirad, Z.M., Jaskólski, M., Pawłowski, L., Model, P., 2017. Cryo-conditioned rocky coast systems: a case study from Wilczekodden, Svalbard. *Science of The Total Environment* 607–608, 443–453. <https://doi.org/10.1016/j.scitotenv.2017.07.009>.

- Svendsen, J.I., Mangerud, J., 1992. Paleoclimatic inferences from glacial fluctuations on Svalbard during the last 20 000 years. *Clim. Dyn.* 6 (3–4), 213–220. <https://doi.org/10.1007/BF00193533>.
- Svensson, H., 1971. Pingos i yttre delen av Adventdalen. (Pingos in outermost Adventdalen valley.). 1969. *Nor. Polarinst. Årb.*, pp. 168–174.
- Szymański, W., Skiba, S., Wojtuń, B., 2013. Distribution, genesis, and properties of Arctic soils: a case study from the Fuglebekken catchment. Spitsbergen. *Pol. Polar Res.* 34 (3), 289–304. <https://doi.org/10.2478/popore-2013-0017>.
- Szymański, W., Siwek, J., Waścińska, J., Wojtuń, B., 2016. Texture and geochemistry of surface horizons of Arctic soils from a non-glaciated catchment, SW Spitsbergen. *Polish Polar Research* 37 (3), 361–377. <https://doi.org/10.1515/popore-2016-0019>.
- Telford, W.M., Geldart, L.P., Sheriff, R.E., 1990. *Applied Geophysics*, second ed. Cambridge Univ. Press.
- Tsuji, T., Johansen, T.A., Ruud, B.O., Ikeda, T., Matsuoka, T., 2012. Surface-wave analysis for identifying unfrozen zones in subglacial sediments. *Geophysics* 77. <https://doi.org/10.1190/geo2011-0222.1>.
- Wawrzyniak, T., Osuch, M., Napiórkowski, J., Westermann, S., 2016. Modelling of the thermal regime of permafrost during 1990–2014 in Hornsund, Svalbard. *Polish Polar Research* 37 (2), 219–242. <https://doi.org/10.1515/popore-2016-0013>.
- Williams, P., Smith, M., 1989. *The Frozen Earth: Fundamentals of Geocryology* (Studies in Polar Research). Cambridge University Press, Cambridge <https://doi.org/10.1017/CBO9780511564437>.
- Wiśniewska-Wojtasik, B., 2005. Temperature and salinity of bottom waters in bays of the Hornsund Fjord (S Spitsbergen). *Problemy Klimatologii Polarnej* 15, 155–167 (in Polish).
- Wójcik, A., Ziąja, W., 1993. Relief and Quaternary of the southern Sorkapp Land, Spitsbergen. *Pol. Polar Res.* 14 (3), 293–308.
- Xia, J., Miller, R.D., Park, C.B., 1999. Estimation of near-surface shear-wave velocity by inversion of Rayleigh waves. *Geophysics* 64, 691–700. <https://doi.org/10.1190/1.1444578>.
- You, Y., Yu, Q., Pan, X., Wang, X., Guo, L., 2013. Application of electrical resistivity tomography in investigating depth of permafrost base and permafrost structure in Tibetan Plateau. *Cold Reg. Sci. Technol.* 87, 19–26. <https://doi.org/10.1016/j.coldregions.2012.11.004>.
- Young, N.E., Lamp, J., Koffman, T., Briner, J.P., Schaefer, J., Gjermundsen, E.F., Linge, H., Zimmerman, S., Guilderson, T.P., Fabel, D., Holmes, A., 2018. Deglaciation of coastal south-western Spitsbergen dated with in situ cosmogenic ^{10}Be and ^{14}C measurements. *J. Quaternary Sci.* <https://doi.org/10.1002/jqs.3058>.

Paper IV:

Majdański, M., Dobiński, W., **Marciniak, A.**, Owoc, B., Glazer, M., Osuch, M., & Wawrzyniak, T. (2022). Variations of permafrost under freezing and thawing conditions in the coastal catchment Fuglebekken (Hornsund, Spitsbergen, Svalbard). *Permafrost and Periglacial Processes*. <https://doi.org/10.1002/ppp.2147>



Received: 12 April 2021 | Revised: 14 March 2022 | Accepted: 17 March 2022
DOI: 10.1002/ppp.2147

RESEARCH ARTICLE

WILEY

Variations of permafrost under freezing and thawing conditions in the coastal catchment Fuglebekken (Hornsund, Spitsbergen, Svalbard)

Mariusz Majdański¹ | Wojciech Dobiński² | Artur Marciniak¹ |
Bartosz Owoc¹ | Michał Glazer² | Marzena Osuch¹ | Tomasz Wawrzyniak¹

¹Institute of Geophysics, Polish Academy of Sciences, Warsaw, Poland

²Faculty of Natural Sciences, University of Silesia, Sosnowiec, Poland

Correspondence

Mariusz Majdański, Institute of Geophysics, Polish Academy of Sciences, Warsaw, Poland.
Email: mmajd@igf.edu.pl

Funding information

National Science Centre, Poland (NCN), Grant/Award Number: UMO-2015/21/B/ST10/02509

Abstract

Two seismic field surveys were organized in the Fuglebekken coastal catchment of Hornsund, Spitsbergen, Svalbard, to map frozen and unfrozen ground and assess the spatial and temporal state of the permafrost. Surveys were conducted during maximum thawing in September and maximum freezing in April of the following year. The obtained seismic wavefields were interpreted using three methods: the dispersion of surface waves, seismic refraction, and travel time tomography. The seismic experiments were supported by nearby boreholes with continuous thermal monitoring. In the frozen survey, a gradual increase in ice content of water-filled sediments was found, farther from the coast. In September the shallow sensors in the boreholes validated positive ground temperatures down to 3.0 m depth, with below-zero temperatures at greater depths. However, seismic tomography indicated that the ground was unfrozen down to 30 m. The ground probably remained unfrozen due to intrusion of high-salinity seawater, even though it had been below 0°C. In April, in the area 300 m and farther from the coast, the ground below 3 m depth was frozen, except for a 19-m-deep open talik identified in a borehole at the slope of Fugle Mountain. We attribute the complex spatial extent, form, and condition of permafrost in the Fuglebekken coastal catchment to multiple factors, including variable solar energy, snow and ground cover, thermal and humidity properties of the soil, subsurface water flow, and seawater intrusion. The presented combination of seismic methods provides a new robust and precise approach to assess the spatial variability of permafrost in a coastal environment. The proposed interpretation shows deep percolation of subsurface flow into permafrost and its seasonal unfreezing at a depth of 30 m in both the zone of saltwater intrusion and the slope area.

KEYWORDS

Arctic, near-surface methods, permafrost, seismic method, Spitsbergen

1 | INTRODUCTION

Permafrost plays an important role in high-latitude and high-altitude ecosystems, underlying 25% of the terrestrial parts of Earth.¹ The

thermal state of and changes to permafrost are crucial indicators of environmental changes occurring in the Arctic. In Svalbard, permafrost underlies almost all land areas that are not covered by glaciers. Changes in climatic variables, especially air temperature, snow depth,

and the increased duration of the period with positive air temperature, have resulted in an increase of permafrost temperature and deepening of the active layer.¹

In SW Spitsbergen, Svalbard, the changes in air temperature observed at the Hornsund meteorological site over the last four decades (1979–2018) are more than six times higher than the global average.² Degradation of permafrost results in a change in hydrogeological and geotechnical properties of the ground, hydrological and biogeochemical processes, landforms, and other components of the ecosystems. The thickness of the active layer, which has increased globally from 0.2 to 1.0 m in the last four decades, is expected to increase, especially in the Arctic due to polar amplification phenomenon.³

Ground thermal conditions near Ny-Ålesund, Longyearbyen, Barentsburg, Kapp Linné, and Hornsund were described by Christiansen et al.,^{4,5} in Petuniabukta by Rachlewicz and Szczuciński,⁶ in Bellsund by Marsz et al.,⁷ and on the Kaffiøyra Plain by Sobota and Nowak.⁸ Lowland permafrost is at temperatures close to 0°C, making it very sensitive to climate change. Moreover, the warmest permafrost in Svalbard has been found in Hornsund. Temperatures observed at 12 m depth are only −1.1°C on average.^{5,9} Unfortunately, *in situ* point monitoring of the ground thermal state is insufficient to evaluate the spatial variability of permafrost thickness. Spatial heterogeneity of the thaw depth is influenced by the local solar and atmospheric conditions, ground surface albedo, exposure, thermal and humidity properties of the soil, thickness and duration of snow cover and vegetation, and the depth of permafrost itself.⁵

Geophysical measurements, apart from thermal monitoring, cannot measure the temperature of the subsurface directly, but they can indirectly detect changes in physical parameters and properties of the ground. Laboratory analysis shows that at temperatures exceeding 0°C low-porosity rocks experience a significant (~11%) increase in seismic P-wave velocity when compared with the same rocks at negative temperatures.¹⁰ This is sufficient to identify the presence of permafrost within a single rock unit.¹¹ Locally, where the velocity, lithology, and distribution of rocks do not vary significantly, such a change at the edge of permafrost can be detected by seismic methods, even at great depths. The P-wave velocity in high-porosity rocks will double after freezing.^{12–14} Recent scientific efforts have focused on studying permafrost in high mountains and polar regions using a variety of geophysical methods, including gravity measured by satellite,¹⁵ electrical resistivity tomography (ERT),^{16,17} surface waves analysis,^{18,19} travel time tomography,²⁰ shear waves,²¹ and reflection seismic imaging.^{22–25} However, little information is available regarding the impact of active layer seasonal changes on seismic wavefields. Most research has been conducted during the summer thaw. Seismic measurements have been performed on Svalbard in Adventdalen, including imaging of deep structure to store CO₂ safely.²⁶ These experiments showed that imaging at high spatial precision is possible down to 1 km.

Periglacial studies have been conducted in the Hornsund area since the 1950s, resulting in a description of the geomorphological characteristics of this area,²⁷ and the long-term measurement of near-

surface ground temperature (up to 1 m) was initiated in 1978 at the meteorological site of the Polish Polar Station.²⁸ The post-glacial evolution of the Hornsund coast, which is also important for the development of permafrost in this area, was described by Pękala and Repelewska-Pękłowa.²⁹ The thermal state of the ground and active layer thickness in the Hornsund area have been discussed in several studies. Jahn^{30,31} and Grzes³² analysed soil structures and permafrost-related geomorphological processes. Migata^{33,34} and Dolnicki³⁵ described the influence of snow cover on ground temperatures. Miętus,³⁶ Miętus and Filipiak,³⁷ Leszkiewicz and Caputa,³⁸ and Dolnicki^{39,40} described variability of the active layer thickness in the Hornsund area. Dobiński and Leszkiewicz⁴¹ analyzed permafrost occurrence by the first application of geophysical methods near Hornsund and indicated the possibility that water can penetrate deeply into the ground and interact with permafrost. The thermal regime of permafrost in Hornsund was studied by Wawrzyniak et al.²⁸ The permafrost state near the Polish Polar Station Hornsund was modeled using the numerical heat transfer model CryoGrid 2, which was calibrated with borehole data and validated with available observations from the period 1990–2014. The simulated subsurface temperature indicated that multi-annual variability in that period can reach 25 m in depth.

Further, ERT studies in this area showed a relationship between soil structure and the permafrost table,⁴² but also found an effect of seawater on the coastal permafrost, imaged as a permafrost wedge in the near-surface onshore permafrost,⁴³ and described the active layer in the coastal permafrost.⁴⁴ Finally, using a combination of ERT and multichannel analysis of surface waves (MASW) techniques, the occurrence of permafrost was recognized in the Hornsund area with a distinction between ice-free, ice-bearing, and cryotic permafrost.⁴⁵

This study aims to analyze the applicability of seismic methods, surface wave dispersion, seismic refraction and travel time tomography, to obtain new high-resolution information on key permafrost characteristics in deglaciated areas. Due to the prevalence of climate warming, the form and condition of permafrost are changing, which require additional validation in the studied area. High spatial resolution in the imaging of the velocity field of the seismic method and direct monitoring of ground temperature allow validation of the hypothesis that a wide extent of unfrozen ground exists proximal to the coast, probably influenced by saltwater intrusion and mineralization of the groundwater (the cryotic state⁴⁶). Seismic studies can also provide information about the thickness of the active layer and be compared with the distance to the shoreline, elevation, and the presence of streamwater. Another interesting interface is the boundary between the sedimentary material and the solid rock beneath it. In these two media the seismic wave velocities can be different, and can change seasonally depending on the depth at which the ground freezes. Our study, based on two surveys in spring and late summer, estimates the minimum thaw depth and active layer thickness, the depth of surface temperature influences on the permafrost, and the extent of permafrost in the coastal catchment Fublebecken. We show links between the permafrost characteristics (frozen and ice-bearing zones) and the distance to the coast, slope, and geology. We rely on time-

lapse seismic image, results of a previous ERT survey,⁴⁵ and *in situ* borehole data to conduct this study.

2 | METHODS—TWO ARCTIC SURVEYS

2.1 | Fuglebekken—Geological setting

The study site, the Fuglebekken coastal catchment, is located on the northern shore of Hornsundfjord, near the Polish Polar Station Hornsund (SW Spitsbergen; see Figure 1). The region is underlain by Precambrian basement rocks, which are part of the Lower and Middle Hecla Hoek succession. The crystalline basement of metamorphic quartzites, schists, paragneisses, marbles, and amphibolites is covered by Cambrian and Ordovician sedimentary successions containing a mixture of sand and gravel with clay.⁴⁷ The Fuglebekken catchment (1.27 km²) is heterogeneous in terms of land cover and topography and occupies the southern slopes of the Arikammen–Fugleberget mountain ridge and the elevated marine terraces of the Fuglebergsletta coastal plain. The slopes are covered with washed rubble sediments, solifluction tongues, rock streams, alluvial cones, and bare solid rock. The bottom of the slope is covered with sea gravel, sediments, and diverse types of tundra vegetation. The

hydrographic cover includes several tributaries of Fuglebekken Stream, which drains into Isbjørnhamna Bay.^{48,49} Glazer et al.⁴⁵ and Humlum et al.⁵⁰ provide a detailed history of the permafrost in the area during the Holocene, from the mountain region through the system of elevated marine terraces, due to marine incursions.

2.2 | Thermal monitoring

To verify the results obtained using seismic methods, three shallow boreholes were drilled in April 2018, down to 20 m (Borehole 1), 5 m (Borehole 2), and 10 m (Borehole 3) as presented in Figures 1 and 2. Boreholes were located at previous monitoring sites, but our seismic data were acquired along with the previous ERT survey line. As a result, only Borehole 1 lies on our seismic line, whereas Borehole 2 is 100 m from the seismic line, and Borehole 3 is 250 m from the seismic line. Those out-of-line measurements cannot be directly compared with seismic data. The studied structures are complex and a variety of factors, such as geomorphology, sedimentary structure, water content and snow cover, contribute to variability of the permafrost. They are presented to show the thermal state and its temporal dynamics in this small area. Due to environmental restrictions, the operation of heavy equipment is allowed only on thick snow cover, so boreholes were

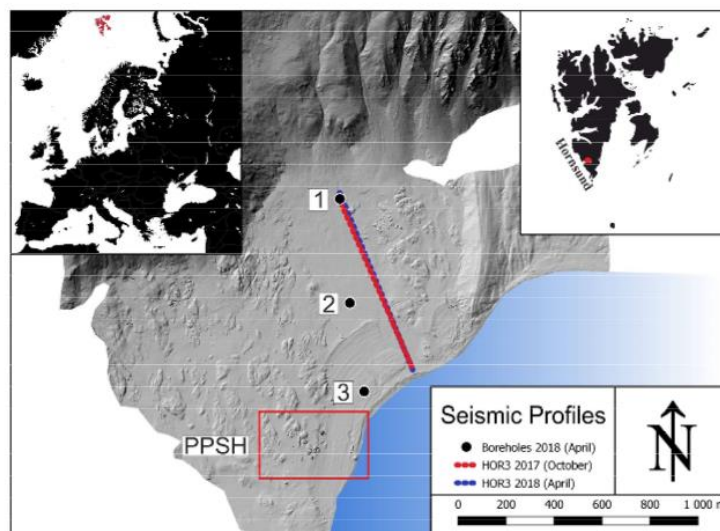


FIGURE 1 Digital terrain map of the study area in the Fuglebekken catchment close to the Polish Polar Station in Hornsund (PPSH, red box). The locations of the two seismic surveys are marked: Unfrozen survey in October 2017 (red) and Frozen survey in April 2018 (blue). Both lines match the previous ERT survey. Numbers 1–3 mark the position of shallow boreholes with thermal and piezometer measurements. Borehole 2 lies 50 m and Borehole 3 lies 250 m out-of-the-line in the position of previous monitoring sites. Insets show the position of Svalbard (left) and Hornsund (right) [Colour figure can be viewed at wileyonlinelibrary.com]

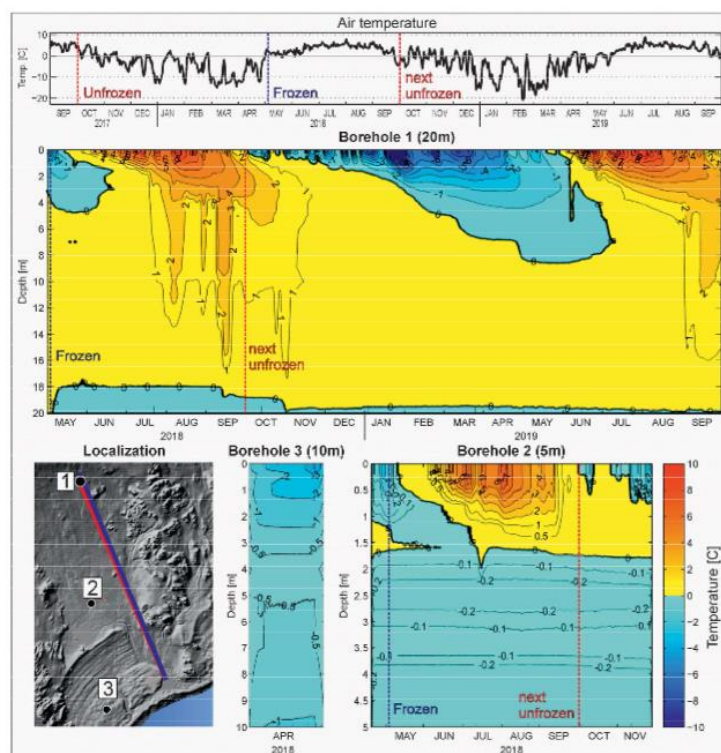


FIGURE 2 Daily mean air temperature at the meteorological station in the PSPH (top) with marked time (dashed lines) of both surveys: Frozen (blue) and Unfrozen conditions (red). Continuous ground temperature measurements were recorded in three boreholes (see inset for a location with marked closest points on the line). Clear seasonal variation was observed. The time of both seismic surveys (red and blue dashed lines) is marked. The next unfrozen line marks the time in the following year showing similar thermal conditions in which the seismic Frozen survey was acquired [Colour figure can be viewed at wileyonlinelibrary.com]

drilled during the second survey. Automatic sensors (Geoprecision M-Log5W) were installed at irregular intervals from 0.2 to 20 m (maximum of 18 sensors in a single borehole) to measure ground temperatures in the active layer and permafrost. In addition to thermal measurements, piezometers were installed to measure the depth of groundwater level as far as 5 m below the surface. Hourly measurements were recorded for different periods from installation: Borehole 3 (12 days), Borehole 2 (7 months), Borehole 1 (17 months and still active).

The thermal data were interpolated and are presented in Figure 2. The longest series (17 months) collected in Borehole 1 shows seasonally repeated heat transfer down to 4 m. Extreme temperatures were recorded by the shallowest sensor (at a depth of 20 cm), reaching $+16^{\circ}\text{C}$ on 28 July and -19°C on January 21, 2019.

Surprisingly, 0°C was observed at a depth of 19 m. The behavior of Boreholes 1 and 2 was found to be closer to expectation, with heat waves reaching 2 m and continuous subzero temperatures below that depth, similar to the results described by Kasprzak et al.⁴³ Figure 2 also shows air temperatures measured at the Polish Polar Station Homsund (Vaisala QMT107) with the dates of both surveys marked (red and blue lines). As borehole measurements were not available during the first survey, and the cycle repeats annually, the temperatures from September of the subsequent year were used in further analysis.

The fact that Borehole 3 was made at the end of winter is particularly noteworthy as the temperatures recorded are relatively high, ranging from about -3°C at the surface to about -0.5°C at a depth of 10 m. However, Borehole 3 recording was operational for only

12 days and located too far from the line to allow reliable calibration of seismic data. Note that during drilling, the ground, except for a thin layer at the surface, was not frozen. The most surprising temperature profile of the ground was found at Borehole 1. The 16-month sequence of temperatures revealed that seasonal freezing reaches a depth of 8 m, but the summer thaw is much deeper. In July and August 2018, in particular, a sharp increase in temperature was visible, reaching 12–18 m. This is interpreted as evidence of a strong under-ground flow that percolates deep into the ground, resulting in the occurrence of an extremely deep active layer at this site, ranging from about 18 m in 2018 to almost 20 m in 2019. This is one of the few places in the world where the active layer reaches such a depth. In addition to that detected in Hornsund, a similar depth has also been recorded in the Rocky Mountains and Labrador.⁴⁶

2.3 | Two active seismic surveys

For the first time in SW Spitsbergen, a multimethod approach was applied to reveal the spatial distribution of frozen ground and the active layer. Most permafrost studies in the High Arctic are conducted in summer because of the availability of daylight and easier logistics. Two fieldwork campaigns were conducted during different seasons: (a) during ground at maximal thaw (September 21–28, 2017, Unfrozen survey) and (b) during maximum snow cover with minimal thaw (April 15 to May 10, 2018, Frozen survey). The seismic data were collected twice on the same profile located between the seashore and the

mountain slope (see Figure 1). Sixty standalone seismic stations (DATA-CUBE, Omnirecs) with 1C 4.5-Hz geophones in walking spread deployments were used to obtain a high-resolution near-surface seismic dataset. The survey was designed to provide the longest offsets for observations without sacrificing resolution (see Figure 3 for details). For the first survey, both receivers and sources were deployed every 2 m (each source was stacked three times), while in the second survey the receivers were positioned every 5 m and sources every 2.5 m (each source was stacked six times, because of longer offsets). Attenuation of the seismic waves in frozen ground is significantly lower; thus it is possible to observe refraction at a much larger offset. Changing receiver spread to 5 m gave a maximum of 350-m offsets. Additionally, 20 m of overlapping shot locations were established. The PEG-40 accelerated weight-drop with 40 kg of usable mass was used as a seismic source. The seismic signal was generated by striking a steel plate. An additional strike was made before actual acquisition of data for each shot point to compact the ground and snow cover. The seismic source was mounted on an in-house built cart, and a sledgehammer (8 kg) was used as the source in places that were difficult to access during the first survey.

In the second survey, during maximum snow cover, the seismic source was mounted on a sledge. In this open terrain, snow cover ranged from 0 to 0.4 m. Both devices were equipped with power generators and a GPS-based timing system designed in-house (timing dispersion of <2 ms) to determine the excitation time. Precise source timing enabled correct vertical stacking to be achieved, resulting in a high signal-to-noise ratio. Measurements at the level of the snow

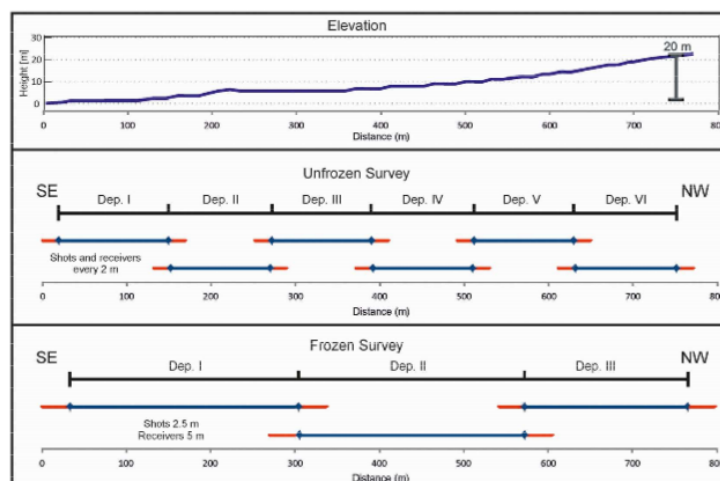


FIGURE 3 Schematic geometry of both seismic fieldwork arrangements. Elevation along the profile (top) with the position of boreholes marked, and acquisition geometry in two seasons: Unfrozen (middle) in 2017, Frozen (bottom) in 2018. The survey in 2018 used 5-m receiver spacing, resulting in much larger offsets (up to 350 m) [Colour figure can be viewed at wileyonlinelibrary.com]

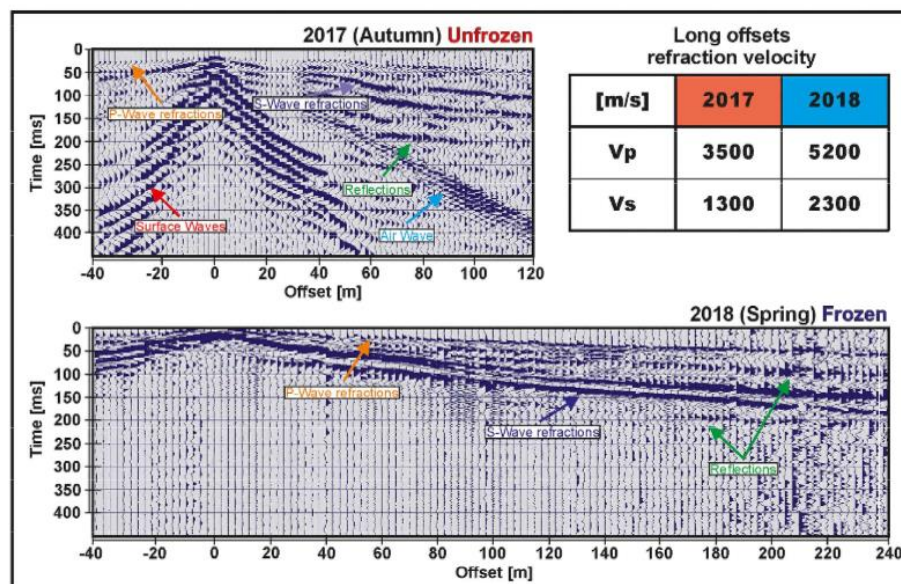


FIGURE 4 Example of a seismic wavefield recorded at the same shot location (shot position 142 m) in the two seasons: Unfrozen (top) and Frozen (bottom). Clear P- and S-wave refractions and wide-angle reflections are visible. No surface waves were recorded in frozen conditions. The table presents refraction velocities measured at large offsets showing a significant change in apparent velocities [Colour figure can be viewed at wileyonlinelibrary.com]

caused a large mismatch of the time of the first strike due to snow compaction, so all the first strikes recorded had to be discarded from the vertical stacking. The elevation data were gathered from the DTM model based on laser scanning (Riegl system) and GPS measurements.

2.4 | Recorded seismic wavefields

Seismic records from separate deployments (see Figure 3) were merged into a single dataset, after manual quality control, vertical stacking, and adding geometry information. An example of a seismic wavefield recorded from the same shot location during both surveys is presented in Figure 4. There are clear arrivals at all measured offsets that were longer in the frozen ground during the 2018 survey due to a change in the acquisition method (larger receiver spacing, resulting in an elongation of the profile using the same number of sensors). Both P- and S-wave refractions are visible at large offsets in both surveys. In near-surface applications, near-field observations (offsets shorter than 20 m) are difficult to perform for P-waves, and not possible for S-waves. Also, clear wide-angle reflections are visible at larger offsets. In the unfrozen conditions (in 2017), surface waves were the strongest signals in the wavefield, while in the frozen survey in 2018

they were observed only for several shots at rocky outcrops without snow cover. In these conditions even thin snow cover suppresses surface waves. However, high-amplitude, nondispersive S-wave refractions were observed. Shot gathers of long offset refractions (Figure 4) show P-wave velocities (V_p) of 3,500 m/s in unfrozen conditions and 5,200 m/s in frozen conditions, both with uncertainty ± 100 m/s, and S-wave velocities (V_s) of 1,300 m/s and 2,300 m/s, respectively, with uncertainty ± 150 m/s. Only apparent velocities are measured, not including layer thickness and dipping layers from a single gather. Nevertheless, the seasonal difference is very large, almost double, confirming the laboratory observations made by Draebing.¹⁴

2.5 | Near-surface techniques—MASW and seismic refraction

MASW⁵¹ is a well-known technique that is sensitive to changes in shear velocity (V_s) in the shallow subsurface. This technique is also known to be difficult to apply to complex structures due to its low precision. As surface waves were occasionally recorded in the frozen ground survey, only results from the unfrozen survey are discussed. Globe Clarity and Geopsy software were used to calculate the classic

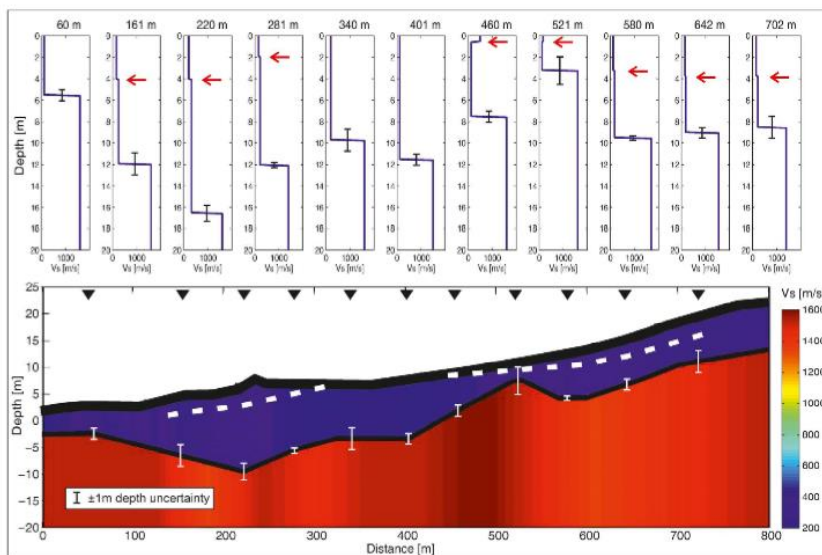


FIGURE 5 Results of surface wave dispersion analysis (MASW) for unfrozen survey data: 1D models for areas are marked with black triangles (top); 2D interpolation (bottom). The main S-wave velocity change (300–1,300 m/s) is identified as the sediment–bedrock boundary; the shallow smaller change (200–300 m/s) corresponds to the interpreted groundwater table. Vertical lines mark MASW depth uncertainty. No surface waves were observed in the frozen survey [Colour figure can be viewed at wileyonlinelibrary.com]

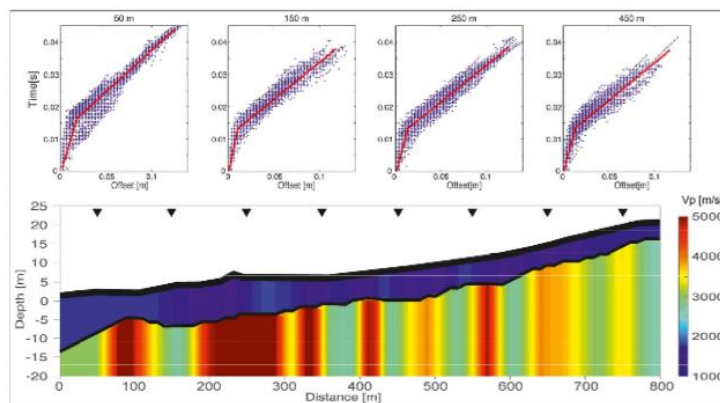


FIGURE 6 Shallow P-wave velocity distribution from the unfrozen survey, based on 1D fitting at regular intervals, marked with triangles (top), and 2D short offset seismic refraction (bottom). The velocity jump at about 10 m depth (1,500–3,500 m/s) corresponds to the depth of bedrock [Colour figure can be viewed at wileyonlinelibrary.com]

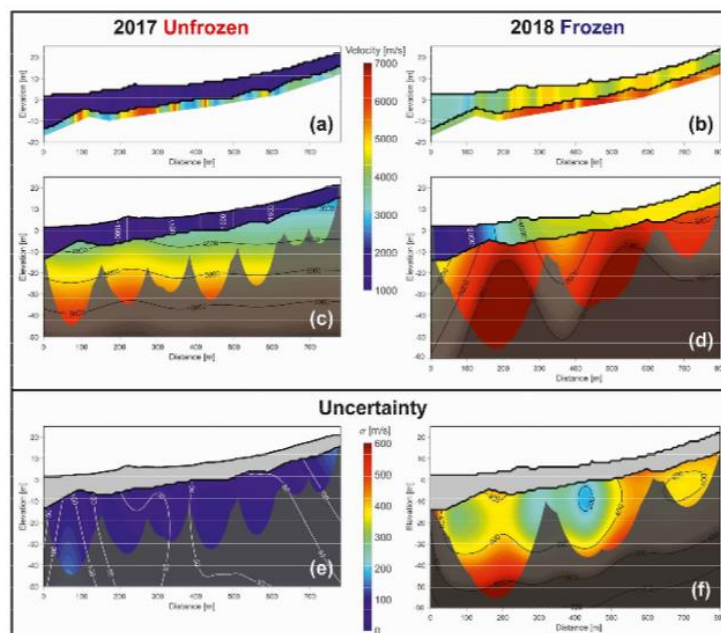


FIGURE 7 Seismic refraction (a, b) and ray-based tomography results (c, d) for both seasons: Unfrozen 2017 (left) and Frozen 2018 (right). The uncertainty of the tomography (e, f) shows the significance of the results down to 30 m. Higher velocities are visible at a depth of 30 m in the frozen survey [Colour figure can be viewed at wileyonlinelibrary.com]

inversion of the surface wave dispersion curve for 30-channel data blocks resulting in 11 1D Vs profiles. To limit the near-field effects, short offset channels (<20 m) were not used in the analysis. Also, all refraction and reflection signals were muted or filtered out of the data using a 2–50-Hz bandpass filter to increase the visibility of surface waves and thus enhance the dispersion curve. The results (Figure 5, top) present a consistent strong Vs contrast between the layers, the top layer with an average velocity of 300 m/s and the lower layer with an average velocity of 1,300 m/s, visible at a depth varying from 3 to 16 m with average uncertainty of ± 1 m. The velocity uncertainty is estimated as ± 100 m/s in the top layer and is much larger (± 500 m/s) in the bottom layer. This strong contrast is the boundary between fluvial sediments and compacted bedrock. The 1D results also show a much weaker, but consistent, change in Vs from 200 to 300 m/s at 0.5–4 m depth. This corresponds to the underground water table that was determined by the piezometers in Borehole 1. Moreover, stream water at the surface was also observed in this area at a distance of 330–430 m of the analysed profile, where this change is not visible in Vs. Figure 5 shows the interpolation of 1D results into a pseudo-2D Vs model.

The second near-surface technique used was the analysis of short-offset P-wave refraction arrivals (details in⁵²). Because of the complex

structure along the profile, including rocky outcrops, a stream, and varying levels of the water table, an initial model for inversion was created using 1D analysis at eight regular intervals, separately (Figure 6 top). Observations from the unfrozen survey clearly show a rapid change in Vp at about 10 m, confirming the depth to bedrock described using MASW with higher precision (Figure 6). The 2D models, for both seasons, were calculated using all the refraction observations for offsets smaller than 40 m, generating the detailed shape of the bedrock (Figure 7a,b). The independent results from the two seasons described an almost identical shape for the bedrock, confirming it is a lithological, not a thermal, feature. Vp in the sediments changed significantly between the seasons, with an average of 1,500 m/s in the unfrozen survey and reaching >5,000 m/s in the frozen survey. Moreover, in the unfrozen state, all values of Vp along the profile were similar, while the frozen survey found significant differences depending on distance from the coast. Close to the coast (up to 120 m away), the medium remained partially unfrozen, with Vp of $3,500 \pm 100$ m/s, while farther away it was fully frozen ($Vp > 4,500 \pm 100$ m/s).

More importantly, a change in Vp is also visible in the bedrock; in the unfrozen survey, bedrock Vp ranged from 3,300 to 5,500 m/s, while in the frozen survey all values of Vp were >5,000 m/s. Both

near-surface techniques using P- and S-waves provided independent information regarding the thickness and internal velocity structure in the sedimentary layer and just below the boundary. However, both methods are useful only at shallow depths.

2.6 | Ray-based refraction tomography

To reach lower depths and utilize all refraction observations, it is necessary to use refraction travel time tomography. Ray-based JIVE3D code⁵³ was used to identify the velocity distribution in this study. The seismic refraction results were used as an initial model for tomographic inversion. Inversion results for both seasons are presented in Figure 7c,d with uncertainty analysis in Figure 7e,f.

The grayed-out areas in Figure 7 are just the results of inversion smoothing and are not confirmed by seismic ray coverage. Both results show dense crystalline material with large Vp at distances of 200 m (corresponding to the rocky outcrop at the surface) for the basement and loosely compacted rock in the center of the profile (330–430 m). The uncertainty of the tomographic velocities was estimated using the statistical analysis of 121 randomly generated starting models (as in⁵⁴). The uncertainty associated with the frozen survey is very good (~50 m/s) down to 40 m, due to the large data set (2.5-m spacing), and for the unfrozen survey the uncertainty is acceptable (<400 m/s) down to 30 m. It would be possible to perform a similar analysis of S-waves, but due to the lack of short offset observations, such results would be highly uncertain.

3 | RESULTS AND DISCUSSION

The results obtained provide new information regarding the recognition of permafrost variability, facilitating better planning and future adaptation of the measurement methodology. In addition, the results provide new information regarding the occurrence of permafrost on the Spitsbergen coast.

3.1 | Optimal seismic refraction survey

Fieldwork in the polar regions is always challenging. For studies of the active layer, the period from August to September seems optimal, as evidenced by the borehole thermal data. During these months, thawing of the active layer is almost maximal, and seismic studies based on surface waves and refractions are possible. The use of lightweight seismic sources makes it possible to generate seismic waves that can easily be observed at 300-m offsets, resulting in the recognition of structures down to 40 m. Moreover, a 2-m spacing of sources and receivers, and a dominant refraction frequency in the range 30–100 Hz, provides precise characterization of the active layer. However, investigations of the deeper structure are significantly simpler to conduct during winter, when stronger seismic sources can be used on snow. Due to environmental restrictions, heavy duty equipment

cannot be used in open tundra areas. Moreover, the presence of a frozen active layer is optimal for deep seismic studies, where waves are not attenuated in near-surface layers. However, as shown in this case study, surface waves were only occasionally observed in the wavefield from the frozen period, making the use of the MASW method impossible.

Due to environmental restrictions, only noninvasive seismic sources are allowed, which automatically limits the possibility of using strong sources. A good methodology for gathering and processing data from relatively weak sources is therefore necessary. As shown, the uncertainty-driven approach (see also⁵⁵), which combines different seismic waves with independent information, seems to be an effective way to obtain results from such demanding datasets.

3.2 | Characteristics of permafrost and its relationship to ground temperature

The results obtained for the near-surface structures were integrated and are presented in Figure 8 with the estimated thermal state of the ground, obtained from nearby boreholes. The most notable feature is the sharp contrast in velocities, for both Vp (1,500–4,000 m/s) and Vs (300–1,300 m/s), located, on average, 10 m below the surface. This interface has been interpreted as a lithological boundary between water-filled unconsolidated and consolidated rocks. The seasonal change of seismic velocities is significant between seasons. On average, the Vp in the sediments was $1,500 \pm 50$ m/s in the unfrozen state and $4,500 \pm 100$ m/s in the frozen state. Such a spread suggests (after¹⁴) the presence of high-porosity and water-saturated fractured metamorphic rocks or a mixture of sand and clay.

As predicted by Gregersen et al.⁵⁶ and Christiansen et al.,⁵⁷ a strong effect of seawater on the freezing of sediments is visible for the frozen survey. At a distance of 150 m from the coast, a rapid change of Vp was observed (Figure 7d). Vp in the section from the coast to around 150 m is significantly lower than in the farther part of the profile. Such results indicate that the sediments did not freeze entirely. Based on air temperature measured in the nearby Polish Polar Station and Borehole 3, which was 250 m out-of-the-line, we suspect that the temperature of the ground was lower than 0°C. Although the distance from the coastline and the elevation for Borehole 3 are similar to those of the relevant part of the seismic line, a direct comparison of those states is not possible. A variety of factors, including geomorphology, snow cover, and water content, affect the local thermal state. To validate the thermal state of the ground it is necessary to have borehole measurements exactly on the seismic line. This area did not freeze probably due to the relatively high salinity level of the seawater penetrating the ground. A comparison of Vp in the first 150 m of the profile (Figure 7c,d) shows a change between seasons (Vp 1,500–2,000 m/s with the uncertainty of 50 m/s) that has been interpreted as a change in the amount of ice in the sediments. The active layer, in which temperature is seasonally positive, lies on top of the cryotic permafrost but its thickness can only be established by direct temperature measurement. Further, between

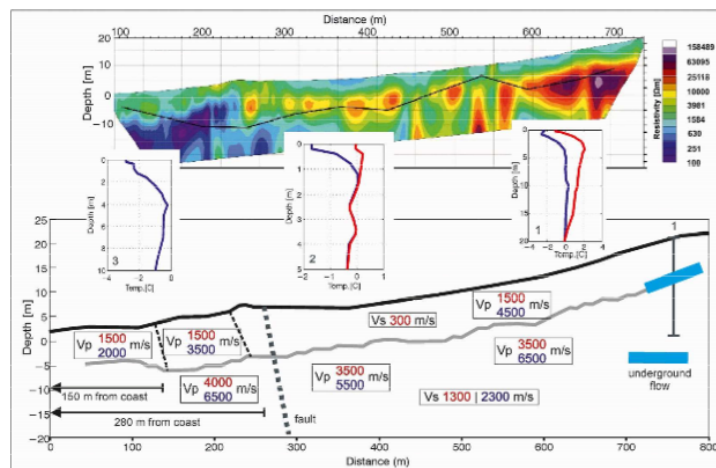


FIGURE 8 Schematic interpretation of seismic velocity and thermal structures. The gray line marks the lithological boundary between fluvial sediments and bedrock. Numbers show the velocities of P- and S-waves observed in the unfrozen (red) and frozen (blue) surveys. The previous ERT result is shown at the top (after⁴⁵). Insets show thermal profiles of the three boreholes in the vicinity. Black dashed lines mark the range of the influence of seawater on freezing in sediments. A thick dashed line marks the deep fault recognized in the area [Colour figure can be viewed at wileyonlinelibrary.com]

150 and 300 m from the coast, a strong velocity gradient (2,000–4,500 m/s) was observed in the sediments as a result of the lower salinity of the water penetrating the ground and a gradual increase in the ice content of the medium. Salt in the ground lowers the freezing point. Therefore, the ground may be below 0°C but not frozen due to salt content. Ice-free subsea permafrost has also been reported by other authors.⁵⁸ At distances greater than 300 m from the coast, the sediments were fully frozen. There was no influence of seawater and the ground was frozen at 0°C. In such conditions, seismic methods can easily distinguish the boundary between the active layer and permafrost. The characteristic velocity (V_p) of unfrozen, water-filled sediments is 1,500 m/s. In frozen conditions, it is 4,500 m/s for sediments and 6,500 m/s for frozen, solid rock. A small-scale talik, which was identified at 10 m during the drilling of Borehole 1, represented an exception because it did not freeze in either season. This talik formed as a result of the underground runoff generated by the steep mountain slope and the stream that exists in the area in summer, so it is classified as a hydrothermal, noncryotic talik. Surprisingly, the bedrock at depths >10 m also demonstrated significant variations in velocity, proving that the medium may undergo seasonal freezing and thawing at such depth. The V_p of the bedrock changed from $3,500 \pm 50$ to $6,500 \pm 400$ m/s between seasons, suggesting they comprise mica schists or plutonic rocks, such as granite.¹⁴ Moreover, significant changes in velocity, larger than the estimated uncertainty, occurred at a depth of 30 m. This result is similar to observations in Adventdalen where ground freezing in late summer was recognized at a depth of

50 m.⁵⁹ Lower velocities are, probably, the effect of the deep groundwater circulation also visible in Borehole 1 (Figure 2). Due to the uncertainty associated with the tomographic technique, changes deeper than 30 m cannot be confirmed, and the depth at which the medium was not affected by seasonal freezing changes remains unknown. Similarly, a change in V_s from 1,300 to 2,300 m/s was observed below the interface. The value of V_s in the frozen active layer cannot be confirmed, because of the lack of surface waves in the observed wavefield.

Figure 8 also presents the ERT result with the MASW-based interphase (modified after⁴⁵). Due to the deployment used and the high resistivity contrasts of the near-surface, structures in the resistivity model of the study area (Figure 8) do not reflect exact lithological boundaries. The profile was designed to observe changes in the horizontal characteristics of the permafrost within the Fuglebekken. Supporting information from the results provided by MASW allowed a qualitative interpretation of subsurface resistive structures in terms of ice content. Geological information below the high-resistivity ice-bearing permafrost structure is very limited, due to current penetration being insufficient over long distances. Based on data from ERT, permafrost with the frozen medium was found to be absent from up to ~250 m of the profile (Figure 8) and the extent of the saltwater intrusion within the Fuglebekken catchment area was suggested to cover up to 450 m of the profile.⁴⁵

Thermal monitoring was active for different periods for each borehole. The thermal profiles marked in Figure 8 show the ground

temperature during the frozen season survey (blue lines). The ground temperature in the unfrozen season, measured in consecutive years, also reflects similar conditions taking into account the air temperatures measured in this area (see Figure 2 top). Correlation of the seismic results with the thermal conditions was not possible for out-of-line boreholes. The shallow central borehole (Borehole 2), with a depth of 5 m, retained a constant temperature below 2 m in both seasons. The surface stream observed in the unfrozen season carries large amounts of warm water which heats the ground. The identified subsurface flow is preventing freezing, by constantly replacing groundwater by the movement and transfer of heat.

The thermal measurements in the last borehole (Borehole 1), at the bottom of the mountain slope, were unusual. A negative temperature was observed down to 8 m in the frozen season, while in the unfrozen season the ground had a positive temperature (max. 2°C at 4 m) down to a depth of 19 m. Such a situation is not typical for the thermal state of the active layer but is the effect of underground flow, which was unexpectedly observed at 10 m during drilling in the frozen season (May). This strong flow on the mountain slope heats the ground significantly during the unfrozen season. Unfortunately, the deep talik identified by measurements from the borehole is below the resolution of the seismic image, as this location is at the edge of the seismic profile.

4 | CONCLUSIONS

The results presented here have demonstrated that the application of multiple seismic methods (MASW, seismic refraction, and travel time tomography) together with borehole data provide new high-resolution observations and insight into the state of permafrost. The borehole data show the local ground thermal regime and high spatial variability, and allowed us to distinguish areas with ground temperatures below and above 0°C. Seismic methods used in time-lapse mode recognize frozen and unfrozen ground, and changes in water content. Comparing the observations from two seasons, we see a significant impact of seasonal changes in the active layer on the seismic wavefield. Analysis of the short offset refractions shows clearly that the thickness of sediments and the top of bedrock are not changing in time. Travel time tomography detects the seasonal variability of seismic velocities due to partial or complete freezing of water in the medium. MASW cannot be used in time-lapse mode as the surface waves are only occasionally observed in area covered by snow. There are large differences between outcomes of the *in situ* borehole data and the seismic analyses due to salinity or mineralization of water. Salt in the ground lowers the freezing point. Therefore, the ground at a temperature below 0°C may be not frozen due to the salt content. Ice-free subsea permafrost has also been reported by other authors.⁵⁸

Determining the boundary characteristics of the permafrost environment in the area under study is difficult via the seismic methods used in this study for the following reasons:

- The boundary between the active layer and the permafrost beneath it overlaps the boundary between sedimentary and bedrock material.
- Marine and glacial sediments fill the spaces between the palsoskerries in the studied area very unevenly, causing the active layer to end in both sedimentary material and solid rock. This is indicated by the seismic velocities along with their seasonal variation in both the sedimentary material and the solid rock.
- In the area characterized by cryotic permafrost, it is only possible to distinguish between the active layer and the permafrost by directly measuring the temperature in the ground.

However, time-lapse geophysical observations show that the characteristics of the cryotic permafrost are changing over time, which is interpreted as being due to a changing amount of ice in the ground. In the Hornsund region, we are dealing with a complex form of permafrost, which is produced by a diverse set of factors. This environment is a good analog for other coastal permafrost environments, which also probably exhibit such complexities, but the Hornsund region, as with the entire region of southern Svalbard, is experiencing the fastest climate change in the Arctic. The Hornsund region can therefore serve as a specific example of permafrost degradation and act as a kind of field laboratory where permafrost degradation is clearly visible. Water-permafrost interactions have a significant effect that is expected to grow in the future, further increasing the slope processes and resulting in larger geohazards.

Permafrost occurring on the sea coast of Hornsund is undergoing to rapid degradation. We interpret this degradation as being caused by the following factors: the rapid increase in air temperature, intrusion of seawater into the shore (which is no longer subject to freezing but remains in a cryotic state), and deep penetration of freshwater into the fractured bedrock.

ACKNOWLEDGEMENTS

This research was funded by the National Science Centre, Poland (NCN), Grant UMO-2015/21/B/ST10/02509. Jarosław Grzyb, Adam Nawrot, and Wojciech Gajek are thanked for their fieldwork assistance. We thank associate editor Seth Campbell as well as an anonymous reviewer for many comments and suggestions that improved the manuscript.

DATA AVAILABILITY STATEMENT

The data that support the findings of this study are available in the Institute of Geophysics repository (https://dataportal.igf.edu.pl/dataset/hor3_seismic). The data are open and available under DOI 10.25171/instgeoph_pas_igdata_hor3_seismic_2021_004

ORCID

Mariusz Majdański  <https://orcid.org/0000-0002-8909-4407>

Wojciech Dobirski  <https://orcid.org/0000-0002-6249-7273>

Marzena Osuch  <https://orcid.org/0000-0002-1887-3569>

Tomasz Wawrzyniak  <https://orcid.org/0000-0003-3393-753X>

REFERENCES

- Christiansen HH, Gilbert GL, Neumann U, et al. Ground ice content, drilling methods and equipment and permafrost dynamics in Svalbard 2016-2019 (PermaSval), 2021. doi:10.5281/zenodo.4294095
- Wawrzyniak T, Osuch M. A 40-year High Arctic climatological dataset of the Polish Polar Station Hornsund (SW Spitsbergen, Svalbard). *Earth Syst Sci Data*. 2020;12(2):805-815. doi:10.5194/essd-12-805-2020
- IPCC. In: Shukla PR, Skea J, Buendia EC, et al., eds. *Climate Change and Land: an IPCC special report on climate change, desertification, land degradation, sustainable land management, food security, and greenhouse gas fluxes in terrestrial ecosystems*; 2019 In press.
- Christiansen HH, Gilbert GL, Demidov N, et al. SESS Report 2019 - The State of Environmental Science in Svalbard, Svalbard Integrated Arctic Earth Observing System, Longyearbyen. 2019a.
- Christiansen HH, Gilbert GL, Demidov N, et al. Permafrost temperatures and active layer thickness in Svalbard during 2017/2018 (PermaSval). In: den Heuvel, ed. *SESS Report 2019*. Longyearbyen: Svalbard Integrated Arctic Earth Observing System; 2020:236-249.
- Rachlewicz G, Szczuciński W. Changes in thermal structure of permafrost active layer in a dry polar climate, Petuniabukta, Svalbard. *Pol Polar Res*. 2008;29:261-278.
- Marsz AA, Styszynska A, Pekala K, Repelewska-Pekalowa J. Influence of meteorological elements on changes in active-layer thickness in the Bellsund region, Svalbard. *Permafrost Periglacial Process*. 2013;24(4):304-312. doi:10.1002/ppp.1790
- Sobota I, Nowak M. Changes in the dynamics and thermal regime of the permafrost and active layer of the High Arctic coastal area in north-west Spitsbergen, Svalbard. *Geogr Ann Ser B*. 2014;96(2):227-240. doi:10.1111/geoa.12045
- Christiansen HH, Gilbert GL, Demidov N, et al. Permafrost thermal snapshot and active-layer thickness in Svalbard 2016-2017. In: Orr, ed. *SESS Report 2018*. Longyearbyen: Svalbard Integrated Arctic Earth Observing System; 2019b:26-47.
- Draebing D, Krautblatter M. P-wave velocity changes in freezing hard low-porosity rocks: a laboratory-based time-average model. *Cryosphere*. 2012;6(5):1163-1174. doi:10.5194/tc-6-1163-2012
- Hauck C, Kneisel C. *Applied Geophysics in Periglacial Environments*. Cambridge University Press; 2009 10.1017/CBO9780511535628.
- Carcione J, Seriani G. Wave Simulation in Frozen Porous Media. *J Comput Phys*. 2001;170(2):676-695. doi:10.1006/jcph.2001.6756
- Dou S, Ajo-Franklin JB. Full-wavefield inversion of surface waves for mapping embedded low-velocity zones in permafrost. *Geophysics*. 2014;79(6):EN107-EN127. doi:10.1190/geo2013-0427.1
- Draebing D. Application of refraction seismics in alpine permafrost studies: A review. *Earth Sci Rev*. 2016;155:136-152. doi:10.1016/j.earscirev.2016.02.006
- Gido NAA, Bagherbandi M, Sjöberg LE, Tenzer R. Studying permafrost by integrating satellite and in situ data in the northern high-latitude regions. *Acta Geophys*. 2019;67(2):721-734. doi:10.1007/s11600-019-00276-4
- Dobiński W. *Permafrost in the selected areas of Tatra Mts, the Scandinavian Mts, and Spitsbergen in the light of extensive geophysical studies and climatological analyses*, *Prace naukowe Uniwersytetu Śląskiego w Katowicach nr 2850*. Wydawnictwo Uniwersytetu Śląskiego; 2011 (in Polish with English and German summary).
- Minsley BJ, Abraham JD, Smith BD, et al. Airborne electromagnetic imaging of discontinuous permafrost. *Geophys Res Lett*. 2012;39(2):L02503. doi:10.1029/2011GL050079
- Rossi G, Accaino F, Boaga J, Petronio L, Romeo R, Wheeler W. Seismic survey on an open pingo system in Adventdalen Valley, Spitsbergen, Svalbard. *Near Surf Geophys*. 2017;16(1):89-103. doi:10.3997/1873-0604.2017037
- Tsuji T, Johansen TA, Ruud BO, Ikeda T, Matsuoka T. Surface-wave analysis for identifying unfrozen zones in subglacial sediments. *Geophysics*. 2012;77(3):EN17-EN27. doi:10.1190/geo2011-0222.1
- Hilbich C. Time-lapse refraction seismic tomography for the detection of ground ice degradation. *Cryosphere*. 2010;4(3):243-259. doi:10.5194/tc-4-243-2010
- Lecomte I, Polom U, Sauvin G, Ruud BO, Christiansen H, Gilbert G. Shear-wave Reflection-seismic Pilot Study at the UNIS CO2 Lab site, Longyearbyen. Svalbard 76th EAGE Conference Proceedings, 2014, WE P04 05, 5 pp.
- Johansen TA, Digraanes P, van Schaak M, Lonne I. Seismic mapping and modeling of near-surface sediments in polar areas. *Geophysics*. 2003;68(2):566-573. doi:10.1190/1.1567226
- Johansen TA, Ruud BO, Bakke NE, Riste P, Johannessen EP, Henningsen T. Seismic profiling on Arctic glaciers. *First Break*. 2011; 29(1768):65-71. doi:10.3997/1365-2397.2011004
- Oye V, Braathen A, Polom U. Preparing for CO2 storage at the Longyearbyen CO2 Lab: microseismic monitoring of injection tests. *First Break*. 2013;31(7):95-101. doi:10.3997/1365-2397.31.7.70361
- Strobbia C, Glushchenko A, Laake A, Vermeer P, Papworth TJ, Ji Y. Arctic near surface challenges: the point receiver solution to coherent noise and statics. *First Break*. 2009;27(2):1-5. doi:10.3997/1365-2397.27.1296.28785
- Baelum K, Johansen TA, Johnsen H, Rod K, Ruud BO, Braathen A. Subsurface structures of the Longyearbyen CO2 Lab study area in Central Spitsbergen (Arctic Norway), as mapped by reflection seismic data. *Nor J Geol*. 2012;92:377-389.
- Baranowski S. Thermic Conditions of the Periglacial Tundra in SW Spitsbergen, Acta Universitas Wratlaviensis 68, *Studia Geograficzne X* (in Polish with Eng abstract), 1968; 74
- Wawrzyniak T, Osuch M, Napiórkowski J, Westermann S. *Modelling of the thermal regime of permafrost during 1990-2014 in Hornsund, Svalbard*. Polish Polar Research; 2016 10.1515/popore-2016-0013.
- Pekala K, Repelewska-Pekalowa J. *Relief and stratigraphy of Quaternary deposits in the region of Recherche Fjord and southern Bellsund (Western Spitsbergen)*. Lublin, Poland: Wyprawy Geograficzne na Spitsbergen, UMCS; 1990.
- Jahn A. Soil thawing and active layer of permafrost in Spitsbergen. *Acta Univ Wratislavi*. 1982;525:57-75.
- Jahn A. Periglacial soil structures in Spitsbergen and in central Europe, V International Conference on Permafrost, Trondheim, 769-800. 1988.
- Grześ M. Characteristics of the active layer of permafrost in Spitsbergen. XI Sympozjum Polarne, Poznań, 65-83, 1984. (in Polish)
- Migala K. Effect of winter season and snow cover on the active layer of permafrost in the region of Hornsund (SW Spitsbergen). *Wyprawy Geograficzne na Spitsbergen*, Lublin, 248. 1991. (in Polish)
- Migala K. The characteristic features of the active layer of the permafrost in the climate of Spitsbergen. *Acta Univ Wratislavi*. 1994;1590:79-111. (in Polish with Eng. abstract)
- Dolnicki P. Spatial distribution of permafrost level and its connection with variable disappearance snow cover in the area of Fuglebergsetta (SW Spitsbergen). *Polish Polar Studies. XXXI Sympozjum Polarne*, Kielce, 34-45, 2005. (in Polish)
- Miętus M. Short period changes of soil temperature against advective changes of air temperature in Hornsund, Spitsbergen. *Pol Polar Res*. 1988;9:95-103.
- Miętus M, Filipiak J. Variability of ground temperature in Hornsund in the period 1979-1999. *Przegl Geofizyczny*. 2001;46(4):323-337. (in Polish)
- Leszkiewicz J, Caputa Z. The thermal condition of the active layer in the permafrost at Hornsund, Spitsbergen. *Pol Polar Res*. 2004;25:223-239.
- Dolnicki P. Changes of thermic of the ground in Hornsund (SW Spitsbergen) in the period 1990-2009. *Probl Klim Polar*. 2010;20:121-127. (in Polish with English summary)
- Dolnicki P, Grabiec M, Puczek D, Gawor Ł, Budzik T, Klementowski J. Variability of temperature and thickness of permafrost active layer at

- coastal sites of Svalbard. *Polish Polar Res.* 2013;34(4):353-374. doi:10.2478/popore-2013-0026
41. Dobiński W, Leszkiewicz J. Active layer and permafrost occurrence in the vicinity of the Polish Polar Station, Hornsund, Spitsbergen in the Light of Geophysical Research. *Probl Klim Polar.* 2010;20:129-142. (in Polish with English summary)
 42. Kasprzak M. High-resolution electrical resistivity tomography applied to patterned ground, Wedel Jarlsberg Land, south-west Spitsbergen. *Polar Res.* 2015;34(1):25678. doi:10.3402/polar.v34.25678
 43. Kasprzak M, Strzelecki MC, Kondracka M, et al. On the potential for a bottom active layer below coastal permafrost: the impact of seawater on permafrost degradation imaged by electrical resistivity tomography (Hornsund, SW Spitsbergen). *Geomorphology.* 2017;293:347-359. doi:10.1016/j.geomorph.2016.06.013
 44. Kasprzak M. Seawater intrusion on the Arctic coast (Svalbard): The concept of onshore-permafrost wedge. *Geosciences.* 2020;10(9):349. doi:10.3390/geosciences10090349
 45. Glazer M, Dobiński W, Marciniak A, Majdański M, Błaszczyk M. Spatial distribution and controls of permafrost development in non-glacial Arctic catchment over the Holocene, Fuglebekken, SW Spitsbergen. *Geomorphology.* 2020;358:107128. doi:10.1016/j.geomorph.2020.107128
 46. Dobiński W. Permafrost active layer. *Earth Sci Rev.* 2020;208:103301. doi:10.1016/j.earscirev.2020.103301
 47. Czerny J, Kieres A, Manecki M, Rajchler J. *Geological Map of the SW part of Wedel Jarlsberg Land, Spitsbergen, 1:25000.* Kraków: Institute of Geology and Mineral Deposits; 1993.
 48. Osuch M, Wawrzyniak T, Nawrot A. Diagnosis of the hydrology of a small Arctic permafrost catchment using HBV conceptual rainfall-runoff model. *Hydrol Res.* 2019;50(2):459-478. doi:10.2166/nh.2019.031
 49. Wawrzyniak T, Majerska M, Osuch M. Hydrometeorological dataset (2014–2019) from the high Arctic unglaciated catchment Fuglebekken (Svalbard). *Hydrol Process.* 2021;35(1):e13974. doi:10.1002/hyp.13974
 50. Humlum O, Instanes A, Sollied JL. Permafrost in Svalbard: a review of research history, climatic background and engineering challenges. *Polar Res.* 2003;22(2):191-215. doi:10.3402/polar.v22i2.6455
 51. Park CB, Miller RD, Xia J. Multichannel analysis of surface waves. *Geophysics.* 1999;64(3):800-808. doi:10.1190/1.1444590
 52. Schrott L, Hoffmann T. *Refraction seismics.* Cambridge University Press; 2008:57-80. doi:10.1017/CBO9780511535628.004.
 53. Hobro JWD, Singh SC, Minshull TA. Three-dimensional tomographic inversion of combined reflection and refraction seismic traveltimes data. *Geophys J Int.* 2003;152(1):79-93. doi:10.1046/j.1365-246X.2003.01822.x
 54. Owoc B, Górszczyk A, Majdański M. The discussion of the uncertainty in the traveltime seismic tomography, EAGE conference proceedings, 2018; TU 24P2 04, 5 pp.
 55. Marciniak A, Stan-Kleczeck I, Idziak A, Majdański M. Uncertainty based multi-step seismic analysis for near-surface imaging. *Open Geosci.* 2019;11:727-737.
 56. Gregersen O, Phukan A, Johansen T. Engineering properties and foundations design alternatives in marine Svea clay, Svalbard. Permafrost, Fourth International Conference Proceedings, National Academy Press Washington D.C. 1983.
 57. Christiansen HH, Etzelmüller B, Isaksen K, et al. The thermal state of permafrost in the Nordic area during the international polar year 2007–2009. *Permafrost Periglacial Process.* 2010;21(2):156-181. doi:10.1002/ppp.687
 58. Millero FJ, Feistel R, Wright DG, McDougall TJ. The composition of Standard Seawater and the definition of the Reference-Composition Salinity Scale. *Deep-Sea Res I Oceanogr Res Pap.* 2008;55(1):50-72. doi:10.1016/j.dsr.2007.10.001
 59. Albaric J, Kuhn D, Ohnberger M, et al. Seismic monitoring of permafrost in Svalbard, Arctic Norway. *Seismol Res Lett.* 2021;92(5):2891-2904. doi:10.1785/0220200470







How to cite this article: Majdański M, Dobiński W, Marciniak A, et al. Variations of permafrost under freezing and thawing conditions in the coastal catchment Fuglebekken (Hornsund, Spitsbergen, Svalbard). *Permafrost and Periglacial Process.* 2022;1-13. doi:10.1002/ppp.2147

Paper V:

Marciniak, A., Osuch, M., Wawrzyniak, T., Owoc, B., Dobiński, W., Glazer, M., & Majdański, M. (2022). Multi-method geophysical mapping of ground properties and periglacial geomorphology in Hans Glacier forefield, SW Spitsbergen. *Polish Polar Research*, 43(2), 101–123. <https://doi.org/10.24425/ppr.2022.140363>



Multi-method geophysical mapping of ground properties and periglacial geomorphology in Hans Glacier forefield, SW Spitsbergen

Artur Marciniak^{1*} , Marzena Osuch¹ , Tomasz Wawrzyniak¹ ,
 Bartosz Owoc¹ , Wojciech Dobiński² , Michał Glazer²
 and Mariusz Majdański¹ 

¹ Institute of Geophysics, Polish Academy of Sciences, Warsaw, 01-452, Poland

² Faculty of Natural Sciences, University of Silesia, Sosnowiec, 41-200, Poland

* corresponding author <amarciniak@igf.edu.pl>

Abstract: This article presents the results of a geophysical survey from which detailed images of glacial and periglacial landforms and subsurface structures were obtained. Sediments and landforms on newly deglaciated terrain can be used to reconstruct the extent and character of glaciers in the past and add to the understanding of their response to climate and environmental changes. To derive spatial information from complex geomorphological terrain, joint interpretation of three non-intrusive geophysical methods were applied: Electrical Resistivity Tomography (ERT), Ground Penetrating Radar (GPR), and time-lapse Seismic Tomography. These were used to identify subsurface structures in the forefield of the retreating Hans Glacier in SW Spitsbergen, Svalbard. Three main zones were distinguished and described: outwash plain, terminal moraine from the last glacial maximum, and glacial forefield proximal to the glacier front. Geophysical profiles across these zones reveal information on glacio-fluvial sediment thickness and structure, ice thickness and structure, and bedrock topography. The freezing-thawing effect of the active layer has a strong and deep impact, as demonstrated by variations in P-wave velocity in the obtained outcomes. The results are discussed in the context of the current climate in Svalbard. This study provides a snapshot of ground parameters and the current state of the subsurface in southern Spitsbergen. The boundary between sediment-bedrock layers was estimated to be from 5 to 20 m in depth. It is the first such extensive description of periglacial structures in the forefield of the Hans Glacier, utilising the longest ERT profile (1500 m) in Svalbard together with deep GPR and precise seismic tomography.

Keywords: Arctic, Svalbard, geophysical imaging, periglacial environment, glacial landforms.



Copyright © 2022. The Authors. This is an open-access article distributed under the terms of the Creative Commons Attribution-NonCommercial-NoDerivatives License (CC BY-NC-ND 3.0 <https://creativecommons.org/licenses/by-nc-nd/3.0/>), which permits use, distribution, and reproduction in any medium, provided that the article is properly cited, the use is non-commercial, and no modifications or adaptations are made.

Introduction

In recent years, there has been increasing scientific interest in environmental changes within the Arctic and Antarctic regions, as well as in high-altitude landscapes (*e.g.*, Kaushik *et al.* 2021). These areas are highly sensitive to climatic fluctuations and therefore can be used as “natural laboratories” for studying the evolution of periglacial environments, landforms, and processes. In most studies in areas such as Svalbard, the greatest effort is put into the characterisation of air or ground surface temperatures (IPCC 2021). Subsurface parameters and spatial extents of features are usually poorly represented due to an insufficient number of measurements and experiments.

Geophysical imaging is a powerful tool for achieving better spatial insights into subsurface structures. Approaches utilising multiple methods based on different parameters can be effective in recognising structural features and major lithological characteristics, as well as in the indirect estimation of thermal conditions (Maurer and Hauck 2007; Kneisel *et al.* 2008). Freezing of the ground has implications for geomorphic processes, mechanical and hydrogeological properties, and consequently landforms since freezing restricts permeability and subsurface water movement. Materials of different grain sizes have various thermal conductivities and volumetric heat capacities (Zimmerman and King 1986). Most modern permafrost research focuses on the variability of the 0°C isotherm within the ground, known as the permafrost table. Such boundary separates permafrost from the so-called active layer above where seasonal changes in summer reach positive temperatures.

The direct measurement of permafrost, *i.e.*, thermal properties of the ground, can only be done by establishing boreholes equipped with thermistor strings. Such an approach is limited to point observations in a limited number of boreholes and does not provide information about both permafrost/active layer areal changes over time. Instead, multiple geophysical methods can be used in an integrated field investigation to fill this gap. Seasonal changes in both temperature and hydrology of the permafrost/active layer strongly affect the elasticity modulus and, therefore, seismic velocities of rocks (Jacoby *et al.* 1996; Carcione and Seriani 1998). This complicates our understanding of active layer behaviour, which in turn impacts our understanding of the glacial and periglacial environments. As a consequence, integrated seismic studies in permafrost environments remain scarce.

To improve the understanding of landforms–permafrost interactions, joint interpretation of multiple datasets is essential. In this contribution, we present the results of a multi-method geophysical approach utilising Electrical Resistivity Tomography (ERT), Ground Penetrating Radar (GPR) and seismic tomography. These methods were combined to obtain an improved visualisation of subsurface structures of geomorphological landforms in the forefield of the Hans Glacier, including outwash plain (sandur) and terminal moraine.

Study site

The study area is located in SW Spitsbergen near the Polish Polar Station Hornsund (Fig. 1). The station was established in 1957, and since 1978 it has conducted year-round scientific monitoring. Geophysical imaging was conducted in 2015, 2017, and 2018 along with the HOR22 profile in an area partially covered by a glacier up to 2013. The survey was performed on the uplifted marine terraces between the shore of the Hornsund fjord and the slopes of the mountains Fugleberget (569 m a.s.l.) and Arikammen (517 m a.s.l.). These terraces, raised during the Holocene (Lindner *et al.* 1986), consist of sea gravels covered by a wide variety of tundra vegetation types as well as areas of exposed rock. The profile also covers the moraines of the Hans Glacier. The glacier retreated about 1500 m from its maximum extent (König *et al.* 2014) at the end of the Little Ice Age (LIA). To image periglacial and glacial features, the profiles were run during two campaigns through moraines towards the terminus of the retreating glacier. There is a slight difference in the profile line obtained on the frontal moraine between the two data acquisition campaigns.

Climatic conditions. — The climate of the west coast of Spitsbergen is highly influenced by relatively mild polar-marine conditions and has experienced significant changes in the annual average air temperature over the 20th century

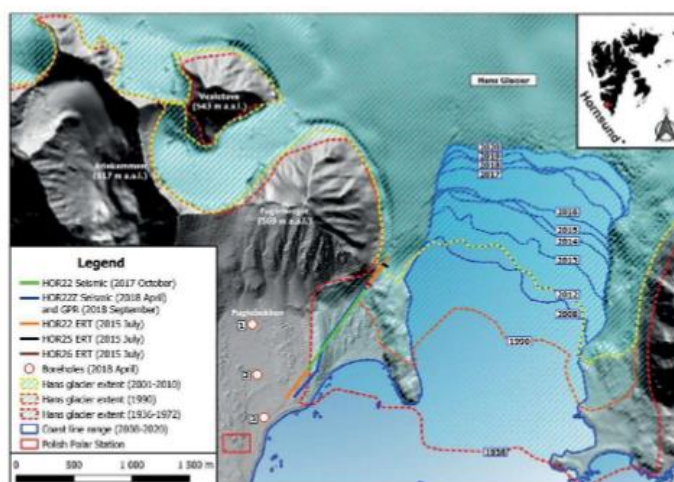


Fig. 1. Study area with marked seismic, ERT, and GPR profiles. Digital elevation model after Błaszczyk *et al.* (2022), glacier extent after König *et al.* (2014).

and after the year 2000 (Nordli *et al.* 2020). Changes in the annual cycles of air temperature during this period are not evenly distributed. Atmospheric warming over Spitsbergen has been pronounced in almost all decades since the end of the LIA, except for the two coldest decades of the 1910s and 1960s. The greatest warming was observed during the past three decades and is amongst the most severe recorded in the Arctic region. The largest impact is seen in the response of glaciers, especially in changes to volume and extent (Van Pelt *et al.* 2019). The location of the front of the Hans Glacier and factors controlling position was described by Blaszczyk *et al.* (2021).

Long-term measurement of meteorological variables at the Hornsund Station enables estimation of changing climatic conditions. Figure 2a shows the variation in mean annual air temperature at Hornsund in the period 1979–2020. The mean air temperature from this period was -3.6°C (and -3.7°C during 1979–2018). Analyses of this data by the modified Mann-Kendall test indicate a statistically significant increasing trend with a slope of $+1.04^{\circ}\text{C}$ per decade, using the method of Sen (1968). This was six times higher than the global warming average for the same period (Wawrzyniak and Osuch 2020). Such changes have many environmental implications, including the prolongation of the ablation season (Osuch and Wawrzyniak 2017b; Nowak *et al.* 2021). Figure 2b shows variation in the number of days with positive air temperature per year observed at Hornsund in the period 1979–2020. The lowest number, 99 days, was observed in 1982, while the highest was 213 days in 2016. A statistically significant increasing trend was estimated with a slope of $+12.86$ days per decade.

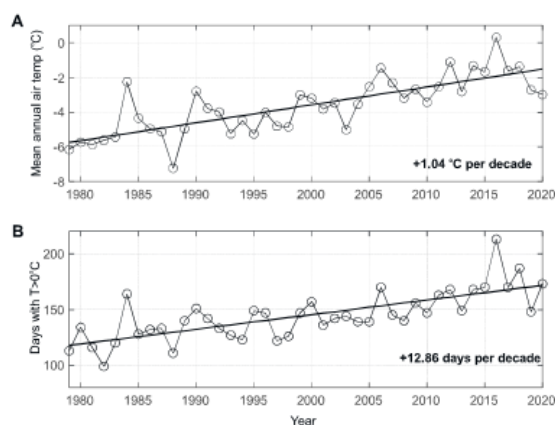


Fig. 2. Variation in (A) annual mean air temperature and (B) number of days with positive air temperatures at Hornsund Station in the years 1979–2020. Trends were estimated by the modified Mann-Kendall test (Hamed and Rao 1998).

Changes in air temperature and precipitation resulted in changes in snow cover thickness and duration (Osuch and Wawrzyniak 2017a). The presence of a seasonal snow cover has a significant influence on the ground thermal regime, with either cooling or warming effects that change over time. Due to high albedo and low thermal conductivity, snow cover acts as an insulator from direct atmospheric influence. Snow cover is a key factor for subsurface processes including both permafrost development and degradation, as it may substantially reduce the seasonal freezing depth. The overall impact of snow cover on the ground thermal regime depends on the timing, duration, thickness, and melting of seasonal snow and ice cover (Wawrzyniak *et al.* 2016; Christiansen *et al.* 2019; 2020, 2021). Figure 3 presents the variation of maximum annual snow depth and the number of days with snow cover at the Hornsund meteorological site in the period 1983–2020. Large decreases in both variables are present with statistically significant trends. The slopes of the trends are -2.35 cm per decade for maximum snow depth and -12.78 days per decade for snow cover duration.

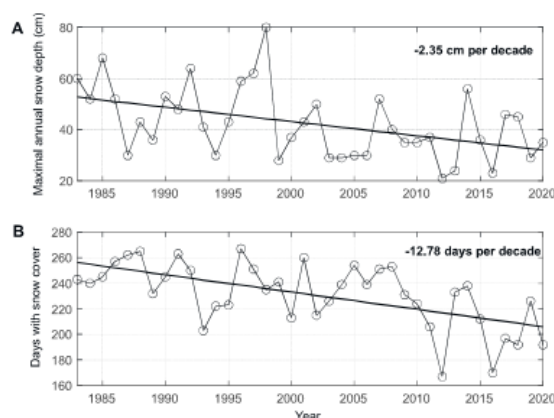


Fig. 3. Variation in (A) maximal annual snow depth and (B) number of days with snow cover at Hornsund Station in the years 1983–2020. Trends were estimated by the modified Mann-Kendall test (Hamed and Rao 1998). The slope of the trend was estimated using Sen's method (Sen 1968).

Geology and geomorphology of the study site. — The geology along the studied profile (Fig. 4) consists of crystalline Precambrian rocks of Lower and Middle Hecla Hoek succession: marbles, schists, metamorphic quartzites, paragneisses, and amphibolites (Czerny *et al.* 1993). These rocks are strongly fractured and loosened in the near-surface zone due to tectonic relief movements and glacial abrasion and frost weathering at the turn of the Pleistocene/Holocene.

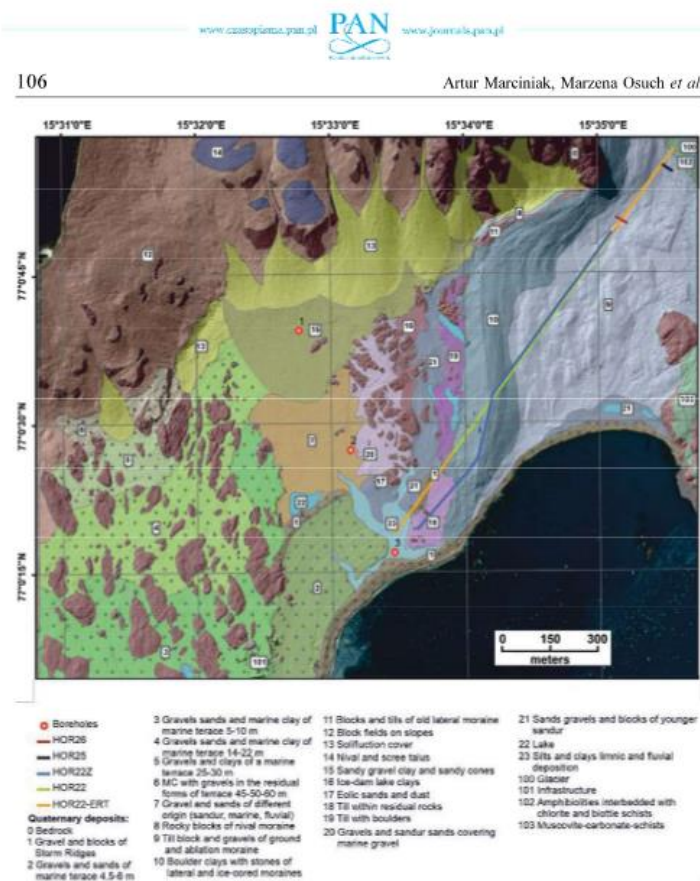


Fig. 4. Map of Quaternary deposits with marked seismic, GPR and ERT lines. Source of data: Pękala (1989) and Glazer *et al.* (2020).

As a result of isostatic uplift, abrasion platforms with variably aged marine sediments were formed. These elevated structures have been largely transformed by erosion, as well as by colluvial accumulation and solifluction on the slopes (Pękala 1989; Dolnicki and Grabiec 2022). Isostatic uplift of terraces on Spitsbergen was irregular and also affected by local tectonic activity (Lindner *et al.* 1986). Uplift depended spatially and dynamically on the distribution of past ice-sheet loads and deglaciation histories (Landvik *et al.* 1998).

In the foreground of the Hans Glacier, landforms of glacial and fluvio-glacial relief in the form of moraines, soil and rock deposits were superimposed on the

uplifted sea terraces. These glacial landforms underwent relatively rapid changes in the periglacial environment following deglaciation especially on slopes and in wetlands. The maximum extent of the Hans Glacier is marked by the frontal part of the ice-cored moraine, which was deposited *ca.* 1900 (Fig. 4), at the end of the LIA (Błaszczyk *et al.* 2013). The frontal moraine is characterised by a particularly large culmination of pushed morainic sediments with a buried ice core. Behind this moraine, an area of degrading dead-ice ground moraine extends up to the current glacier front (Glazer *et al.* 2020). Ground moraine deposits formed during advance and retreat also contain blocks of dead ice, visible in the geophysical imaging described below. Within this area, a system of smaller lateral moraines has been created encircling sediments of the ground moraine.

In southern Spitsbergen, there has been a recent expansion of ice-free areas (Fig. 1), with the most remarkable retreats of the tidewater glaciers (Błaszczyk *et al.* 2013, 2021), therefore the monitoring of changes in the functioning of environmental systems has become critically important.

Methods

The ERT measurements were carried out in June 2015, using a Schlumberger and dipole-dipole array with 5 m electrode spacing (Loke 2018). As an electric method, the ERT is sensitive to water saturation and phase changes, as ice has very high resistivity and water has low resistivity. Due to better resolution, only the results from the dipole-dipole arrays are presented in this study. The ERT profile length was 1500 m and covered parts of the Fugglebekken catchment (past glacial outwash plain), along with the Hans Glacier ice-cored moraine of the glacial maximum and post-glacial sediments with dead ice (Fig. 1). The profile ends close to the current glacier front. The dataset was gathered using ABEM Terrameter LS equipment. Additionally, the data from two 40 m crossline profiles (HOR25 and HOR26) were collected at the end of the HOR22 line. These arrays used dense (1 m) electrode spacing for recognition of active layer thickness, with a dipole-dipole scheme.

The GPR survey along 1115 m profile was conducted when the ground was still in a thawing state in September 2018. It covered the HOR22Z profile so that the results from various geophysical methods could have been compared. A MALÅ GPR with a 30 MHz non-shielded RTA (Rough terrain antenna) system was used, allowing penetration up to 40 m. The sampling interval was 20 cm, providing a dense dataset. Elevation was measured by built-in GPS.

Two seismic campaigns were undertaken in September/October 2017 during maximum active layer thawing and in April/May 2018 with the active layer frozen. In September, the seismic receiver and shot spacing was 5 m, and the seismic profile consisted of three deployments with 50 m lateral offsets, resulting in a length of 900 m (without shot offsets) covered with seismic stations, using 4.5 Hz

geophones connected with standalone Omnirecs Data CUBE stations. In April 2018, the profile consisted of four deployments with offset-shooting and 25 m offset on each side, resulting in a length of 1150 m (without shot offsets) covered with seismic stations. The receiver spacing in 2018 was maintained (5 m), whereas the shot spacing was set at 2.5 m. As a result, the data was spatially twice as dense as in 2017. This significantly increased the seismic data fold (Fig. 5) and enhanced the signal-to-noise ratio and horizontal resolution of the data.

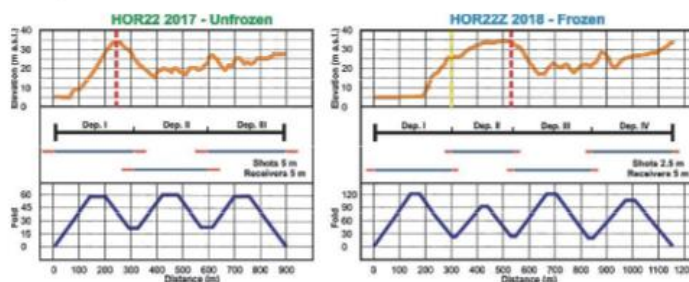


Fig. 5. The survey geometry for seismic profiles during freezing and thawing active layer conditions. The yellow bar crossing the profile marks the edge of the moraine. The red bar marks the beginning of the shared profile in the two seasons, which can be directly compared. Snow coverage during measurements is visible on the elevation profile, however, main landforms can be distinguished and directly compared. Rock outcrops not covered.

Data processing

The program Res2dinv v. 4.06.18 was used to invert the measurement data. For topographic correction, a Digital elevation model (DEM) model with a 1 m resolution was used. More than 50 inversions with respective predetermined parameters were applied to test the behaviour of the resistivity models and to ensure a systematic approach (Glazer *et al.* 2020). Models demonstrated high resilience to structural change upon tested inversion parameters. The resistivity model standard settings from this version of the software for robust data and smooth model were used. The inversion methodology was the same for all three ERT lines.

GPR is one of the most useful tools in cryospheric studies (Farbrot *et al.* 2005; Baelum 2007; Bernard *et al.* 2014; Senderak *et al.* 2021). Data processing was conducted using RadExplorer software. It consists of the removal of instrumental noise (debias), with subsequent basic signal filtering for optimal results. In addition, time zero adjustment was made based on the first breaks of Electromagnetic (EM) waves, with final topography correction based on the GPS data. EM wave velocities were quantified in recognised subsurface structures.

The precise velocity field for depth migration was then determined after manual fitting of parameters, based on tabularized values (Dobiński *et al.* 2011, 2017).

Seismic refraction results were obtained by merging two inversion methods. To image the near-surface layer, the Simultaneous Iterative Reconstruction Technique (SIRT) algorithm (Nolet 2008) was used. Such an approach permits precise estimation of the first seismic boundary, which was fixed for further processing. For modelling of deeper layers, First Arrival Traveltime Tomography (FATT) was applied. This produces a precise estimation of velocity changes and thus gives a smooth velocity field, necessary for recognition of freezing-thawing effects. The starting velocity field model for FATT was a rectangular grid with cell dimensions of 5.0 by 1.0 m in unfrozen conditions (2017) and 2.5 by 1.0 m in frozen conditions (2018). The variation in model cell size is due to different shot spacing for the corresponding survey (Fig. 5). Seismic tomography inversion for both seasons was carried out with the JIVE3D software (Hobro *et al.* 2003). During processing, a set of linearized refinements was applied to the velocity field model for an accurate fit between picked and calculated travel times. For uncertainty analysis, the approach proposed by Owoc *et al.* (2019) was used. It employs a grid search method to statistically generate a set of 1D velocity fields, which are used as starting models in tomographic inversion. To estimate uncertainty, standard deviations of obtained results (inverted velocity fields) were calculated separately for each grid cell.

Results and interpretation

The combined geophysical surveys yielded sufficient data for quantitative and qualitative analysis of the study site. The combination of the different methods allowed resolving the complex characteristics of the subsurface.

Electrical Resistivity Tomography. — The application of ERT with a dipole-dipole array deployment provides insight into the ground structures up to 100 m in depth (Fig. 6). However, due to high resistivity, only the shallowest parts of the image (to a depth of 20–30 m) can be interpreted with certainty. The beginning of the section where the seismic data from profile HOR22Z can be compared with the ERT dataset is located at 520 m of the profile. There is a large variability in resistivity, ranging from 0.1 to 11000 kOhm.m. Such broad variation indicates major changes in conditions for current propagation for different parts of the study site. Multiple bodies of high resistivity can be identified in the profile image. The root mean square error for profile HOR22 was estimated at 5.3%, and 3.7% and 4.5% for profiles HOR26 and HOR25, respectively. The analysis of the ERT results allows for differentiation of 3 zones, where major resistivity distributions can be separated. These zones correspond to the geomorphological overall zonation/landforms: outwash plain (sandur), terminal moraine, and ground moraine (glacier forefield).

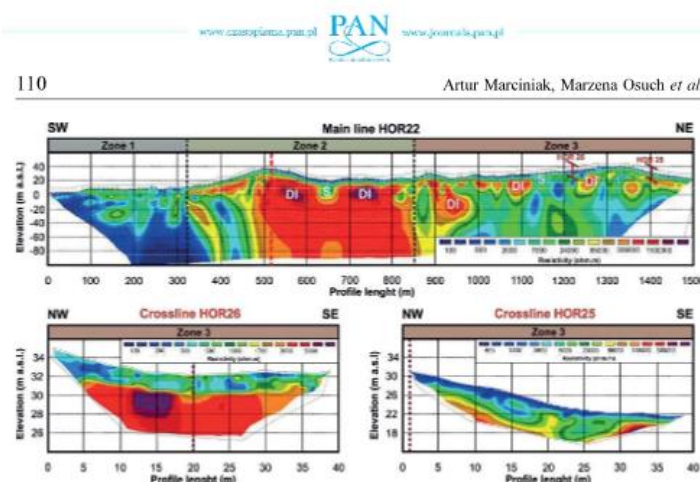


Fig. 6. Profiles generated by ERT survey (summer 2015) using dipole-dipole electrode deployment. High-resistivity anomalies were interpreted as dead-ice (DI). The small low-resistivity anomalies at 640 and 1150 m were identified as an active watercourse (S). The red dashed line indicates the area from which the results of seismic and GPR surveys can be directly compared. The crossline profiles HOR25 and HOR26 show the presence of the active layer with thickness varying from 1 to 2 m. Profiles differ in scale concerning both elevation and resistivity. For the location of the profiles, see Fig. 1.

In zone 1 (outwash plain), from 0 to 320 m on the profile, overall resistivities are low, in the range of 0.1 to 7.0 kOhm.m. This can be attributed to the presence of the water-saturated layers in the Fuglebekken catchment. The lowest resistivity occurs between 0 and 80 m due to the presence of water-saturated sands and gravels of the Fuglebekken channel and floodplain. Increasing resistivity from 80 to 240 m can be attributed to a thin cover of silts, sands, and gravels of the outwash plain, formed as a sandur in the past, by meltwater from the glacier (Glazer *et al.* 2020). Structures located at 150–170 m and 300–320 m can be identified as gravel and blocks of storm ridges, which are visible on the surface as outcrops (Fig. 4).

In zone 2 (terminal moraine), from 320 to 850 m along with the profile, the terminal moraine of the maximum glacial extent during the LIA at around 1900 has the highest resistivity (over 1100 kOhm.m). The structure can be interpreted as dead-ice. On the SW side of the moraine, the ice core is thinner compared to the NE side. Near the surface above these ice cores, a water-saturated sediment cover that is around 10 m thick can be noticed based on estimated resistivity values. In addition, on the NE side of the moraine at 640 m, a stream channel is visible by clearly lower resistivity values. In the profile between 320 up to 850 m, features at a depth greater than 20 m below the surface cannot be identified, as the current is blocked by overlying high-resistivity features. Thus, the interpretation of deeper parts is uncertain and may be misleading.

In zone 3 (glacier forefield proximal to the glacier front), from 850 m to 1500 m, several structures are present with differing resistivities. Multiple areas with lower resistivity (<30 kOhm.m) can be interpreted as a water-saturated layer and stream channels due to the overall shape of the anomalies. Structures with high resistivity (>100 kOhm.m) can be recognised as blocks of dead-ice 10–30 m big. From 1280 m to 1500 m, structures with moderate resistivities can be seen. These are probably solid rock structures, with relatively high values of resistivity, however significantly lower than typical ice formations. Additionally, the shape of the structures is more horizontal in comparison to dead ice blocks. Within the zone 3, periglacial reworking of glaciogenic sediments occurred during ongoing deglaciation. The retreat of the Hans Glacier caused progressive modification of glacial sediments, landforms, and deeper layers through exposure to non-glacial processes, resulting in complex structures.

Crossline profiles gathered in June 2015, HOR25 and HOR26 were used to image the active layer thickness in Zone 3 with denser electrode spacing on 40 m arrays. The difference to mainline HOR22 deployment resulted in shallower recognition depth, however, with higher resolution. The layer varies from 1 to 2.5 m in both crossline profiles. There is an overall difference in resistivity between HOR26 (approx. 5.0 kOhm.m) and HOR25 (380 kOhm.m). This can be explained by the localisation of the profile HOR26 near the active surface stream, while line HOR25 was located on a relatively dry part of the moraine. The increased resolution due to more dense electrode spacing allowed for recognition of active layer – permafrost boundary, which is clearly visible on HOR26 line at a depth of average 2 m. Such boundary is less visible at line HOR25 due to lower contrast between layers in a drier environment. In comparison to profile HOR22, where the active layer is not visible due to resolution limitations, the shorter lines HOR25 and HOR26, in contrast, do not show the sediment-bedrock boundary.

Ground Penetrating Radar. — Due to resolution limitations, the GPR method with a 30 Mhz unshielded RTA provides information about subsurface structures down to 40 m depth but not the near-surface, including the active layer (Fig. 7). The shallowest penetration range was obtained at the end and beginning of the profile and at 100 m of its length, where it reached 20 m. The deepest penetration was in the central part of the terminal moraine. The overall reflection visibility is good, and multiple reflectors can be tracked and distinguished as continuous across the whole profile. Reflections at depths greater than 10 m in front of and behind moraine structures are very irregular. In the dataset, almost no diffraction hyperbolas can be distinguished. These observations indicate that irregular structures are continuous, without visible faults and discontinuities. Similar to the ERT results, the three main zones could be distinguished.

Zone 1 (the outwash plain) ranges from 0 to 220 m of the profile, with shallow sediment cover visible on the GPR section. The thickness of this layer, limited by the green dashed line (Fig. 7), varies from 1 m at the beginning of the profile to about 7 m near the slope of the terminal moraine. Beneath this layer,

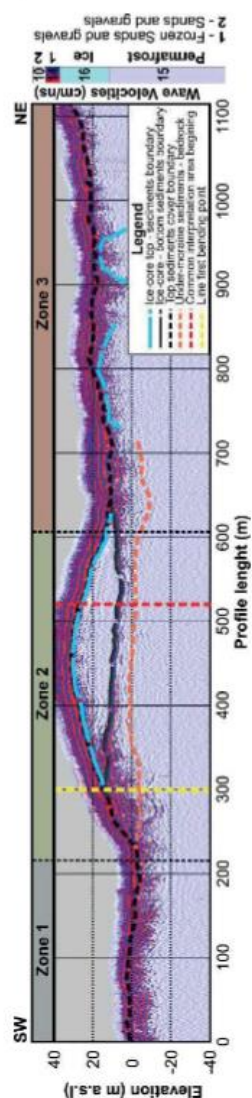


Fig. 7. The GPR images reveal a sediment layer covering the moraine structure and uniform LLA moraine with an ice core inside. The red and yellow dashed lines indicate the profile breaking points.

crystalline bedrock can be distinguished. The uneven shape of this boundary is caused by the presence of gravel and blocks of storm ridges partly covered by sediments (Fig. 4).

Zone 2 (terminal moraine) from 220 to 620 m of the profile length includes the terminal moraine from the maximum glacial extent during the LIA. The ice core was recognised in the processed radargram by its shape from 300 up to 610 m of the profile, beneath 5 to 7 metres of sediment cover. Presumably, a body of glacial ice was buried at the glacier terminus by accumulations of sediment during the glacier recession (Evans 2009). These overlying sediments provide a protective layer that reduces or even prevents the melting of the ice core as the active layer thickness is much smaller than the sediment cover. As the signal in this layer (up to an average of 35 m under the surface) reveals no reflective characteristics, the ice-core can be described as uniform without internal structures. Underneath the ice-core, there is a boundary that strongly reflects EM waves (dark grey dashed line on Fig. 7) that separates it from underlying sediments. The thickness of this lower sediment layer varies from 20 m in the bottom of the terminal moraine to 6 m in its NE slope (540 m of profile length). The shape of the layer at 230–330 m is a result of sediments pushed during glacial advance and debris sliding down from the slopes of the terminal moraine itself. The signal in this layer is strongly dampened, with most energy from the EM wave being propagated to the surface. The use of GPR also allowed for the distinction of the sediment/bedrock boundary and the bedrock layer (orange line on Fig. 7). The elevation of

this boundary is located at around 1 m a.s.l. A uniform ice-core partially isolates the underlying sediments and bedrock from hydrological processes occurring at the surface.

Zone 3 (the glacial forefield proximal to the glacier front), located from 610 m to the end of the profile, is covered by glacial deposits 5–10 m thick. Below this layer, the change in signal characteristics was identified as dead ice blocks mixed with englacial debris. Due to complicated reflections patterns, the interpretation of deeper structures reveals complex transitions. They have very high resistivity and effectively reflect EM waves to the surface. Deeper layers are obscured by these structures and by water saturation of near-surface sediment, which absorbs EM wave energy. As a result, only the tops of the dead-ice blocks can be imaged using the GPR method. Within zone 3, there are various glacio-fluvial landforms, characteristic of young glacial landscapes in a ground moraine. These landforms were formed below and around the margins of the retreating glacier and include old meltwater channels, eskers, and kame terraces, as can be recognised from the irregular topography of this zone and the shape of the sediment-bedrock boundary.

Seismic Tomography. — Seismic tomography imaging was conducted during two seasons, with maximal freezing (April 2018) and thawing conditions (October 2017). The application of seismic tomography was focused on the recognition of lithological structures and the top of permafrost. The tomographic results were obtained with the joint application of two methods. The shallowest layer was identified with short offset refraction travel times and the SIRT algorithm. The deeper layer was imaged using the ray-based FATT approach (Hobro and Singh 1999) with a fixed layer from the SIRT approach (Nolet 2008). Such a combination allowed for the improvement of subsurface recognition, with the derivation of sharp boundaries as well as smooth velocity changes. The initial models for tomographic method inversion were based on the GPR and ERT results. In these models, two layers were approximated: sediment and bedrock. The maximum penetration of imaging reached 80 m under the terminal moraine surface. The method provides a deeper range than GPR, but due to high seismic velocities and resolution limitations, smaller structures such as dead-ice blocks visible on the ERT and GPR in the glacial forefield cannot be recognised. The most important added value from the use of the SRT method is the visibility of seasonal changes in seismic velocity, *i.e.*, the thawing-freezing effect. During the field campaign in October 2017, air temperatures were still above 0°C, and the active layer thickness was estimated to be about 2 m, based on the data from nearest boreholes in Fuglebekken catchment (Fig. 1), while in April 2018, the air temperatures remained below 0°C and the ground was frozen.

Zone 1 (the outwash plain) from 280 to 390 m of the 2017 profile and 0 to 220 m of the 2018 profile, is characterised by uniform velocities across the sediment cover (~2000 m/s and 2500–2700 m/s in consecutive years). This is the smallest seasonal velocity change observed for the sedimentary cover along the

whole profile. A slight mismatch at the 5 m depth is a result of differing profile locations. In the bedrock, differences in the velocity field are visible up to 20 metres under the surface. In the data from 2017, velocities at 10 m depth below the surface are close to 5000 m/s, while for 2018, they were estimated at around 5600 m/s. Such high velocities indicate that the basement was in a cryotic state in April 2018 and September 2017, and the relatively small changes in the velocity compared to the other parts of the study site are probably related to groundwater level changes induced by the freezing-thawing effect of the active layer. However, the effect of velocity change is visible up to even 30 m under the surface. The changes in hydrology can reach even deeper into the rock structures and thus require further studies.

Zone 2 (terminal moraine), from 220 m in 2017 and 400 m in 2018 to 600 m, is characterised by clearly visible changes in velocity in sediment cover (2000 and 3000 m/s) and underlying ice-core (4000 and 5000 m/s in subsequent seasons). Due to the nature of refracted waves, the boundary between the ice-core and underlying structure cannot be recognised. The debris layer, visible in the GPR image underlies the ice-core, has lower velocities thus is transparent for refracted waves. Moreover, due to a mixture of ice and rocks lying on water-filled bedrock, there is no clear velocity change that could be observed in refracted waves. Because of this complicated pattern, the maximum refraction penetration is limited to the depth of 20 m only, as shown in Fig. 8. The uncertainty analysis for the second, deeper layer reveals very good precision, with an average value of ± 50 m/s for the first 20 m and ± 150 m/s in deeper areas in 2017, and not exceeding ± 200 m/s for deeper parts of the 2018 profile.

Zone 3 (the glacier forefield proximal to the glacier front) from moraine to the current glacier shows a simple velocity structure with clear ~ 7 m thick sediment over bedrock. Comparison of results from two seasons shows the change of velocity down to 37 m. The uncertainty in both cases is smaller than the overall velocity change. Below these depth velocities are unaffected by seasons. Velocity changes in the sediment layer reach 2000 m/s, whereas, in bedrock, they exceed 1000 m/s. These differences in the velocity field between the two seasons are due to changes in the state of water/ice. The effects of such changes are visible almost up to 40 m under the surface (see deepest area on Fig. 9), however a more precise estimation of hydrological changes require direct studies and cannot be estimated with higher certainty using currently gathered geophysical data. In September 2017, velocities in the upper sediment layer were around 2000 m/s, corresponding to water-saturated sand, whereas velocities of 4000 m/s in April 2018 correspond to the same mixture in a frozen state. The bedrock in the unfrozen season is characterised by velocities around 4000 m/s, representing fractured due to thaw/freeze cycles and water-filled bedrock. In April 2018, bedrock velocities were significantly larger (6300 m/s) as water between grains was completely frozen. The uncertainty results for that layer are similar to those in zone 1, with an average of ± 100 m/s for the first 20 m. Below

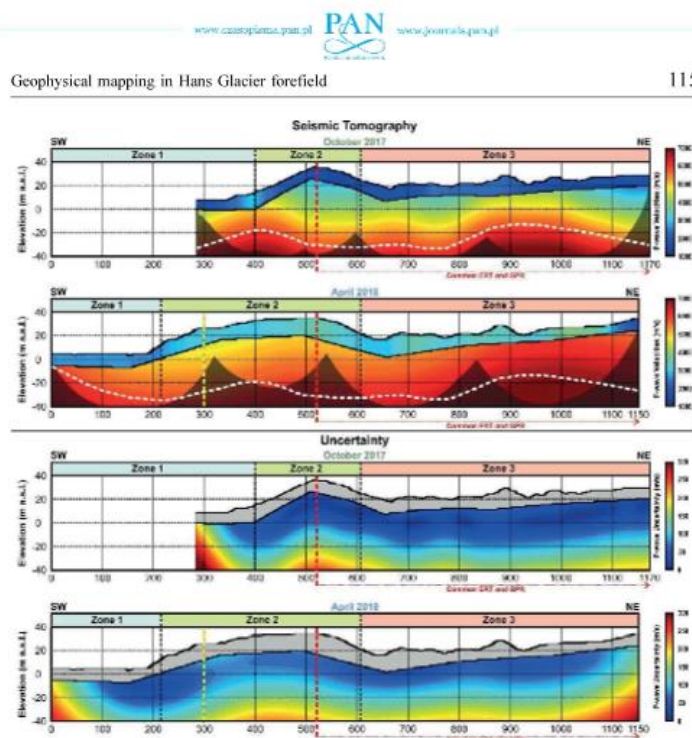


Fig. 8. Results of the Seismic Tomography analysis. The white dashed line marks the boundary of seasonal velocity changes. The uncertainty of the estimated velocity field is small, on average less than 100 m/s. The red and yellow dashed lines indicate the breaking points of the seismic profile. The red line additionally indicates the same location of ERT and GPR profile following NE direction. The grey-shaded masks show the ray propagation depth on tomographic images. Due to the used inversion algorithms for deeper layers imaging, the uncertainty analysis was possible for those layers where ray coverage was precisely estimated.

a depth of 37 m, the uncertainty of the method increases significantly, and thus the seasonal variation of velocity cannot be confirmed.

Integrative approach. — Geophysical remote sensing methods such as GPR, ERT, and active seismic have been used in permafrost research in a few locations in Svalbard to map subsurface structures and composition (Brandt *et al.* 2007; Kasprzak *et al.* 2017; Glazer *et al.* 2020). Although accurate knowledge of active layer thickness distribution and bedrock topography is essential to understand the long-term dynamics of permafrost, data with a time-lapse approach so far were lacking in the forefield of the Hans Glacier and generally in non-glaciated areas of SW Spitsbergen.

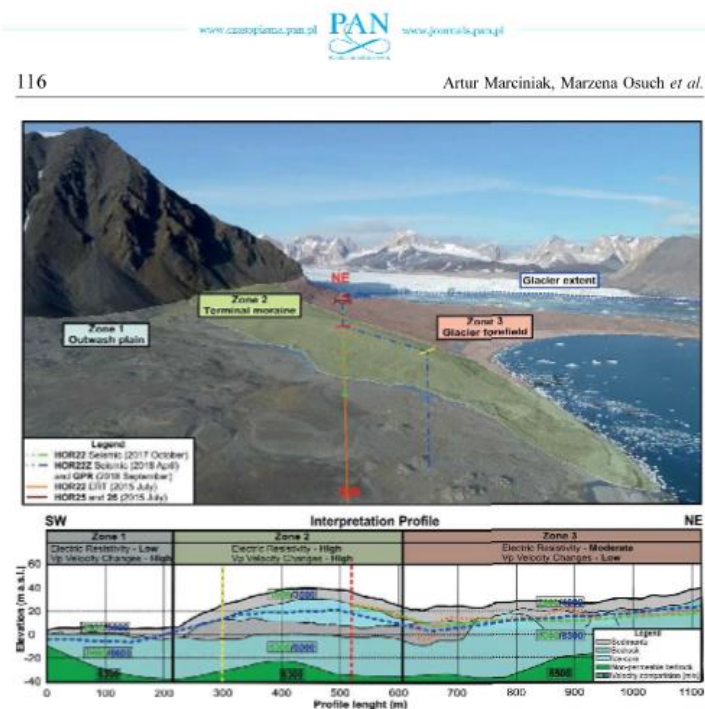


Fig. 9. Interpretation profile from combined methodologies. Several geological structures are present in the study site, with multiple cryotic effects affecting the overall sediment state.

Seismic methods were also used in Svalbard, mainly in the Adventdalen and in waters surrounding the archipelago. The primary purpose of using seismic soundings was to image the deep structures with wide-angle refraction methods (Czuba *et al.* 2008) or reflection seismic imaging (Baelum *et al.* 2012), and both proved successful. In near-surface application, seismic was used to study Pingo structures (Rossi *et al.* 2017; Hammock *et al.* 2021), clearly showing complicated shallow structures.

A key aspect of this study is that the various geophysical methods are complementary, with each method providing additional information on particular characteristics of the subsurface morphology and morphometric features. Similarly to the work of Hammock *et al.* (2021), where ERT and refraction tomography was used to study incipient coastal open-system Pingo in Svalbard, the use of multiple geophysical methods to study the periglacial environment increases the overall quality of final data and solves interpretation misambiguities.

The application of a comprehensive non-intrusive geophysical approach to studying the moraines and forefield of the Hans Glacier reveals the complex glacial and periglacial nature of the study site. From these results, an interpretation profile was created (Fig. 9) and applied to the study area. For correct interpretation of the data, the sensitivities, resolution, limitations, and uncertainties of different geophysical methods have to be fully considered. Each geophysical method is sensitive to different physical parameters, limiting the ability to accurately describe the subsurface periglacial structures (Table 1). In particular, the effects of seasonal freezing-thawing cycles, which can vary from year to year, must be taken into account, and this requires a multi-method approach. As presented, applied geophysical methods resulted in the slightly different mapping of the same structures, which complement and enable an overall interpretation supported by the geomorphological mapping.

Table 1.

A summary of the obtained results. Advantages (+) and disadvantages (-) of using different geophysical methods to recognise underground structures.

| Recognised structure | ERT | GPR | Seismic tomography |
|--|---|---|--|
| The active layer (freezing-thawing effect) | + visible on profiles HOR25 and HOR26 with dense electrode array | - due to 30 Mhz antenna with low resolution and measurement in one season only | + visible as a VP (P-wave velocity) difference in two seasons both for sediment cover and bedrock |
| Moraine's ice-core | + | + | - not sufficient spatial resolution |
| Sediment-bedrock boundary | - due to the high water saturation and complicated geology the boundaries are smoothened | + | + |
| Boundary between ice-core of moraine and underlying sediment | - due to high resistivity values of upper laying ice-core | + | - lack of refraction in low-velocity layers |

The ERT method allowed for recognition of active layer thickness, and the presence of ice cores. The general recognition of the study site across profile HOR22, however, without detailed recognition due to limited resolution of wide electrode spacing. Similar to the work of Kasprzak (2015), the results indicate the active layer thickness by using denser arrays in profiles HOR25 and HOR26. Even though resistivity images are smoothed models of near-surface

data, the overall information is sufficient for the recognition of geomorphological features in the study site without the knowledge of precise boundaries of periglacial structures (Glazer *et al.* 2020). However, the results of the ERT method have to be taken with caution in situations where saline water infiltration can happen and thus act as a conductor (Revil and Glover 1998). Multiple ERT profiles with dense electrode deployment are required to obtain more information about active-layer horizontal changes across the study site. Even though, for obtaining a more detailed image of the subsurface, the integration of both data from dense as well as wider arrays providing deeper insight into the subsurface is necessary.

The GPR with a 30 Mhz antenna allowed for detailed recognition of the shapes of the boundaries between uppermost sediments, bedrock, and ice cores. Similarly as described by Brandt *et al.* (2007), the sediment layering can be recognised and tracked. However, due to the resolution limitations of low-frequency RTA, more detailed recognition of the first two metres is not possible, including the active layer. For such a study, a more resolved antenna of 200 Mhz and above will be more suitable. The sediment-bedrock boundary underneath the ice core of the terminal moraine was mapped this way, which was not possible using other geophysical methods. The potential use of antennas with higher frequencies (100 Mhz and higher) in the imaging of the active layer is high, but at the cost of depth resolution and the visualisation of moraine structures (Sevestre *et al.* 2015; Zhao *et al.* 2016). In addition, the scattering of GPR waves by loose rock, unconsolidated sediment and water in a partially or fully frozen state further limits the imaging potential.

The seismic method provided insight into seasonal changes by visualising stages between thawing and freezing based on the velocity change. Based on a direct comparison of velocity fields gathered in the contrasting thermal conditions, and including the uncertainty estimation, this effect can be quantified. It was estimated that the effects of water penetration into the permafrost can be confirmed down to a depth of 40 m. However, due to a lack of information about the bedrock from the deep boreholes, the deepest borehole near the study site reaches 20 m only, future efforts in this subject should be taken. Hilbich (2010) suggested that refraction is very shallow due to high-velocity contrast at the permafrost table. In contrast, this study suggests that deeper penetration is feasible. In unfrozen materials, when the contrast should be greatest, water penetration smooths the velocity gradient resulting in a gradual increase of seismic velocity with depth. Although the acquisition of seismic data requires more effort and is more time-consuming than other geophysical methods, seismic imaging gives a reliable geophysical characterization of deep structures with quantitative uncertainties. This, combined with precise repeatability in the form of time-lapse images, allows recognition of P-waves velocity changes at depths up to 40 m. Such deep seasonal changes can be attributed to hydrogeological processes like deep water percolation. To verify this interpretation, direct

measurements in deep enough cored boreholes (geological structure), thermal measurements (seasonal temperature change), and hydrogeological piezometers (groundwater flow) are necessary.

Concluding remarks

The goal of the geophysical investigations conducted across multiple landforms from sandur, over a terminal moraine up to the present front of the Hans Glacier was to provide comprehensive information on near-surface structural features and characteristics of the periglacial environment. The results presented here highlight the value of combining geophysical techniques for assessing permafrost characteristics, the extent of bedrock and sediment cover, recognition of active layer behaviour, and resolving complex geological structures. The observed freezing-thawing effects are stronger than expected from previous studies due to an indirect influence on deeper structures reaching about 40 m below the surface as a result of deep water penetration into the rock structures. The new geophysical data from three main zones: outwash plain, terminal moraine, and ground moraine in the glacial forefield strongly vary in measured physical properties. Each zone is characterised by a different response to the freezing and thawing effect. Based on two season observations, thermal and hydrogeological effects on geophysical data can be distinguished from the non-seasonal effects of sedimentary thickness and bedrock topography. The main cause of seasonal variation is deep water circulation and intra permafrost percolation in bedrock.

Recently, snow cover, temperature and precipitation are changing rapidly in the Arctic, especially in Spitsbergen. To estimate the influence of these changes on the shift in the periglacial processes, the ongoing time-lapse characterisation of permafrost is required. As there is a clear need to recognise subsurface changes caused by climate warming, geoelectric, seismic, and GPR measurements should be conducted and repeated along with the common profiles, especially in places important for local communities and vulnerable to geophysical hazards. As shown here, such combinations of geophysical methods are effective tools even in places with complex geomorphology. Geophysical methods are non-invasive and provide 2D or 3D images of subsurface features that relate to the interplay of permafrost, water, and ice in the ground and form an excellent basis for comparative studies.

Acknowledgements. — This research was funded by National Science Centre, Poland Grant UMO-2015/21/B/ST10/02509. Part of this work was supported within statutory activities No. 3841/E-41/S/2018 of the Ministry of Science and Higher Education of Poland. Authors want to thank Daniel Dunkley for the language corrections, which significantly improved the quality of the article. Special thanks to the reviewers who have made important suggestions and contributions to this article.

References

- Baelum K. 2007. Investigations of the subsurface by Ground Penetrating Radar (GPR): Examples from Spitsbergen. *AGU Fall Meeting Abstracts* 2007: NS14A-07.
- Baelum K., Johansen T.A., Johnsen H., Rod K., Ruud B.O. and Braathen A. 2012. Subsurface structures of the Longyearbyen CO₂ Lab study area in Central Spitsbergen (Arctic Norway), as mapped by reflection seismic data. *Norwegian Journal of Geology* 92: 377–389.
- Bernard E., Friedt J.M., Saintenoy A., Tolle F., Griselin M. and Marlin C. 2014. Where does a glacier end? GPR measurements to identify the limits between valley slopes and actual glacier body. Application to the Austre Lovénbreen, Spitsbergen. *International Journal of Applied Earth Observation and Geoinformation* 27: 100–108. doi: 10.1016/j.jag.2013.07.006
- Błaszczak M., Jania J. A. and Kolondra L. 2013. Fluctuations of tidewater glaciers in Hornsund fjord (southern Svalbard) since the beginning of the 20th century. *Polish Polar Research* 34: 327–352. doi: 10.2478/popore-2013-0024
- Błaszczak M., Jania J., Cieply M., Grabiec M., Ignatiuk D., Kolondra L., Kruss A., Luks B., Moskalik M., Pastusiak T., Strzelewicz A., Walczowski W. and Wawrzyniak T. 2021. Factors controlling terminus position of Hansbreen, a tidewater glacier in Svalbard. *Journal of Geophysical Research: Earth Surface* 126: e2020JF005763. doi: 10.1029/2020JF005763
- Błaszczak M., Laska M., Sivertsen A. and Jawak S.D. 2022. Combined use of aerial photogrammetry and terrestrial laser scanning for detecting geomorphological changes in Hornsund, Svalbard. *Remote Sensing* 14: 601. doi: 10.3390/rs14030601
- Brandt O., Langley K., Kohler J. and Hamran S.E. 2007. Detection of buried ice and sediment layers in permafrost using multi-frequency Ground Penetrating Radar: A case examination on Svalbard. *Remote Sensing of Environment* 111: 212–227. doi: 10.1016/j.rse.2007.03.025
- Carcione J.M. and Seriani G. 1998. Seismic and ultrasonic velocities in permafrost. *Geophysical Prospecting* 46: 441–454. doi: 10.1046/j.1365-2478.1998.1000333.x
- Christiansen H.H., Gilbert G.L., Demidov N., Guglielmin M., Isaksen K., Osuch M. and Boike J. 2019. Permafrost thermal snapshot and active-layer thickness in Svalbard 2016–2017. In: Orr E., Hansen G., Lappalainen H., Hübner C. and Lihavainen H. (eds.) *SESS report 2018*. Svalbard Integrated Arctic Earth Observing System, Longyearbyen: 26–47.
- Christiansen H.H., Gilbert G.L., Demidov N., Guglielmin M., Isaksen K., Osuch M. and Boike J. 2020. Permafrost temperatures and active layer thickness in Svalbard during 2017/2018. In: Van den Heuvel F., Hübner C., Błaszczak M., Heimann M. and Lihavainen H. (eds.) *SESS report 2019*. Svalbard Integrated Arctic Earth Observing System, Longyearbyen: 236–249.
- Christiansen H.H., Gilbert G.L., Demidov N., Guglielmin M., Isaksen K., Osuch M. and Boike J. 2021. Ground ice content, drilling methods and equipment and permafrost dynamics in Svalbard 2016–2019 (PermaSval). In: Moreno-Ibáñez M., Hagen J.O., Hübner C., Lihavainen H. and Zaborska A. (eds.) *SESS report 2020*. Svalbard Integrated Arctic Earth Observing System, Longyearbyen: 258–275. doi: 10.5281/zenodo.4294095
- Czerny J., Kieres A., Manecki M. and Rajchel J. 1993. *Geological map of the SW part of Wedel Jarlsberg Land Spitsbergen, 1:25 000*. Institute of Geology and Mineral Deposits. University of Mining and Metallurgy, Cracow.
- Czuba W., Grad M., Gutereh A., Majdański M., Malinowski M., Mjelde R., Moskalik M., Środa P., Wilde-Piórko M. and Nishimura Y. 2008. Seismic crustal structure along the deep transect Horsted'05, Svalbard. *Polish Polar Research* 29: 279–290.
- Dobiński W., Grabiec M. and Gądek B. 2011. Spatial relationship in interaction between glacier and permafrost in different mountainous environments of high and mid-latitudes, based on GPR research. *Geological Quarterly* 55: 375–388.
- Dobiński W., Grabiec M. and Glazer M. 2017. Cold-temperate transition surface and permafrost base (CTS-PB) as an environmental axis in glacier-permafrost relationship, based on research

- carried out on the Storglaciären and its forefield, northern Sweden. *Quaternary Research* 88: 551–569. doi: 10.1017/qua.2017.65
- Dolnicki P. and Grabiec M. 2022. The thickness of talus deposits in the periglacial area of SW Spitsbergen (Fugleberget Mountainside) in the light of slope development theories. *Land* 11: 209. doi: 10.3390/land11020209
- Evans D.J.A. 2009. Controlled moraines: origins, characteristics and paleoglaciological implications. *Quaternary Science Reviews* 28: 183–208. doi: 10.1016/j.quascirev.2008.10.024
- Farbrot H., Isaksen K., Eiken T., Kääb A. and Sollid J.L. 2005. Composition and internal structures of a rock glacier on the strandflat of western Spitsbergen, Svalbard. *Norsk Geografisk Tidsskrift-Norwegian Journal of Geography* 59: 139–148. doi: 10.1080/00291950510020619
- Glazer M., Dobiński W., Marciniak A., Majdański M. and Blaszczyk M. 2020. Spatial distribution and controls of permafrost development in non-glacial Arctic catchment over the Holocene, Fuglebekken, SW Spitsbergen. *Geomorphology* 358: 107128. doi: 10.1016/j.geomorph.2020.107128
- Hamed K.H. and Rao A.R. 1998. A modified Mann-Kendall trend test for autocorrelated data. *Journal of Hydrology* 204: 182–196. doi: 10.1016/S0022-1694(97)00125-X
- Hammock C.P., Kulassa B., Hiemstra J.F., Hodson A.J. and Hubbard A. 2021. Seismic and electrical geophysical characterization of an incipient coastal open-system Pingo: Lagoon Pingo, Svalbard. *Earth and Space Science* 9: e2021EA002093. doi: 10.1029/2021EA002093
- Hilbich C. 2010. Time-lapse refraction seismic tomography for the detection of ground ice degradation. *The Cryosphere* 4: 243–259. doi: 10.5194/tc-4-243-2010
- Hobro J.W. and Singh S. 1999. Joint interface and velocity estimation in three dimensions (JIVE3D). *LITHOS science report*. Department of Earth Sciences, University of Cambridge, Cambridge.
- Hobro J.W.D., Singh S.C. and Minshull T.A. 2003. Three-dimensional tomographic inversion of combined reflection and refraction seismic traveltime data. *Geophysical Journal International* 152: 79–93. doi: 10.1046/j.1365-246X.2003.01822.x
- IPCC 2021. *Climate Change 2021: The physical science basis. Contribution of working group I to the sixth assessment report of the Intergovernmental Panel on Climate Change*. Cambridge University Press, Cambridge.
- Jacoby M., Dvorkin J. and Liu X. 1996. Elasticity of partially saturated frozen sand. *Geophysics* 61: 288–293. doi: 10.1190/1.1443951
- Kasprzak M. 2015. High-resolution electrical resistivity tomography applied to patterned ground, Wedel Jarlsberg Land, south-west Spitsbergen. *Polar Research* 34: 25678. doi: 10.3402/polar.v34.25678
- Kasprzak M., Strzelecki M.C., Traczyk A., Kondracka M., Lim M. and Migala K. 2017. On the potential for a bottom active layer below coastal permafrost: the impact of seawater on permafrost degradation imaged by electrical resistivity tomography (Hornsund, SW Spitsbergen). *Geomorphology* 293: 347–359. doi: 10.1016/j.geomorph.2016.06.013
- Kaushik H., Ramanathan A.L., Soheb M., Shamurailatpam M.S., Biswal K., Mandal A. and Singh C. 2021. Climate change-induced high-altitude lake: Hydrochemistry and area changes of a moraine-dammed lake in Leh-Ladakh. *Acta Geophysica* 69: 2377–2391. doi: 10.1007/s11600-021-00670-x
- Kneisel C., Hauck C., Fortier R. and Moorman B. 2008. Advances in geophysical methods for permafrost investigations. *Permafrost and Periglacial Processes* 19: 157–178. doi: 10.1002/ppp.616
- König M., Nuth C., Kohler J., Moholdt G. and Pettersen R. 2014. A digital glacier database for Svalbard. In: Kargel J.S., Leonard G.J., Bishop M.P., Kaab A. and Raup B. (eds.) *Global land ice measurements from space*. Springer, Berlin, Heidelberg: 229–239.
- Landvik J.Y., Bondevik S., Elverhi A., Fjeldskaar W., Mangerud J., Siegert M.J., Salvigsen O., Svendsen J. and Vorren T.O. 1998. The Last Glacial Maximum of Svalbard and the Barents

- 122
- Artur Marciniak, Marzena Osuch *et al.*
- Sea area: ice sheet extent and configuration. *Quaternary Science Reviews* 17: 43–75. doi: 10.1016/S0277-3791(97)00066-8
- Lindner I., Marks L. and Pękala K. 1986. Outline of Quaternary chronostratigraphy of the northern Hornsund area, southern Spitsbergen. *Bulletin of the Polish Academy of Sciences. Earth Sciences* 34: 427–436.
- Loke M.H. 2018. *Tutorial: 2-D and 3-D electrical imaging surveys*. URL: <http://www.geotomosoft.com/downloads.php> (accessed on 15.06.2018).
- Maurer H. and Hauck C. 2007. Geophysical imaging of alpine rock glaciers. *Journal of Glaciology* 53: 110–120. doi: 10.3189/172756507781833893
- Nolet G. 2008. *A breviary of seismic tomography: Imaging the interior of the Earth and Sun*. Cambridge University Press, Cambridge. doi: 10.1017/CBO9780511984709
- Nordli O., Wyszynski P., Gjeltten H., Isaksen K., Lupikasz E., Niedźwiedz T. and Przybylak R. 2020. Revisiting the extended Svalbard Airport monthly temperature series, and the compiled corresponding daily series 1898–2018. *Polar Research* 39: 1–15. doi: 10.33265/polar.v39.3614
- Nowak A., Hodgkins R., Nikulina A., Osuch M., Wawrzyniak T., Kavan J., Lepkowska E., Majerska M., Romashova K., Vasilevich I., Sobota I. and Rachlewicz G. 2021. From land to fjords: The review of Svalbard hydrology from 1970 to 2019. In: Moreno-Ibáñez M., Hagen J. O., Hübner C., Lihavainen H. and Zaborska A. (eds.) *SESS report 2020*. Svalbard Integrated Arctic Earth Observing System, Longyearbyen: 176–201. doi:10.5281/zenodo.4294063
- Osuch M. and Wawrzyniak T. 2017a. Inter- and intra-annual changes in air temperature and precipitation in western Spitsbergen. *International Journal of Climatology* 37: 3082–3097. doi: 10.1002/joc.4901
- Osuch M. and Wawrzyniak T. 2017b. Variations and changes in snow depth at meteorological stations Barentsburg and Hornsund (Spitsbergen). *Annals of Glaciology* 58(75pt1): 11–20. doi: 10.1017/aog.2017.20
- Owoc B., Marciniak A., Dzierżek J., Kowalczyk S. and Majdański M. 2019. Seismic imaging of the Mesozoic bedrock relief and geological structure under Quaternary sediment cover: The Bolmin Syncline (SW Holy Cross Mountains, Poland). *Geosciences* 9: 447. doi: 10.3390/geosciences9100447
- Pękala K. 1989. Quaternary deposits of the Hans Glacier forefield (Hornsund, Spitsbergen). *Polar Session. Natural Environment Research of West Spitsbergen*, UMCS Lublin: 191–204 (in Polish).
- Revil A. and Glover P.W.J. 1998. Nature of surface electrical conductivity in natural sands, sandstones, and clays. *Geophysical Research Letters* 25: 691–694.
- Rossi G., Accaino F., Boaga J., Petronio L., Romeo R. and Wheeler W. 2017. Seismic survey on an open Pingo system in Adventdalen Valley, Spitsbergen, Svalbard. *Near Surface Geophysics* 16: 89–103. doi: 10.3997/1873-0604.2017037
- Sen P.K. 1968. Estimates of the regression coefficient based on Kendall's tau. *Journal of the American Statistical Association* 63: 1379–1389.
- Senderak K., Kondracka M. and Gądek B. 2021. Processes controlling the development of talus slopes in SW Spitsbergen: The role of deglaciation and periglacial conditions. *Land Degradation & Development* 32: 208–223. doi: 10.1002/ldr.3716
- Sevestre H., Benn D.I., Hulton N.R.J. and Bælum K. 2015. Thermal structure of Svalbard glaciers and implications for thermal switch models of glacier surging. *Journal of Geophysical Research* 120: 2220–2236. doi: 10.1002/2015JF003517
- Wawrzyniak T. and Osuch M. 2020. A 40-year High Arctic climatological dataset of the Polish Polar Station Hornsund (SW Spitsbergen, Svalbard). *Earth System Science Data* 12: 805–815. doi: 10.5194/essd-12-805-2020
- Wawrzyniak T., Osuch M., Napiórkowski J.J. and Westermann S. 2016. Modelling of the thermal regime of permafrost during 1990–2014 in Hornsund, Svalbard. *Polish Polar Research* 37: 219–242. doi: 10.1515/popore-2016-0013

- Van Pelt W., Pohjola V., Pettersson R., Marchenko S., Kohler J., Luks B., Hagen J.O., Schuler T., Dunse T., Noel B. and Reijmer C. 2019. A long-term dataset of climatic mass balance, snow conditions, and runoff in Svalbard (1957–2018). *The Cryosphere* 13: 2259–2280. doi: 10.5194/tc-13-2259-2019
- Zhao W., Forte E., Colucci R.R. and Pipan M. 2016. High-resolution glacier imaging and characterization by means of GPR attribute analysis. *Geophysical Journal International* 206: 1366–1374. doi: 10.1093/gji/ggw208
- Zimmerman R.W. and King M.S. 1986. The effect of the extent of freezing on seismic velocities in unconsolidated permafrost. *Geophysics* 51: 1285–1290. doi: 10.1190/1.1442181

Received 20 December 2021

Accepted 22 April 2022

Paper VI:

Marciniak, A., Kowalczyk, S., Gontar, T., Owoc, B., Nawrot, A., Luks, B., Cader, J., & Majdański, M. (2021). Integrated geophysical imaging of a mountain landslide – A case study from the Outer Carpathians, Poland. *Journal of Applied Geophysics*, 191. <https://doi.org/10.1016/j.jappgeo.2021.104364>



Integrated geophysical imaging of a mountain landslide – A case study from the Outer Carpathians, Poland



Artur Marciniak^{a,*}, Sebastian Kowalczyk^b, Tadeusz Gontar^b, Bartosz Owoc^a, Adam Nawrot^a, Bartłomiej Luks^a, Justyna Cader^c, Mariusz Majdański^a

^a Institute of Geophysics, Polish Academy of Sciences, Warsaw, Poland

^b Faculty of Geology, University of Warsaw, Warsaw, Poland

^c Mineral and Energy Economy Research Institute, Polish Academy of Sciences, Cracow, Poland

ARTICLE INFO

Article history:

Received 8 September 2019

Received in revised form 16 February 2021

Accepted 5 May 2021

Available online xxx

Keywords:

Seismic

Electrical resistivity tomography (ERT)

Landslide

Multichannel analysis of surface waves

(MASW)

Uncertainty analysis

Outer Carpathians

ABSTRACT

In the presented case study, the authors applied the multimethod approach utilising geophysical imaging with estimated uncertainty to the landslide in Cisiec, southwest Poland. Application of multiple geophysical methods such as electrical resistivity tomography (ERT), multichannel analysis of surface waves (MASW), refraction seismic method, ray-based seismic tomography, and reflection imaging was aimed at obtaining a detailed and high-resolution image of the subsurface. Drone-based digital terrain models (DTM) supported the subsurface imaging by providing a detailed view of the landslide surface. Accurate GPS-based geodesy conducted during data gathering was used to complete information about the topography of the area and correlate the results of geophysical surveys. The combination and transfer of information between methods allow solving multiple reflection imaging problems, especially lack of borehole information. The final result presents the detailed geophysical images of the landslide with a recognized depth of main slip surface ranging from 16 to 36 m. Because the study site is used as a ski slope, detailed information about the landslide structure is needed to provide safety for nearby construction. The methodology proposed in this paper can be used in similar case studies, where fast and cost-effective recognition of a landslide is required.

© 2021 Elsevier B.V. All rights reserved.

1. Introduction

Landslides are one of the most challenging geohazards causing losses both in infrastructure and human lives (Petley, 2012). Although geophysical methods are widely used to determine their extent, thickness and depth of failure planes, an overall recognition of the landslide structure is still challenging in mountain conditions. Very often the chaotic internal structure makes geophysical investigations of landslides demanding and susceptible to errors. In Poland, 95% of all landslides occur in the Carpathian region (Poprawa and Rączkowski, 2003). Since 1997, when heavy rainfalls caused one of the biggest floods in Poland's modern history, slope stability became one of the most important subjects for geological and geophysical studies in the country (Nescieruk et al., 2016).

By using high-resolution geophysical methods, the variability of physical properties that can describe the landslide formation and development can be observed. Seismic, ERT (electrical resistivity tomography), VLF (very low frequency) Electromagnetic Method and ground-penetrating radar or a combination of these methods

(Bogoslovsky and Ogilvy, 1977; McCann and Forster, 1990; Bruno and Martillier, 2000; Bichler et al., 2004; Lapenna et al., 2005; Godio et al., 2006; Bednarczyk, 2008; Eichkitz et al., 2009; Renalier et al., 2010; Travelet et al., 2010; Mantovani et al., 2013; Kowalczyk et al., 2014; Malehmir et al., 2016; Wang et al., 2016; Yalcinkaya et al., 2016; Bellanova et al., 2018; Crawford et al., 2018; Orozco et al., 2018; Harba et al., 2019; Karcioğlu, 2019; Pasierb et al., 2019) has been used for years to locate slip surfaces and reduce the ambiguity of interpretation.

In the Outer Carpathians (Southern Poland), the usefulness of combining various geophysical methods to characterize landslides was investigated in the 1970s (Białostocki, 1974). Since then, many geophysical studies have been performed in the Polish Carpathians area (e.g. Bestyński, 2001; Bestyński and Thiel, 2005; Pilecki et al., 2007; Bednarczyk, 2008; Ostrowski et al., 2013; Gawruciencow et al., 2017), however without using reflection imaging techniques.

The utilisation of multiple geophysical techniques with the use of uncertainty as a processing parameter of each method to reduce the ambiguity of the results (Majdański et al., 2018; Marciniak et al., 2019) was carried out. The applied scheme (Fig. 1) where all seismic related methods (MASW, refraction seismic method, ray-based seismic tomography, reflection seismic), and geoelectrical method (i.e. ERT) were used. The combination of four different geophysical methods

* Corresponding author.

E-mail address: amarciniak@igf.edu.pl (A. Marciniak).

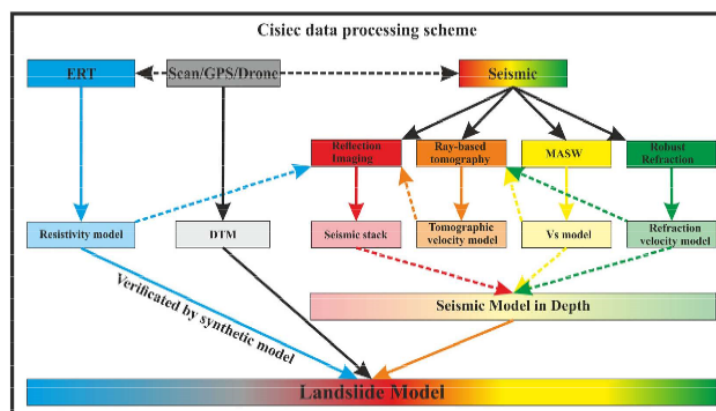


Fig. 1. The multimethod approach. Migration of the data, (dashed lines) in terms of uncertainty, allowed to combine different methods and utilize the information in a more complete and precise way. The solid lines present the information that was directly migrated to the next processing step without recalculations.

resulted in minimizing errors and improving imaging of the landslide body. A digital terrain model (DTM) based on drone photogrammetry was created to interpret and correlate surface data with subsurface images. The proposed methodology is based on combining information from multiple geophysical methods.

The main objectives of the study were to determine the spatial variability of the Cisiec landslide and the depth of its slip surface. The second goal was to check the proposed methodology based on mutual verification of results obtained from each method used. This was done by transferring information from one geophysical method to another during processing steps in a way that uncertainty is treated as a parameter to reduce interpretation ambiguity. Application of high-resolution geophysical imaging as presented in this paper can provide a universal approach for studying similar cases.

2. Geology

The Cisiec landslide is located on the northeast slope below Czerwieniska Grapa mountain (southwest Poland) in the Outer West Carpathians, Silesian Nappe unit (Fig. 2). About a kilometre south of the described location, the Silesian Nappe is overlapped by Foremagura units and the Magura Nappe unit. The described slope is situated on lithostratigraphic units named Hieroglyphic Beds and Variegated Shales (Burtan et al., 1956; Kucharska and Kamiński, 2008). Hieroglyphic Beds consist of interbedded layers of fine-grained sandstones and shales, varying in thickness from a few centimetres up to one metre. Shale layers can be black, grey, green, or even red. The thickness of the whole unit may reach up to 200 m (Golonka and Wałkowska-Oliwa, 2007). The observed dip readings vary from 45 to 85 degrees, while the strike varies from 170 to 190 degrees. The age of the Hieroglyphic Beds, according to Wałkowska-Oliwa (2014), is Lutetian (Middle Eocene). This estimation is based on foraminifera from the Reticulophragmium amplexans zone. The depositional environment of the Hieroglyphic Beds was classified by Leszczyński (1985) as the D-fation (Mutti, 1977), which stands for a basin plain subjected to diluted turbidity currents, where interbeds of clay-rich shales and fine-grained sandstones occur. Hieroglyphic Beds are an example of flysch, which is a regional term used to describe rocks deposited in cycles by turbidity

currents in a deep, marine environment. In the described area, the Variegated Shales interlock with the Hieroglyphic Beds appearing above and below each other (Burtan et al., 1956; Golonka and Wałkowska-Oliwa, 2007). Those units were accumulated in rather deep, bathyal to abyssal environments below the calcite compensation depth. Their red and green colours indicate oxidising conditions of deposition (Leszczyński and Uchman, 1991). As stated by Bestyński and Thiel (2005) and Bestyński et al. (2017), geological conditions, like those in the Cisiec area (alternating shales and sandstones), increase the probability of slope instability and mass movements. A few kilometres south from Cisiec, on the Milowka landslide, quantitative assessment of slope stability was calculated based on the classification index KFG (geophysical classification of flysch) dependent on the P-waves velocity and electrical resistivity (Bestyński, 2001; Bestyński et al., 2017). In 2008, the Cisiec landslide was described and incorporated into the Landslide Counteracting System database (LCS; SOPO in Polish) (Kucharska and Kamiński, 2008). From 2011 to 2013, construction of the ski lift at the Cisiec slope caused deforestation and prolonged the snow retention period, increasing the risk of landslide movements.

3. Fieldworks

To investigate the subsurface structure and obtain input data for Cisiec landslide characterization, four ERT and one seismic profile were acquired in October 2018. The used approach aimed at gathering a dataset for multiple geophysical methods was cost-effective due to the usage of the same shot gathers for all seismic methods. The profile lines covered the area of the ski slope in a way that the landslide body is located in the middle of those lines. Between ERT lines 2 and 3, a seismic profile with a length of 230 m was deployed (Fig. 2C, yellow line). To obtain dense datasets, both geophone and electrode spacing was set to 5 m. This electrode spacing is quite optimal because it allows for an investigation up to 70 m depth using a gradient array giving the distribution of the data points as shown in Fig. 3. A total of 76 electrodes connected to resistivity meter equipment (ABEM Terrameter LS) were used on each ERT line (Table 1). To gather seismic data, 48 geophones with an ABEM Terraloc recorder were deployed, enabling recognition of Rayleigh waves up

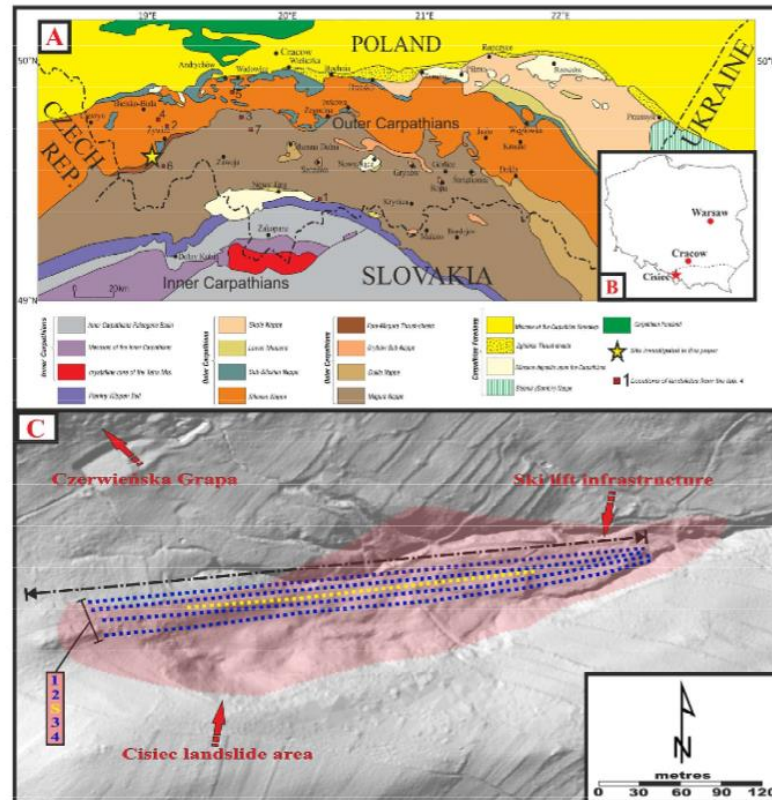


Fig. 2. Tectonic sketch map of the Polish Carpathians (A) (after Żytko et al., 1989; Oszczytko et al., 2008; Kłopotowska and Łukasiak, 2017; modified) with locations of the site investigation (the yellow star) and local landslides presented in Table 4. The Cisiec landslide area, located in southwest Poland (B). The red marked area (C) is based on the information from the Landslide Counteracting System database (LCS; SOPO in Polish). The blue dotted lines present the location of the ERT profiles (1–4), while the yellow one shows the seismic profile (S). (For interpretation of the references to colour in this figure legend, the reader is referred to the web version of this article.)

to 20–30 m deep (Park et al., 2002). For the seismic signal excitation, an 8-kg sledgehammer was used as the source. The precise GPS location of each measurement point was done using the Geomax Zenith 10 GPS Real Time Kinematics (RTK) system.

The DTM of the ski slope was constructed using aerial photogrammetry. A drone DJI Phantom IV Pro was used for obtaining the images. The flight program was set up as a double-grid mission, 50 m in height with a 70° angle, and 80% overlap.

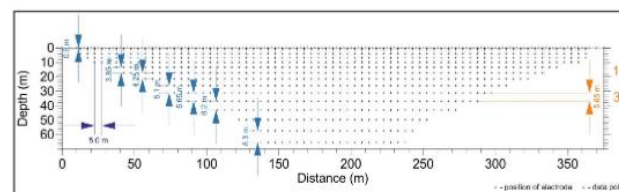


Fig. 3. The distribution of the data points. Depth of investigation, vertical and horizontal resolution obtained in ERT surveys.

Table 1
Characteristics of the ERT profiles.

| Number of profile | Type of array | Electrode spacing (m) | Profile length (m) | Number of measured data points | Number of inverted data points | Number of iterations | RMS (%) |
|-------------------|---------------|-----------------------|--------------------|--------------------------------|--------------------------------|----------------------|---------|
| Profile 1 | Gradient | 5 | 375 | 960 | 929 | 5 | 2.49 |
| Profile 2 | Gradient | 5 | 375 | 960 | 940 | 5 | 2.37 |
| Profile 3 | Gradient | 5 | 375 | 960 | 945 | 5 | 2.50 |
| Profile 4 | Gradient | 5 | 375 | 960 | 947 | 5 | 2.50 |

4. Uncertainty driven data processing

The interpretation of reflection seismic images is difficult, especially for researchers without extensive experience in the data processing. Often interpretation details are way below the uncertainty of the given method. With experience in processing, it is possible to distinguish between processing artefacts and recognized features. Here we propose a simple estimation of the uncertainty for the final reflection images that will allow neglecting characteristics of the studied structure that are not directly related to observed data. The idea is to use several methods in steps from the shallowest and the least precise (refraction seismic method, MASW and ERT) to deeper traveltimes tomography to estimate the stacking velocity with its uncertainty (see seismic part of Fig. 1). The strategy proposed yields characterization of horizons of interest via three independent information obtained from handling the same dataset differently. This allows showing estimated depth range for each element and obtaining the best stacking velocity. The proposed approach is a simple Monte Carlo method based on the random generation of a set of starting models for each inversion from parameter range described by the previous method. Further, the optimal data fit solution is selected, and its uncertainty is estimated by statistical means and standard deviation of parameters (Owoc et al., 2019). There are other solutions to joint analysis of multimethod datasets with the numerical superiority of simultaneous inversions in large parameter space (e.g. Nolet, 2008; Bodin and Sambridge, 2009; Tarantola, 1987), but they require significantly larger complexity and generate additional problems like the stability of inversion. Moreover, advanced techniques like covariance matrices or reversible-jump Monte Carlo Markov Chain analysis, that are state of the art in geophysical inversion and are crucial in tectonic scale and global seismology problems, are not needed in the near-surface scale. Still, as the borehole verification is not always possible, even a simple uncertainty estimation of the final model is essential.

Parallel to the seismic processing (Table 2), the ERT resistivity model was calculated and verified by synthetic models. GPS RTK was used for precise geodesy measurements. The post-processing of the aerial photography was done using Pix4D software. The DTM was calculated from the digital surface model (DSM) that includes vegetation. The DTM resolution is 2.33 cm/pixel.

4.1. Electrical resistivity tomography

The apparent resistivity data from the field investigation was inverted using Res2DInv software (Loke, 2018). Before processing several steps were carried out. Topographical corrections based on the GPS RTK measurements were prepared. All the datasets were checked for negative resistivity values and also outliers were removed. Only a small number of apparent resistivity data points were removed (up to 3.2%) (Table 1). Both inversion methods, the smooth L_2 norm, the robust L_1 norm, and several different inversion settings were tested. Finally, the L_1 norm was chosen because the images obtained seemed to be more consistent with the expected geology (Burtan et al., 1956; Kucharska and Kamiński, 2008) as described in Geology chapter.

The data were inverted using the robust constraints and the Gauss-Newton method for calculating the Jacobian matrix. Mainly the default

Table 2
Seismic data processing steps.

| Number | Seismic processing step | Aim |
|--------|--|--|
| 1 | Data QC | Removal of dead and oversteered noisy traces |
| 2 | Geometry building | Filling SEG-Y headers with data from the GPS and precise building of the acquisition line geometry |
| 3 | First break picking | Gathering data for static and residual corrections. Export of the first breaks to ray-based tomography with geometry information |
| 4 | MASW data preparation and export | Preparing of the selected shot records for MASW analysis. Data filtering using 1D Bandpass (8–10 to 70–80 Hz) and 2D FK filter. Applying front mute to remove refracted waves. Additional use of AGC (500 ms time window) for amplitude normalisation |
| 5 | Elevation, static and residual corrections | Corrections for slope elevation, statics, and residual zones. The short offsets were used for calculations. |
| 6 | Noise attenuation | The attenuation of the air-wave and ground rolls. Removal of refracted waves using front mute. Application of 1D Bandpass (20–25 to 100–110 Hz) and 2D FK filters |
| 7 | Signal normalisation | Deconvolution and signal normalisation using AGC in a 100 ms time window. The final pass of the FK filter, and application of the second, more precise front mute |
| 8 | Velocity field estimation | Fitting of the tomographic velocity field by analysing the NMO correction effect on reflections. Extrapolation of the tomographic data to higher times. Recalculation of the tomographic velocity into interval velocity using the DIX formula for time to depth migration |
| 9 | Data horizontal stacking | The NMO data correction and horizontal stacking of reflections |
| 10 | Time to depth conversion and uncertainty information | Time to depth conversion using the interval velocities calculated in step 8. Creation of two additional interval velocity fields using the tomographic uncertainty. Application of those velocities to the data and comparison of TTD correction results. Verification of horizons depth changes |
| 11 | Filtering of the final stack | The final data filtering using 1D filter (32–35 to 100–110 Hz) with an additional pass of the FK bandpass filter and 2D FK filtration |

inversion parameters were used such as no extended model, normal model cells with the same widths of one unit spacing (5 m), and the finite-element method with trapezoidal elements. The robust inversion method was used with 0.05 cut-off factor constrain. That means that a threshold of 5% was selected for the differences between the measured and calculated apparent resistivity values. The differences above a threshold value were strongly reduced. After five iterations, a good fit was achieved between apparent resistivities measured in the field and resistivities calculated as a result of inverse modelling. The RMS (Root Mean Square) error values ranged from 2.37% to 2.5% (Table 1). The

geological interpretation was based on the block model, not on the contour model with a smooth gradient of colours. Finally, the interpretation of the slip surface and thickness of the colluvium layer based on the inverted resistivity models was verified by synthetic models.

4.2. MASW

The MASW method, which allows estimating Vs velocities in the shallowest part is additionally sensitive to the low-velocity zones (which is a zone with a seismic velocity lower than surrounding layers, especially referred to layers not visible on refraction methods). MASW processing was performed using the GeoPsy (Wathelet et al., 2020) program to pick dispersion curves for each shot and Vs profiles calculations. Only the positive offsets were used in the scheme assuming utilisation of 24 channels for each shot position (24 1D profiles). Additionally, 12 profiles with less than 24 geophones (23–12) were calculated and used for 2D model construction (Prolongation of the imaging on the East side of the profile). Pre-inversion parameters were assumed for each shot point separately. In general, they consisted of the five-layer model with the Poisson's ratio between 0.2 and 0.5, the density of 2000 kg/m³, fixed Vp velocities from 500 m/s for the top layer up to 3500 m/s for the bottom one and loose constraints for Vs velocities, ranging from 100 to 450 m/s in the top layer and up to 2000 m/s at the bottom. The depth of MASW models was limited to 20 m, i.e. the maximum reliable penetration depth of this method in this particular case. The midpoint of each profile was assigned to the centre of each subprofile considered.

The total length of the MASW profile is 135 m and covers the area between 72.5 m and 207.5 m of the seismic profile. It consists of 36 1D profiles, which were interpolated using a natural neighbourhood approach. The Chi² parameter, an overall measure of the misfit between the theoretical dispersion curve and the real data (the example is shown in Fig. 4), was used as an estimator of the uncertainty. The 2D misfit model was created analogically to the 2D MASW Vs model. However, the rapid increase in uncertainty, limited resolution, and penetration depth, as well as obtaining the S-wave velocity field do not allow the use of MASW as a standalone method for estimating the velocity field for reflection imaging purposes.

4.3. Refraction seismic

A robust short offset refraction seismics method is widely used to recognize the shallow structure from karst landforms, valley-fill deposits, and landslides (Hoffmann and Schrott, 2003; Schrott et al., 2003; Bichler et al., 2004), and the most often for static corrections (Law and Trad, 2017). In our case, it is an estimation of the first significant velocity change between the weathered and water-filled colluvium and the bedrock. This information is however averaged for a whole layer and cannot image low-velocity layers caused by water saturation. Those characteristics are clearly imaged by MASW, but to correctly interpret those two datasets the information about Vp/Vs ratio is essential. Moreover, an uncertainty for refraction seismic has been estimated in a statistical test based on randomly generated starting models as in previous method (MASW).

The refraction calculations were done during the estimation of static corrections for reflection imaging in the Refstat module of Globe Claritas package. Using refraction first breaks, the 2D model was obtained using Claritas Software. It was done by calculating an average Vp and thickness of each layer for all shots and fitting the velocity model to the given data. Such an effective approximation of average Vp velocities allowed the estimation of Vp/Vs ratio by comparison with the average Vs velocities from the MASW in the same layers giving the value of c. a. 1.9 (Table 3), where the theoretical is 1.7. The comparison between MASW velocities and refraction ones, as well as correlation of layers between methods, was based on 2D models (Fig. 5).

4.4. Ray-based travel time seismic tomography

Compared to the short-offset, refraction seismic approach based on generalized linear inversion method, yielding only depth and velocity beneath every source and/or receiver employed previously, in this part we employ a grid-based - raytracing traveltimes tomography to obtain the velocity variation in the shallow subsurface. The ray-based first breaks travel time refraction tomography, which allows estimating velocities of the layers, also has limitations. The most difficult is the dependence from the starting model (Nolet, 2008) and common vertical to horizontal anisotropy of Vp. The recalculated MASW model was used

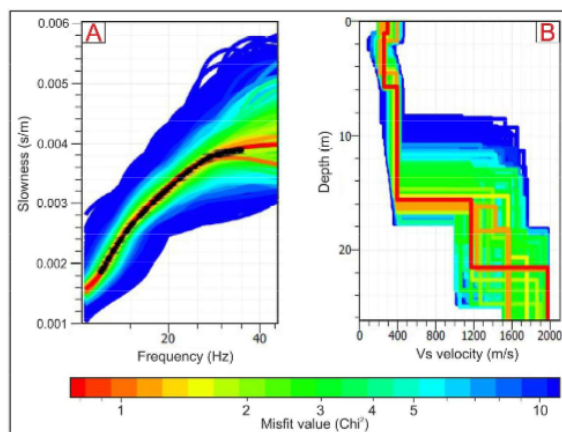


Fig. 4. The example of the dispersion curve modelling (A) and 1D shear velocity model (B) for shot 1006. The dispersion curve (black line with uncertainty bars) shows a good fit between data and synthetic models. The best theoretical curve has a Chi² value less than one.

Table 3
Comparison of MASW and Seismic refraction average velocities and layer thicknesses.

| Layer | Seismic refraction (Vp) velocity (m/s) | Seismic refraction layer thickness (m) | MASW (Vs) velocity (m/s) | MASW layer thickness (m) | Vp/Vs |
|-------|--|--|--------------------------|--------------------------|-------|
| 1 | 450 | 11 | 230 | 10 | 1.95 |
| 2 | 2100 | – | 1150 | 11 | 1.82 |

in the ray-based seismic tomography. The Jive3D tomographic code (Hobro et al., 2003), which is based on the ray approximation, was used to obtain the P-wave velocity field. The starting model in seismic tomography is usually based on a priori knowledge or extracted from the velocities of both direct and refracted arrivals and depth to the refractor/refractors as seen in the seismic data (Nolet, 2008). In the proposed approach, the seismic Vs velocities model with its uncertainties based on the MASW were recalculated into Vp domain. Such information with refraction seismic model was used to obtain initial models for ray-based tomography. This approximated model with the estimated uncertainty information from previous methods was used to limit the solution space in the inversion process of ray-based seismic tomography. The use of the approach proposed by Meléndez et al. (2015) in Tomo3D code was applied to estimate the uncertainty of the tomographic model from the 2D MASW misfit model. To estimate the uncertainty of the ray-based seismic tomography (Owoc et al., 2018), the set of starting models was randomly created based on the MASW result and its uncertainty range. In total, 121 initial models were generated. Finally, an optimal tomographic model and its deviation were obtained. That model, representing the horizontal Vp velocities, was used in the reflection imaging as a starting point in solving the velocity estimation problem.

4.5. Seismic imaging

The tomographic velocity field was recalculated using the Dix formula (Dix, 1955), then applied to the dataset during normal moveout (NMO) correction and time-to-depth conversion. Because the tomographic velocity field representing horizontal velocities is faster than the vertical velocity field required for seismic imaging, the fine fitting was required. We used the Globe Claritas software for seismic imaging and data pre-processing. The effect of key data processing steps, the data filtration, and signal enhancement is presented in Fig. 6. These procedures improved the visibility of the reflections. The velocity analysis modules were used to improve the velocity field from the ray-based tomography. Due to the short offsets, this effect is small. By manually changing the percentage of the velocity field and, it was found that the value of 48% of the tomographic velocities was optimal for the flattening of the reflecting horizons (Fig. 7). By modification of the best fitted seismic velocity field in uncertainty range from the ray-based seismic tomography, two marginal velocity fields were prepared and used during the time to depth conversion to evaluate reflection horizon depth and uncertainty of the result. Seismic data processing steps with their aim are presented in Table 2.

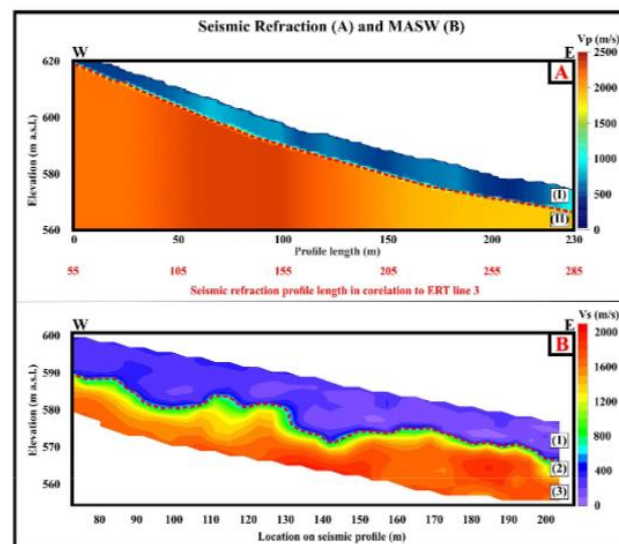


Fig. 5. The result of the refraction seismics method (A). The MASW result (B) presents a strong velocity contrast, which may be related to the landslide movement influencing the water-saturated layer (red dashed line). The velocity estimation in the third layer for the MASW method is estimated with high uncertainty, thus not included in the interpretation. (For interpretation of the references to colour in this figure legend, the reader is referred to the web version of this article.)

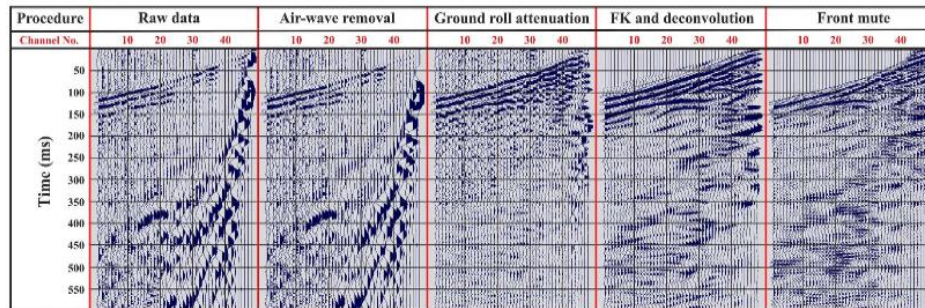


Fig. 6. The effect of key data processing steps on the exemplary shot record. The data filtration and signal enhancement procedures allowed for strengthening the visibility of reflections.

5. Results

The outcomes of applied methods are presented in the following order based on prospecting depth and resolution. In the result of refraction seismics (Fig. 5A) two layers significantly different in P-wave velocity (V_p) can be distinguished. The first layer (I) has an average thickness of approx. 11 m with an average P-wave velocity of 450 m/s and can be connected with (1) layer from the MASW result (Fig. 5B). The second layer (II) is characterized by an average V_p velocity of 2100 m/s and is probably the same layer as (2) from the surface wave analysis. The surface wave analysis using the MASW method (Fig. 5B), which prospecting depth was up to c.a. 26 m, detected three layers significantly different in shear-wave velocity (V_s) in the colluvium: (1) with a velocity of approx. 200–400 m/s and a thickness of 10–16 m; (2) with a velocity of approx. 1100–1200 m/s and a thickness of 4–8 m and (3) with a velocity of approx. 1800 m/s and higher with an unknown thickness (inversion and interpretation limited to 20 m due to a geometry of the survey). However, the third layer was not interpreted

due to its high uncertainty, connected with assumptions described in the processing paragraph. The MASW results do not allow recognition of the bedrock but made it possible to observe a diversity of colluvial properties.

ERT measurements on different profiles showed coherent distributions of resistivities and show similar anomalies and interpreted features (Fig. 8). A layer of low resistivity values (below 40 Ωm), identified as a landslide body, occurs just below the surface. Also, high resistivity anomalies (values up to 200 Ωm) were found within the generally low-resistivity landslide body. The spatial range of colluvium increases from profile 1 to 4 (i.e. from north to south). In the bedrock, two resistivity series were distinguished, the high-resistivity series is interpreted as a sandstone (marked in Fig. 8 as Sst) and low-resistivity series is identified as a shale and sandstone complex with a significant amount of shale (marked in Fig. 8 as Sh). Based on ERT measurements, the maximum thickness of the landslide in profile 1 was estimated at 16 m, in profile 2 at 33 m, in profile 3 at 34 m and in profile 4 at 36 m. However, it should be taken into account that with an electrode spacing of 5

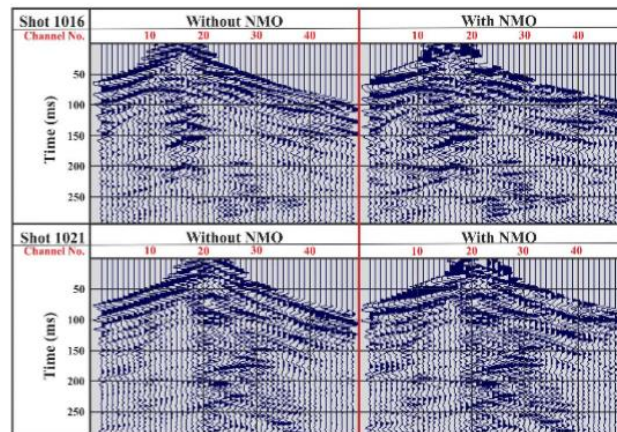


Fig. 7. The effect of NMO correction, after the application of smooth tomographic velocity field on two exemplary shot records. Because of short offsets straightening of reflections is not perfect, but sufficient to obtain a clear reflection image.

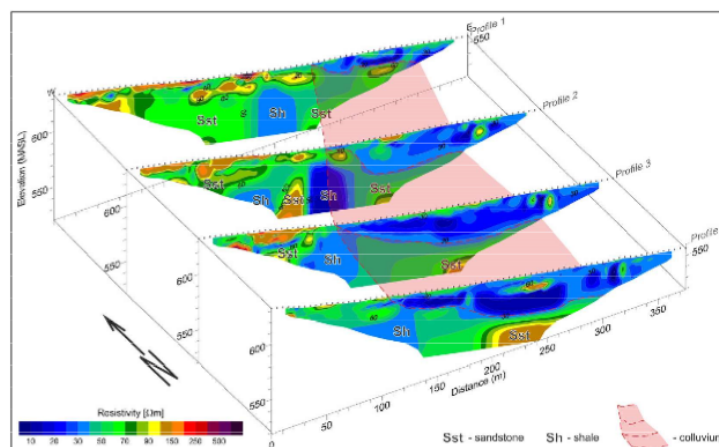


Fig. 8. The result of ERT. The landslide slip surface in each profile is marked by a red dashed line. The bottom surface of colluvium of the landslide is shown by a red plane. The slip surface dips from the north to the south of the study site. (For interpretation of the references to colour in this figure legend, the reader is referred to the web version of this article.)

m, the vertical resolution at depths of 16 and 34 m is 3.85 m and 5.65 m, respectively (Fig. 3). This, of course, indicates that the uncertainty of thickness estimation increases with depth to the bottom of the landslide body. The verification of the thicknesses evaluated in individual ERT profiles was done using synthetic resistivity models generated in the Res2Dmod forward solver, with a high correlation between the real data and the model. The distribution of resistivity values in the bedrock of the landslide in all of the images from the forward modelling process is different from that obtained from the field data. That indicates complex geological structure at the study site which is difficult to image in the Res2Dmod software. Interpolation of ERT results allowed estimating the spatial extent of colluvium and the position of the slip surface of the landslide (Fig. 8). The thickness of the landslide decreases to the north and the maximum is estimated at 36 m.

The calculated velocities from MASW and seismic ray-based tomography methods (Fig. 9A), with the interpretation of geologic boundaries from ERT, allowed for the construction of the velocity field that was applied in the reflection imaging. The ratio of vertical to horizontal seismic P-wave velocity was estimated at 0.48. The lower values of this parameter are caused by the presence of the colluvial material. Moreover, ERT and surface wave methods allowed recognition of the first few metres of the rock structures, which is difficult to perform using other seismic methods in used acquisition geometry. The assessment of colluvial thickness and landslide extent based on the seismic profile located between ERT profiles 2 and 3 shows a high correlation of these features with the ERT profile 3.

The seismic section displays the shape of the landslide body, as well as the presence of discontinuities in the study site (Fig. 9B–D). This result correlates well with the ERT data, where similar structures can be observed. The ERT images show colluvium (the red plane in Fig. 8) visible as a strong resistivity contrast, whereas the seismic image provides additional knowledge about the shape of sliding structures and discontinuities occurring below the landslide body (green dashed line in Fig. 9D), as well as discontinuity between two main active landslide bodies (red dashed line in Fig. 9D). The deeper parts of the seismic image below 50 m of depth reveal multiple horizontal reflections (orange area). The reflection seismic method determined the thickness of the main landslide body, which was estimated to be approximately 35

± 3 m in the middle of the study area (detailed uncertainty field in Fig. 9C). The high-resolution seismic image also additionally indicates the possibility of a second landslide body, with different amplitude characteristics (Fig. 9D). Compared to the main body marked by the strong reflection signature, the non-reflective zone likely connected with freshly disturbed rocks might be an indicator of the secondary landslide body.

The comparison of landslide dimensions determined on the basis of geophysical measurements against the background of the terrain model is shown in Fig. 10. In the DTM model, the slip surface can be recognized. With the information from subsurface methods well correlated with the structures visible on the DTM, the complete view of the landslide shape was obtained (Fig. 10).

6. Discussion

Previous refraction seismics surveys have been used to identify the Carpathian landslides (Bestyński and Thiel, 2005; Pilecki et al., 2007; Bestyński, 2008; Ostrowski et al., 2013; Bestyński et al., 2017; Gawrucienczow et al., 2017). Based on the variation in the velocity of the longitudinal wave V_p , the referenced authors were able to estimate the geometry of the landslides as well as to demonstrate that the colluviums within the landslides are usually bipartite. Differences in average V_p within the colluvium and bedrock are presented in Table 4. Bestyński et al. (2017) juxtaposed refraction boundaries identified as slip surfaces with the depth determined based on borehole data and inclinometer measurements. Their comparison shows a correlation between results. The deviations of in-depth estimation range from 0.5 m to several metres.

Geological and inclinometer studies of the nearby Miłówka landslide showed the occurrence of two slip surfaces at a depth of about 12 and 28 m, which correlate with refraction boundaries (Bestyński et al., 2017). According to these studies, the V_p in the bedrock was between 2.6 and 3.2 km/s. Both the depth values of discontinuity zones and the V_p propagation in the bedrock are similar to the results presented in this paper.

Based on the ERT measurements, the maximum thickness of the Cisiec landslide is estimated at 36 m. In other parts of the Carpathians,

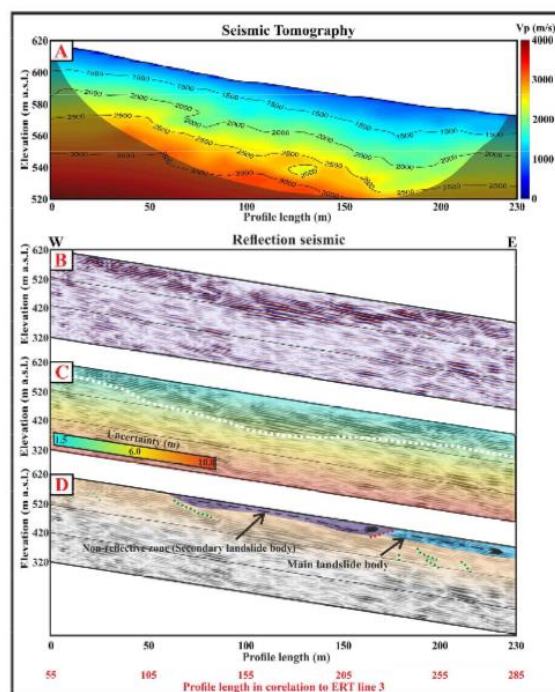


Fig. 9. The results of the smooth ray-based tomography (A), the depth section (B), and the depth uncertainty of the seismic imaging (C). The white dotted line marks 4-m depth uncertainty. Schematic interpretation (D) shows two active landslide bodies. Green and red dashed line marks discontinuities. (For interpretation of the references to colour in this figure legend, the reader is referred to the web version of this article.)

the thickness of colluvium which extended 30 m was also recognized by Ostrowski et al. (2013) and Gawriuczenkow et al. (2017) using the ERT method.

Bestyński and Thiel (2005), based on research on Carpathian slopes, indicated that the combination of the results of electrical-resistivity studies (profiling, vertical soundings and ERT) with refraction seismics method is the efficient way of landslide investigation. They indicated that these methods are effective to delineate landslide geometry and position of the slide boundaries. The combination of ERT and seismic methods is the most reasonable approach. However, more sophisticated seismic imaging methods should be used nowadays, because they provide more information at a higher resolution. Moreover, the problem of uncertainty analysis of the results is often skipped or minimized to the most basic form. That additional information is useful in the final correlation of the results from different methods and can improve data interpretation. Each technique increased the amount of information about the landslide, allowing for cross-validation of the results.

The slide of rock material disturbs its original structure, reducing its mechanical and changing physical properties. As Bestyński (2008) points out, it most often causes an increase in electrical resistivity values. However, this is not always the case. Bochnacka (2013), investigating the landslide no. 23 in the area of the Świnna Poręba reservoir (Carpathians), noticed that the electrical resistivity of the slope-building medium, interpreted as flysch with a predominance of shale

(sandstone content up to 35%), is in the range of 30–70 Ωm , while the resistivity values of the colluvium were lower. For the region of this landslide, the Vp velocities were in the range of 1900–3200 m/s for the bedrock while for the two layers of weathered rock material lying above, they were in the range of 1200–1700 m/s and 500–800 m/s. Obviously, lower velocities indicate a reduction in the mechanical properties of the weathered layers.

Ambiguity in the interpretation of geophysical measurements can be reduced in several ways. The most appropriate approach would be to combine all of them. First, at least two different measuring methods should be used. Second, confirming the interpretation by forward modelling based on a model of resistivity distribution in the tested medium should be implemented. Of course, the most optimal solution would be to drill boreholes in the area where geophysical anomalies were identified. However, verification with core drillings that provide direct and accurate information is costly, especially when the drillings are deep. Additionally, the borehole data provides only point information (1D), not spatial (2D or 3D). As stated in the introduction, one of the purposes of this paper was to verify the results obtained from each method used. The idea of uncertainty analysis allowed to build a coherent and high-resolution landslide model using all of the obtained results from different geophysical methods along with knowledge of their accuracy. This proposed method is the only one giving quantitative depth estimation in seismic imaging.

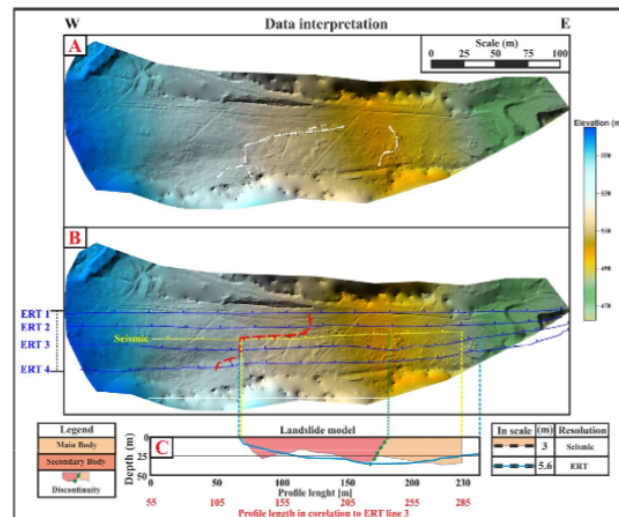


Fig. 10. Projection of the data on the DTM. The white line presents the discontinuities visible on the surface (A). The red line indicates the headscarp of the landslide based on the ERT data (B). The model (C) directly compares the result of ERT profile 3 and Reflection imaging interpretation. In both cases, the slip surface depth is about 34–35 m. The depth uncertainty for both methods is presented in scale with (C). (For interpretation of the references to colour in this figure legend, the reader is referred to the web version of this article.)

Table 4
Comparison of Vp wave velocity values in landslides in the Polish Carpathians.

| Authors | Place (number in Fig. 2A) | Longitudinal wave velocity Vp in the layer (km/s) | | |
|----------------------------|--|---|--------------|---------|
| | | Colluvium | Bedrock | Bedrock |
| | | First layer (strongly weathered) | Second layer | Bedrock |
| Bestyński and Thiel (2005) | Czorsztyn–Niedzica water reservoir (1) | 0.6 | 1.6–2.4 | 3.0 |
| | Miedzybrodzie Żywieckie (2) | 0.3–0.5 | – | 2.3–3.4 |
| Pilecki et al. (2007) | Mucharz (3) | 0.23–0.28 | 1.7 | 2.4 |
| Ostrowski et al. (2013) | Miedzybrodzie Bialskie (mountain Zar slopes) (4) | 0.4 | 1.0–1.4 | 3.0 |
| | Łańcucha (Łanckorona area) (5) | 0.4 | 1.3–1.8 | 2.2–2.5 |
| | Northside of the Miłówka stream (6) | 0.3 | 2.0 | 3.0 |
| Gawrużenkov et al. (2017) | Landslide no. 43958 in LCS (7) | 0.2–1.0 | – | 2.0 |
| This paper | Cisiec, landslide no. 24–17–152–029130 in LCS (the yellow star in Fig. 2A) | 0.5–0.7 | 1.5–2.0 | 2.5–3.0 |

7. Conclusions

The Cisiec landslide was characterized using a combination of multiple geophysical methods in an approach that uses information about the uncertainty of the results of each method used. Application of MASW, ERT, refraction seismics method, ray-based seismic tomography and reflection imaging permitted the creation of a high-resolution image of the subsurface of the landslide in a geologically and tectonically complex area, where information obtained from a single method was insufficient. All seismic data were recorded on a single seismic survey. No separate field measurements were needed, thus the cost of field works is small in this approach. Different data handling techniques allowed the use of all parts of the recorded seismic wavefield by a variety of methods (MASW, two refraction seismics, reflection imaging), suggesting the overall cost-effectiveness of the methodology.

The DTM of the surface created using aerial photogrammetry, combined with the geophysical methods provided a complete view of the landslide structure. The MASW survey made it possible to recognize

and distinguish different layers in the colluvium zone. The ERT modelled physical boundaries which can be correlated with various lithologies. The ray-based seismic tomography result allowed construction of a velocity field essential for reflection imaging. The obtained velocity range in each layer is comparable with the results of other seismic studies from the Polish Carpathians region. The model obtained by the ERT method allowed to estimate the northeast direction of the slope movement. Seismic imaging allowed the identification of discontinuities inside and below the landslide body. The analysis of uncertainty was necessary for direct comparison of results, as well as the correct transfer of information between them. In ERT and reflection seismic methods, interpreted depth of the slip surface shows great convergence, confirming the narrow uncertainty of the obtained results. The resolution of the ERT method was estimated to be 5.6 m at the depth c.a. 35 m, whereas reflection imaging uncertainty at the depth of 30–40 was ± 3 m. The final correlation of the information gathered from various methods enabled a thorough and high-resolution characterization of the Cisiec landslide.

A. Marciniak, S. Kowalczyk, T. Gontar et al.

Declaration of Competing Interest

The authors do not have any conflict of interest to declare.

Acknowledgements

This research was funded by the National Science Centre, Poland (NCN) Grant UMO-2015/19/B/ST10/01833. Part of this work was supported within statutory activities No. 3841/E-41/S/2018 of the Ministry of Science and Higher Education of Poland.

References

- Bednarczyk, Z., 2008. Application of GPR Scanning for Landslide Investigations in Polish Carpathians. Near Surface 2008-14th EAGE European Meeting of Environmental and Engineering Geophysics, pp. 372–376. <https://doi.org/10.3997/2214-4609.20146273>.
- Bellanova, J., Calamita, G., Giocoli, A., Luongo, R., Macchiato, M., Perrone, A., Uhlemann, S., Piscitelli, S., 2018. Electrical resistivity imaging for the characterization of the Montaguto landslide (southern Italy). Eng. Geol. 243, 272–281. <https://doi.org/10.1016/j.enggeo.2018.07.014>.
- Bestyński, Z., 2001. Geophysical investigations of the flysch built landslide slopes. Proceedings ISRM Regional Symposium EUROCK 2001. Rock Mechanics a Challenge for Society, Finland.
- Bestyński, Z., 2008. Metody geofizyczne w rozpoznaniu flišowych stoków osuwiskowych. Geofizyka: Biuletyn Informacyjny 7, 62–71.
- Bestyński, Z., Thiel, K., 2005. Geophysical investigations of the Carpathian slide slopes. In Proceedings of the Conference Mass Movements Hazard and various Environments. Pol. Geol. Inst. Spec. Pap. 20, 35–39.
- Bestyński, Z., Pacanowski, G., Śleński, E., 2017. Geophysical investigation and geotechnical classifications for stability assessment of carpathian flysch slopes. Prz. Geol. 65 (10/2), 717–724.
- Białostocki, R., 1974. Wytczne do stosowania metod geofizycznych w badaniach hydrogeologicznych i geologiczno-inżynierskich. Wydawnictwa Geologiczne, Warszawa.
- Bichler, A., Bobrowsky, P., Best, M., Douma, M., Hunter, J., Calvert, T., Burns, R., 2004. Three-dimensional mapping of a landslide using a multi-geophysical approach: the Quesnel Forks landslide. Landslides 1, 29–40. <https://doi.org/10.1007/s10346-003-0008-7>.
- Bochnacka, A., 2013. Stateczność zboczy osuwiskowych zbiornika Świnna Poręba. Geofizyka: Biuletyn Informacyjny 11, 73–86.
- Bodin, T., Sambridge, M., 2009. Seismic tomography with the reversible jump algorithm. Geophys. J. Int. 178 (3), 1411–1436. <https://doi.org/10.1111/j.1365-246X.2009.04226.x>.
- Bogoslavsky, V.A., Ogilvy, A.A., 1977. Geophysical methods for the investigation of landslides. Geophysics 42 (3), 562–571. <https://doi.org/10.1190/1.1440727>.
- Bruno, F., Martillier, F., 2000. Test of high-resolution seismic reflection and other geophysical techniques on the Boup landslide in the Swiss Alps. Surv. Geophys. 21 (4), 335–350. <https://doi.org/10.1023/A:1006736824075>.
- Burtan, J., Silora, W., Sokolowski, S., Zytka, K., 1956. Serial Geological Maps of Poland 1:50 000. Sheet 1029 – Międzybóże (Radziechów) (M-34-87-a).
- Crawford, M.M., Bryson, L.S., Woolery, E.W., Wang, Z., 2018. Using 2-D electrical resistivity imaging for joint geophysical and geotechnical characterization of shallow landslides. J. Appl. Geophys. 157, 37–46. <https://doi.org/10.1016/j.jappgeo.2018.06.009>.
- Dix, C.H., 1955. Seismic velocities from surface measurements. Geophysics 20, 68–86.
- Eichkitz, C., Schreiechner, M., Amtmann, J., Schmid, C., 2009. Shallow seismic reflection study of the schlieflgraben landslide deposition area - interpretation and three dimensional modeling. Austrian J. Earth Sci. 102 (2), 52–60.
- Gawruzenkow, I., Kaczmarek, L., Kielbasiński, K., Kowalczyk, S., Mieszkowski, R., Wójcik, E., 2017. Slope stability and failure hazards in the light of complex geological surveys. Sci. Rev. Eng. Environ. Sci. 26, 85–98. <https://doi.org/10.22630/PNIKS.2017.26.1.08>.
- Godio, A., Strobbia, C., De Bacco, G., 2006. Geophysical characterization of a rockslide in an alpine region. Eng. Geol. 83, 273–286. <https://doi.org/10.1016/j.enggeo.2005.06.034>.
- Golonia, J., Waśkowska-Oliwa, A., 2007. Stratygrafia polskich Karpat flišowych pomiędzy Bielskiem-Białą a Nowym Targiem. Geologia, Akademia Górniczo-Hutnicza im. Stanisława Staszica w Krakowie 33 (4/1), 5–27.
- Harba, P., Pilecki, Z., Krawiec, K., 2019. Comparison of MASW and seismic interferometry with use of ambient noise for estimation of S-wave velocity field in landslide subsurface. Acta Geophys. 67, 1875. <https://doi.org/10.1007/s11600-019-00344-9>.
- Hobro, J.W.D., Singh, S.C., Minshall, T.A., 2003. Three-dimensional tomographic inversion of combined reflection and refraction seismic traveltime data. Geophys. J. Int. 152 (1), 79–93. <https://doi.org/10.1046/j.1365-246X.2003.01822.x>.
- Hoffmann, T., Schrott, L., 2003. Determining sediment thickness of talus slopes and valley fill deposits using seismic refraction – a comparison of 2D interpretation tools. Z. Geomorphol. Suppl. 132, 71–87.
- Karçioğlu, G., 2019. Near-surface resistivity structure near avicular landslide in Istanbul, Turkey by 2D inversion of VLF data. J. Appl. Geophys. 163, 73–83. <https://doi.org/10.1016/j.jappgeo.2019.02.012>.
- Kłopotowska, A., Łukasiak, D., 2017. Estimation of lithogenetic features of flysch sandstones based on ultrasonic tests. Prz. Geol. 65, 177–182.
- Kowalczyk, S., Mieszkowski, R., Pacanowski, G., 2014. The stability evaluation of Warsaw slope selected pieces based on Electrical Resistivity Tomography survey (ERT). Prz. Geol. 62, 634–640.
- Kucharska, M., Kamiński, M., 2008. Karta rejestracyjna osuwiska (numer ewidencyjny 24-17-152-029130) w miejscowości Cisiec.
- Lapenna, V., Lorenzo, P., Perrone, A., Piscitelli, S., Rizzo, E., Sdao, F., 2005. 2D electrical resistivity imaging of some complex landslides in Lucanian Apennine chain, southern Italy. Geophysics 70 (3), 811–818. <https://doi.org/10.3997/2214-4609-pdb.6.P093>.
- Law, Bernard, Trad, Daniel, 2017. Robust refraction statics solution using feedback from reflection data, p. 2666. <https://doi.org/10.1190/segam2017-17738085.1>.
- Leszczyński, S., 1985. Piaszkowe pasy z warstw hieroglifowych w Jastrzębiej k. Ciepłkowice [Banded sandstones of the Hieroglyphic Beds at Jastrzębia near Ciepłkowice]. Kwartalnik Geol. 29 (2), 395–403.
- Leszczyński, S., Uchman, A., 1991. To the origin of variegated shales from flysch of the Polish Carpathians. Geol. Carpath. 42, 279–289.
- Loke, M.H., 2018. Tutorial: 2-D and 3-D Electrical Imaging Surveys. Geotomo Software <https://www.geotomosoft.com/downloads.php> (accessed 28 May 2019).
- Majdański, M., Grzyb, J., Owoc, B., Krogulec, T., Wysocka, A., 2018. Near-surface structure of the Carpathian Foredeep marginal zone in the Roztocze Hills area. Acta Geophys. 66 (2), 179–189. <https://doi.org/10.1007/s11600-018-0131-4>.
- Malehmir, A., Socco, L.V., Bastani, M., Krawczyk, C.M., Pfaffhuber, A.A., Miller, R.D., Maurer, H., Frauenfelder, R., Suto, K., Bazin, S., Merz, K., Dahlin, T., 2016. Near-surface geophysical characterization of areas prone to natural hazards: a review of the current and perspective on the future. In: Nielsen, L. (Ed.), Advances in Geophysics, pp. 51–146. <https://doi.org/10.1016/b.sagph.2016.08.001>.
- Mantovani, M., Devoto, F., Forte, E., Mocnik, A., Pasuto, A., Piacentini, D., Soldati, M., 2013. A multidisciplinary approach for rock spreading and block sliding investigation in the north-western coast of Malta. Landslides 10, 611–622. <https://doi.org/10.1007/s10346-012-0347-3>.
- Marciniak, A., Stan-Kleczek, I., Idziak, A., Majdański, M., 2019. Uncertainty based multi-step seismic analysis for near-surface imaging. Open Geosci. 11 (1), 727–737. <https://doi.org/10.1515/geo-2019-0057>.
- McCann, D., Forster, A., 1990. Reconnaissance geophysical methods in landslide investigations. Eng. Geol. 29 (1), 59–78. [https://doi.org/10.1016/0013-7952\(90\)90082-C](https://doi.org/10.1016/0013-7952(90)90082-C).
- Meñéndez, A., Korenaga, J., Sallares, V., Miniussi, A., Ranero, C., 2015. TOMO3D: 3-D joint refraction and reflection traveltime tomography parallel code for active-source seismic data synthetic test. Geophys. J. Int. 203, 158–174. <https://doi.org/10.1093/gji/ggv292>.
- Mutti, E., 1977. Distinctive thin-bedded turbidite facies and related depositional environments in the Eocene Hecho Group (South-central Pyrenees, Spain). Sedimentology 24 (1), 107–131. <https://doi.org/10.1111/j.1365-3091.1977.tb00122.x>.
- Nescieruk, P., Wojciechowski, T., Perski, Z., 2016. Monitoring osuwisk w ramach Systemu Osłony Przeciwosuwiskowej. II Ogólnopolskie Sympozjum Geodyscyplinarnych Metod Badawczych 46.
- Nolet, G., 2008. A Breviary of Seismic Tomography: Imaging the Interior of the Earth and Sun. Cambridge University Press, Cambridge <https://doi.org/10.1017/CBO9780511984709>.
- Orozco, A.F., Bücker, M., Steiner, M., Malet, J.P., 2018. Complex-conductivity imaging for the understanding of landslide architecture. Eng. Geol. 243, 241–252. <https://doi.org/10.1016/j.enggeo.2018.07.009>.
- Ostrowski, S., Rybak-Ostrowska, B., Lasocki, M., 2013. Application of near-surface geophysical survey for recognition of the geology of landslide areas in the Carpathians – a case study. Prz. Geol. 61 (1), 67–73.
- Oszczypko, N., Ślęcka, A., Zytka, K., 2008. Tectonic subdivision of Poland: Polish Outer Carpathians and their foredeep. Prz. Geol. 56, 927–935.
- Owoc, B., Górszczyk, A., Majdański, M., 2018. The discussion of the uncertainty in the traveltime seismic tomography. EAGE Near Surface 2018. <https://doi.org/10.3997/2214-4609.201802559>.
- Owoc, B., Marciniak, A., Dzierżek, J., Kowalczyk, S., Majdański, M., 2019. Seismic Imaging of the Mesozoic Bedrock Relief and Geological Structure under Quaternary Sediment Cover: the Bolmin Syncline (SW Holy Cross Mountains, Poland). Geosciences 9, 447.
- Park, C.B., Miller, R.D., Miura, H., 2002. Optimum field parameters of a MASW survey [Exp. Abs.] SEG-J. Tokyo May 22–23, 2002.
- Pasierb, B., Grodecki, M., Gwóźdź, R., 2019. Geophysical and geotechnical approach to a landslide stability assessment: a case study. Acta Geophys. 67, 1823–1834. <https://doi.org/10.1007/s11600-019-00338-7>.
- Pettley, D., 2012. Global patterns of loss of life from landslides. Geology 40, 927–930. <https://doi.org/10.1130/G33217.1>.
- Pilecki, Z., Zietek, J., Karczewski, J., Pilecka, E., Klosinski, J., 2007. The effectiveness of recognizing of failure surface of the Carpathian flysch landslide using wave methods. Near Surface 2007-13th EAGE European Meeting of Environmental and Engineering Geophysics, pp. 256–260. <https://doi.org/10.3997/2214-4609.20146664>.
- Poprawa, D., Rączkowski, W., 2003. Carpathian landslides (southern Poland). Prz. Geol. 51, 685–692.
- Renalier, F., Jongmans, D., Campillo, M., Bard, P.Y., 2010. Shear wave velocity imaging of the Avignonet landslide (France) using ambient noise cross correlation. J. Geophys. Res. 115, F03032. <https://doi.org/10.1029/2009JF001538>.
- Schrott, L., Hufschmidt, G., Hankammer, M., Hoffmann, T., Dikau, R., 2003. Spatial distribution of sediment storage types and quantification of valley fill deposits in an upper Alpine basin, Reintal, Bavarian Alps, Germany. Geomorphology 55, 45–63.
- Tarantola, A., 1987. Inverse Problem Theory: Methods for Data Fitting and Model Parameter Estimation. Elsevier, Amsterdam.
- Travelletti, I.J., Demand, J., Jaboyedoff, M., Marillier, F., 2010. Mass movement characterization using a reflexion and refraction seismic survey with the sloping local base level concept. Geomorphology 116, 1–10. <https://doi.org/10.1016/j.geomorph.2009.10.006>.

A. Marciniak, S. Kowalczyk, T. Gontar et al.

Journal of Applied Geophysics 191 (2021) 104364

- Wang, S., Malehmir, A., Bastani, M., 2016. Geophysical characterization of areas prone to quick-clay landslides using radio-magnetotelluric and seismic methods. *Tectonophysics* 677–678, 248–260. <https://doi.org/10.1016/j.tecto.2016.04.020>.
- Waśkowska-Oliwa, A., 2014. The Eocene Hieroglyphic beds and Green shales in the Rożnów Lake area (Silesian Nappe, Outer Carpathians) – facies development and biostratigraphy. *Geol. Geophys. Environ.* 40, 5–26. <https://doi.org/10.7494/geol.2014.40.1.5>.
- Wathelet, M., Chatelain, J.-L., Cornou, C., Di Giulio, G., Guillier, B., Ohrnberger, M., Savvaidis, A., 2020. Geopsy: a user-friendly open-source tool set for ambient vibration processing. *Seismol. Res. Lett.* 91 (3), 1878–1889. <https://doi.org/10.1785/0220190360>.
- Yalcinkaya, E., Alp, H., Ozel, O., Gorgun, E., Martino, S., Lenti, L., Bourdeau, C., Bigarre, P., Coccia, S., 2016. Near-surface geophysical methods for investigating the Buyukcekmece landslide in Istanbul, Turkey. *J. Appl. Geophys.* 134, 23–35. <https://doi.org/10.1016/j.jappgeo.2016.08.012>.
- Żytko, K., Zając, R., Gucik, S., Rylko, W., Oszczytko, N., Garlicka, I., Nemčok, J., Eliáš, M., Menčík, E., Stráňík, Z., 1989. Map of the tectonic elements of the Western Outer Carpathians and their foreland. In: Poprawa, D., Nemčok, J. (Eds.), *Geological Atlas of the Western Outer Carpathians and their Foreland*. Państwowy Instytut Geologiczny Warszawa/GUDS Bratislava/Uag Praha.

Author contribution statements

Załącznik nr 2

do Szczegółowego trybu postępowania w sprawie nadania
stopnia doktora przez Instytut Geofizyki Polskiej Akademii Nauk

Author contribution statement

Publication:

Marciniak, A., Stan-Kłeczek, I., Idziak, A., & Majdański, M. (2019). Uncertainty based multi-step seismic analysis for near-surface imaging. Open Geosciences, 11(1), 727–737. <https://doi.org/10.1515/geo-2019-0057>

Author contribution: 70%

Author contribution according to Contributor Roles Taxonomy (CRediT):

Conceptualization – Fieldworks and experiment design, **Data curation** – Data maintaining and validation after gatherings, **Formal analysis** – Application of statistical analysis to seismic data, Seismic data processing (LVL, MASW, Tomography, RI), **Investigation** – Fieldwork data gathering, Interpretation of the results, **Methodology** – Development of methodology presented in the article, **Software** – Code refactoring for use in data gathered during the study (Refraction tomography, LVL), **Validation** – Final results common interpretation and validation, **Visualization** – Figures and tables preparation for publication, **Writing – original draft** – Preparation of all draft paragraphs, **Writing – review & editing** – Revision of the article after reviews

Author signature

.....

Supervisor signature

.....

Załącznik nr 2

do Szczegółowego trybu postępowania w sprawie nadania
stopnia doktora przez Instytut Geofizyki Polskiej Akademii Nauk

Author contribution statement

Publication:

Owoc, B., Marciniak, A., Dzierżek, J., Kowalczyk, S., & Majdański, M. (2019). Seismic Imaging of the Mesozoic Bedrock Relief and Geological Structure under Quaternary Sediment Cover: The Bolmin Syncline (SW Holy Cross Mountains, Poland). *Geosciences* (Switzerland), 9(10). <https://doi.org/10.3390/geosciences9100447>

Author contribution: 20%

Author contribution according to Contributor Roles Taxonomy (CRediT):

Conceptualization – Fieldworks and experiment design, **Data curation** – Data QC and pre-processing, **Formal analysis** – Seismic data processing (MASW, RI), **Investigation** – Fieldwork data gathering, Interpretation of the results, **Methodology** – Design of methodology, **Software** – Code refactoring for use in data gathered during the study (MASW), **Visualization** – Figures and tables preparation for publication (MASW, RI), **Writing – original draft** – Draft Preparation (Contribution in all paragraphs), **Writing – review & editing** – Revision of the article after reviews

Author signature

Supervisor signature

.....

.....

Załącznik nr 2

**do Szczegółowego trybu postępowania w sprawie nadania
stopnia doktora przez Instytut Geofizyki Polskiej Akademii Nauk**

Author contribution statement**Publication:**

Glazer, M., Dobiński, W., Marciniak, A., Majdański, M., & Błaszczuk, M. (2020). Spatial distribution and controls of permafrost development in non-glacial Arctic catchment over the Holocene, Fuglebekken, SW Spitsbergen. *Geomorphology*, 358. <https://doi.org/10.1016/j.geomorph.2020.107128>

Author contribution: 10%

Author contribution according to Contributor Roles Taxonomy (CRediT):

Formal analysis – Data processing (MASW), **Software** – Code refactoring for use in data gathered during the study (MASW), **Visualization** – Figures and tables preparation for publication (MASW), **Writing – original draft** – Draft Preparation (Data processing and interpretation), **Writing – review & editing** –Final draft validation, Revision of the article after reviews

Author signature

Supervisor signature

.....

.....

Załącznik nr 2

do Szczegółowego trybu postępowania w sprawie nadania
stopnia doktora przez Instytut Geofizyki Polskiej Akademii Nauk

Author contribution statement

Publication:

Majdański, M., Dobiński, W., Marciniak, A., Owoc, B., Glazer, M., Osuch, M., & Wawrzyniak, T. (2022). Variations of permafrost under freezing and thawing conditions in the coastal catchment Fuglebekken (Hornsund, Spitsbergen, Svalbard). Permafrost and Periglacial Processes. <https://doi.org/10.1002/ppp.2147>

Author contribution: 20%

Author contribution according to Contributor Roles Taxonomy (CRediT):

Conceptualization – Fieldworks and experiment design, **Data curation** – Data maintaining and validation after gatherings, **Formal analysis** – Application of statistical analysis to seismic data, Seismic data processing (MASW, Tomography), **Investigation** – Fieldwork data gathering, Interpretation of the results, **Methodology** – Development of methodology presented in the article, **Software** – Code refactoring for use in data gathered during the study (MASW), **Validation** – Final results common interpretation and validation, **Visualization** – Figures and tables preparation for publication, **Writing – original draft** – Preparation of all draft paragraphs, **Writing – review & editing** – Language and methodological corrections, Revision of the article after reviews

Author signature

Supervisor signature

.....

.....

Załącznik nr 2

do Szczegółowego trybu postępowania w sprawie nadania
stopnia doktora przez Instytut Geofizyki Polskiej Akademii Nauk

Author contribution statement

Publication:

Marciniak, A., Osuch, M., Wawrzyniak, T., Owoc, B., Dobiński, W., Glazer, M., & Majdański, M. (2022). Multi-method geophysical mapping of ground properties and periglacial geomorphology in Hans Glacier forefield, SW Spitsbergen. Polish Polar Research, 43(2), 101–123. <https://doi.org/10.24425/ppr.2022.140363>

Author contribution: 50%

Author contribution according to Contributor Roles Taxonomy (CRediT):

Conceptualization – Fieldworks and experiment design, **Data curation** – Data maintaining and validation after gatherings, **Formal analysis** – Application of statistical analysis to seismic and georadar data, Data processing (Tomography, GPR) **Investigation** – Fieldwork data gathering, Interpretation of the results of all methods, **Methodology** – Development of methodology presented in the article, **Software** – Code refactoring for use in data gathered during the study (Tomography), **Validation** – Final results common interpretation and validation, **Visualization** – Figures and tables preparation for publication, **Writing – original draft** – Preparation of all draft paragraphs, **Writing – review & editing** – Language and methodological corrections, Revision of the article after reviews

Author signature

Supervisor signature

.....

.....

Załącznik nr 2

do Szczegółowego trybu postępowania w sprawie nadania
stopnia doktora przez Instytut Geofizyki Polskiej Akademii Nauk

Author contribution statement

Publication:

Marciniak, A., Kowalczyk, S., Gontar, T., Owoc, B., Nawrot, A., Luks, B., Cader, J., & Majdański, M. (2021). Integrated geophysical imaging of a mountain landslide – A case study from the Outer Carpathians, Poland. Journal of Applied Geophysics, 191. <https://doi.org/10.1016/j.jappgeo.2021.104364>

Author contribution: 30%

Author contribution according to Contributor Roles Taxonomy (CRediT):

Conceptualization – Fieldworks and experiment design, **Data curation** – Data maintaining and validation after gatherings, **Formal analysis** – Application of statistical analysis to seismic data, Seismic data processing (LVL, MASW, Tomography, RI), **Funding acquisition** - Acquisition of the financial support for the project leading to this publication, **Investigation** – Fieldwork data gathering, Interpretation of the results, **Methodology** – Development of methodology presented in article, **Project administration** – Management and coordination responsibility for the research activity planning and execution, **Software** – Code refactoring for use in data gathered during study (Refraction tomography, LVL, MASW), **Supervision** – Oversight and leadership responsibility for the research activity planning and execution, **Validation** – Final results common interpretation and validation, **Visualization** – Figures and tables preparation for publication, **Writing – original draft** – Preparation of all draft paragraphs, **Writing – review & editing** – Revision of the article after reviews

Author signature

Supervisor signature

.....

.....